Spring 2018

ORTHOPHOSPHATE REMOVAL FROM SIMULATED AGRICULTURAL RUNOFF USING ZEROVALENT IRON ENHANCED SOIL MEDIA

Zachary Wallin
University of New Hampshire, Durham

ORTHOPHOSPHATE REMOVAL FROM SIMULATED AGRICULTURAL RUNOFF USING ZEROVALENT IRON ENHANCED SOIL MEDIA

BY

ZACHARY DANIEL WALLIN

B.S., University of New Hampshire, 2015

THESIS

Submitted to the University of New Hampshire

In Partial Fulfillment of

The Requirements for the Degree of

Master of Science

In

Civil Engineering

May 2018

This thesis has been examined and approved in partial fulfillment of the requirements for the degree of Master's of Science in Civil Engineering.

Thesis Director, Dr. Thomas P. Ballestero, Associate Professor of Civil and Environmental Engineering, University of New Hampshire

Dr. Michael Robin Collins, Professor of Civil and Environmental Engineering, University of New Hampshire

Dr. Iulia Barbu, Water Resources Engineer, AECOM

On April 6, 2018

Original approval signatures are on file with the University of New Hampshire Graduate School.

Acknowledgments

I would like to thank my advisor, Dr. Ballestero, for giving me the opportunity to work on this project and for all the guidance along the way. I would also like to thank Dr. Collins and Dr. Barbu for providing feedback on my research and for being a part of my Thesis Committee. Thank you to Tim Puls, Dr. Houle, and my fellow grad students for working with me throughout these years and for giving me the assistance that I often needed. I would like to thank my parents and siblings for their love and support. I also want to thank them for modeling what it looks like to work hard and overcome obstacles while still remembering what is most important in life. Most of all, I would like to thank my amazing wife, Emily, for putting up with me during this crazy time and for never ceasing to encourage, support, and love me.

Table of Contents

List of Tables

List of Figures

List of Equations

Abstract

ORTHOPHOSPHATE REMOVAL FROM SIMULATED AGRICULTURAL RUNOFF USING ZEROVALENT IRON ENHANCED SOIL MEDIA

by

Zachary Daniel Wallin

University of New Hampshire, May 2018

Agricultural runoff often contains high orthophosphate (ortho-P) loads due to the accumulation of phosphorus (P) in soils. This accumulation can be caused by fertilizer application, manure and litter application, or animal waste where feed contained significant amounts of P. With increasing knowledge of the environmental impacts of ortho-P, efforts have been made to research effective treatment solutions for this runoff and minimize receiving water impairments. An emerging trend in this field has been the use of zerovalent iron (ZVI) as an adsorbent. ZVI has been shown to improve the removal of dissolved ortho-P from stormwater over traditional filtration and sedimentation systems.

The removal of ortho-P from simulated runoff using ZVI-amended media was investigated in this study. The main objective of this research was to gather data to better understand and predict the lifespan of ZVI when treating high concentrations of ortho-P. Column tests were performed with varying depths and percentages of sand, loam, and ZVI composing the media. Sand and loam percentages were roughly 70% and 30%, respectively, while ZVI percentages tested were 0.5%, 1%, and 3%. These media mixes were tested at 6-inch and 12-inch media depths. The columns were subjected to target influent ortho-P concentrations of 4.57 mg-P/L over decades of simulated runoff. After roughly nine years of simulated runoff, all columns except for the column containing 3% ZVI and 12-inch media depth had lost their adsorption capacities. This last column lost its adsorption capacity around year twenty.

The results indicated a strong correlation between ZVI mass in the columns and adsorption capacity. Columns with more ZVI mass correlated to higher cumulative ortho-P mass removed and longer ZVI lifespans. Though increased media depth also corresponded to better removal percentages, it was determined that this increased performance was likely due to the higher ZVI mass in the columns. Time-series percent ortho-P removal results for each column were used in the creation of a tool for estimating ZVI lifespan in field applications. This tool employed the Langmuir isotherm as the basis for predicting adsorption over time for the ZVI-amended media. Removal data from each column was used in developing this model. This tool allows the user to input values for the expected yearly volume of runoff at a site, the expected average ortho-P concentration, and the desired media depth and ZVI percentage. Using these inputs, the tool produces a predictive percent removal curve over a number of years that can estimate when the ZVI's useful life will end, and therefore, when actual system maintenance (ZVI addition) is necessary.

Chapter 1: Introduction

1.1 Background

Agricultural runoff often poses a significant risk to receiving waters due to its high phosphorus (P) loading from fertilizer application (He, Zhang, Stoffella, Yang, & Banks, 2006). Other factors contributing to this high P loading can include manure and litter application, erosions of soils that have accumulated high P concentrations, and waste from animals where feed is high in P (Sharpley, et al., 2003). Excess phosphorus largely contributes to eutrophication in these receiving waters, which is a clear sign of deteriorating water quality (Bartsch, 1972). Eutrophication leads to low dissolved oxygen levels and sometimes fish kill in water bodies as harmful algal blooms and aquatic plants are rapidly produced (Fry, 1969). Fish kill, the increased cost of water treatment, and impacts on recreational activities attributable to eutrophication can all have severe consequences on the environment and economy (Carpenter, 2005). As this problem affects environmental, social, and economic aspects of society, it is clear that working toward simple eutrophication solutions can help improve sustainability on local and global levels.

The fertilization of croplands and subsequent runoff can contribute to nutrient pollution in receiving waters. Over-fertilization with respect to phosphorus can easily occur when farmers cannot purchase mixes with the desired nutrient ratio due to availability or cost (Stewart, Woolhiser, Wischmeier, Caro, & Frere, 1975). However, this over fertilization could also occur with the ideal fertilizers being over applied. As point sources of nutrient pollution have become more regulated, agricultural runoff has become the primary cause of eutrophication in many regions due to this over application of fertilizer (Carpenter, 2005). The volume of runoff generated from agricultural lands can be significantly higher than lands with undisturbed soils due to compaction and other factors (Burt & Slattery, 2006). With high P loadings and high runoff volumes for these agricultural sites, it is clear that

stormwater management practices should be employed to ensure the health and quality of receiving waters. As a point of reference, Pitt et al. (2005) reported that the median dissolved P (DP) concentration in urban runoff reported in a nationwide survey of municipalities was 0.12 mg-P/L, while a synthesis of study data from agricultural runoff discussed later in Section 2.1.3 was shown to be almost five times higher at 0.58 mg-P/L. It has been documented that eutrophication is accelerated at concentrations as low as 0.02 mg/L (Sharpley, et al., 2003).

Bioretention systems are commonly used in urban areas to reduce runoff volumes and to remove suspended solids and particulate contaminants through filtration and sedimentation (Stone, 2013). Though particulate phosphorus can be filtered out using a standard bioretention system, dissolved orthophosphate (ortho-P, PO_4-P) can only be removed from the stormwater by adsorption. Ortho-P is bioavailable, and its introduction to receiving waters can lead to excessive plant and algae growth (DePinto, Young, & Salisbury, 1986). Ortho-P, also known as dissolved inorganic phosphorus, is considered the most important phosphorus source for algae because algal cells can use it immediately (Li, Wang, Cao, Wang, & Zheng, 2015). Removal of this dissolved phosphorus requires a modified bioretention system that includes amendments such as iron or aluminum oxides in the media mix (Stone, 2013). Water treatment residuals (WTR), available from water treatment plants that use alum for flocculation, often contain these iron or aluminum oxides, but their quality and availability can often be unpredictable (Barbu, Ballestero, & Ballestero, 2014). Zerovalent iron (ZVI) is a more consistent and uniform product than the WTR and can be purchased through many providers who will guarantee its initial quality.

Several recent studies have shown that ZVI-amended treatment systems can efficiently remove P from stormwater. Erickson et al. (February 23, 2010) performed a column study in which sand columns amended with 5%, 2%, and 0.3% iron filings demonstrated overall DP removals of 93%, 86%, and 35%, respectively when treating simulated runoff. These sand-ZVI treatment systems were also tested in the

field. Erickson and Gulliver (2010) tested four full-scale filtration trenches in Prior Lake, Minnesota amended with 7.2%, 10.7%, 11.3%, and 18.2% iron filings by weight. The majority of tests showed DP removals greater than 50% and the removals for all tests ranged from 29% to 90%. These studies clearly demonstrated the feasibility of using iron-amended systems in treating DP.

According to the EPA (Nutrient pollution policy and data, 2018), 54% of US states have no numerical criteria for nitrogen (N) or P loads entering receiving waters. 32% of the states have partial N and P criteria for lakes, 4% have statewide N and P criteria for lakes, 8% have statewide P criteria for lakes and rivers, and only Hawaii has statewide N and P criteria for lakes, rivers, and estuaries. Because many states lack criteria for phosphorus entering receiving waters, farmers may lack the incentive to implement phosphorus runoff treatment on their lands. However, many states have plans to add numerical criteria in the coming years. This means that farmers and landowners may be searching for simple but effective ways to limit their phosphorus contribution. A ZVI-modified bioretention system could be one option for people seeking simple solutions for treating phosphorus runoff from their fields.

1.2 Research Objectives

The first objective of this study was to examine the applicability of adding ZVI to a bioretention media mix in order to treat phosphorus from agricultural runoff. With high concentrations of ortho-P in this runoff, the lifespan of this ZVI becomes a concern. As the iron retains ortho-P and complexation of its adsorption sites continues, it becomes less effective over time (Erickson, Gulliver, & Weiss, 2007). This method of treating orthophosphate is only viable if landowners can expect high removal percentages for a year or more before amendment replacement. This study explores the P-removal ability of bioretention systems with varying percentages of ZVI and media depths.

The second objective was to create a ZVI- lifespan prediction tool that includes factors such as depth of media, percentage of ZVI, and influent ortho-P concentration. By including these factors, it may

be possible for those looking to implement a modified bioretention system to predict the performance of their system over time depending on the expected influent concentrations. The tool would be useful for both the design and maintenance of the system. By knowing the expected level of treatment over time, those wishing to implement a ZVI-enhanced system can plan for the costs and future maintenance of their system.

1.3 Description of Research

A column study was used to determine ortho-P removal efficiencies over time for different media mixes. Columns were packed with differing media depths and percentages of sand, loam, and ZVI in order to determine how these factors affect removal efficiencies using simulated runoff. Several columns contained no ZVI and were used as controls in the study.

A watershed to filter area ratio of 14.3:1 was used for each column with a yearly-simulated rainfall depth of 40 inches (102 cm). This watershed to filter area ratio was decreased from the desired 40:1 due to volume and time constraints with the existing column setup. Originally a 1.63 mg-P/L concentration of ortho-P (5 mg-PO_4/L) was selected based on the maximum concentrations found in other agricultural runoff studies. However, the decrease in watershed to filter area ratio meant that this ortho-P concentration would increase to 4.57 mg-P/L (14 mg-PO_4/L) when holding constant the yearly mass of ortho-P applied to the columns. This 4.57 mg/L concentration was still within the range of values reported in the agricultural runoff studies (see Figure 1).

The simulated yearly agricultural runoff was dispensed into each column with influent and effluent samples being collected. These samples were sent to a local analytical laboratory to determine their ortho-P concentrations. With this data, the columns' removal efficiencies could be calculated for each year of simulated runoff as well as the time at which the ZVI P-Removal capacity was exhausted. Simulated yearly runoff was run through each column until its removal efficiency was negligible.

Chapter 2: Literature Review

2.1 Phosphorus in Agricultural Runoff

2.1.1 Forms of Phosphorus

P loss from agricultural runoff can occur with both dissolved and sediment-bound P forms (Elrashidi et al. 2005). Elrashidi et al. (2005) define sediment-bound P as being P associated with minerals and organic matter, and it is not readily bioavailable like dissolved P. However, sediment-bound P can remain a long-term source of P for organisms like algae to use after undergoing chemical changes in anaerobic conditions (Sharpley, 1993). Ortho-P is often referred to using different names in research depending on the study, such as dissolved inorganic phosphorus (DIP), soluble reactive phosphorus (SRP) (Erickson, Gulliver, & Weiss, 2017), dissolved reactive phosphorus (DRP), dissolved phosphorus (DP) (Erickson, Gulliver, & Weiss, 2017), or bioavailable phosphorus (BAP) to name a few. Ortho-P is immediately available for organisms like algae to use without any prior chemical processes, meaning it is bioavailable (DePinto, Young, & Salisbury, 1986). This bioavailability means it is the most important P source for the growth of microalgae (Li, Wang, Cao, Wang, & Zheng, 2015), though dissolved organic P (DOP) has also been correlated to increased phytoplankton and bacterial growth in some natural waters (Rinker & Powell, 2006). DIP is often found in agricultural runoff due to inorganic fertilizer use while DOP content is attributable to organic fertilizers like poultry litter (Nichols, Edwards, & Edwards, 1994). According to Sharpley et al. (1992), roughly 10-40% of the total P (TP) runoff from agricultural land is dissolved. TP content is inclusive of all P forms, whether inorganic, organic, dissolved, sediment-bound, particulate, or bioavailable. BAP can also be found in particulate forms, and particulate P (PP) can comprise 20-80% of BAP in the TP content of agricultural runoff based on land use or management practices (Sharpley, Smith, Jones, Berg, & Coleman, 1992). As P can greatly range in size, researchers commonly distinguish between dissolved and particulate P by their ability to pass through a

0.45 µm filter (Hart, Quin, & Nguyen, 2004). Dissolved P will pass through this filter size while particulate P will not.

2.1.2 Phosphorus Runoff and Environmental Impacts

P enters receiving waters from agricultural lands mainly by way of surface runoff, though in some regions subsurface export of P is more likely to occur (Sharpley, et al., 2003). Overfertilization of croplands can often occur with high-value crops, but farmers have a cost incentive to not purchase or apply excess fertilizers (Sharpley, et al., 2003). Even when farmers supply crops with the proper amount of fertilizer for optimum production, there is still a likelihood that surface runoff and erosion from this land will introduce harmful levels of soluble and sediment P to receiving waters (Sharpley, et al., 2003). Irrigation on agricultural lands can also lead to significantly increased P loss by runoff and surface erosion, especially if furrow irrigation is implemented (Sharpley, et al., 2003). It is not uncommon for farmers to use furrow irrigation where the furrow sizes are too large, or slopes are too steep, which greatly increases the opportunity for soil erosion (Berg & Carter, 1980). This increased soil erosion is directly attributable to the volume and velocity of water (Stewart, Woolhiser, Wischmeier, Caro, & Frere, 1976). According to Stewart et al. (1976), mineral forms of P have very low solubility and easily adsorb to clays. Because of this, P content can then be directly transferred to receiving waters as P adsorbs to these fine clay particles that can stay suspended in the water as it moves (Stewart, Woolhiser, Wischmeier, Caro, & Frere, 1976). Stewart et al. (1976) describe sediment erosion as a significant method of nutrient transport. The threshold inorganic P concentration for accelerated algal growth is 0.02 mg/L in inorganic P (Sharpley, Daniels, Sims, & Pote, 1996), and this concentration is corroborated by a study of Chaohu Lake in China where this threshold was determined to be 0.019 mg-P/L of SRP (Yin, Lan, Zhao, & Bernhardt, 1992). Stewart et al. (1976) set the threshold even lower at

0.015 ppm of inorganic P. These low thresholds could be problematic as optimum soil P concentrations for plant growth are roughly one hundred times higher at 0.2 ppm in solution (Sharpley, et al., 2003).

Eutrophication is the primary environmental concern with respect to nutrient runoff from agricultural lands. Stewart et al. (1976) define eutrophication as excess plant growth caused by nutrient enrichment. Algae is the foremost concerning organism with respect to eutrophication (Aly & Faust, 1964). There are clear environmental and water treatment concerns associated with the rapid growth of algae. As algae die and begin to decay, this process causes a loss of dissolved oxygen in the water, which is essential to other plants and wildlife, and the production of toxins (Fry, 1969). In water treatment systems, increased algae can clog screens and cause taste and odor problems that inevitably become costlier to remedy (Borchardt, 1970).

2.1.3 Phosphorus Concentrations

There have been many studies exploring the P concentration in runoff coming from agricultural lands. However, it is often difficult to directly compare the results of these studies because they can have inherently different experimental setups, assumptions, soil types, sampling timelines, runoff volumes, or data analysis methods. For the purposes of this study and literature review, these differences were largely put aside to gain an understanding of the general range of ortho-P concentrations that could reasonably be expected for a variety agricultural watersheds. Table 1 shows a summary of mean and maximum reported P concentrations from various studies. The studies are very diverse in setup and data analysis, but the reported concentrations can help provide a range of acceptable influent values when testing adsorption methods for agricultural runoff. Ideally, all concentrations would have been explicitly reported as BAP or ortho-P, but DP, STP, and DRP can be synonymous with ortho-P as discussed in Section 2.1.1. Under the assumption that these tests were

measuring the same basic parameter, a range of realistic agricultural P concentrations could be evaluated.

Table 1: Mean and maximum P concentrations for agricultural runoff from previous studies

	P Concentration (mg/L)				
Year of Study	**Mean**	**Max**	**Measurement Type**	**Location**	**Source**
2005	0.194	0.738	DP	Nebraska	a
1989	0.215	0.392	STP	Oklahoma	b
2001	0.389	2.635	DRP	Lake Taihu, China	c
2005	0.72	1.37	PO_4-P	Florida	d
1980	0.695	1.512	PO_4-P	Iowa	e
1995	0.640	0.96	BAP	Oklahoma and Texas	f.1
1995	0.730	0.82	BAP	Oklahoma and Texas	f.2
1995	1.120	1.87	BAP	Oklahoma and Texas	f.3
1995	0.520	1.43	BAP	Oklahoma and Texas	f.4
2017	0.162	0.358	PO_4-P	Montana	g
1976	N/A	3.3	DIP	Massey U, New Zealand	h
1997	N/A	6.4	DRP	Whatawhata, New Zealand	i
1997	N/A	31.5	DRP	Waipawa, New Zealand	i
2001	N/A	6.5	DRP	Herefordshire, UK	j
2003	N/A	13.34	DRP	Changshu, China	k
2003	N/A	2.76	DRP	Anzhen, China	k
1997	N/A	1.296	DRP	Devon, UK	l

a. (Elrashidi, Mays, Harder, Shroeder, & Brakhage, 2005)

Cropland in Nebraska's Wagon Train watershed had runoff water tested for dissolved P concentrations and soil P tests were performed. These tests were used along with the NRCS Technique for estimating P losses from agricultural lands. The concentrations listed in Table 1 are predicted P concentrations based on this estimating technique. The maximum value in Table 1 corresponds to the crop with the highest estimated DP concentration. The mean value corresponds to the area-weighted average DP concentration across all croplands. Runoff samples were taken from ancillary streams running into the main stream feeding the Wagon

Train Lake. These ancillary streams carried direct runoff from the cropland. Crops included soybean, corn, wheat, sunflower, and alfalfa.

b. (Sharpley, Smith, & Menzel, 1989)

Soluble total P (STP) was measured over a decade from cropped watersheds in Oklahoma. The study area included wheat, peanuts, and grain from the El Reno, Fort Cobb, and Little Washita Basin watersheds. Crops had varying amounts of fertilizer applied ranging from 12 kg-P/ha/yr to 20 kg-P/ha/yr. The maximum value in Table 1 corresponds to the cropland with the highest mean annual flow-weighted STP concentration. The mean value corresponds to the average mean annual flow-weighted STP concentration across all cropped lands tested.

c. (Yan, Huang, Zhang, & Tang, 2001)

Six 2 x 5-meter plots were evaluated under simulated rainfall for DRP concentrations in runoff in China's Lake Taihu watershed. Various fertilizer applications were used among the small plots. Volume weighted mean concentrations of DRP for each plot were reported. Table 1 shows the average concentration across these plots and the maximum of the weighted mean concentrations.

d. (He, Zhang, Stoffella, Yang, & Banks, 2006)

Eleven sites in the Indian River area of South Florida were monitored over a year and included citrus groves and vegetable farms. Varying fertilizers were used on these separate plots of land. Water was collected at the drainage outlets for each site for PO_4-P analysis. Mean values of the quarterly median concentrations were reported in this study for each plot. Table 1 shows the average and maximum of these reported PO_4-P concentrations across all plots.

e. (Johnson & Baker, 1984)

Data were collected over two years for corn, soybean, and pasture fields in Iowa. The crops had varying amounts of applied fertilizer. Annual flow-weighted PO_4-P concentrations were reported

for each plot of land. Table 1 shows the average of these annual concentrations as well as their maximum reported value.

f. (Sharpley, Robinson, & Smith, 1995)

Croplands in Texas and Oklahoma were tested for BAP concentrations in their runoff. These croplands were in Bushland, TX, El Reno, OK, Ft. Cobb, OK, and Woodward, OK. Croplands included wheat, peanuts, and native grass and had varying fertilizer applications and amounts of till. Mean annual flow-weighted BAP concentrations for a four-year period were reported for each plot. The average and maximum BAP concentrations across all plots are shown in Table 1.

f.1 – Conventional till

f.2 – Reduced till

f.3 – No till

f.4 – Native grass

g. (Erickson, Gulliver, & Weiss, 2017)

A tile-drained plot of farmland (90% corn and soybean crops with 10% pasture) in Wright County, Montana was studied. This study is discussed further in Section 2.2.1.

h. (Sharpley & Syers, 1976)

Grazed and ungrazed plots of land were studied at Massey University in Australia. Some plots were fertilized with superphosphate and showed higher DIP concentrations in runoff. The maximum reported mean DIP concentration of surface runoff from these plots is shown in Table 1.

i. (Gillingham, et al., 1997)

DRP concentrations in runoff from microplots of crops were tested using simulated rainfall. These tests were conducted in Whatawhata and Waipawa, New Zealand. Mean DRP

concentrations at each test site were reported following fertilizer application. The maxima of these reported values are shown in Table 1.

j. (Withers, Clay, & Breeze, 2001)

Fifteen small, sloped experimental plots (32 sq. m each) were tested in the UK over a two-year period. The plots were cropped to cereals each year and fertilizers were applied. The plots were subject to natural rainfall. The average DRP concentration for the plots' collected runoff reached a maximum immediately after fertilizer was applied. This maximum value is shown in Table 1.

k. (Zhang, Cao, Wang, Zhang, & Wong, 2003)

Experimental plots (30 sq. m each) were tested at sites in Changshu and Anzhen China under wheat crops. Fertilizer was applied at varying rates at these sites. The maximum reported DRP concentrations reported at each of the sites during testing are shown in Table 1.

l. (Haygarth & Jarvis, 1997)

Grazed plots in Devon, UK were tested for DRP concentrations in runoff. They were fertilized with triple superphosphate at varying rates. Immediately following fertilizer application, the maximum DRP concentrations across these plots were recorded. The highest recorded DRP value across these plots is shown in Table 1.

The data for mean and max P concentrations in Table 1 is also displayed by year of study in Figure 1. The median values from each dataset are shown in the plot. Although the studies often had unique setups and data analyses, these median values could be used as a reasonable starting point when estimating bioavailable P concentrations from agricultural lands. These values could be useful for farmers who have no framework for what P concentrations may be exiting their land, or as previously mentioned, researchers could use these values as reasonable influent concentrations for treatment infrastructure testing.

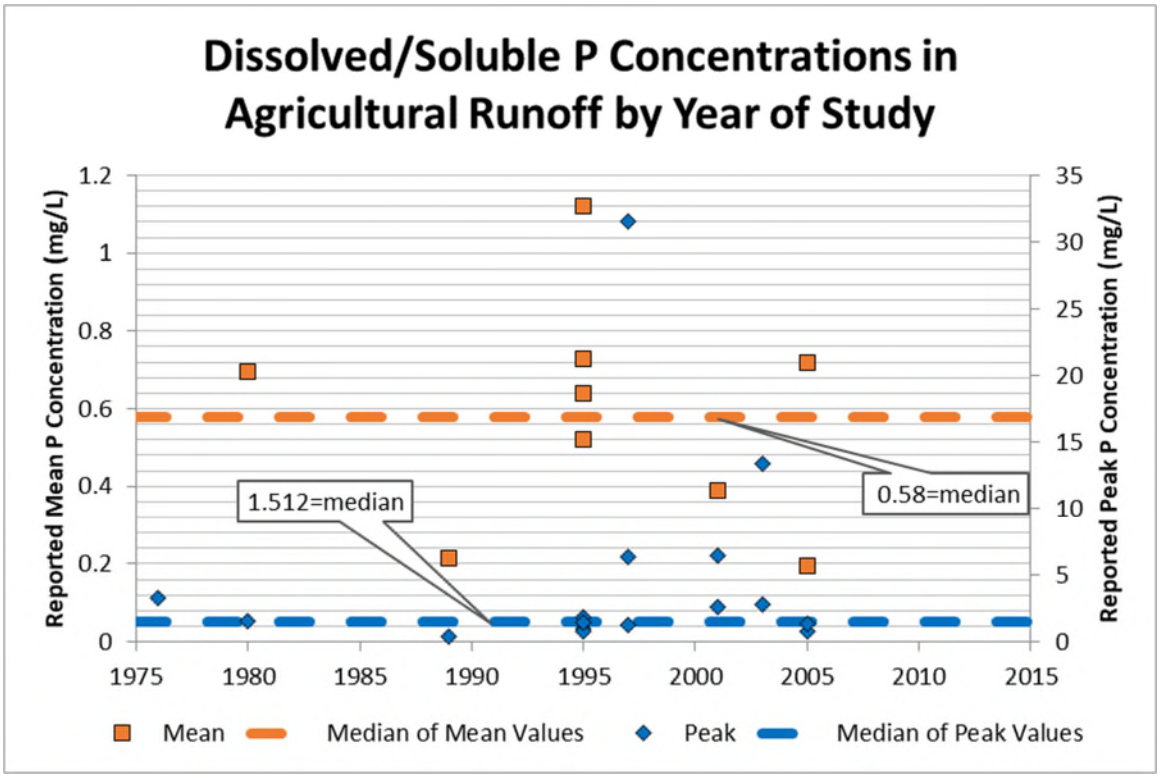

Figure 1: Mean and max reported P concentrations by year of study shown in Table 1

2.2 Dissolved P Adsorption by Iron

2.2.1 Summary of DP Removal Results from Iron-Enhanced Systems

There have been several studies exploring the removal of dissolved P from solution by using iron of various forms as an adsorbent. These studies varied from full-scale stormwater treatment testing in the field to column tests with simulated runoff. Some studies also included laboratory batch testing in which iron and phosphate were mixed in beakers to test adsorption with varying concentrations, pH, and temperatures.

Erickson et al. (2007) performed batch studies testing the adsorption capacity of chopped granular steel wool and other materials such as sand, limestone, aluminum oxide, etc. From the results of the batch study, it was determined that a filter with chopped granular steel mixed with C 33 sand could be a feasible solution for P removal from stormwater runoff. Based on this determination, column

tests were run with various percentages of steel wool mixed with sand. Synthetic stormwater, consisting of tap water mixed with KH_2PO_4, was used at varying concentrations throughout experimentation. These concentrations ranged from 0.1 to 0.8 mg PO_4-P/L. The media depth in the columns was roughly 46 cm and the diameter of each column was 5.08 cm. Columns enhanced with steel wool had depths of stormwater treated ranging from 40 to 90 m by the end of testing. These columns removed between 25 and 99% of the dissolved P during testing and significantly outperformed the sand-only control column. The total mass of P retained for the columns ranged from roughly 19 to 34 mg.

The presentation and proceedings paper by Erickson et al. (February 23, 2010) at the 2010 IUWMC Conference state that column studies were performed with C 33 sand mixed with 5%, 2%, and 0.3% iron filings by weight. Synthetic stormwater of varying DP concentration was applied to the columns at concentrations between 0.25 and 0.55 mg PO_4-P/L with a flow volume weighted mean of 0.340 mg PO_4-P/L. Methods were performed in the same manner as those outlined in Erickson et al. (2007) and columns contained 40 cm of sand mixed with the varying percentages of iron filings. After 20 m of treated depth, the 5% iron filings mix yielded 13 times more cumulative phosphorus retained than the sand control while the 0.3% iron filings mix outperformed sand by a factor of three. The total water depth treated ranged from roughly 50 m to 85 m for the iron-enhanced columns while the cumulative mass of P retained ranged from roughly 0.01 to 0.06 g. It was determined that the short-term P retention for iron-enhanced columns was similar, regardless of iron percentage. Though similar in the short-term, it was determined that higher percentages of iron would provide enhanced P retention capacity with long-term treatment, meaning greater than 50 m of depth treated. Columns with higher iron percentages were not as efficient as those with lower percentages when considering the mass of P retained per mass of iron. This trend was also found in the Erickson et al. (2007) study when comparing columns of varying steel wool percentages. In the end, the 5% iron filings yielded an average of 93% P removal by mass while the 2% and 0.3% iron filings yielded 86% and 35%, respectively. The sand control

column had negligible long-term removal capacity. It was estimated that systems with 5% iron filings could capture 80% of DP for more than thirty years while 2% iron filings could lead to roughly fifteen years of 80% DP capture. It was estimated that 0.3% iron filings would not perform nearly as well with only a 30% estimated DP capture after five years. All of these estimates were based on a hydraulic loading rate of 5.6 m/year.

Erickson and Gulliver (2010) reported the installation and testing of four full-scale sand filtration trenches that were enhanced with iron filings. These trenches were constructed in Prior Lake, MN. The four trenches were constructed with approximately 7.2%, 10.7%, 11.3%, and 18.2% iron filings by weight. The 7.2% and 10.7% trenches were approximately 40 ft by 5 ft by 2 ft deep with a 15 ac drainage area while the 11.3% and 18.2% trenches were approximately 36 ft by 5 ft by 1.5 ft deep. These trenches were exposed to natural rainfall events as well as synthetic stormwater testing provided by nearby fire hydrants. Five runoff events were tested for influent and effluent P concentrations where two of these were synthetic. From these five events, the DP removal efficiency ranged from 29% to 90%, but many of the effluent concentrations were below the 0.01 mg-P/L detection limit. The removal efficiency for most tests was greater than 50%, and as the influent concentrations increased, the removal efficiency increased in-turn. Based on typical P concentrations in stormwater, these tests showed that 85% to 90% of the DP could reasonably be captured by these systems. The average filtration rates in the trenches ranged from 3.6 to 6.4 in/h during the testing.

Reddy et al. (2014) performed batch studies to test the ability of iron filings to remove phosphate from solution. Concentrations in the P solution ranged from 0.25 to 5 mg-TP/L while the dry mass of iron filings used was 10 g. All testing was conducted over a 24-hour period. P-removal rates for the tests ranged from 73 to 100%, and it was found that increases in initial phosphate concentration caused a general reduction in removal efficiency. It was also found that oxidizing conditions prevailed at

low phosphate concentrations while reducing conditions were observed at the higher phosphate concentrations.

Chiu et al. (2016) performed a column study using sand-ZVI columns. The columns were operated in up-flow conditions at a rate of 1 mL/min. The sand-ZVI mix contained 5% ZVI by volume and was wet-packed. Influent concentrations of PO_4-P included 1.6 ppm, 3.2 ppm, 8 ppm, and 16 ppm. Testing was conducted such that a pulse of one pore volume of each concentration would run through the column before switching the influent back to a blank solution. It was determined that the sand control column did not show any P removal potential while the ZVI-enhanced column showed removals near 100% for the 1.6 ppm influent. Chiu et al. (2016) concluded that adding ZVI to bioretention systems could be beneficial, especially when considering the comparatively low influent P concentrations in expected the field.

Erickson et al. (2017) reported the results from an iron enhanced sand filter (IESF) study. This study measured the phosphate and TP retention of an IESF treating tile drainage from agricultural lands in Wright County, MT. The IESF treated tile drainage from 7.45 ha of farmland composed of 90% corn and soybean crops with 10% pasture. The IESF was approximately 6.1 m by 15.2 m by 30 cm thick with pea gravel and an underdrain system below. It contained C-33 sand with 6% iron filings by weight and was lined with an impermeable liner so that water could only enter from the surface. Because the media was rarely submerged from downstream, oxygen could readily interact with the iron through the underdrains and the surface. Throughout the testing of the system, all events showed a positive retention of TP. Influent concentrations of TP for 20 events were generally between 0.2 and 0.8 mg/L while almost half of the events had effluent values less than 0.1 mg/L. Influent phosphate concentrations ranged from 0.018 to 0.358 mg/L while the effluent concentrations ranged from 0.008 to 0.127 mg/L. The system produced an average phosphate load reduction of roughly 64%.

Barbu et al. (2014) performed a column study with varying percentages of ZVI mixed with bioretention media from the UNH Stormwater Center. This bioretention mix consisted of 60% sand, 20% wood chips, 10% loam, and 10% leaf and yard waste containing low amounts of P. Ten simulated storms of varying depths were run through the columns with influent concentrations of roughly 0.9 mg PO_4/L (0.29 mg PO_4-P/L). One column contained 24 inches of media with 3% ZVI. The simulated watershed to filter area ratio for this column was 80:1 and the cumulative depth of the simulated storms was 8.7 inches. This column was shown to remove 98.6% ortho-P after all storms were simulated. Another column was subjected to the same hydraulic loading and contained 24 inches of media with 6% ZVI. This column removed 98.8% ortho-P after all storms were simulated. A third column contained 12 inches of media with 3% ZVI. The simulated watershed to filter area ration for this column was 25:1 with the same cumulative depth of 8.7 inches after all storms were simulated. This column removed 99.0% ortho-P after all storms were simulated. A column containing 12 inches of media with 0.5% ZVI was also tested under the 25:1 watershed to filter area ratio loading with an 8.7 in cumulative storm depth. This column was shown to remove 93.5% ortho-P after simulating all storms.

2.2.2 Iron-Phosphate Adsorption Mechanism

While particulate or sediment-bound P can be removed from stormwater using sedimentation or filtration, DP removal requires a chemical process (Jenkins, Ferguson, & Menar, 1971). Common adsorbents for removing DP include aluminum and iron (Erickson, Gulliver, Weiss, & Huser, February 23, 2010). As iron encounters moisture and oxygen, it oxidizes and forms rust. When the iron rusts, it becomes free to remove P from solution by one or more processes. The iron and P can form precipitates, P can be adsorbed electrostatically, or it can be removed from solution by ligand exchange (Allred & Racharaks, 2014). According to Erickson et al. (2007), the P removal capacity of iron increases as it rusts. This conclusion seems to be consistent across the many studies reviewed.

2.2.3 Factors Influencing P-Sorption by Iron

pH:

Iron-P adsorption is dependent on pH according to Erickson et al. (February 23, 2010). P adsorption to iron is best in acidic conditions, but the adsorption rate can still approach 50% at a pH of 10 (Stumm & Morgan, 1981). Almeelbi & Bezbaruah (2012) state that at higher pH, phosphate desorption is more likely occur, but at lower pH, phosphate adsorption is dominant. They also state that when the pH is less than 7.7 for nano-ZVI (NZVI), the NZVI surface is positively charged which makes it readily available for phosphate anion adsorption. Sellner (2016) performed a column study using steel byproducts to treat P-enriched water. In this study, little correlation was found in relation to pH and P adsorption. The pH range tested was from pH 5 to pH 9 in this study. These results indicate that there may be more than one mechanism affecting P adsorption based on the pH.

Temperature:

Almeelbi & Bezbaruah (2012) performed NZVI-phosphate batch testing under various temperatures. The experiments were run at 4, 22, and 60°C, and it was found that the phosphate removal rates increased with higher temperatures. But after roughly 30 minutes, this discrepancy had diminished, and the removal rates were not found to be significantly different.

Contact time:

Erickson et al. (2007) state that increased contact time between DP in the water and iron allows for better phosphorus removals. Therefore, as hydraulic conductivity in the soil decreases, the increased contact time should yield higher removals. In the Sellner (2016) study, it was concluded that longer empty bed contact time increased P removal efficiencies of the columns enhanced with steel byproducts.

Iron Percentage:

The Erickson et al. (2007) and Erickson et al. (February 23, 2010) studies showed that increasing the percentage of iron-based amendment in the columns led to higher overall P removal efficiencies. Although the short-term efficiencies were somewhat similar between the columns of varying percentages, it was clear that the columns with higher iron percentages would have significantly better long-term removals.

Iron PSD:

The Almeelbi & Bezbaruah (2012) study showed a correlation between particle size and P adsorption. When comparing 16 nm NZVI particles to 10 μm micro-ZVI (MZVI) particles in batch testing, it was shown that MZVI only removed 23% P from the 5 mg PO_4-P/L solution in 30 min while NZVI was able to remove 96%. The surface areas of MZVI and NZVI were kept equal by using 5 g/L MZVI and 400 mg/L MZVI during testing. The much smaller concentration of NZVI outperformed the MZVI even though the surface areas were theoretically equal. Setting aside the assumption of equal surface areas, it was clear that the smaller iron particles significantly outperformed the larger particles, even with a mass disadvantage.

Competing chemicals:

In a four-year study involving tile drained cropland, it was found by Baker et al. (1974) that variable concentrations of nitrate, phosphorus, and sulfate could be found in the drainage. Sellner (2016) reported that P adsorption by iron was not affected by the presence of high levels of nitrate (50 mg NO_3-N/L) or sulfate (500 mg SO_4/L). Dissolved organic carbon (DOC) derived from humic acid and woodchip leaching (both at 50 mg/L) caused a reduction in removal capacity of 10% and 17%, respectively. These results indicate that DOC could negatively affect P removal using iron, though there is still significant P removal capacity in the presence of DOC.

2.3 Isotherm Models for P-Adsorption

2.3.1 Freundlich and Langmuir Isotherms and Removal Efficiency Analysis

Reddy et al. (2014) showed that Langmuir and Freundlich isotherm models can describe P adsorption to iron filings and that based on the maximum adsorption capacity of the iron, one could estimate the volume of stormwater that can be treated given the iron content in a system. The Freundlich and Langmuir isotherms are often applied as empirical representations of experimental data, but this does not mean that any underlying physical models used to derive these isotherms directly applies to this experimental data (LeVan & Vermeulen, 1981). The Freundlich isotherm models cumulative adsorption onto a wide variety of sites in a system while the Langmuir isotherm models adsorption onto only one type of site (Benjamin, 2002). Stone (2013) stated that, in essence, the Freundlich isotherm is based on multilayer adsorption and the Langmuir isotherm assumes single layer adsorption. The Freundlich and Langmuir isotherm equations are shown below (Stone, 2013).

Freundlich:

$$q_e = \frac{V(C_0 - C_e)}{M_{ad}} \qquad \text{Equation 1}$$

$$q_e = KC_e^{1/n} \qquad \text{Equation 2}$$

Where:

q_e = Mass of adsorbate retained per unit weight of adsorbent (mg/g)

V = Known sample volume (L)

C_0 = Influent concentration (mg/L)

C_e = Effluent concentration (mg/L)

M_{ad} = Mass of adsorbent (g)

K = Freundlich adsorption capacity constant $(mg/g)(L/mg)^{-1/n}$

n = Freundlich adsorption intensity constant (unitless)

The Freundlich equation can also be linearized as follows:

$$log(q_e) = log(K) + \frac{1}{n} log(C_e)$$ Equation 3

Langmuir:

$$q_e = \frac{q_m K_L C_e}{1 + K_L C_e}$$ Equation 4

Where:

q_e = Mass of adsorbate retained per unit weight of adsorbent (mg/g) (See Equation 1)

C_e = Effluent concentration (mg/L)

q_m = Maximum adsorbent-phase concentration when surface sites are saturated (mg/g)

K_L = Langmuir adsorption constant (L/mg)

The Langmuir equation can also be linearized as follows:

$$\frac{C_e}{q_e} = \frac{1}{q_m K_L} + \frac{C_e}{q_m}$$ Equation 5

Although it is still common to estimate the adjustable parameters (i.e. q_m, K_L, K, and n) for the Freundlich and Langmuir isotherms by linear regression, the better way to estimate these parameters is by nonlinear least squares (NLLS) (Kinniburgh, 1986). When the isotherms are linearized, the original error distribution is also transformed (Kinniburgh, 1986). Kinneburgh (1986) also states that root mean squared error (RMSE) is the principal criterion for goodness of fit among isotherms. He says that RMSE can be used as a direct comparison between different isotherms for the same set of data. The equation for RMSE is expressed as follows:

$$RMSE = \sqrt{\frac{1}{n}\sum_{i=1}^{n}(M_i - O_i)^2}$$ Equation 6

Where:

n = number differences

M = Observed value

O = Value obtained from model

When comparing the performances of different treatment systems, it is often useful to calculate their removal efficiencies (RE). Removal efficiency can be calculated as follows (Stone, 2013):

$$\%RE = \left(1 - \frac{C_e}{C_0}\right) x100$$ Equation 7

Where:

C_0 = Influent concentration (mg/L)

C_e = Effluent concentration (mg/L)

Chapter 3: Methods and Materials

3.1 Column Contents

3-foot (91.4 cm) long, clear, 1.5-inch (3.81 cm) diameter columns were packed with varying amounts of sand, loam, and ZVI. Based on the UNHSC bioretention media design (UNHSC, 2017), it was determined that each column would contain 70% sand and 30% loam by volume with the exception of the sand-only control column. These percentages roughly coincide with typical UNHSC bioretention media mixes (University of New Hampshire Stormwater Center 2012 Biennial Report, 2012)[1]. The relatively high percentage of sand allows for higher infiltration rates and therefore smaller system footprints. The loam percentage in columns with ZVI was slightly lower than 30% to account for the ZVI volume. The media composition of each column is shown in Table 2. In addition to this media, each column contained a 1-2-inch (2.5-5.1 cm) layer of crushed stone on the top and bottom of the media mixture (Barbu, Ballestero, & Ballestero, 2014). The bottom layer of gravel allowed for drainage of the effluent while blocking media from exiting the bottom of each column. The top layer of gravel protected the media from the impact of water dropping from the dispensers above.

[1] Please note: Most citations throughout Chapter 3 are used to indicate procedural similarities to the cited source.

Table 2: Summary of column media compositions

Column Number	Media Depth (in), (cm)	Sand Percentage	Loam Percentage	ZVI Percentage	ZVI Mass (g)
1	12, 30.5	70%	30%	0%	0
2	6, 15.2	70%	30%	0%	0
3	6, 15.2	100%	0%	0%	0
4	12, 30.5	70%	29.5%	0.5%	3.2
5	12, 30.5	70%	29%	1%	6.3
6	12, 30.5	70%	27%	3%	19.0
7	6, 15.2	70%	29.5%	0.5%	1.6
8	6, 15.2	70%	29%	1%	3.2
9	6, 15.2	70%	27%	3%	9.5

The sand used in each column was Quikrete Tubesand with a particle size distribution shown in Figure 2. ASTM D 422-63 methods were used for this analysis. Particle size distributions were also recorded for the smaller batches of sand used for each column. These particle size distributions are shown in Figures 131 through 135 in Appendix C.

The loam used in each column was collected from a UNH bioretention system during its construction. ASTM D 422-63 methods were used to find the particle size distribution of this loam, shown in Figure 2. The ash content of 94.8% and organic matter content 5.2% of the loam were found using ASTM D 2974-00 methods. The particle size distributions from the smaller batches of loam for each column are shown in Figures 136 through 138 in Appendix C. The fine particles from each batch were removed in order to increase the infiltration rates of the columns.

The ZVI used in the columns had the particle size distribution shown in Figure 2. It was bought from The Science Company (Cat. No. 1381) and produced in India. Figure 3 displays the size and consistency of ZVI particles used in the columns' media mixes. This ZVI was able to show obvious rusting after only one cycle of wetting and drying in a beaker as shown in Figure 4.

When comparing the particle size distributions of the media components in Figure 2, the ZVI was entirely finer than the sand. The ZVI was also largely finer than the loam in the columns, though there was a small percentage of loam that was finer or at least as fine as the ZVI. This finer portion of the loam would help to keep the ZVI from washing through the column. Though finer ZVI has been shown to yield better removals as discussed in Section 2.2.3, it is important to ensure that the size distributions of media allow for proper infiltration rates while protecting against ZVI loss in the effluent. If a finer ZVI were chosen, there would be more opportunity for it to be washed through the sand and loam.

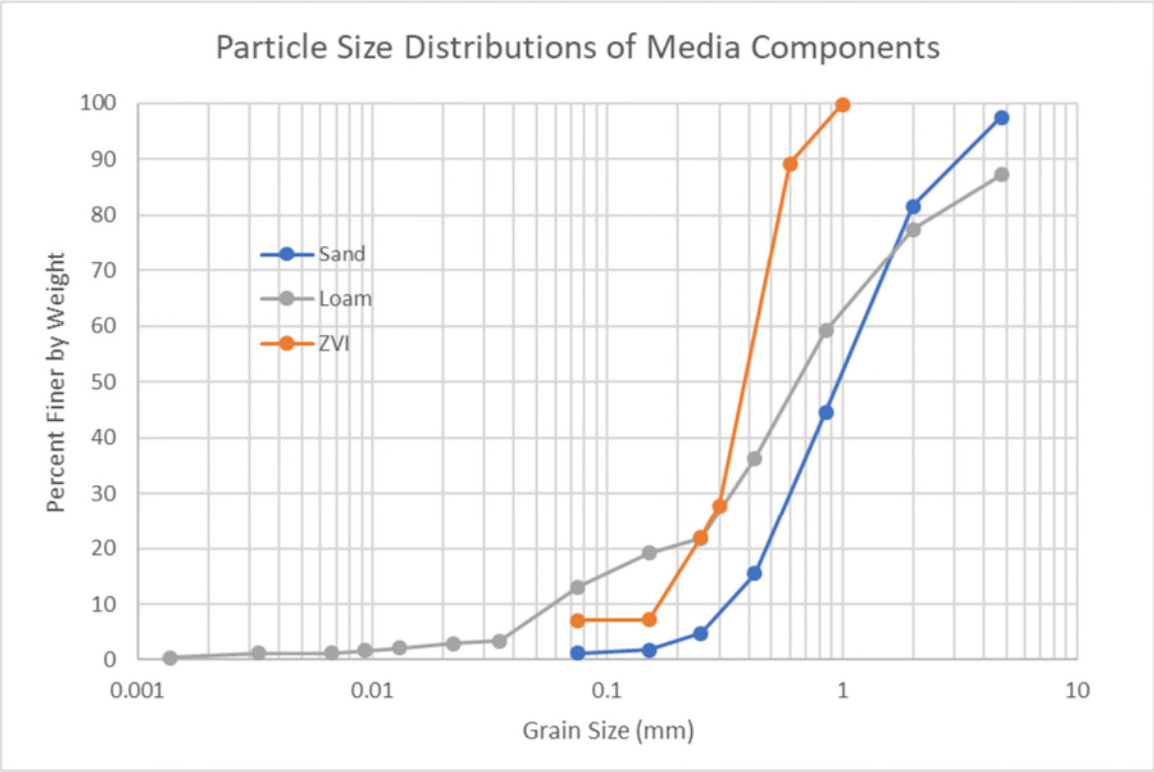

Figure 2: Particle size distributions for Tubesand, loam, and ZVI

Figure 3: ZVI used in media mixes

Figure 4: ZVI rust show after one wetting and drying cycle

3.2 Column Construction and Setup

Column construction and setup closely followed procedures outlined by Barbu et al. (2014). Columns were constructed using 3-foot (91.4 cm) long clear, PVC pipe sections with inner diameters (ID) of 1.5 inches (3.81 cm). A rubber cap with a hole in it was placed on the bottom of each column. The hole would allow for effluent collection under the columns. A layer of crushed stone was then placed on top of the rubber cap. The sand, loam, and ZVI were mixed together thoroughly with a spoon and then the mix was dropped into the column by the spoonful. The media was added in 6-inch (15.2 cm) lifts, with light rodding for compaction. After the desired depth of media had been established, a final layer of crushed stone was placed on top of the media.

An overflow bypass hole was drilled near the top of each column, and a small tube would lead to a collection jar. This would allow for overflowing water to be collected and later documented when flows from the dispensers were set too high. However, flows were controlled during testing such that these overflow tubes were never utilized.

Above each column was placed a 5-gallon carboy with a spigot that would drip simulated stormwater onto the soil media. 5-gallon buckets would collect the effluent below each column during periods when the effluent was not to be analyzed for phosphorus concentrations (Figure 5). ISCO containers with funnels would collect effluent below the columns when the last liter of simulated stormwater was running through the columns (Figure 6). This last liter of effluent would reveal the columns' phosphate removals at the end of each simulated year of stormwater treatment.

Figure 5: Column operation with 5-gallon buckets

Figure 6: Column operation with ISCO containers

3.3 Hydraulic and Phosphorus Loading

With each column representing a stormwater management system for a certain watershed, a yearly hydraulic loading was determined to be 46.3 L (12.2 gal). This volume was based on a watershed to filter ratio of 40:1 (within the range for biorentention systems tested at UNH), the 1.5-inch (3.81 cm) inside diameter of each column, and 40 inches (102 cm) yearly precipitation. However, this volume was decreased by a factor of 2.8 to be 16.6 L (4.4 gal) so that the simulated yearly runoff could be contained in a 5-gallon carboy. The hydraulic loading rate for each column was roughly 47.8 ft/year. This smaller volume would also significantly decrease the duration of experiments. It was determined that an influent concentration of 1.63 mg-P/L (5 mg- PO_4/L) would be realistic for agricultural runoff. With the decrease in yearly volume to 16.6 L (4.4 gal), this influent concentration increased to 4.57 mg-P/L (14 mg-PO_4/L) while maintaining the original P-mass that would have passed through each column under the original conditions. The simulated stormwater was composed of tap water and KH_2PO_4 standard solution (Erickson, 2007).

3.4 Column Operations and Sampling

For each simulated year of runoff, a batch of 14 mg-PO_4/L solution was mixed in a 55-gallon tank sitting on a scale with 0.1 kg (0.2 lb) resolution. The appropriate amount of KH_2PO_4 standard solution would be added to the tank and then the tank would be filled until the desired volume of 166 L (43.9 gal) was reached in the tank. This volume was achieved when the mass on the scale reached the appropriate value. The tank was then stirred thoroughly with an aluminum paddle to ensure proper mixing of the phosphate throughout. Each column's 5-gallon carboy was then filled to a volume of 15.6 L (4.1 gal) including an extra carboy that would be used for influent values data analysis. This extra carboy would not drain into a column, but only into collection containers. After each column had drained 15.6 L (4.1 gal) into the 5-gallon collection buckets seen in Figure 5, 10 L (2.6 gal) of 14 mg-PO_4/L

solution were mixed in a separate bucket and 1 L (0.26 gal) was poured into each carboy. These final 1 L (0.26 gal) volumes going through each column would be collected in the ISCO containers shown in Figure 6 and were sent to the Absolute Resource Associates lab in Portsmouth, NH for phosphate analysis. This would conclude the testing for one simulated year of agricultural runoff. Columns would then rest for roughly 1 day before testing of the next simulated year of runoff began. The only exception to this procedure was that the first simulated year of testing was split into four smaller testing periods because of the large anticipated loss of removal efficiency within the first year. This entire process would continue until it was determined that the phosphate removal percentage for each column was zero.

Because of the large volume of water running through each column, it was imperative that they have high infiltration rates. These high infiltration rates would allow for the duration of testing to decrease, though this would affect the contact time between the phosphate and ZVI. When drainage durations were unsatisfactory, the media within specific columns were taken out, mixed thoroughly with a spoon, and then put back in. Care was taken to ensure that iron particles were not lost during these steps. The media mixing helped to break up layers of finer particles that had made the media less permeable.

3.5 Hydraulic Conductivity Testing

Hydraulic conductivity testing was performed on Columns 1 through 3 prior to running any simulated stormwater testing. These columns were chosen because they did not contain any ZVI. Introduction of water to media containing ZVI would begin the rusting process and could have skewed the removal efficiencies once actual simulated stormwater testing began. All of the columns, including Columns 1 through 3, would undergo hydraulic conductivity testing after all simulated stormwater testing was complete. The comparison of hydraulic conductivity for Columns 1 through 3 before and after this testing would have demonstrated any changes due to compaction. However, because the

media in Columns 1 and 2 were taken out of the column and remixed, a fair comparison could not be made.

Hydraulic conductivity testing followed the same procedure for each column. The columns were backfilled through the bottom outlet cap with tap water. This minimized any bubbles from being trapped in the soil media during testing. Once the columns were saturated, the outlet tube was set at an elevation above the soil media. A water dispenser then directed water at constant flowrate into the column. The water dispenser above the column would then run so that the water level above the media remained constant (constant head permeameter). Water was collected at the tube outlet for a known amount of time to determine the total column discharge. Three different flowrates were performed on each column with the tube outlet at a constant elevation and the water level at three distinct elevations. Hydraulic conductivity results are shown in Appendix C.

Chapter 4: Results and Discussion

4.1 Percent Removal Results

Although a single target influent P concentration was set, results from the ARA laboratory showed that the concentrations fluctuated for the simulated years. Because of these fluctuations, calculations of percent removal over time were performed to standardize the data and facilitate performance comparisons. Time series data for percent ortho-P removal is shown for each column in Figures 7 through 15. Figures 7 through 9 show data for each control column containing no ZVI (Columns 1, 2, and 3). Column 1 showed significant ortho-P removal, or adsorption, within the first year of simulated runoff even though it contained no ZVI. This adsorption capacity could be connected to clay particles in the loam (Stewart, Woolhiser, Wischmeier, Caro, & Frere, 1976). However, the trend showed a sharp decline in the first year and dropped below 15% for the second year. This sharp decline indicates it has a very limited adsorption capacity. Column 2 showed a similar trend to Column 1, but its removals were roughly 30% lower for each data point within the first year. Because the two columns had the same media mix, this discrepancy in performance indicates that the depth of soil media played a role in ortho-P removal efficiency. The simulated runoff would likely have contact with more adsorption sites when passing through a thicker layer of media giving Column 1 the clear removal advantage over Column 2. Column 3 consistently showed no removal capacity across all simulated years, which was to be expected due to the inert nature of sand. Erickson et al. (February 23, 2010) reported similar findings. With the only difference between Columns 2 and 3 being the percentage of loam in Column 2, it is theorized that there is ortho-P adsorption capacity within the loam and not sand. Assuming a column with 12 inches of sand would produce the same results as Column 3, there would be an even larger discrepancy between the removal efficiencies when compared to Column 1.

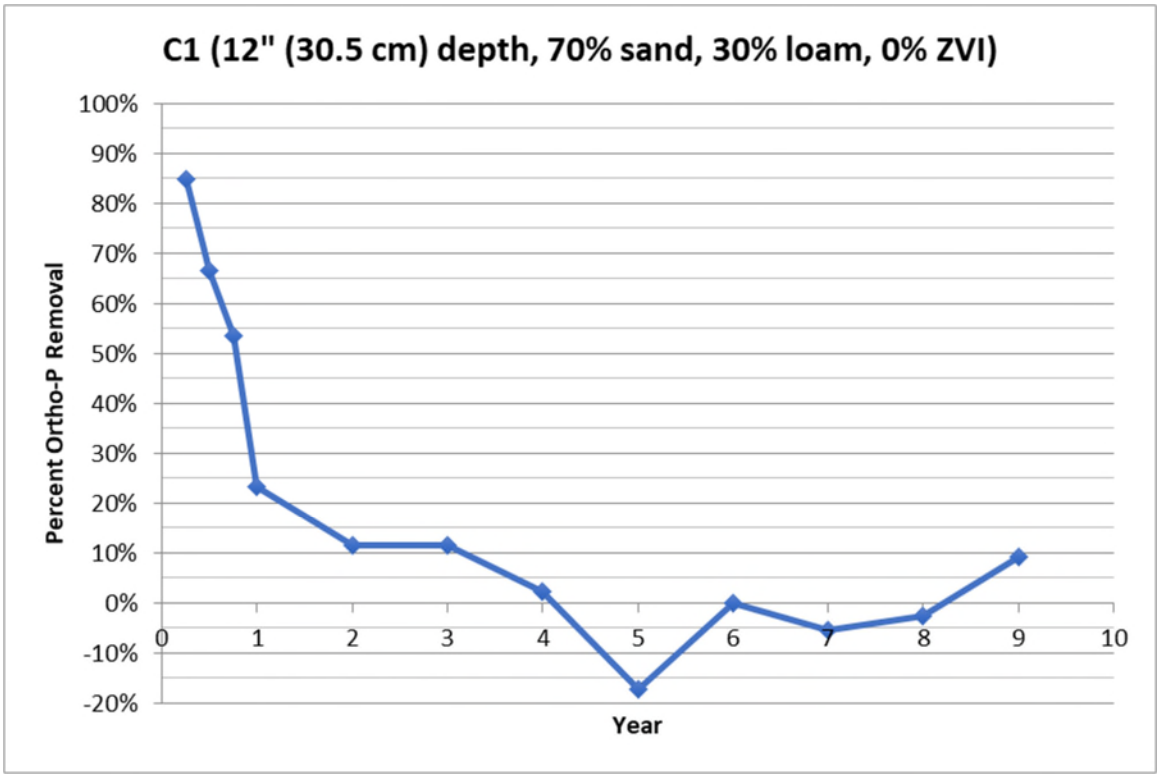

Figure 7: Column 1 percent ortho-P removal results based on simulated year

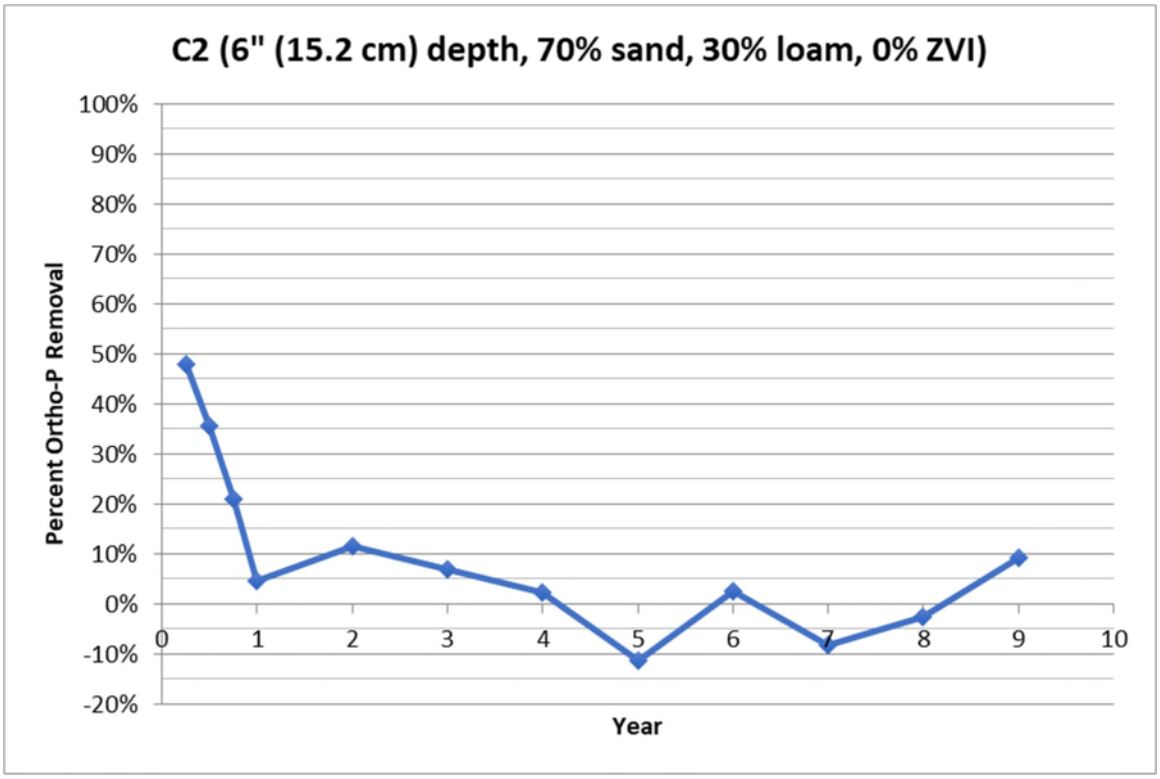

Figure 8: Column 2 percent ortho-P removal results based on simulated year

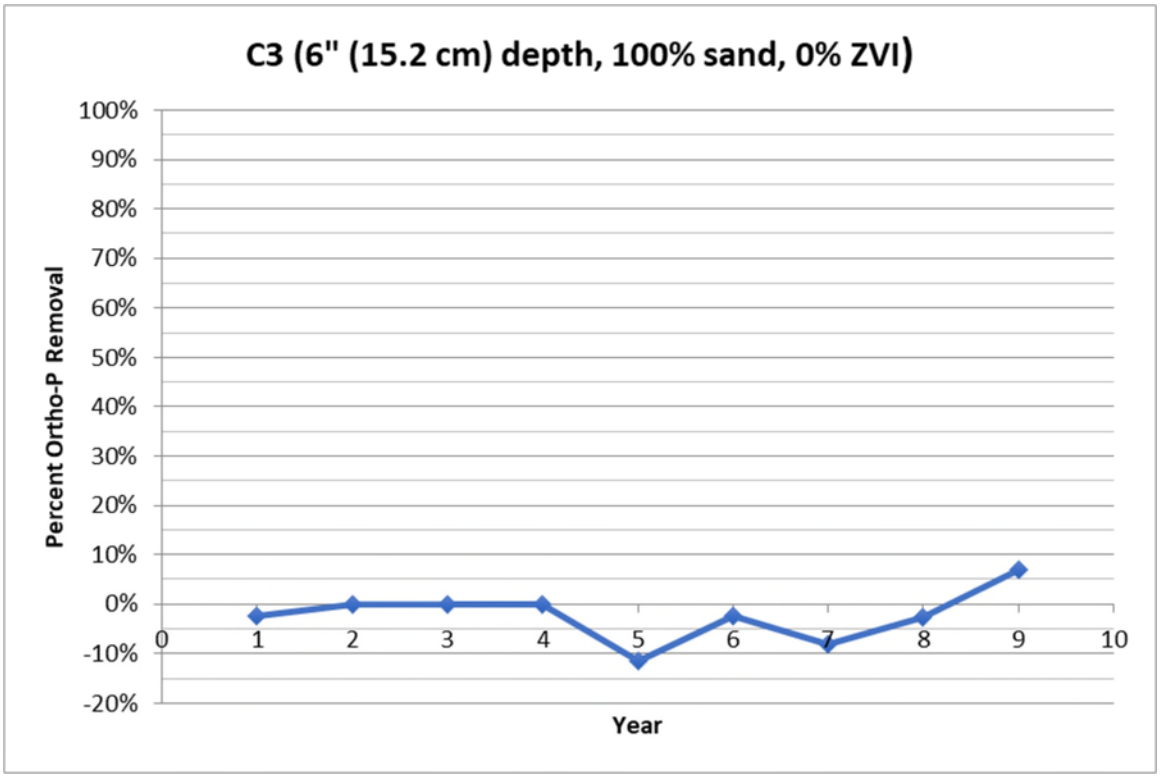

Figure 9: Column 3 percent ortho-P removal results based on simulated year

Figures 10 through 12 show data for each column containing varying amounts of ZVI but the same 12-inch depth of media. Each figure displays the raw data values calculated simply by comparing the effluent ortho-P concentrations to the influent concentrations. These figures also display values calculated by subtracting the percent removal values from Column 1 from the raw values for each column. The “Control Subtracted” lines are meant to roughly display the percent ortho-P removal that could be attributed to ZVI adsorption and not the combined ZVI-loam adsorption. However, these lines could be slightly misleading because they do not take into account that adsorption to ZVI and loam could be, and likely is, occurring at the same time. They indicate that the ZVI starts removing ortho-P after the loam’s adsorption capacity is expended. If adsorption to ZVI and loam were occurring simultaneously, this could mean that the adsorption capacity of the loam might be extended in the testing process due to the shared load instead of being mostly limited to the first year as the control

columns showed. But for simplicity of comparison, it would be easiest to assume for now that the ZVI takes on the load of ortho-P adsorption after the capacity of loam in the control columns has been expended. The “Control Subtracted” lines are useful for showing when the ZVI percentage in the media becomes an important factor in the removal of ortho-P from simulated runoff. In Figure 10 the “Control Subtracted” line starts at a low percentage and increases rapidly as the adsorption capacity of the loam decreases. As this line hits its peak just before Year 1, it indicates the point where the ZVI content becomes significant in the ortho-P removal process. Before this point, the loam itself could achieve a substantial portion of the removal without any assistance from the ZVI. After this point, the line begins to follow the “Raw Values” trend more closely. Figures 11 and 12 also show that the “Control Subtracted” line increases in the early years but then conforms to the “Raw Values” trend. The ZVI is doing the majority of the ortho-P adsorption when the trends are matching. Figures 10 through 12 all show that the ZVI can be responsible for most of the adsorption after Year 1.

From the raw data values in Figure 10, it is clear that media in Column 4 is removing a significant amount of ortho-P within the first year. These high removals were short-lived, however, and dramatically decreased from the first year on. There are several simulated years for Column 4 that display negative removals, meaning that the ortho-P concentrations in the effluent were higher than those for the influent. Every column displayed these negative removals during at least one of the simulated years. Several factors could have caused these negative values. It is possible that phosphate ions previously adsorbed to the soil media were desorbing due to variable flows or adverse pH conditions. However, when examining the percent removal trends in Years 6-9 versus trends in pH data from Table 19 (Appendix A), there seems to be no correlation. The erratic behavior of these columns in Years 5-9 is, therefore, more likely caused by variable flows or other unknown factors.

Column 5 followed a very similar trend to Column 4 as shown in Figure 11 with good removals at the beginning followed by a steep decline. Of all nine columns, Column 6 proved to be the most

effective in terms of maintaining high removal percentages for the longest amount of time. This high performance is likely because it contained the most ZVI mass. Figure 12 shows that the removals were above ninety percent for the first three years, and then the decline in performance was much more gradual than the other columns. Testing concluded for all columns except Column 6 at Year 9 due to the indication that their adsorption capacity had been expended, but testing continued for Column 6 until Year 20 when there was an indication that its capacity was exhausted as well.

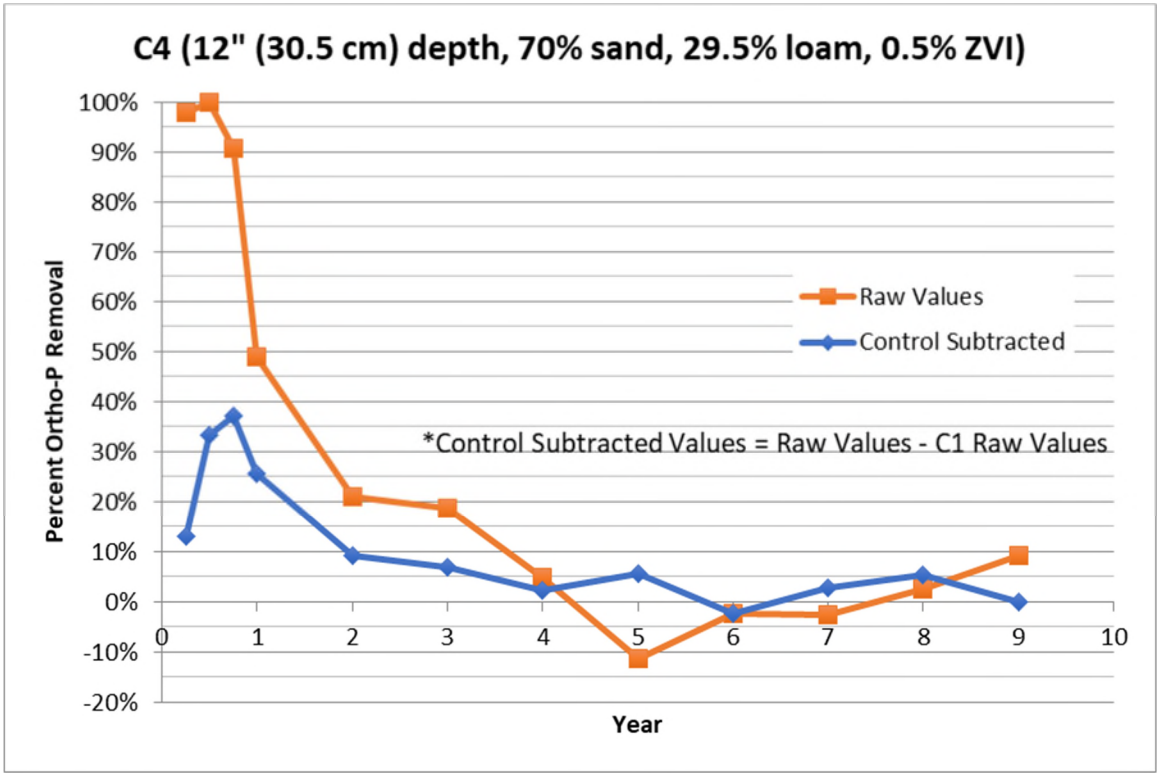

Figure 10: Column 4 percent ortho-P removal results based on simulated year

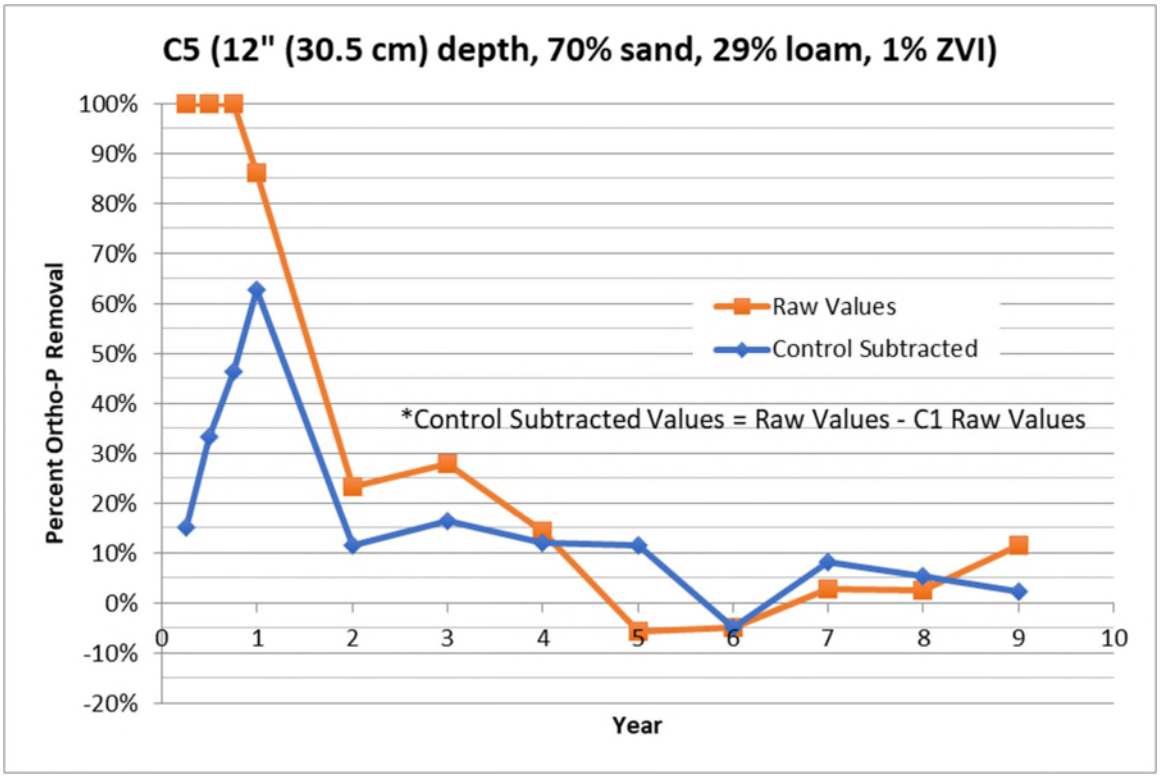

Figure 11: Column 5 percent ortho-P removal results based on simulated year

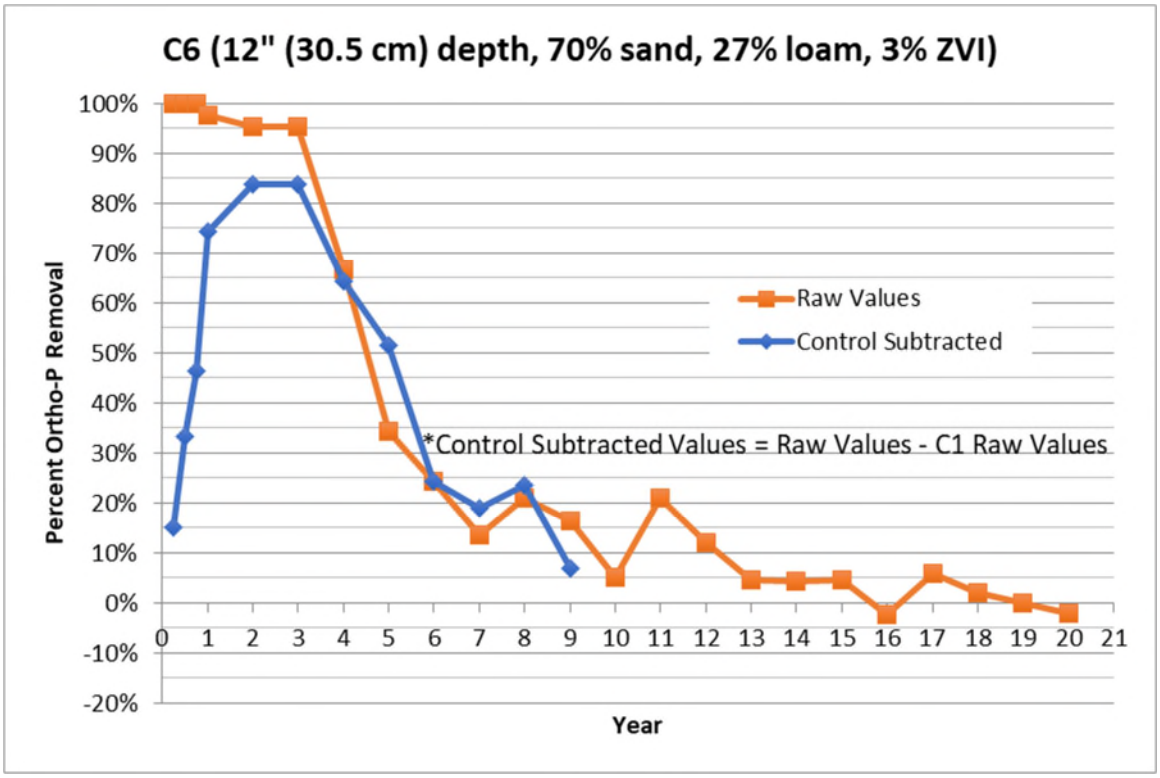

Figure 12: Column 6 percent ortho-P removal results based on simulated year

Figures 13 through 15 show data for each column containing varying amounts of ZVI but the same 6-inch depth of media. As with Columns 4 through 6, the "Control Subtracted" trends generally increase until they reach their maximum around Year 1 and then they follow the "Raw Values" trend after that point. As described before, once these lines follow the same trend and their values are closer for each simulated year, the ZVI is likely responsible for the majority of adsorption.

The "Raw Values" in Figure 13 show that Column 7 experienced high removal percentages in the first few trials but quickly declined by the end of Year 1 to a removal percentage under forty percent. For Columns 8 and 9, the declines were more gradual as shown in Figures 14 and 15. Column 8 did not drop below 40% until Year 2 and Column 9 did not drop below that percentage until Year 3.

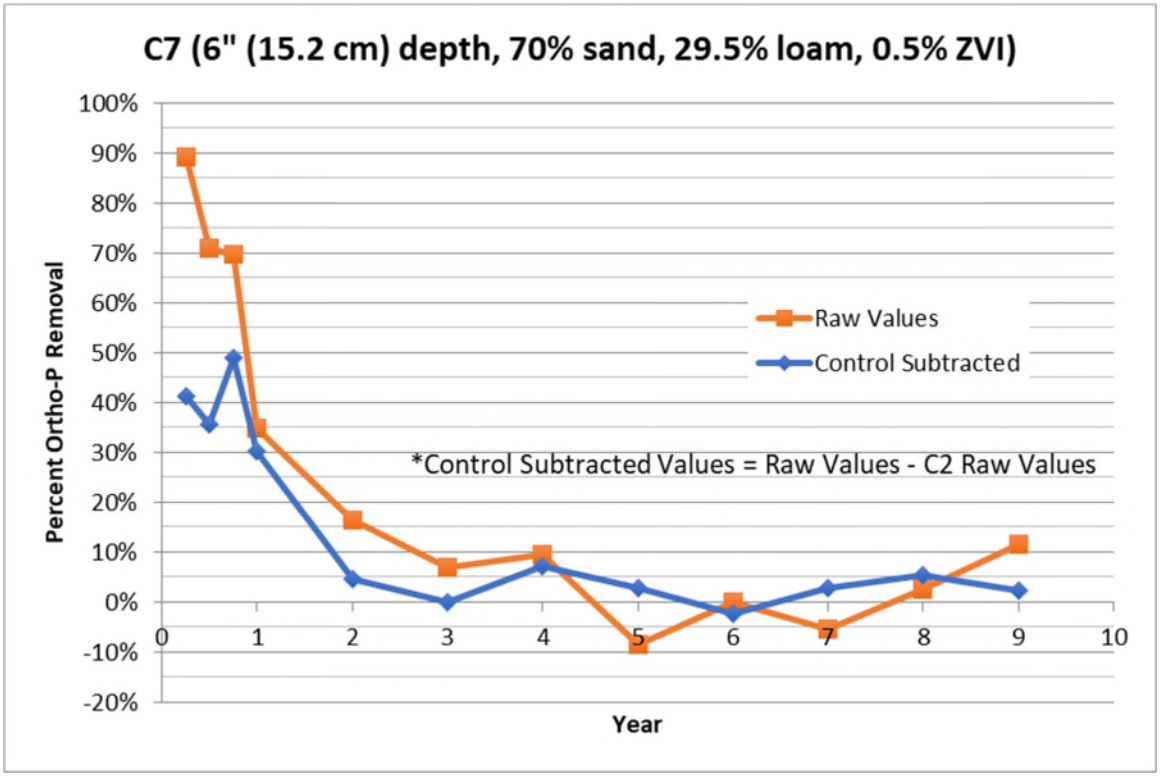

Figure 13: Column 7 percent ortho-P removal results based on simulated year

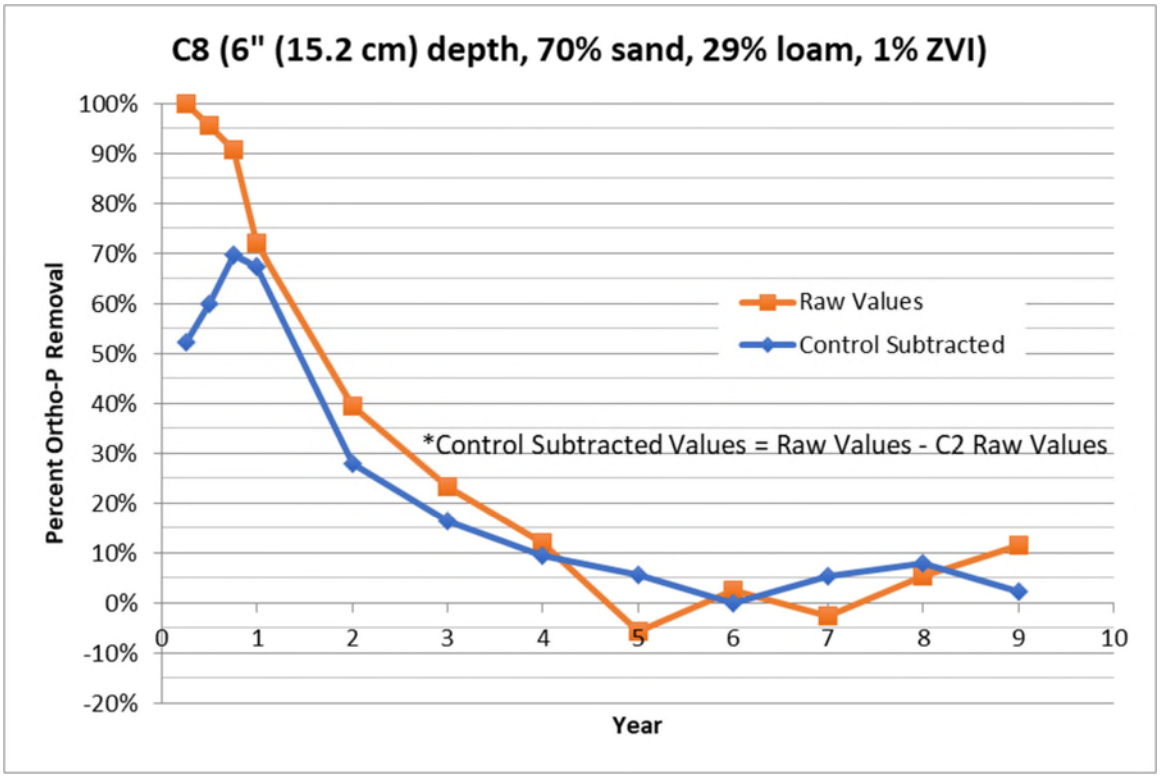

Figure 14: Column 8 percent ortho-P removal results based on simulated year

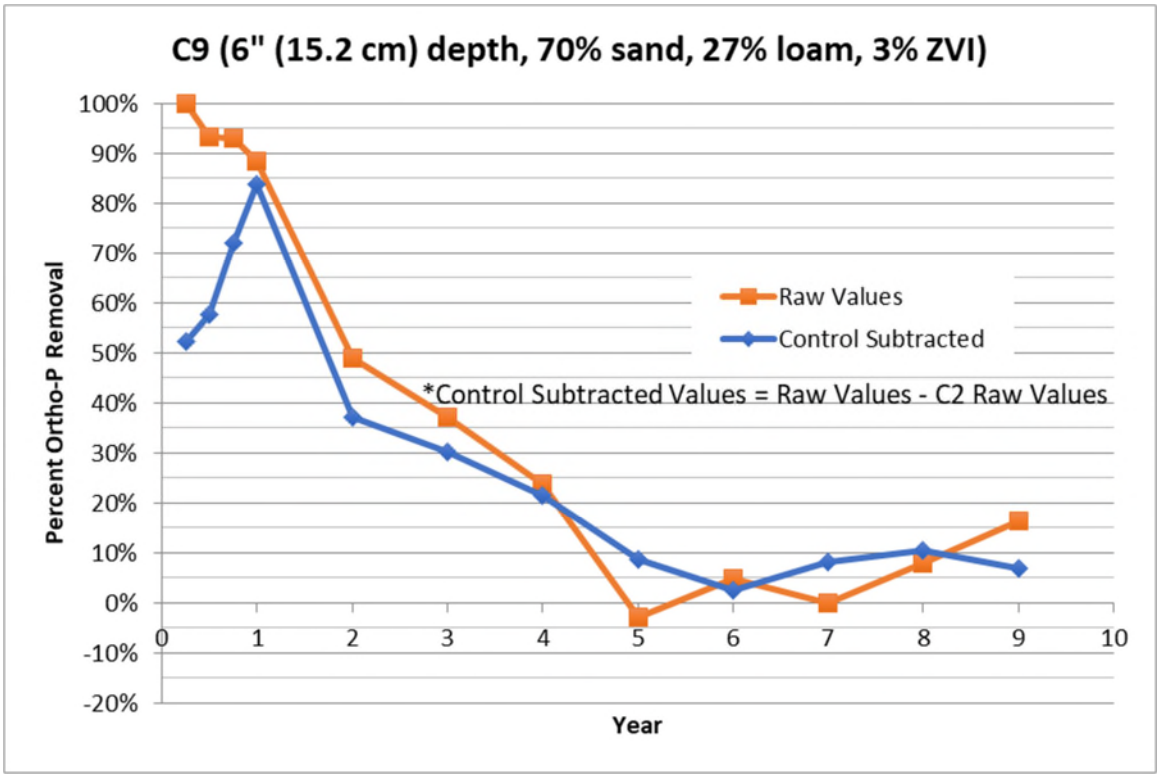

Figure 15: Column 9 percent ortho-P removal results based on simulated year

Figure 16 shows a comparison of percent ortho-P removal over time for all columns with a 12-inch (30.5 cm) depth of soil media. These curves are shown without the subtraction of control values. Column 6 displays the highest removals for the longest amount of time. This was to be expected because it had the highest percentage of ZVI. Column 5 shows the second highest removals followed by Column 5, Column 4, and Column 1. This order also closely relates to the percentage of ZVI in the columns, with Column 1 having none at all.

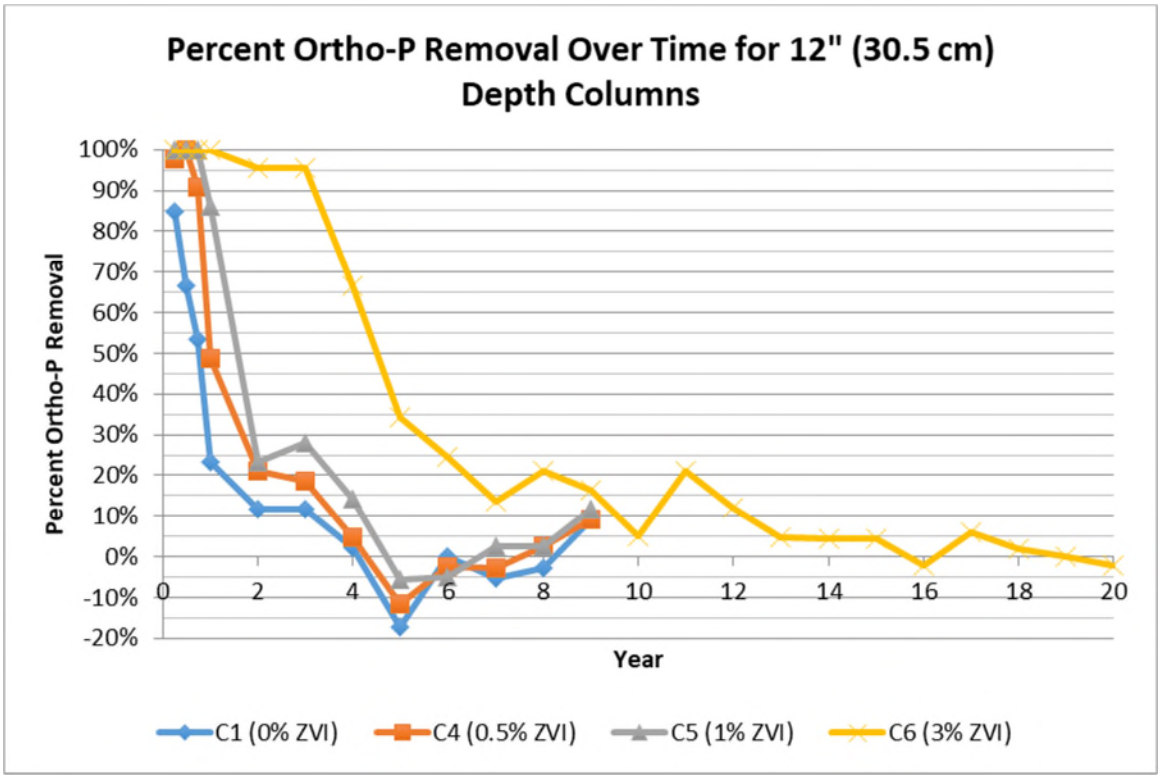

Figure 16: Comparison of percent ortho-P removal results for columns with 12” (30.5 cm) media depth

Figure 17 shows a comparison of percent ortho-P removal over time for all columns with a 6-inch (15.2 cm) depth of soil media. The removal trends in this figure follow those from Figure 16 where the order from the best performing column to the worst coincides with the percentage of ZVI in the media mix. Although Column 9 had the same percentage of ZVI as Column 6, it did not outperform the other columns as much as Column 6 did in Figure 16. It could have reasonably been expected that

Columns 6 and 9 would outperform the other columns by at least the same ratio, but the results did not seem to follow this pattern. Several inconsistent experimental factors could have influenced results from all columns, including flow rate from the dispensers, resting time between experiments, media mixing for increased infiltration rates, and loss of media through the effluent tube. There was occasionally small amounts of media found in the effluent of the columns, even from the control columns. From the particle size distributions shown in Figure 2, it makes sense that some of the loam and ZVI could wash through the columns as both were finer than the sand. This loss of media could have decreased the adsorption capacity of the media for subsequent simulated years. Using coarser loam and ZVI could have remedied the loss of media, but coarser ZVI could have also corresponded to smaller removals as discussed in Section 2.2.3.

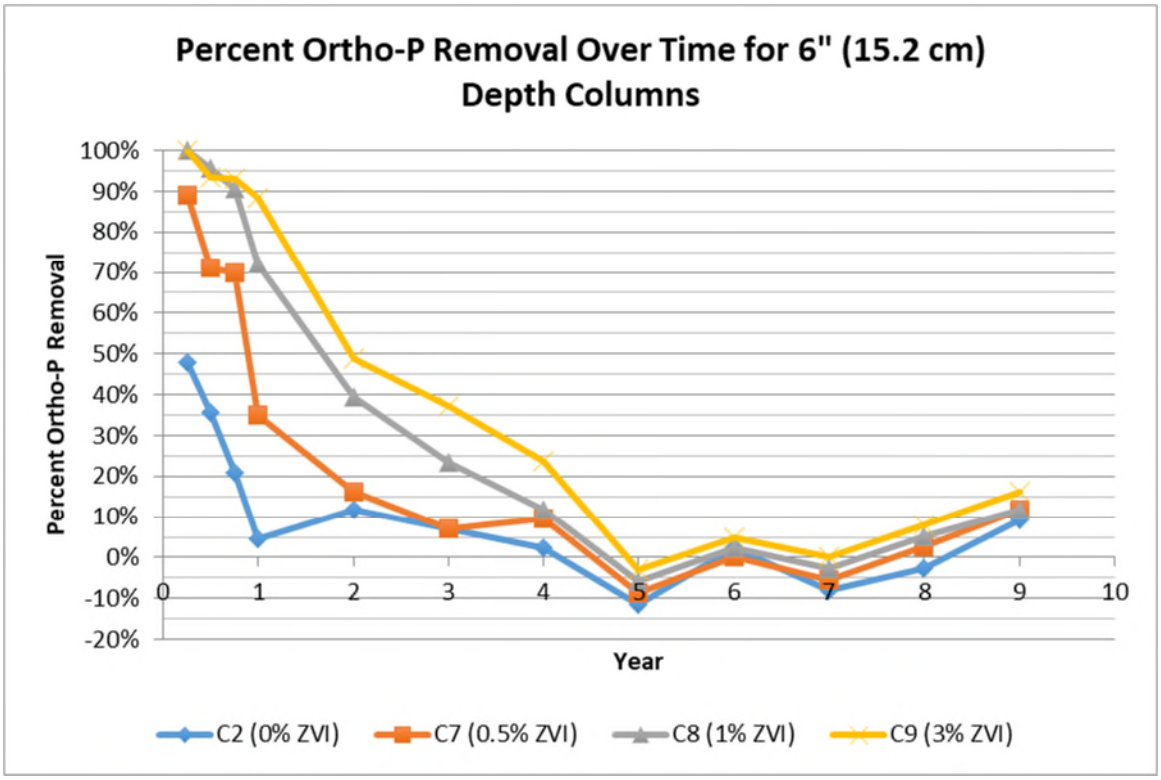

Figure 17: Comparison of percent ortho-P removal results for columns with 6” (15.2 cm) media depth

Figures 18 through 21 compare the removal percentages of columns with the same percentage of ZVI but different media depths. In each of these figures, it is the column with the greater depth that has better performance. There are occasional data points where columns with lesser media depths outperform the larger depth columns, but the majority of data shows larger depth performing better for the years before the removals go to zero. Once the trends reach 0% removal, they become much more unpredictable and the top performing column often switches from year to year.

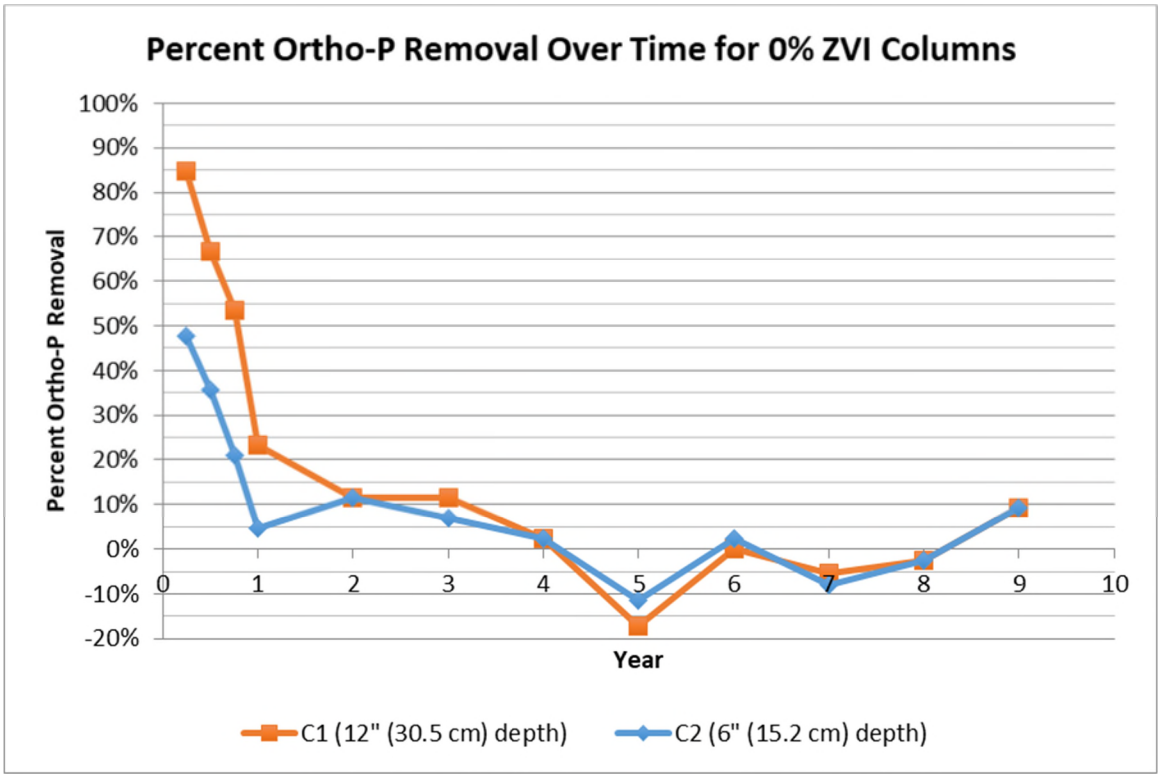

Figure 18: Comparison of percent ortho-P removal results for columns with 0 percent ZVI

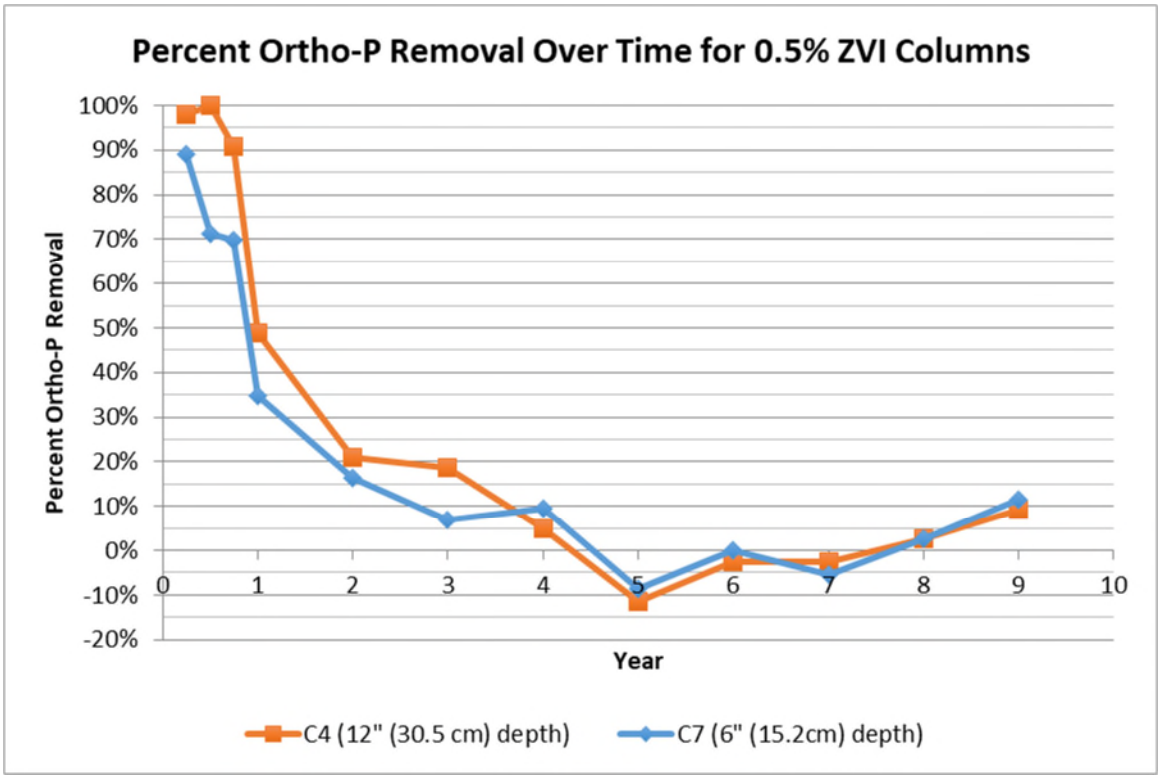

Figure 19: Comparison of percent ortho-P removal results for columns with 0.5 percent ZVI

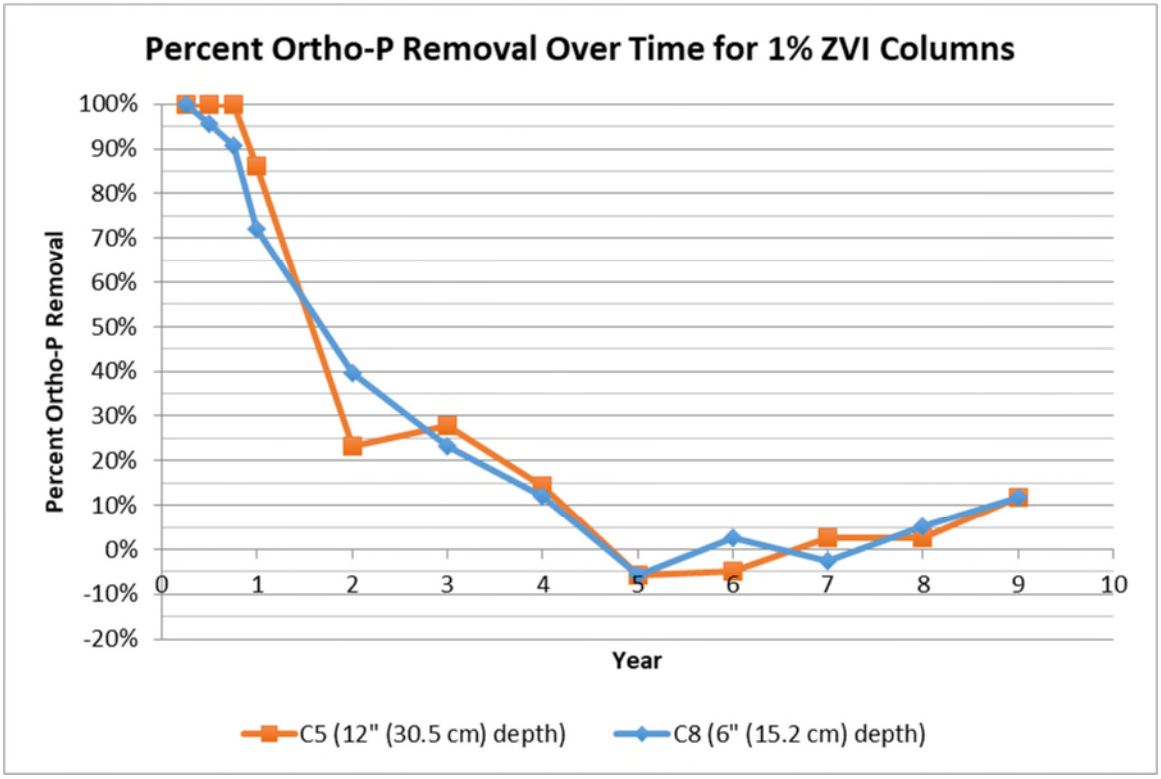

Figure 20: Comparison of percent ortho-P removal results for columns with 1 percent ZVI

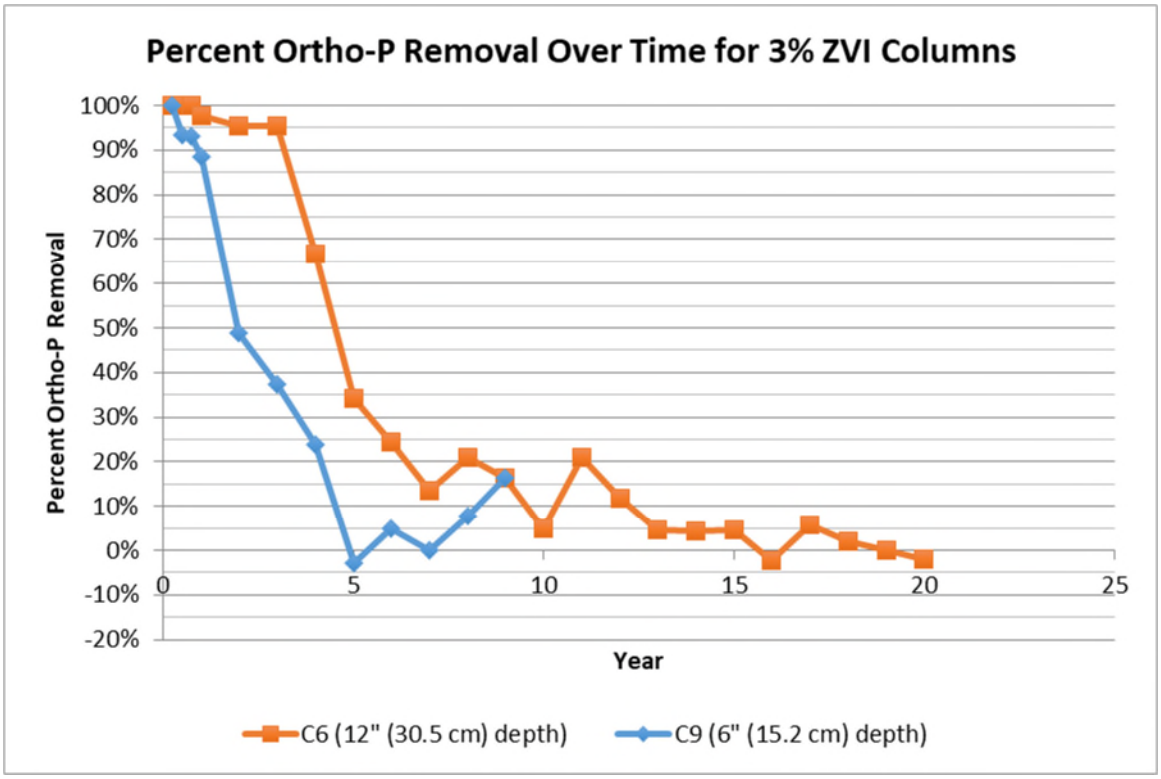

Figure 21: Comparison of percent ortho-P removal results for columns with 3 percent ZVI

All columns except for Column 6 showed negative removals for year 5, and the shapes of their curves are very similar beyond that point when testing was stopped in year 9. Many of the columns showed positive removals after it was assumed their adsorption capacities were exhausted. Because the shapes of these curves do not seem to correlate to pH trends from Table 19 in Appendix A, it may be that these removal percentage trends are a function of small errors in the reported influent concentrations. With ortho-P being reported in low concentrations at 0.1 mg/L sensitivity, small discrepancies in this data can lead to significant differences in removal percentage. Column 3, which was very consistent at 0% removal for years 1 through 4, suddenly had fluctuating removals starting in year 5. This control column containing only sand was expected to remain constant at 0% removal. Because it followed the same general trend as the other columns, it is more likely that there were small errors in the influent measurements than the sand suddenly leaching ortho-P or developing adsorption capacity

in year 9. There is a small chance that the columns did, in fact, regain some adsorption capacity, but based on the available data it is difficult to determine why that could have occurred.

The box and whisker plot in Figure 22 shows a summary of the ortho-P removal efficiencies for the columns across simulated Years 1 through 9. Testing was continued for Column 6 for twenty simulated years, but in order to standardize the comparison, only data up to Year 9 was used in the analysis. The data in this experiment is much better suited for time series analysis, but there are several conclusions that can be made from Figure 22 that support previously stated trends. When considering the median removal percentage for each column, columns with 12 inches (30.5 cm) of media all have larger removals than their 6-inch (15.2 cm) counterparts with the same ZVI percentages. Similarly, columns with higher percentages of ZVI have higher median removals without exception when comparing against columns of the same media depth. Column 6 had the highest median percent removal while Column 3 had the lowest. Ortho-P would have had the most opportunity to adsorb to ZVI and loam in Column 6 due to its 12-inch (30.5 cm) depth and high percentage of ZVI. Conversely, there was very little opportunity for adsorption in Column 3 due to its media's lack of depth, loam, and ZVI.

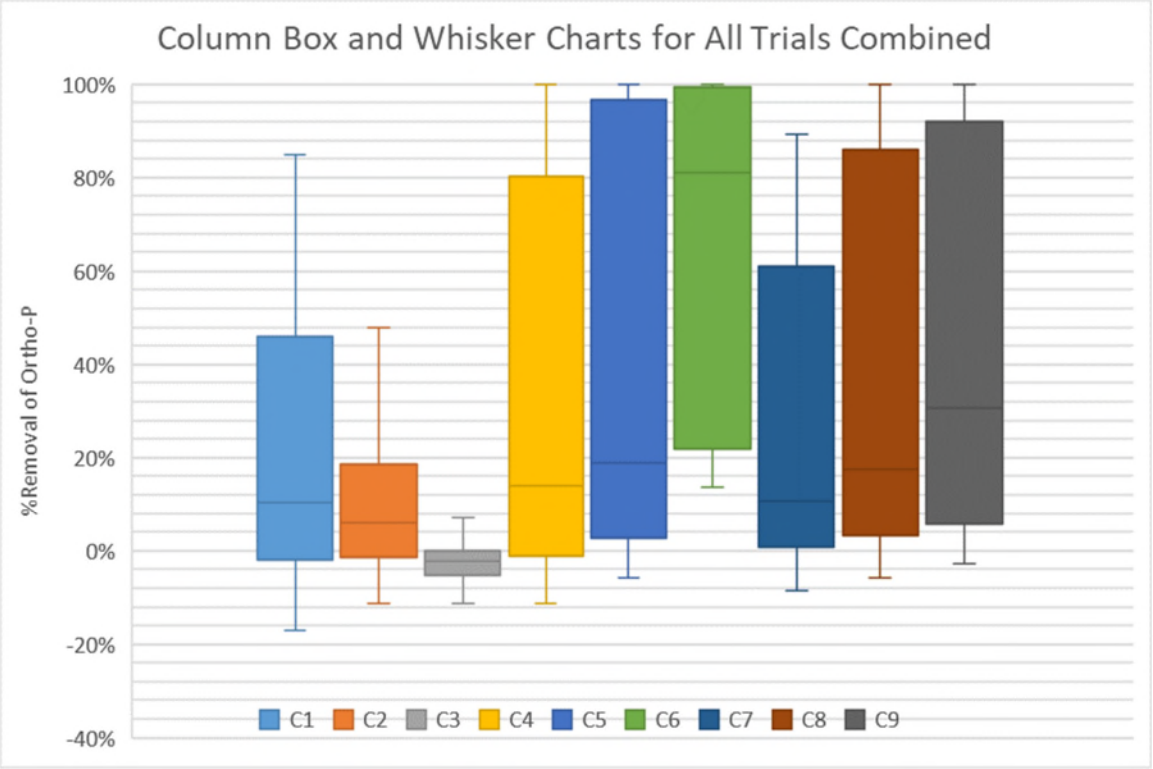

Figure 22: Box and whisker comparison of percent ortho-P removal for each column over combined simulated years

4.2 Cumulative Ortho-P Retention Results

Figure 23 shows the cumulative mass of ortho-P retained in the media of each column for every gram of ZVI contained in the column. This plot effectively shows how efficiently each column can remove ortho-P from the simulated runoff. Column 7 had the highest efficiency while containing the smallest mass of ZVI. The more ZVI mass a column contains, the less efficient it is according to Figure 23. Erickson et al. (February 23, 2010) also found this to be the case. The mass of ZVI for each column can be found in Table 2. As previously discussed, Column 6 had the best performance by far in terms of removal percentages for each year, but this figure is showing it was the least efficient due to its extremely high ZVI mass. Conversely, Column 7 had only about 8% of the ZVI that Column 6 had, and its moderate removals were enough to make it the most efficient column. A possible explanation for this trend is that increasing the ZVI mass in a column does not necessarily corelate to a proportional increase in ZVI

surface area if the ZVI particles stick together. If particles stick together, there could be less surface area for adsorption of ortho-P as adsorption sites are sheltered in the middle of a cluster.

Figure 24 shows the cumulative mass of ortho-P retained in each column over time. Because Column 6 had the highest removal percentages for the longest period of time, it also had the highest cumulative mass of ortho-P retained by the end of Year 9. It was also able to adsorb ortho-P long after the other columns had stopped. The column order in terms of most cumulative mass retained roughly coincides with the mass of ZVI in each column. The more ZVI mass a column contained, the more ortho-P was adsorbed in total. This displays a simple relationship between the mass of ZVI and mass of ortho-P adsorbed. In looking at the curves for Columns 1 and 2, the loam clearly showed some adsorption capacity even though it was exhausted very early in the testing. Column 1 roughly doubled the mass adsorbed by Column 2 which can be explained by Column 1 containing twice the loam content of Column 2. As previously stated, Column 3 showed no adsorption capacity due to its lack of loam and ZVI.

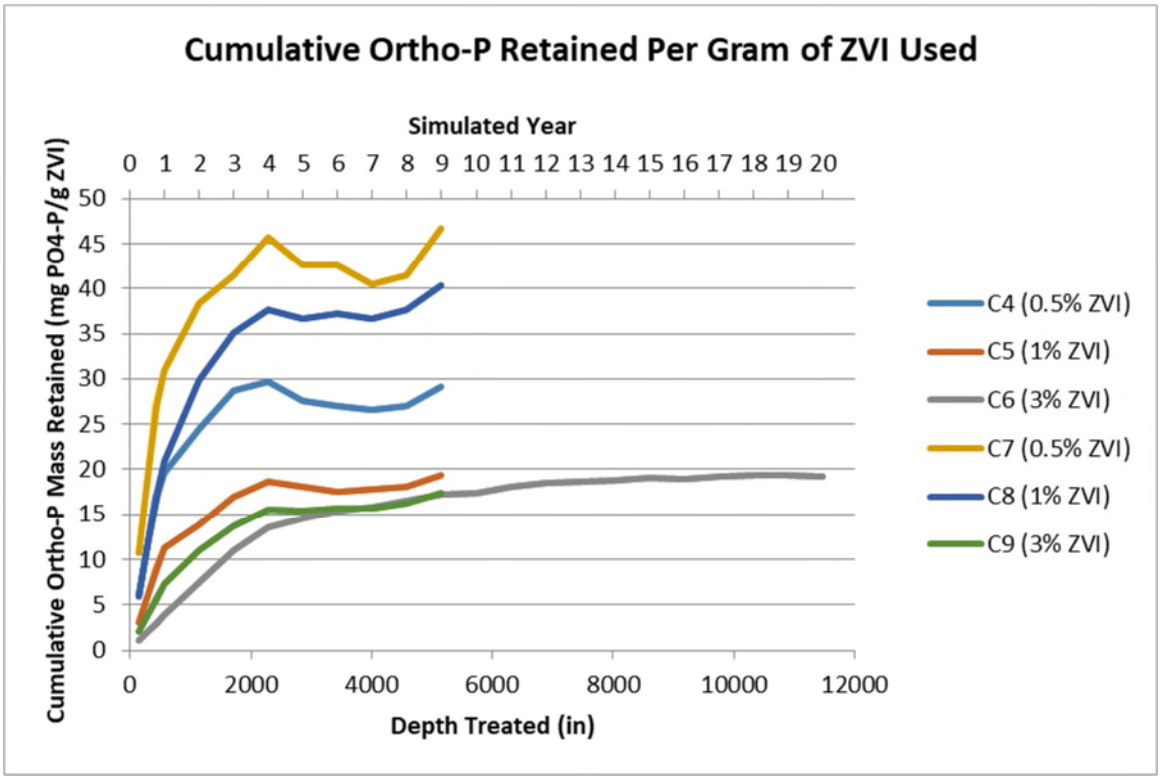

Figure 23: Cumulative ortho-P retained per gram of ZVI used

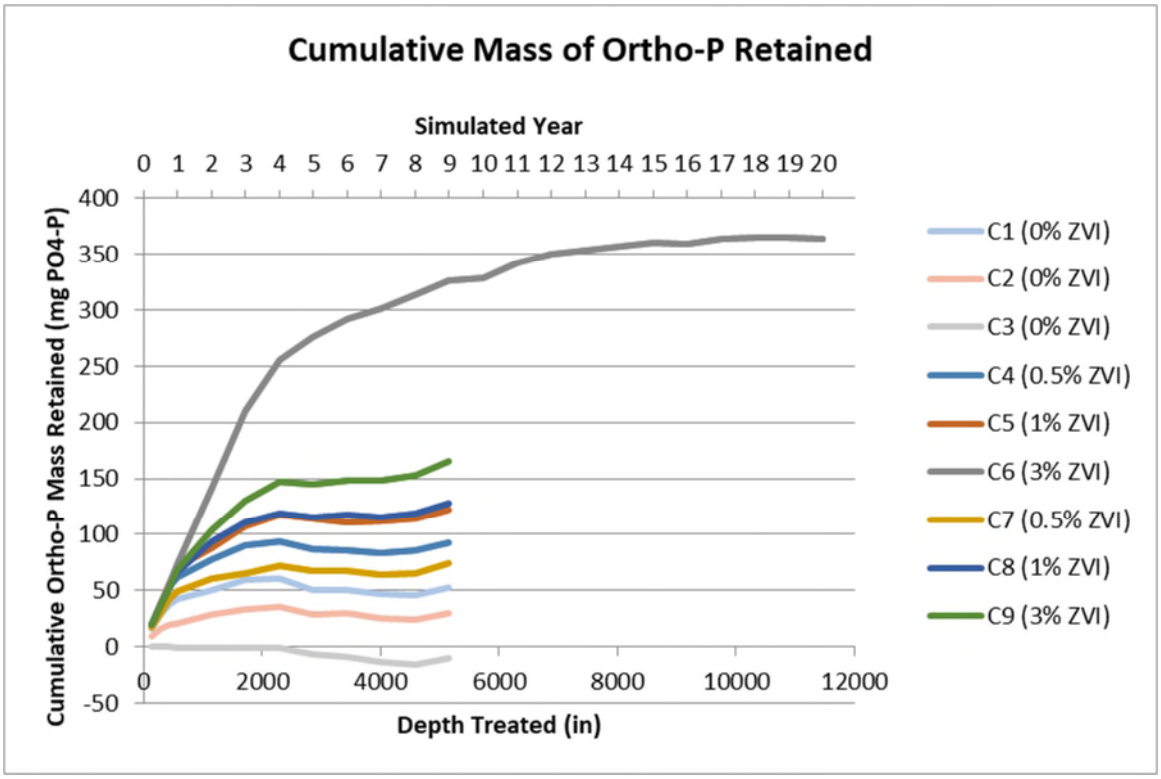

Figure 24: Cumulative mass of ortho-P retained for each column

4.3 Isolation of Loam Adsorption Effect

In order to create a flexible and accurate model for predicting ZVI lifespan, it was important to isolate the effects of loam's ortho-P adsorption throughout testing. Isolating the loam effect would allow for easier lifespan prediction comparisons to ZVI adsorption studies that did not use loam in the mix. This concept of removing the loam effect was previously explored when Figures 10 through 15 showed the "Control Subtracted" curves to indicate the adsorption that is likely attributable to only the ZVI. However, these curves do not fit well with Freundlich and Langmuir isotherms due to their inherent assumption that all the loam adsorption occurs at the beginning and occurs separately from ZVI adsorption. As previously noted, adsorption is likely occurring simultaneously, so these "Control Subtracted" lines do not paint a completely accurate picture of the system. With this in mind, a second method was developed to correct for the loam effect. Table 3 shows the total loam effect percentage and effect per data point collected for each column. These percentages are based on the cumulative

masses of ortho-P retained by each column as compared to their respective control columns of similar media depths. By determining a loam effect percentage for each data point, the natural curvature of the percent removal plots can be maintained and allow for better results when performing analyses based on the Freundlich and Langmuir isotherms.

Table 3: Loam effect percentage based on column

Column	Cumulative Mass Retained (mg)	Total Loam Effect (%)	Loam Effect Per Data Point Collected (%)
1	60.6	N/A	N/A
2	35.3	N/A	N/A
3	0.0	N/A	N/A
4	93.8	65	5.4
5	117.4	52	4.3
6	365.6	17	0.7
7	72.2	49	4.1
8	119.1	30	2.5
9	146.9	24	2.0

4.4 ZVI Performance Longevity Analysis

With both the Freundlich and Langmuir adsorption isotherms being accepted means for fitting phosphorus adsorption data, a comparison between the two was necessary to determine which would be better for predicting the longevity of ZVI under varying loading conditions. The following subsections display the completed analyses to choose the preferred isotherm for use in the final automated longevity prediction spreadsheet. All data points used in Freundlich and Langmuir analyses include a loam effect correction based on Table 3. It is also important to note that Freundlich and Langmuir isotherms are usually applied when a solution has reached equilibrium. As this equilibrium condition was likely not achieved during most of the testing, applying the Freundlich and Langmuir isotherms to this data could be described as creating fit curves that still retain physical meaning in their variables. This method is preferred over applying best fit functions to the data that have no scientific derivation or

physical meaning. The automated spreadsheet is a tool intended to assist in treatment system designs by predicting the lifespan of ZVI in soil media under varying hydraulic and ortho-P loads.

4.4.1 Freundlich Isotherm Fit Lines for Rate Constant Determinations

Figures 25 through 34 show the process of determining the Freundlich rate constants for each column. For each trial, q was calculated and plotted against C_e. Then a power function was fit through the points to determine K and n. Because the Freundlich isotherm equation takes the form of $q = KC_e^{1/n}$, n was the inverse of the exponent in these best-fit equations and K was the coefficient.

Data from Columns 4, 6, 7, and 8 did not naturally fit the shape of a Freundlich isotherm. The best-fit power functions in Figures 25, 28, 30, and 32 had negative n values whereas a Freundlich isotherm should always have a positive n. A Freundlich isotherm was then forced fit to the data points as shown in Figures 26, 29, 31, and 33 to facilitate rate constant comparisons between columns and a final comparison of the Freundlich model itself to the Langmuir model. These force fit equations were determined by minimizing the RMSE between the best fit line and the data points using Excel's Solver add-in. Solver would run through iterations of values for K and n until it arrived at the optimal values for these variables that minimized the RMSE. The $1/n$ exponent values for these force fit equations are very large because relatively flat lines are the closest these functions can get to being negative again as they had been in Figures 25 and 27.

Although the Freundlich model yielded acceptable equations for the rest of the columns, the best fit curves were not a strong representation of the data. For example, the best R^2 value among all columns was 0.0621 for Column 9 in Figure 34. Because the Freundlich model was expected to be useful in predicting ortho-P removals over time for systems with varying media percentages and hydraulic loading conditions, it was not discounted outright for these weak fitting equations.

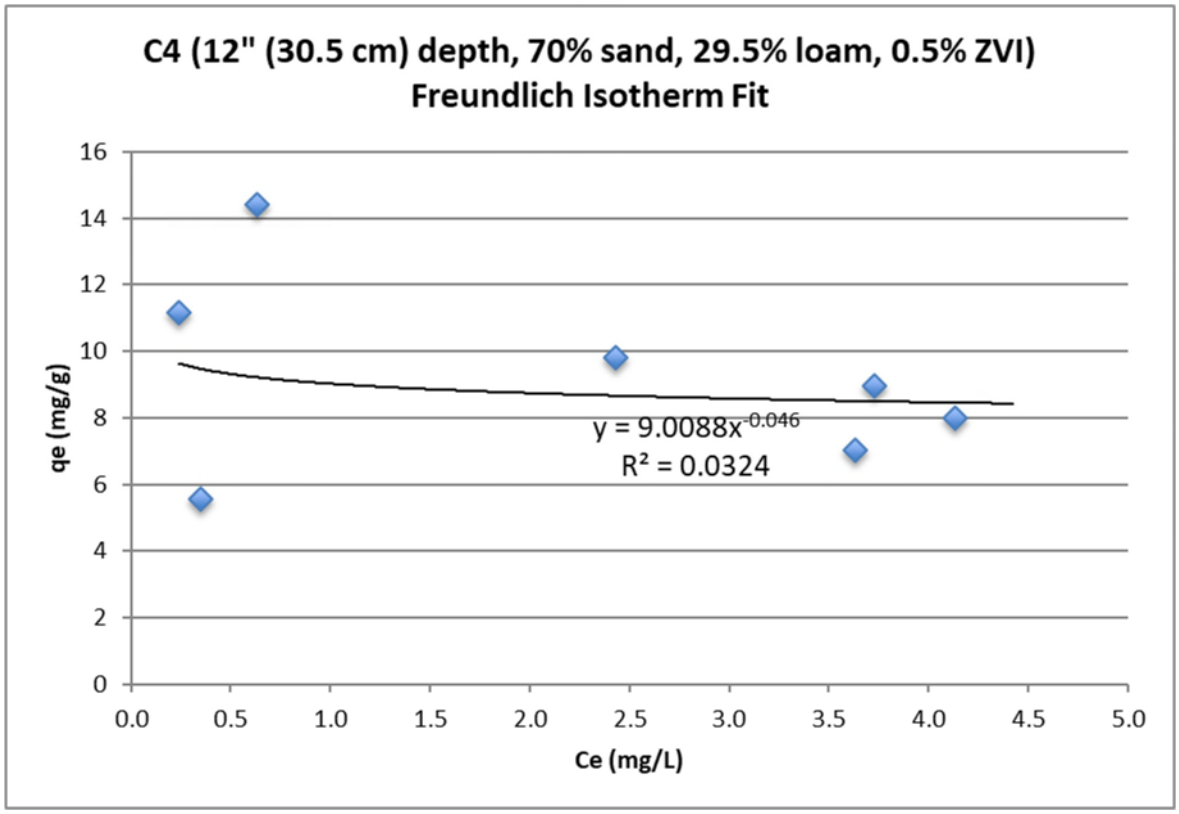

Figure 25: Freundlich isotherm best fit power function for Column 4

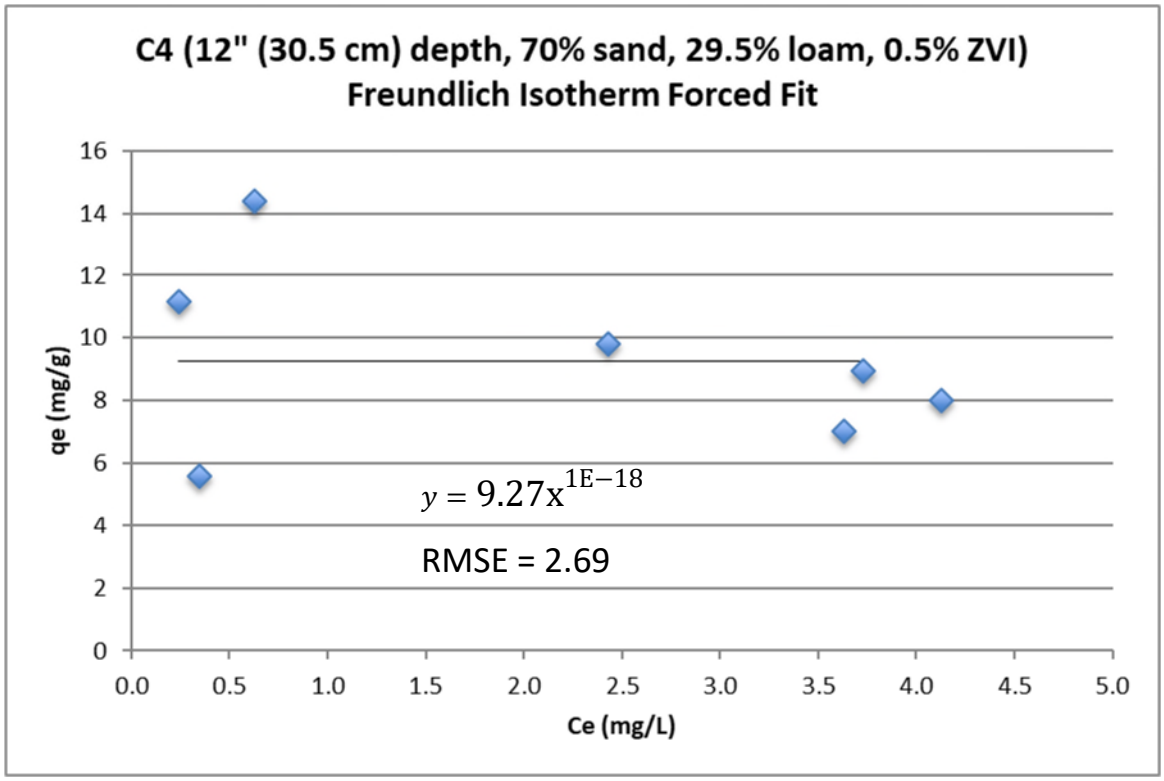

Figure 26: Freundlich isotherm forced fit power function minimizing RMSE for Column 4

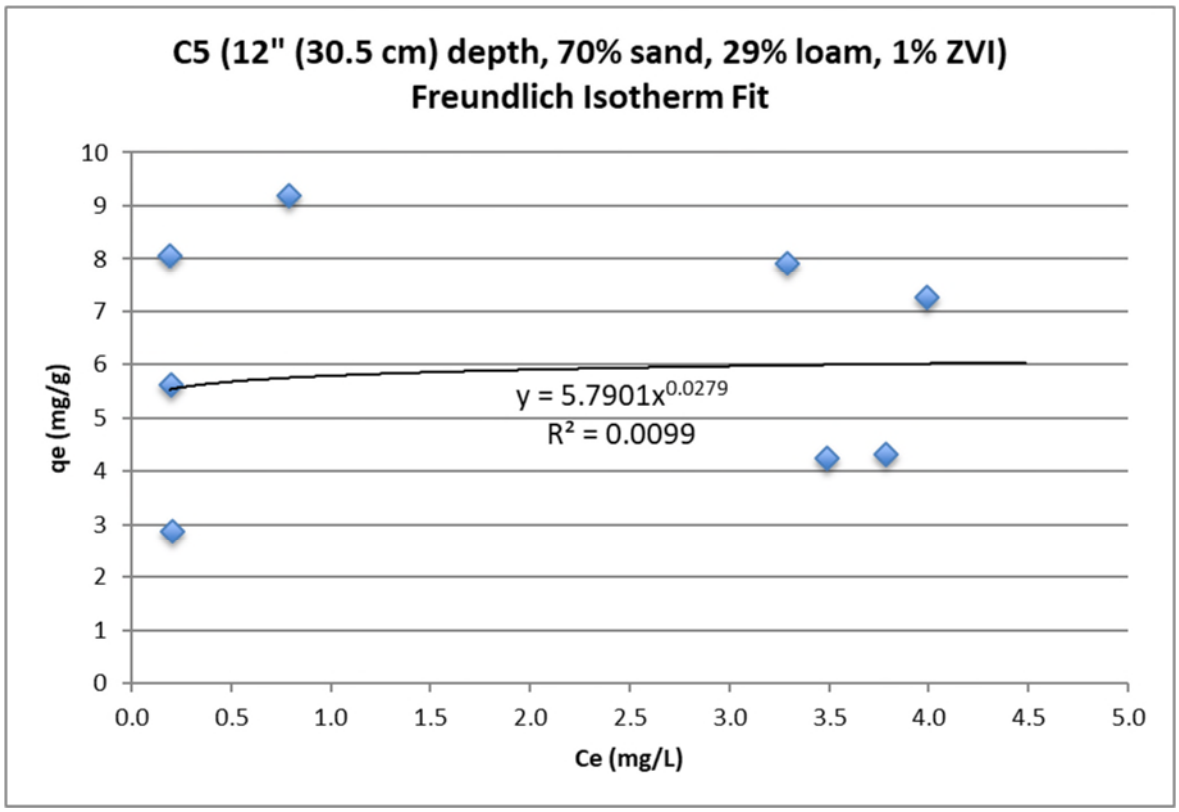

Figure 27: Freundlich isotherm best fit power function for Column 5

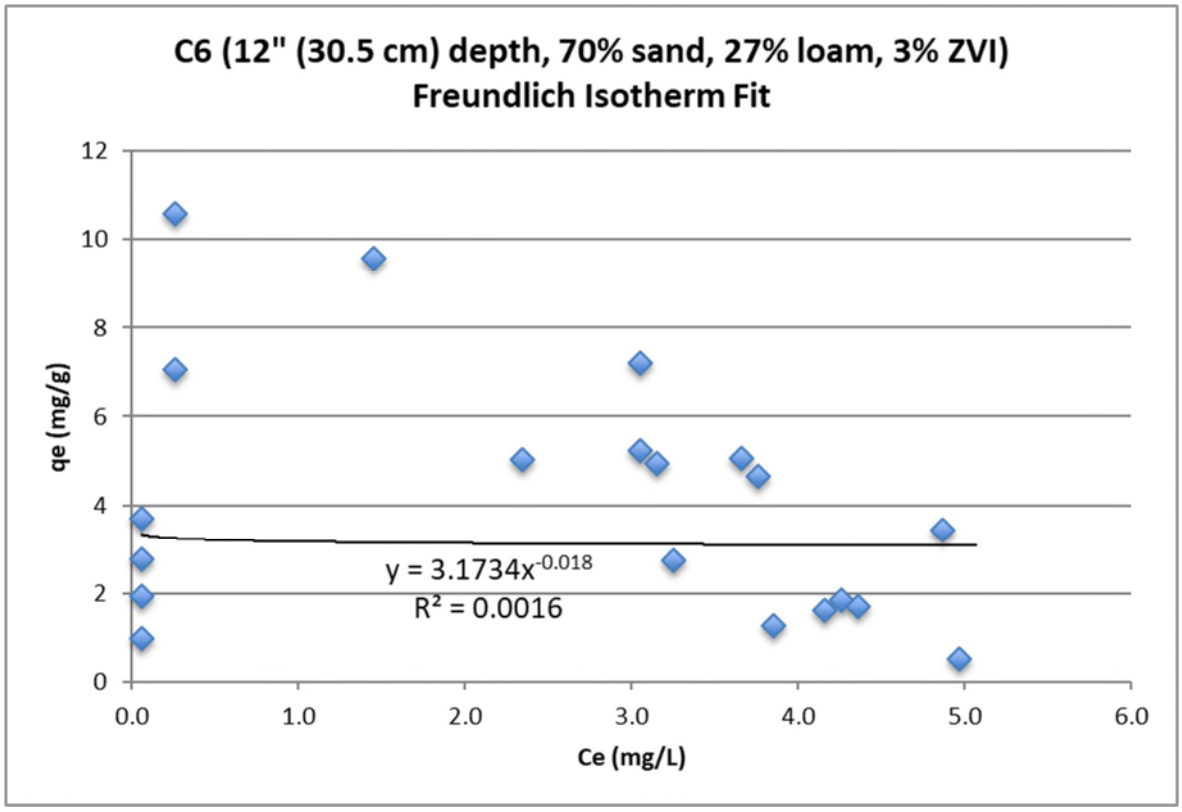

Figure 28: Freundlich isotherm best fit power function for Column 6

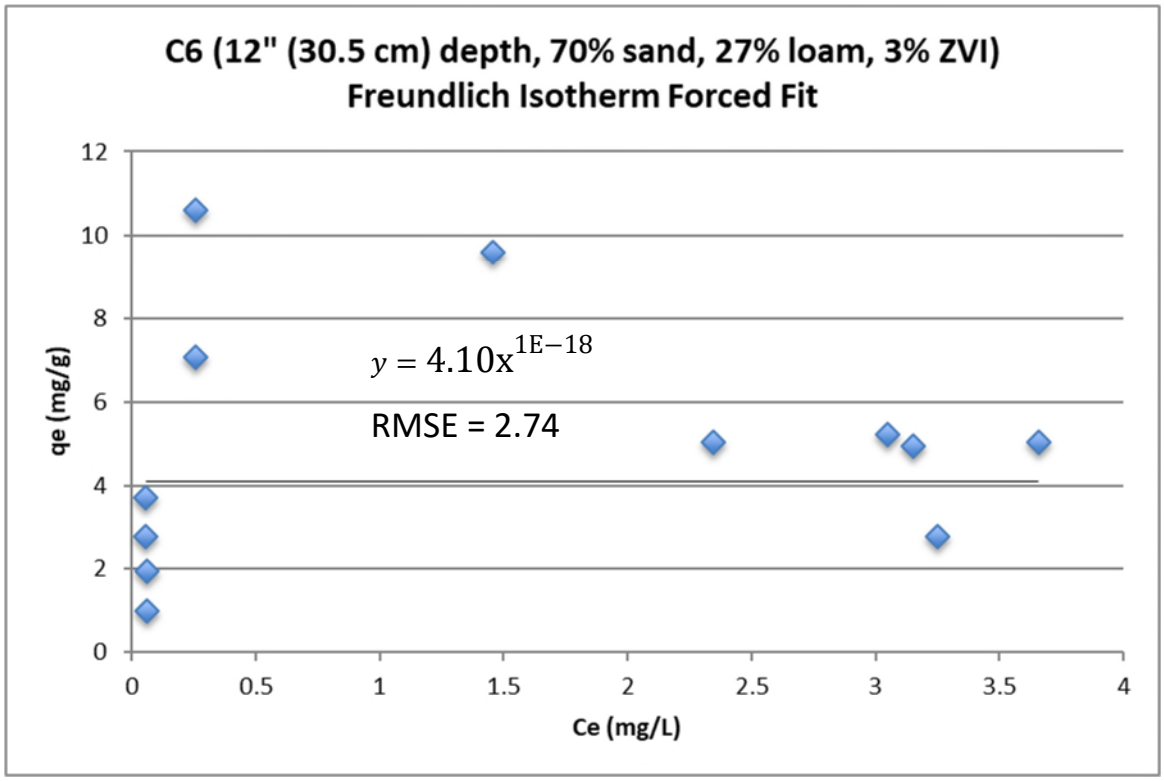

Figure 29: Freundlich isotherm forced fit power function minimizing RMSE for Column 6

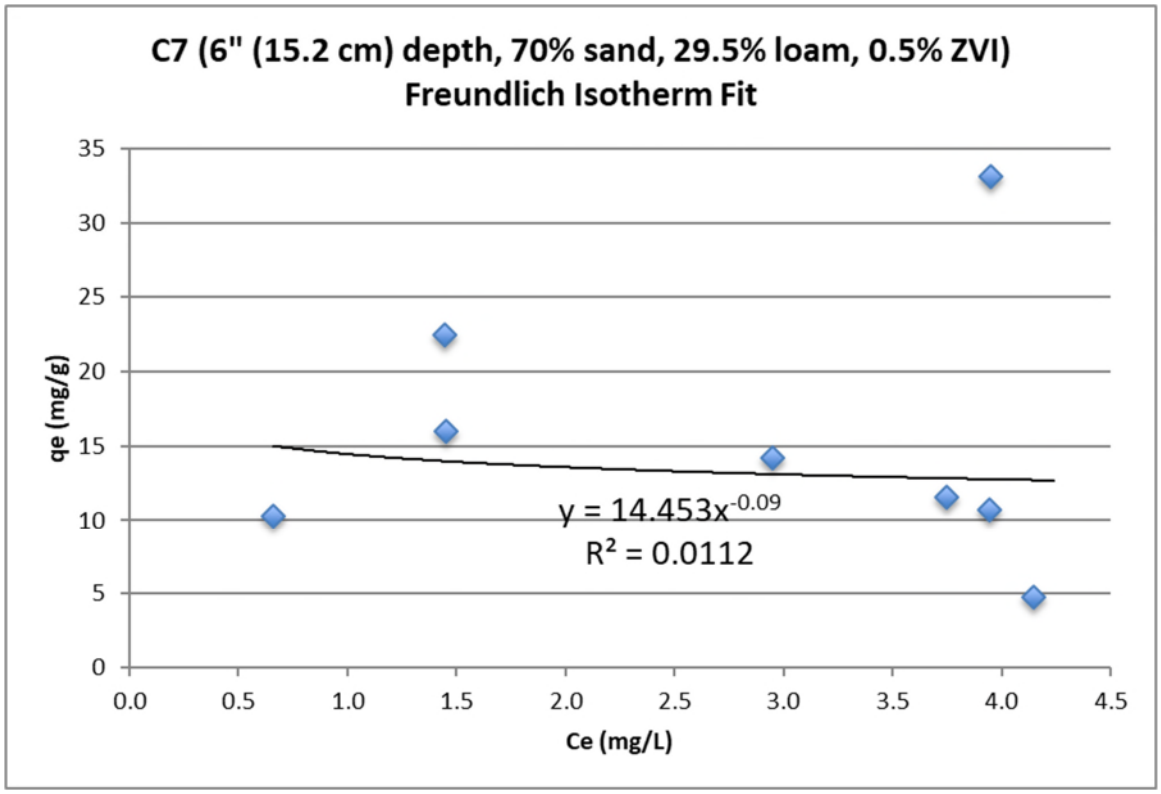

Figure 30: Freundlich isotherm best fit power function for Column 7

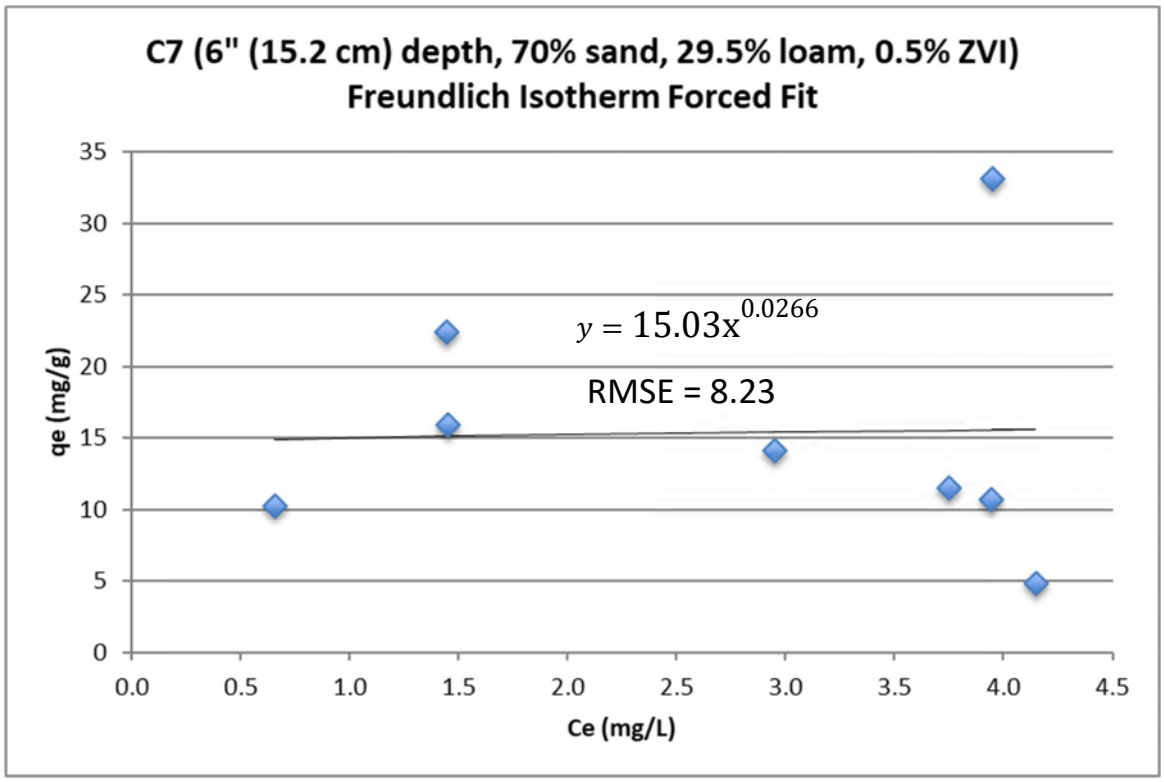

Figure 31: Freundlich isotherm forced fit power function minimizing RMSE for Column 7

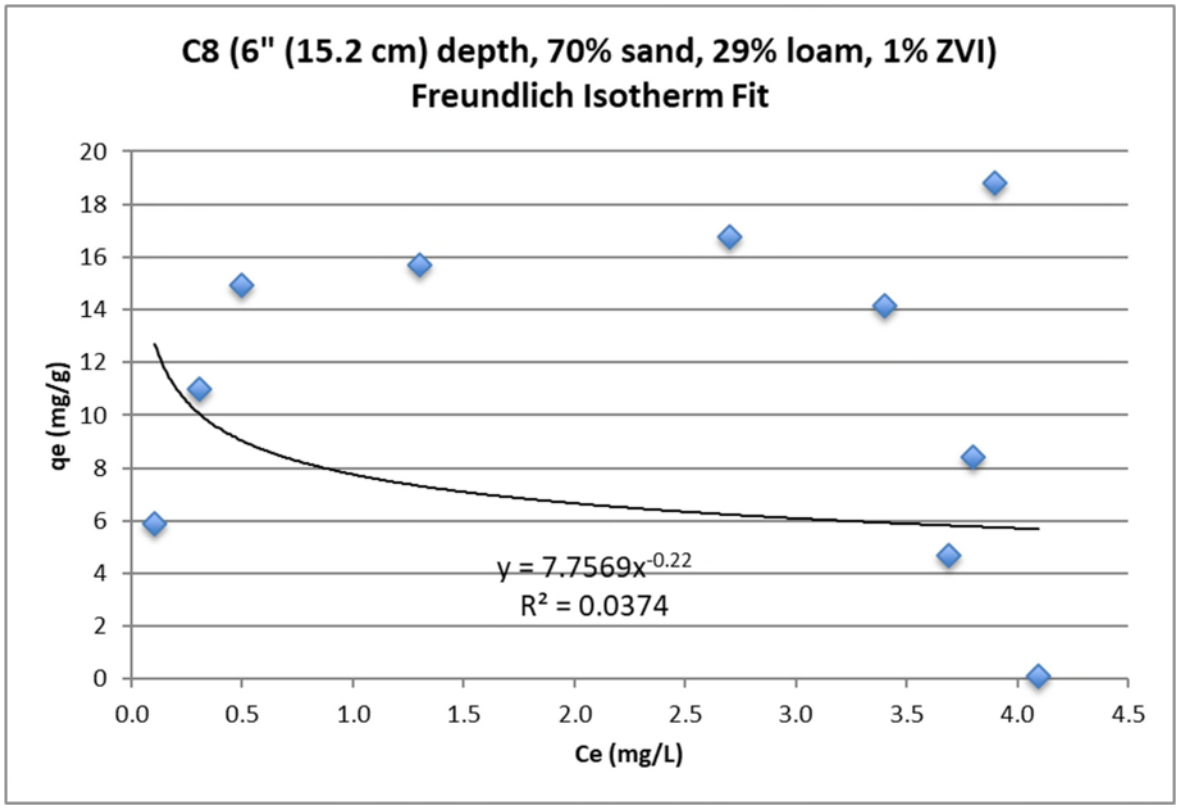

Figure 32: Freundlich isotherm best fit power function for Column 8

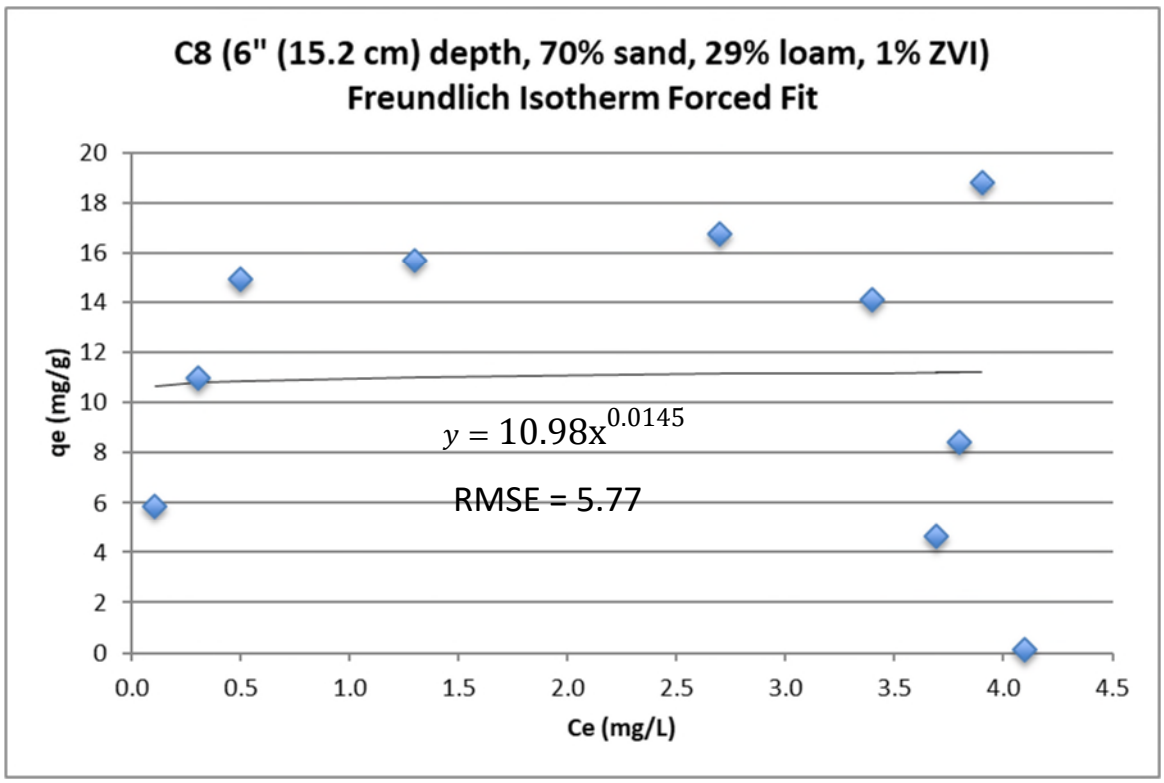

Figure 33: Freundlich isotherm forced fit power function minimizing RMSE for Column 8

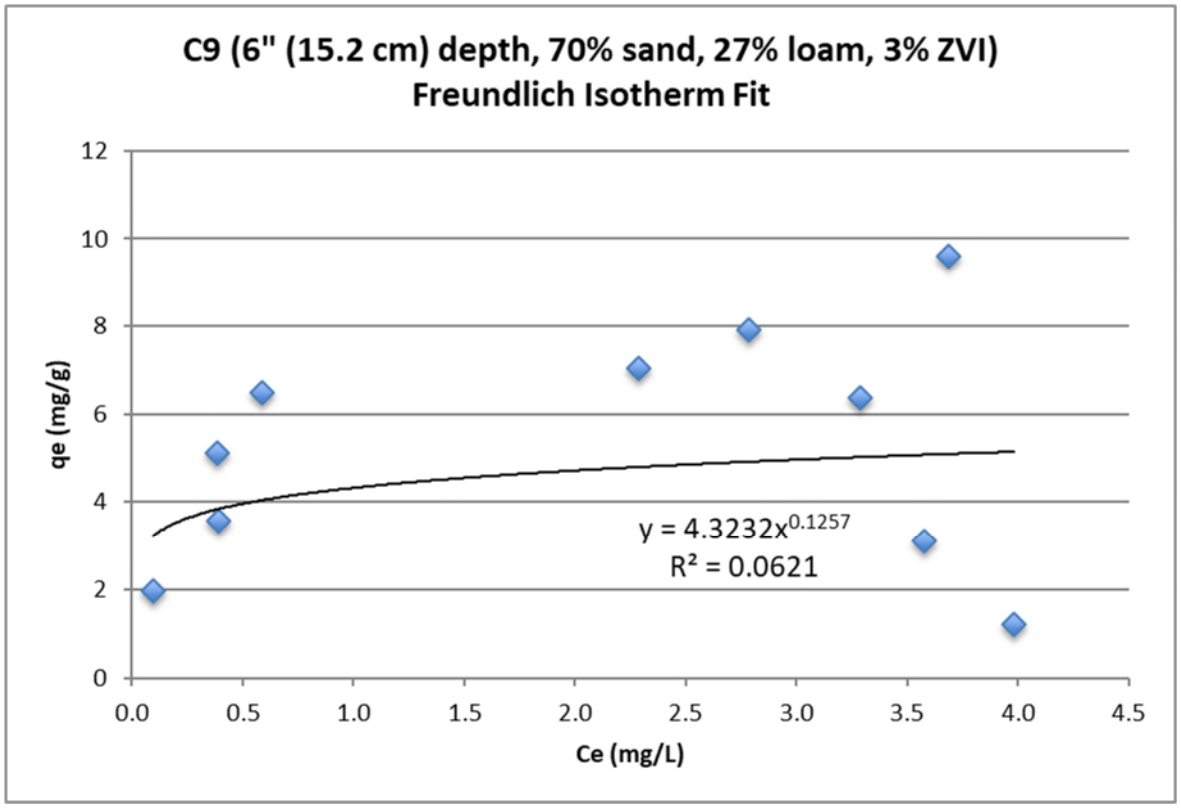

Figure 34: Freundlich isotherm best fit power function for Column 9

4.4.2 Freundlich Isotherm Best Fit Percent Removal Curves

Figures 35 through 40 show the difference between the experimental percent removal values and the best-fit Freundlich isotherms using rate constants for each column determined in Figures 25 through 34. Each figure displays the RMSE between the best-fit curve and the experimental data. These figures are useful in the comparison between Freundlich and Langmuir isotherms. Because data for several columns needed isotherms to be force fit in Sections 4.4.1 and 4.4.3, a simple comparison of R^2 values for Freundlich and Langmuir fit lines was not reasonable. Creating percent removal plots for Freundlich and Langmuir (Section 4.4.5) isotherms allowed for a consistent method of comparison using RMSEs.

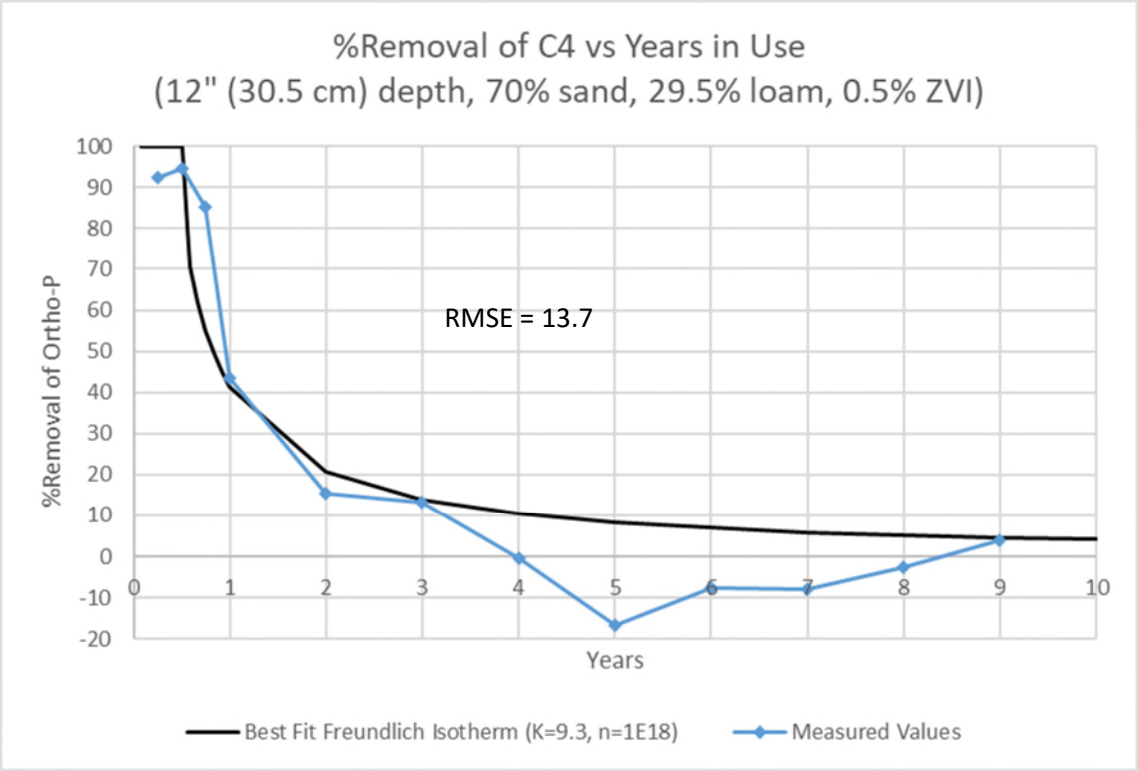

Figure 35: Column 4 comparison of percent ortho-P removal for raw values and values calculated using Freundlich rate constants determined in Figure 26

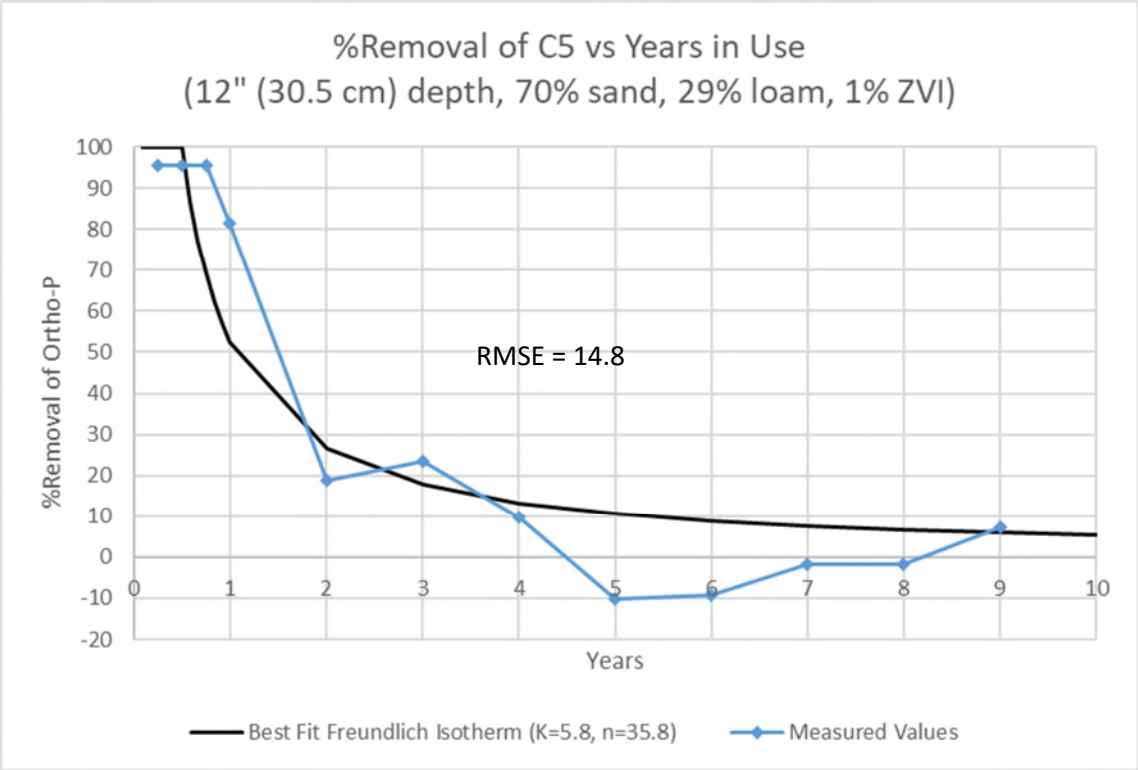

Figure 36: Column 5 comparison of percent ortho-P removal for raw values and values calculated using Freundlich rate constants determined in Figure 27

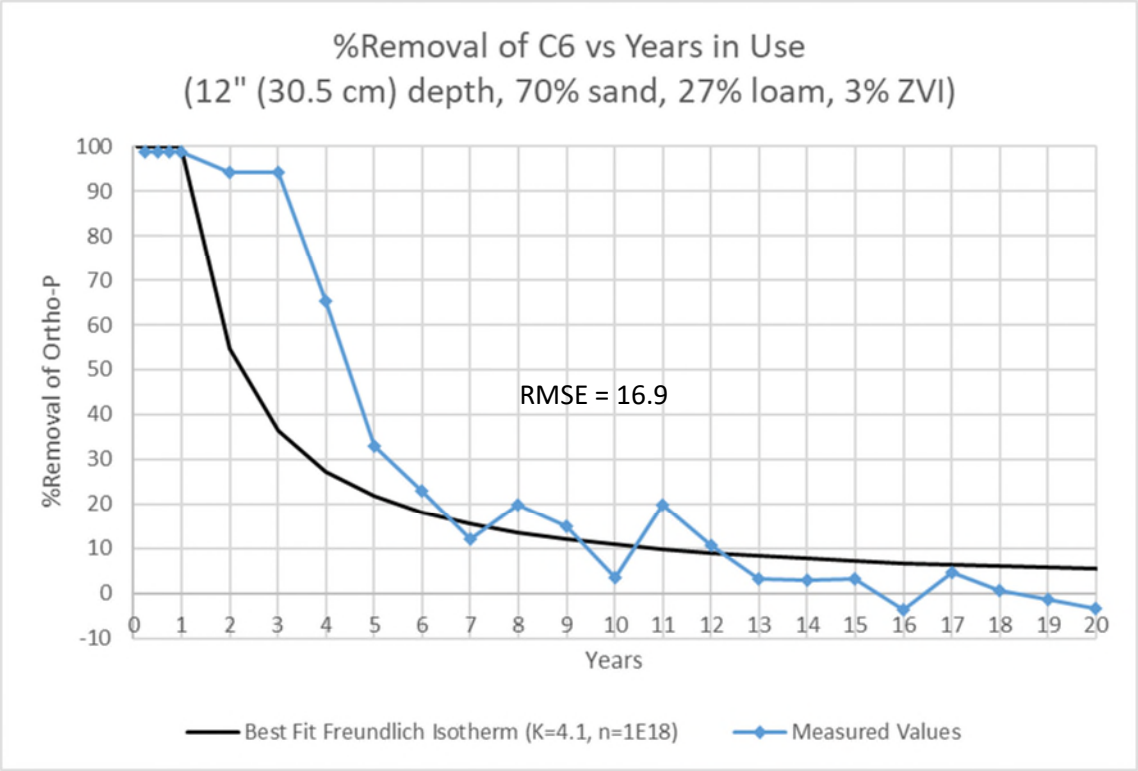

Figure 37: Column 6 comparison of percent ortho-P removal for raw values and values calculated using Freundlich rate constants determined in Figure 29

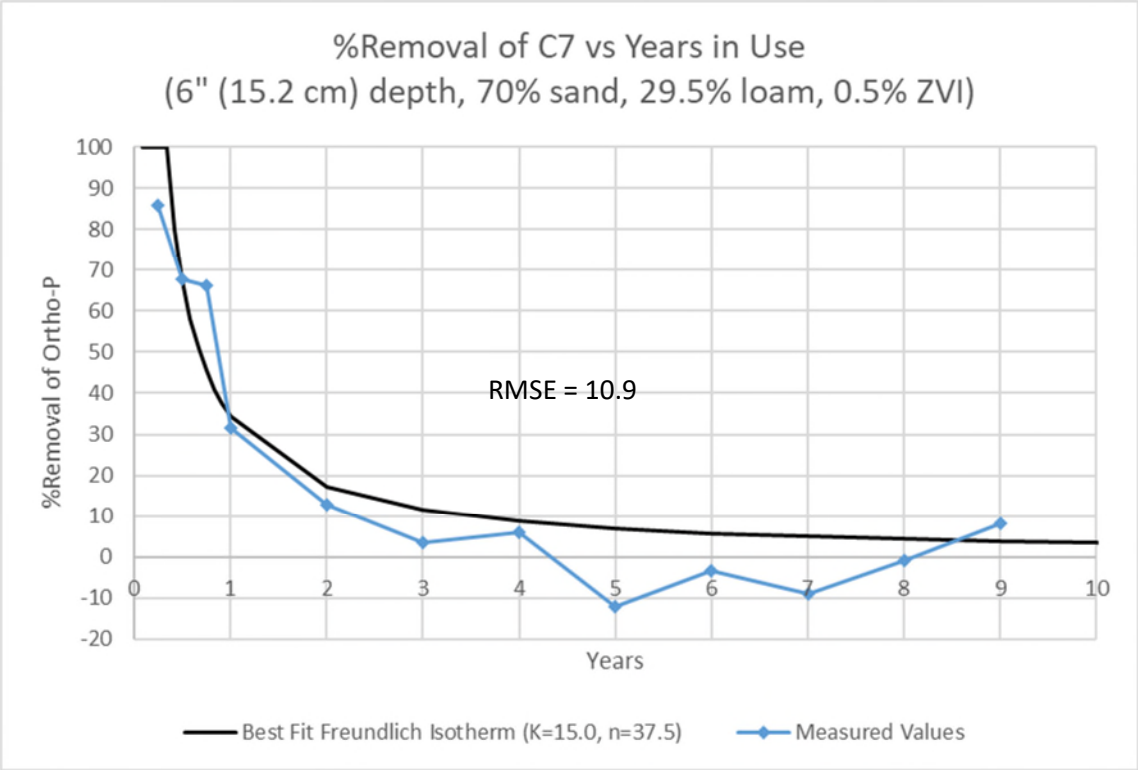

Figure 38: Column 7 comparison of percent ortho-P removal for raw values and values calculated using Freundlich rate constants determined in Figure 31

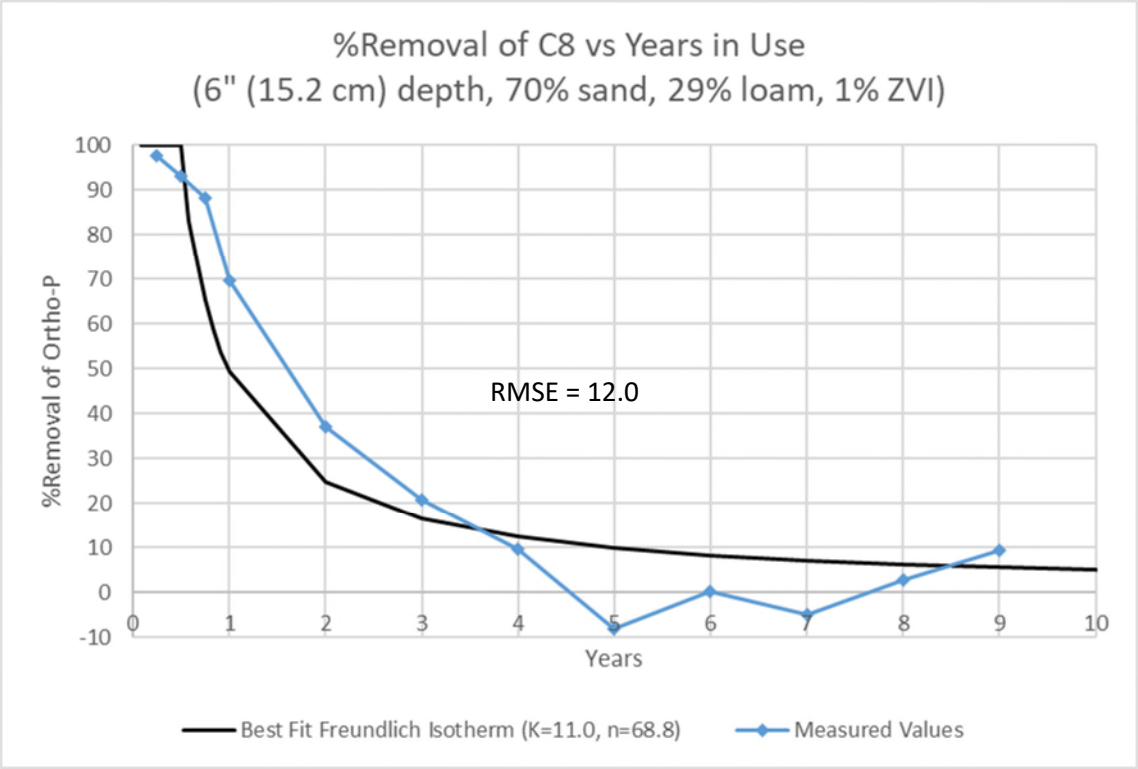

Figure 39: Column 8 comparison of percent ortho-P removal for raw values and values calculated using Freundlich rate constants determined in Figure 33

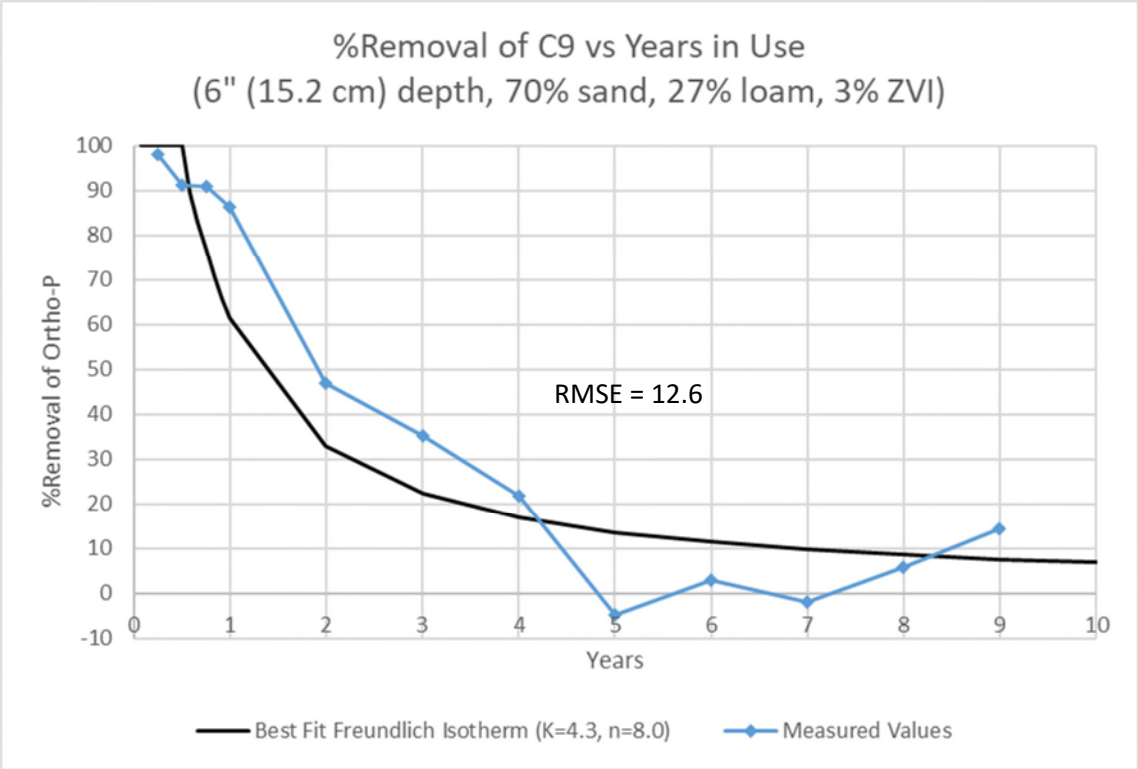

Figure 40: Column 9 comparison of percent ortho-P removal for raw values and values calculated using Freundlich rate constants determined in Figure 34

Table 4 shows a summary of Freundlich constants used in Figures 35 through 40 as well as the associated RMSE for each of these percent removal plots. The average RMSE for these columns was 13.5.

Table 4: Summary of Freundlich constants and RMSE values from percent removal plots

Column	Freundlich K, n	Freundlich RMSE
4	9.3, 1E18	13.7
5	5.8, 35.8	14.8
6	4.1, 1E18	16.9
7	15.0, 37.5	10.9
8	11.0, 68.8	12.0
9	4.3, 8.0	12.6
	Average	**13.5**

Table 5 shows a multiple regression analysis performed for determining *K* based on %ZVI and depth of media. It shows the coefficients of these variables and intercept required to estimate *K* at ZVI percentages and media depths not tested in this study. Equation 8 shows how the coefficients from the multiple regression analysis can be arranged within an equation to determine *K*. This estimation of constants at intermediate percentages is important for creating a robust ZVI lifespan prediction tool. The multiple regression method for determining *K* was compared against a simple power function based on only %ZVI shown in Figure 41, and it was concluded that the multiple regression yielded better results when comparing RMSEs for all of the columns. More information on the comparison of methods is included in Section 4.4.3.

Table 5: Multiple regression analysis for *K* based on %ZVI and media depth

Regression Statistics	
Multiple R	0.916587913
R Square	0.840133402
Adjusted R Square	0.733555669
Standard Error	2.227926731
Observations	6

ANOVA

	df	*SS*	*MS*	*F*	*Significance F*
Regression	2	78.25526756	39.12763378	7.882823027	0.063919976
Residual	3	14.89097255	4.963657518		
Total	5	93.14624012			

	Coefficients	*Standard Error*	*t Stat*	*P-value*	*Lower 95%*	*Upper 95%*	*Lower 95.0%*	*Upper 95.0%*
Intercept	18.13174142	3.141372928	5.771916241	0.010338662	8.134490755	28.12899209	8.134490755	28.12899209
% ZVI	-2.864703328	0.842077153	-3.401948763	0.042400561	-5.544568652	-0.184838005	-5.544568652	-0.184838005
Depth (in)	-0.62077597	0.303182426	-2.047532824	0.133079128	-1.585637762	0.344085823	-1.585637762	0.344085823

$$K = (-2.86)(\%ZVI) + (-0.62)(\text{Depth (in)}) + 18.13 \qquad \text{Equation 8}$$

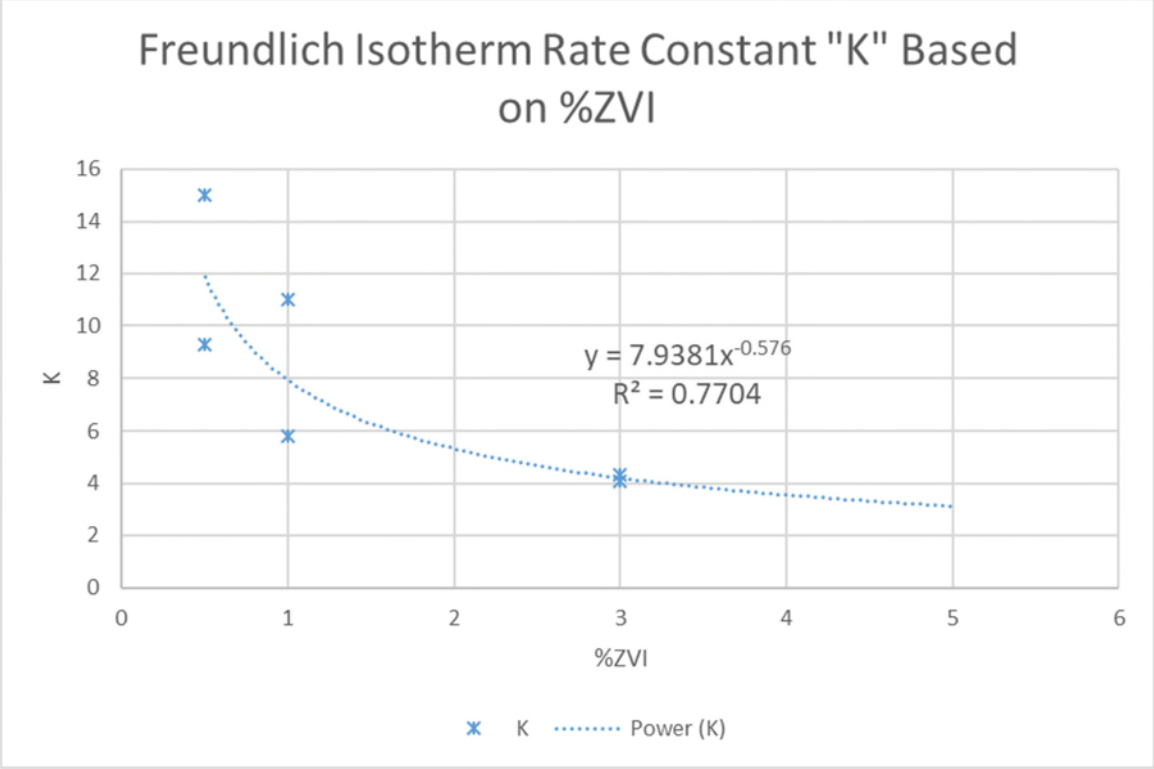

Figure 41: Trendline for K based on K values from Table 14 and ZVI percentage

It was also determined that for the purposes of this study, *n* could be held constant at the median value of all the columns (n=53.2) with little effect on the RMSEs of each column. Instead of fitting a trendline through the highly variable *n* values, it was determined that holding it constant would be sufficient. Section 4.4.3 shows more information on this analysis.

4.4.3 Freundlich Comparison of Methods for K and n Estimation

Because *n* values from the best fit Freundlich isotherms in Table 4 had such a wide range, it was difficult to develop a reasonable trendline for determining *n* at intermediate ZVI percentages without removing the two highest values. These values account for a third of the data, so it would not be ideal to exclude them. Instead, using a constant *n* value was tested to determine how much it influenced the RMSE of each column. The median value of *n* across all columns, *n*=53.2, was selected for analysis. Figures 95 through 100 in Appendix B1.1 show the percent removal plots used to compare the RMSEs for a constant *n* versus the original best fit *n* values shown in Table 4. Table 6 shows that the RMSEs for each column are only minimally different when using a constant *n* value, so it was determined that a constant *n* would be used for all further analyses.

Table 6: Comparison of best fit *K* and *n* RMSEs to RMSEs using the best fit *K* with a constant *n* value

	RMSE			
Column	**K and n from Table 4**	**K from Table 4 with Constant n (n=53.2)**	**|Difference in RMSE|**	**% Difference**
4	13.722	13.695	0.028	0.203
5	14.780	14.818	0.037	0.253
6	16.859	16.607	0.252	1.494
7	10.863	10.870	0.007	0.060
8	12.048	12.010	0.038	0.317
9	12.550	13.425	0.875	6.971
Average	**13.471**	**13.571**	**0.206**	**1.550**

After it was determined that it was reasonable for *n* to be held constant, different methods for estimating *K* at various ZVI percentages were explored. As explained in Section 4.4.2, the

purpose of estimating *K* at different ZVI percentages is to facilitate the facilitate lifespan predictions at ZVI percentages that were not used in this study. Figure 41 shows a trendline created using *K* values from Table 4 and their corresponding ZVI percentages. Figures 101 through 106 in Appendix B.1.2 show the percent removal plots created to determine the new RMSEs based on *K* values from the Figure 41 trendline. Table 7 shows the comparison of RMSEs between the original best fit *K* and *n* values versus when *K* was determined from the Figure 41 trendline with a constant *n* value.

Table 7: Comparison of best fit *K* and *n* RMSEs to RMSEs using the *K* from the Figure 41 trendline with a constant *n* value

	RMSE			
Column	**K and n from Table 4**	**K from Figure 41 with Constant n (n=53.2)**	**|Difference in RMSE|**	**% Difference**
4	13.722	13.340	0.382	2.786
5	14.780	12.465	2.315	15.660
6	16.859	16.202	0.657	3.896
7	10.863	12.822	1.959	18.031
8	12.048	18.610	6.562	54.466
9	12.550	13.960	1.410	11.233
Average	**13.471**	**14.567**	**2.214**	**17.679**

As an alternative to creating the simple trendline for estimating *K* based on only ZVI percentage as shown in Figure 41, a multiple regression analysis was completed to estimate *K* based on both ZVI percentage and depth of media. This analysis was previously shown in Table 5, where the output showed the coefficients of %ZVI and depth and the intercept when determining *K* from an equation with those two variables. Figures 107 through 112 in Appendix B.1.3 show the percent removal plots created to determine the new RMSEs based on *K* values from the multiple regression trend from Table 5. Table 8 shows the comparison of RMSEs between the original best fit *K* and *n* values versus when *K* was determined from the multiple regression trend from Table 5 with a constant *n* value.

Table 8: Comparison of best fit *K* and *n* RMSEs to RMSEs using K from the Table 5 multiple regression trend with a constant *n* value

	RMSE			
Column	**K and n from Table 4**	**K Using Table 5 with Constant n (n=53.2)**	**|Difference in RMSE|**	**% Difference**
4	13.722	14.118	0.395	2.881
5	14.780	12.383	2.397	16.216
6	16.859	26.233	9.374	55.604
7	10.863	11.869	1.006	9.263
8	12.048	11.188	0.859	7.134
9	12.550	9.752	2.798	22.297
Average	**13.471**	**14.257**	**2.805**	**18.899**

4.4.4 Langmuir Isotherm Fit Lines for Rate Constant Determinations

Figures 42 through 47 show the process of determining the Langmuir rate constants for each column. Because the Langmuir isotherm takes the form of $C_e/q_e = 1/(q_m K_L) + C_e/q_m$, C_e/q_e can be plotted against C_e to determine the Langmuir rate constants q_m and K_L. The intercept for Langmuir isotherms in linear form should always be a positive number. However, for all columns in Figures 42 through 47, the intercepts turned out negative. Instead of abandoning the Langmuir isotherm, force fit plots were created where the RMSE of the fit line to the experimental values would be minimized to obtain the rate constants for each column. These force fit plots are shown in Figures 48 through 53. As with the Freundlich force fit lines, some columns showed nearly flatlines when the RMSEs were minimized.

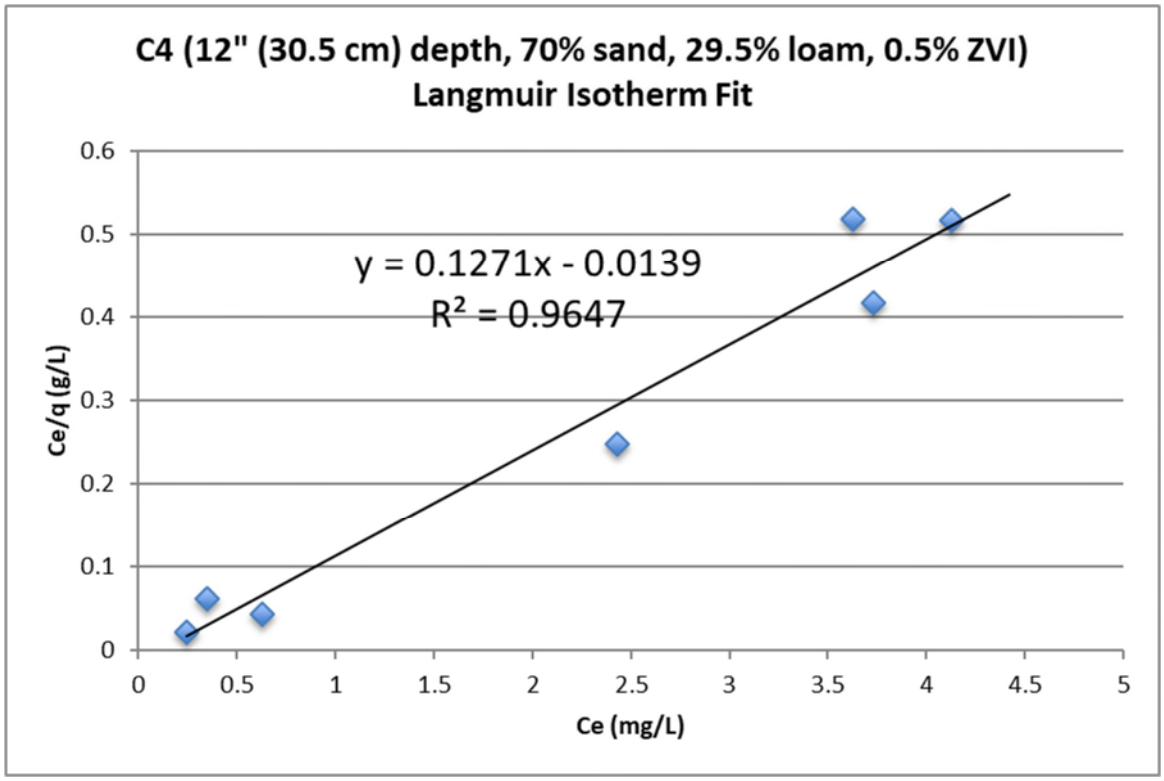

Figure 42: Langmuir isotherm best fit linear function for Column 4

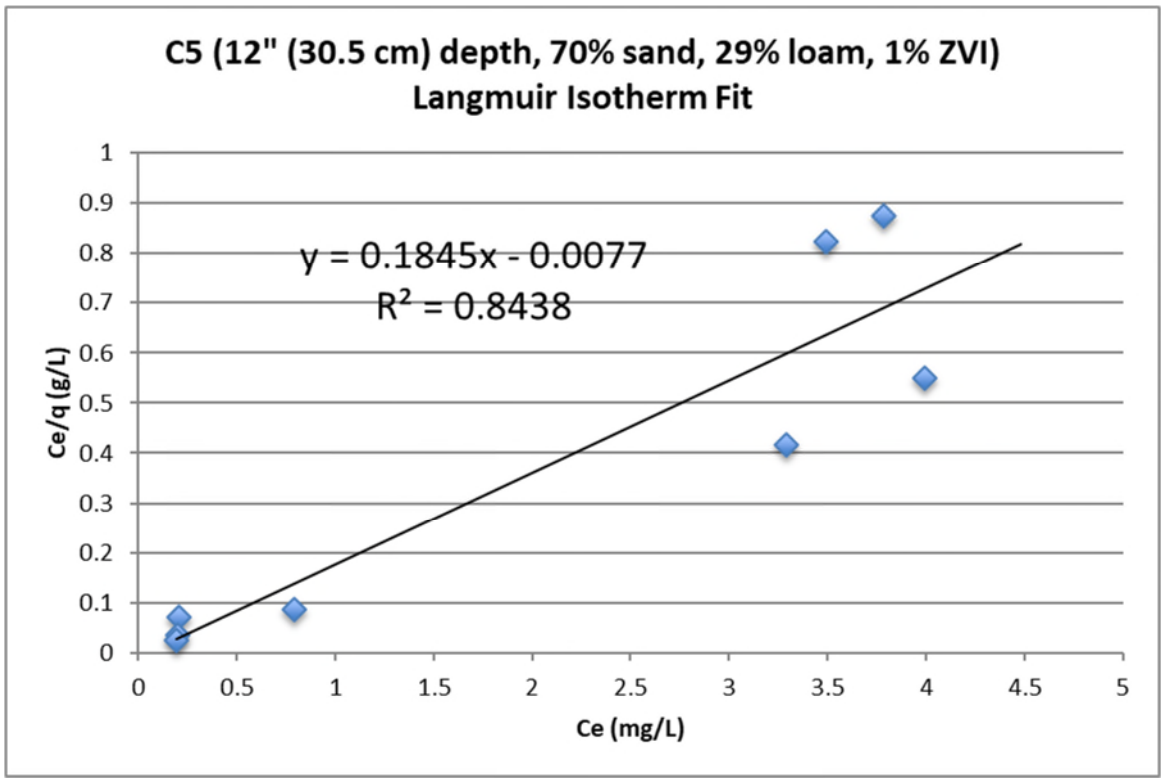

Figure 43: Langmuir isotherm best fit linear function for Column 5

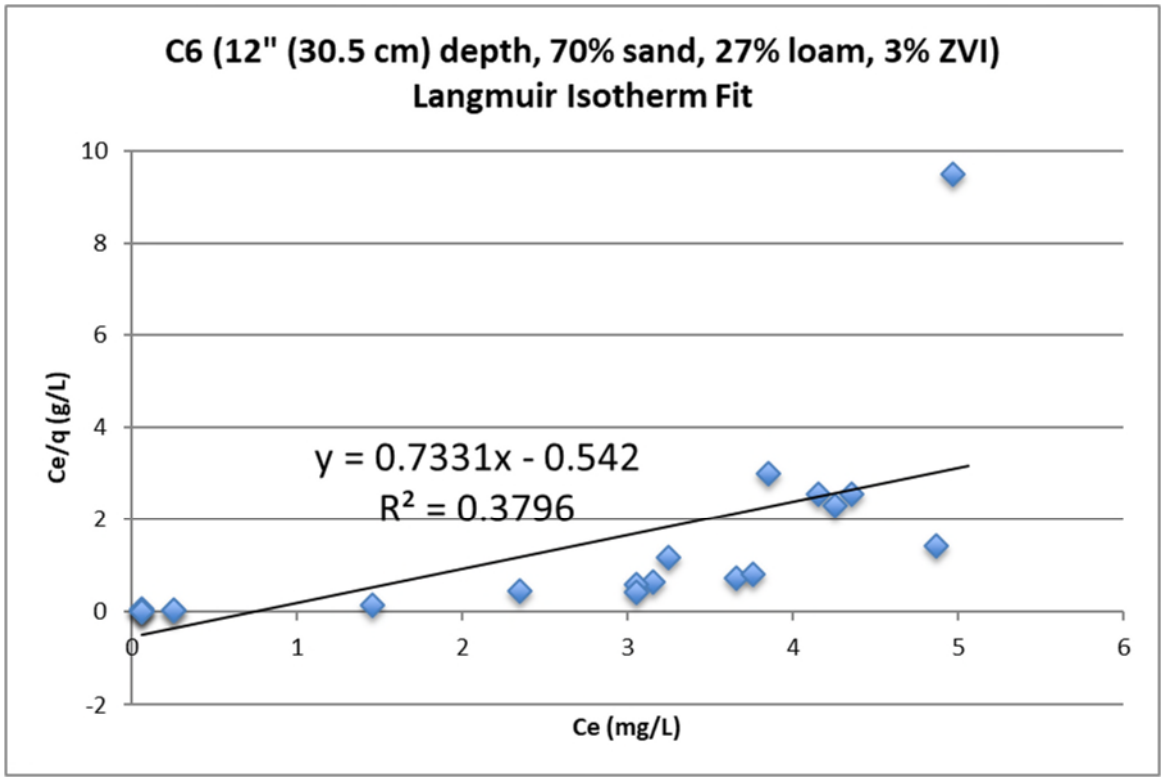

Figure 44: Langmuir isotherm best fit linear function for Column 6

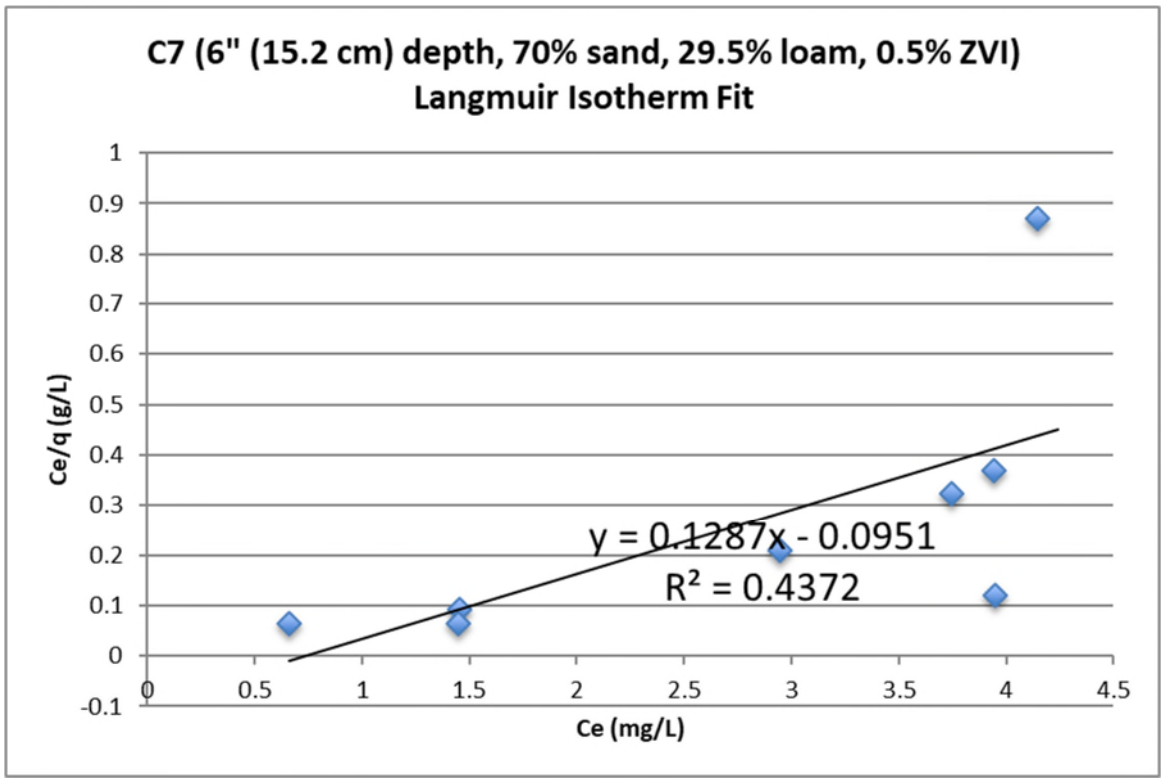

Figure 45: Langmuir isotherm best fit linear function for Column 7

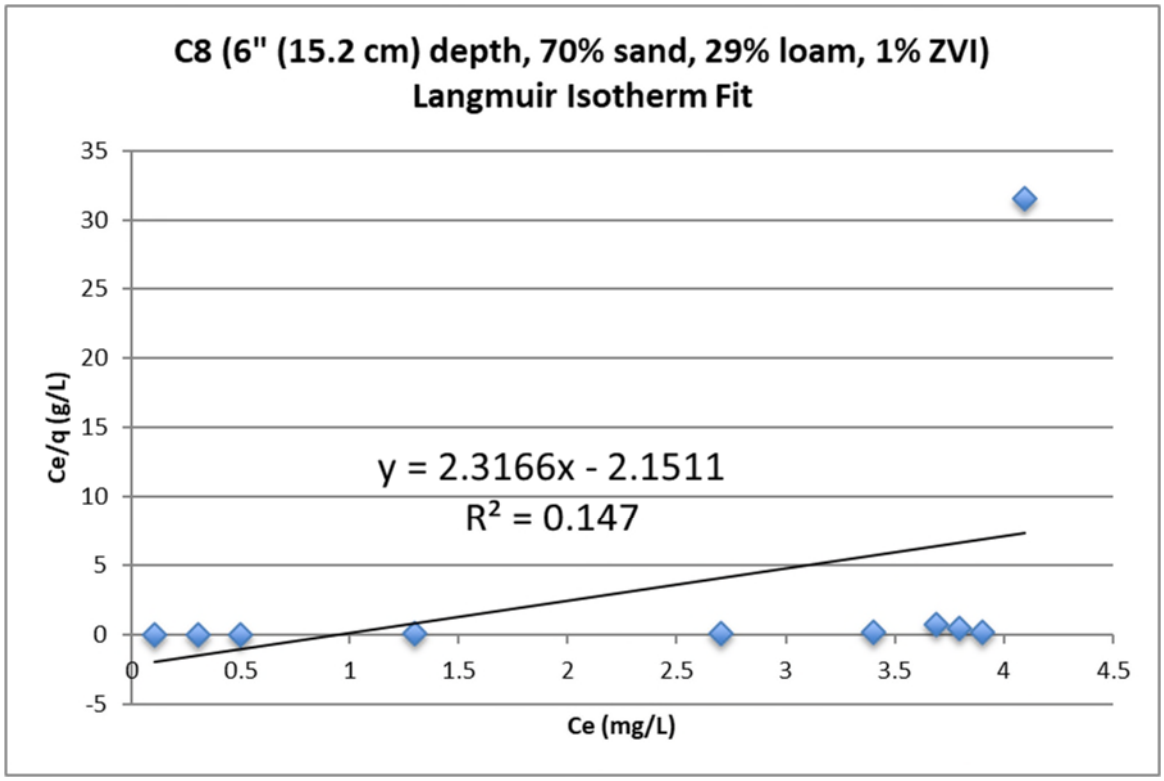

Figure 46: Langmuir isotherm best fit linear function for Column 8

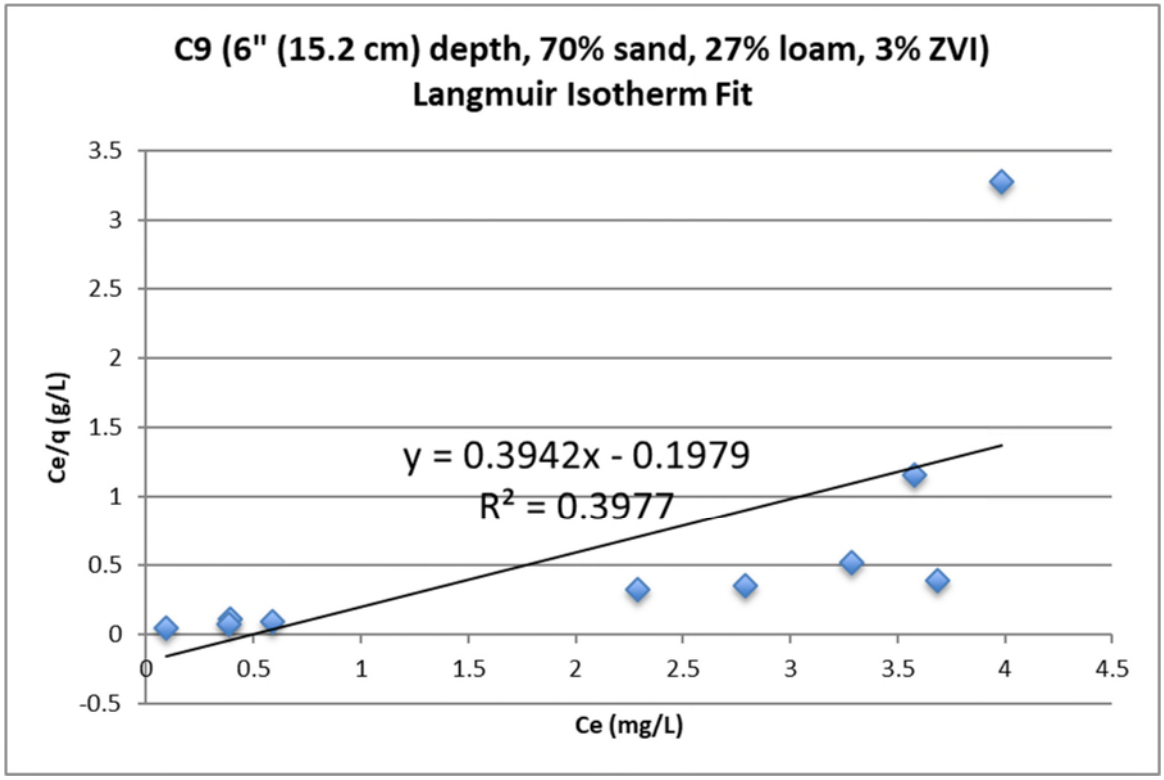

Figure 47: Langmuir isotherm best fit linear function for Column 9

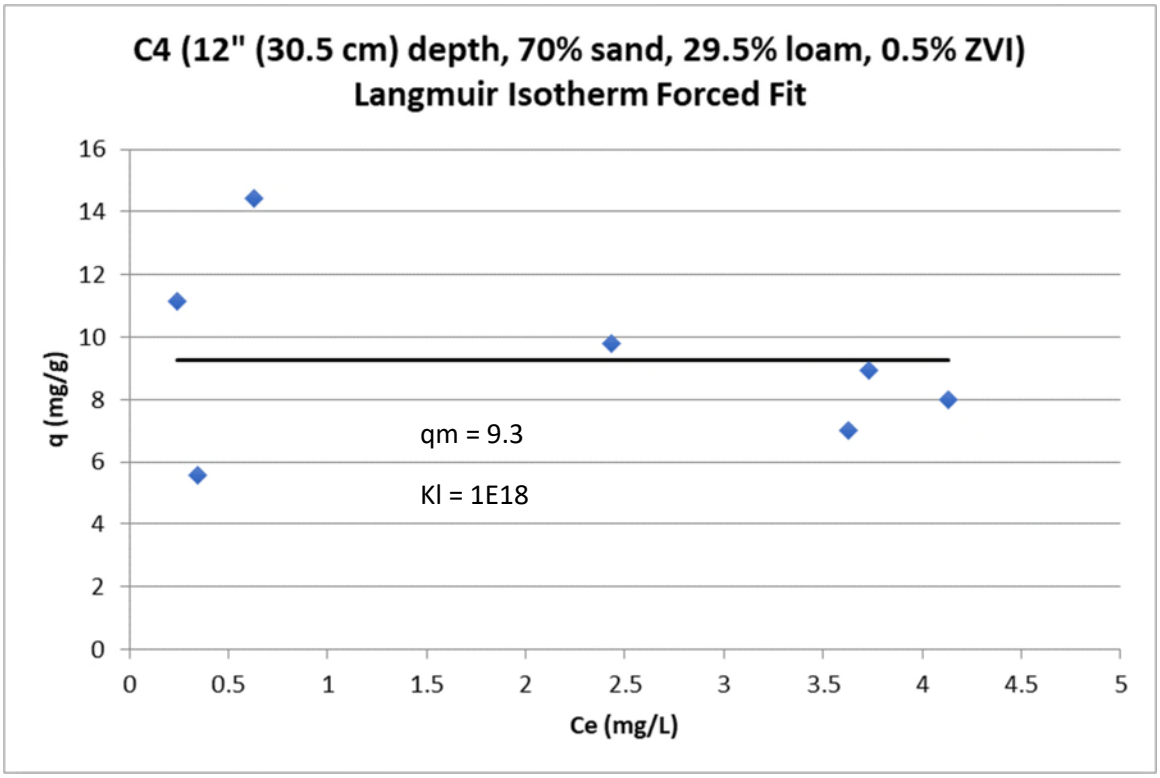

Figure 48: Langmuir isotherm forced fit function minimizing RMSE for Column 4

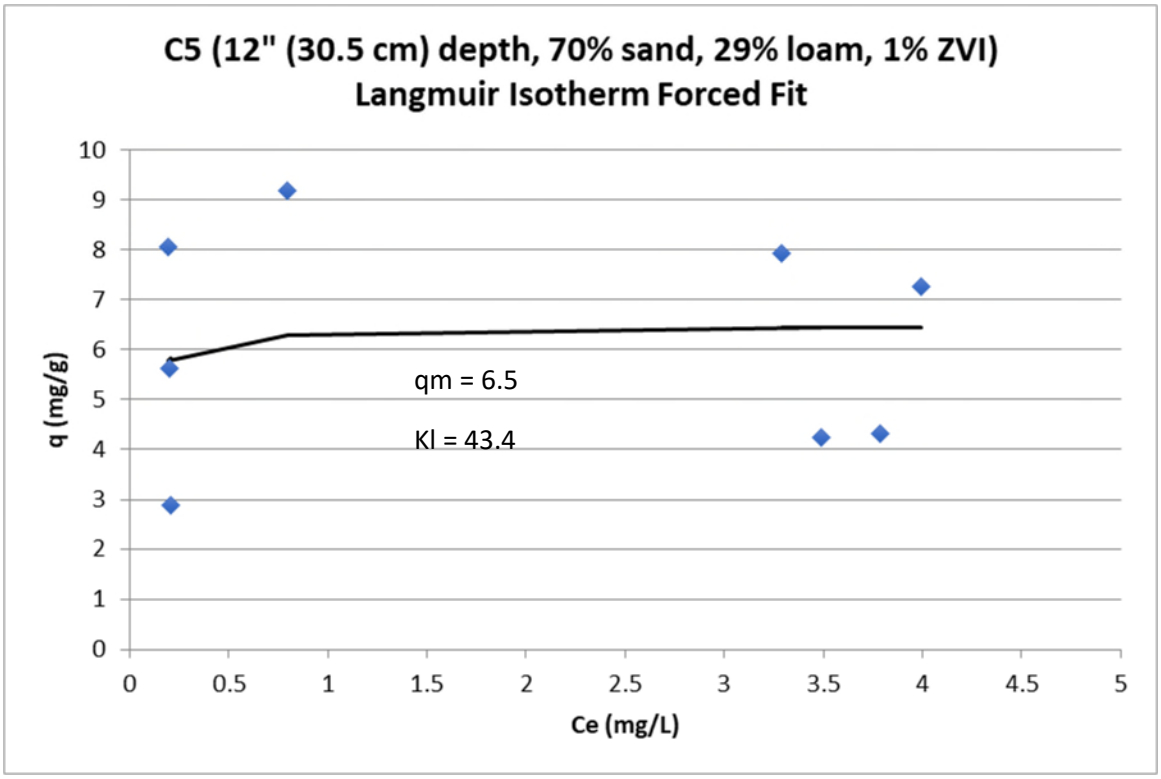

Figure 49: Langmuir isotherm forced fit function minimizing RMSE for Column 5

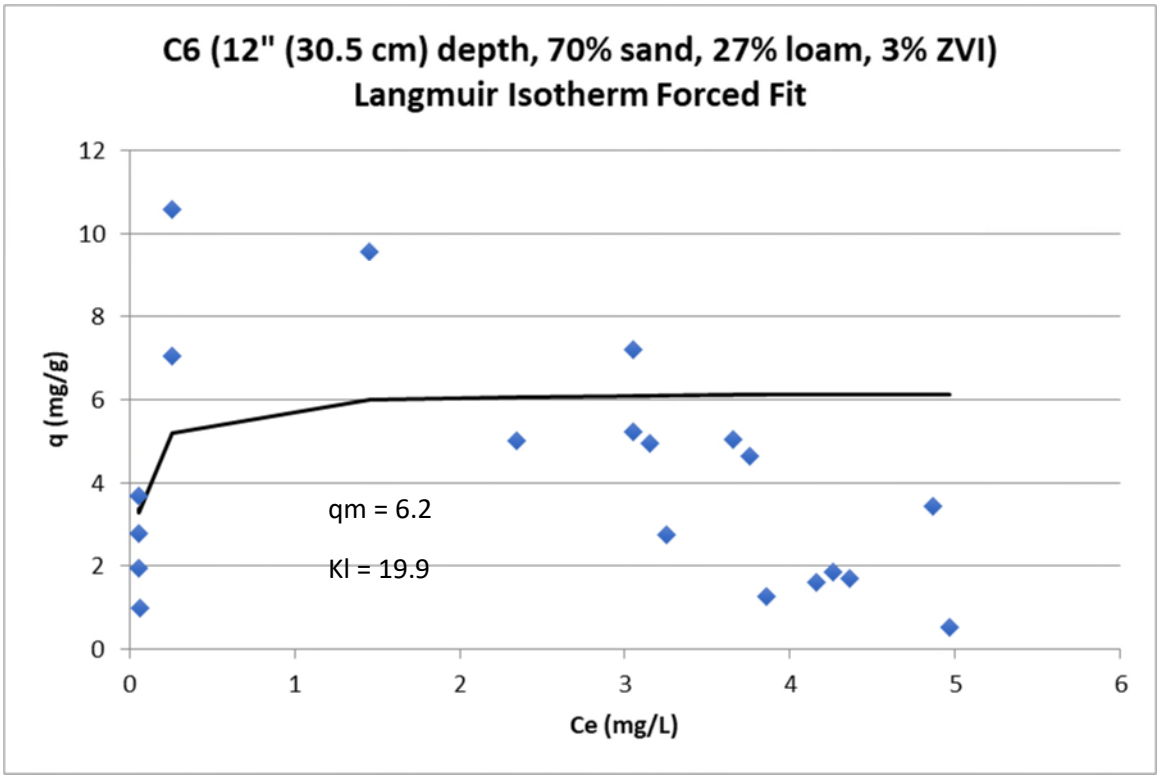

Figure 50: Langmuir isotherm forced fit function minimizing RMSE for Column 6

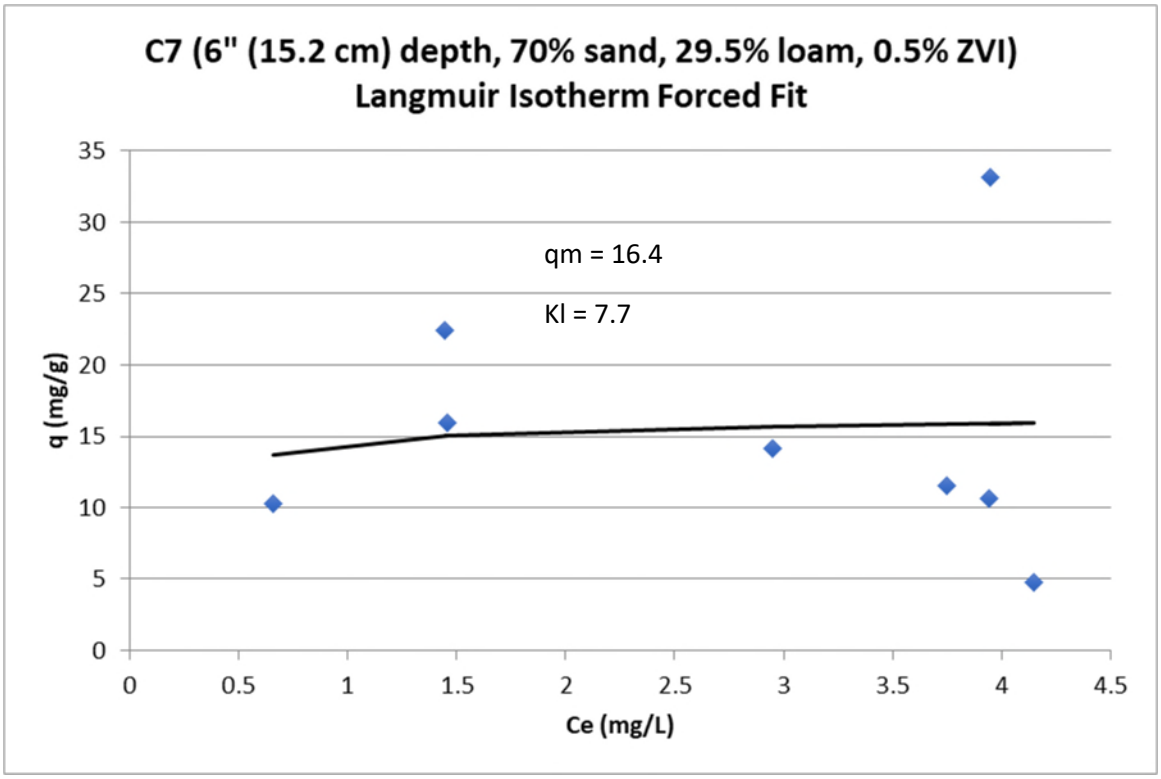

Figure 51: Langmuir isotherm forced fit function minimizing RMSE for Column 7

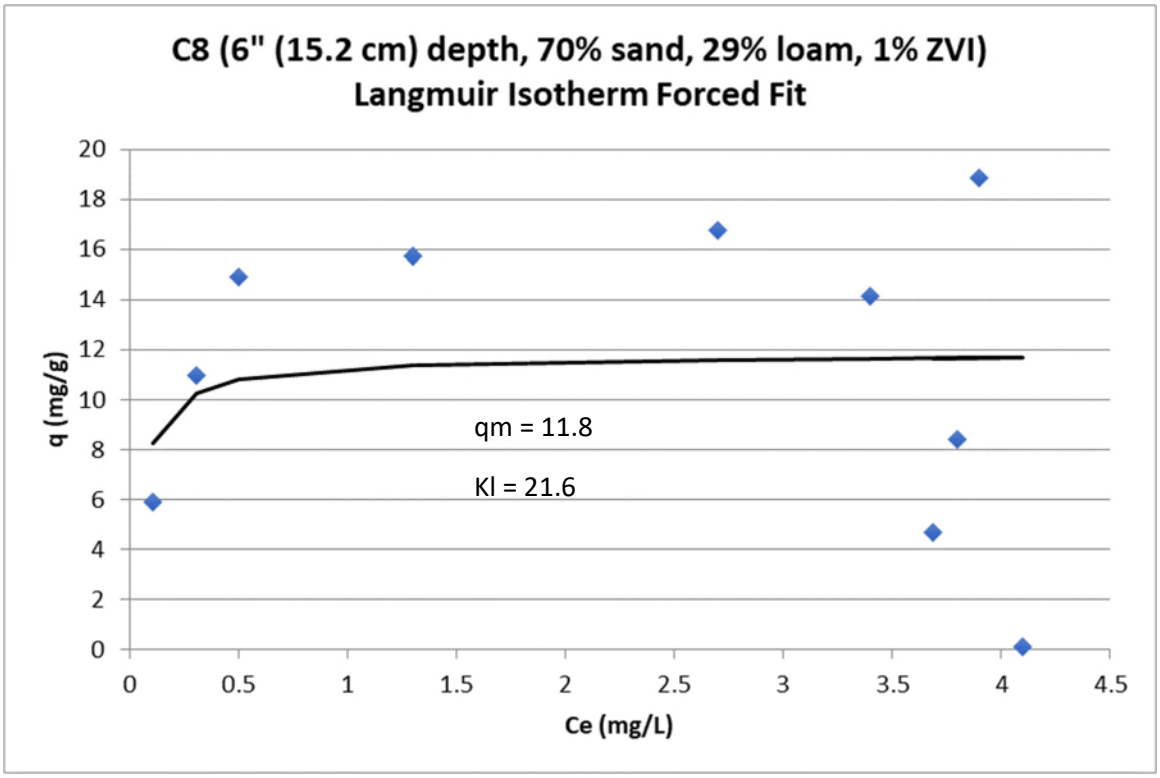

Figure 52: Langmuir isotherm forced fit function minimizing RMSE for Column 8

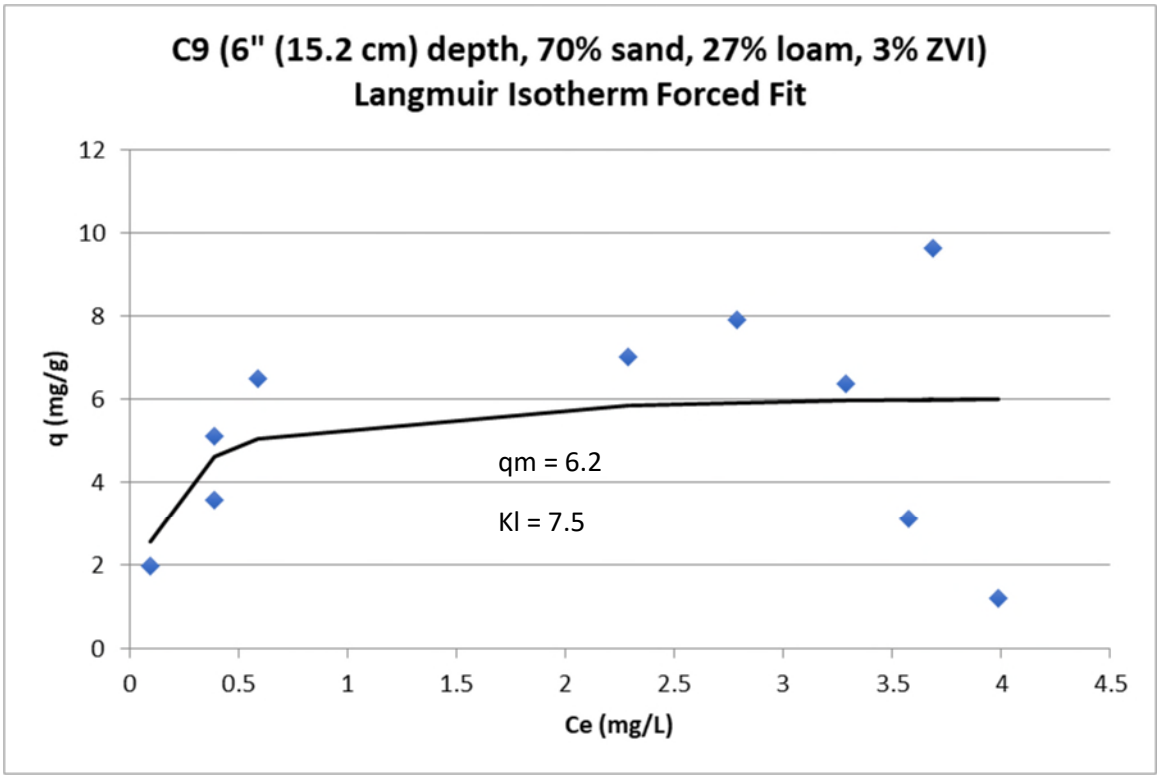

Figure 53: Langmuir isotherm forced fit function minimizing RMSE for Column 9

4.4.5 Langmuir Isotherm Best Fit Percent Removal Lines

Figures 54 through 59 show the difference between the experimental percent removal values and the best-fit Langmuir isotherms using rate constants for each column determined in Figures 48 through 53. The RMSE for each column is shown in these percent removal plots based on the best-fit Langmuir isotherm and the experimental values.

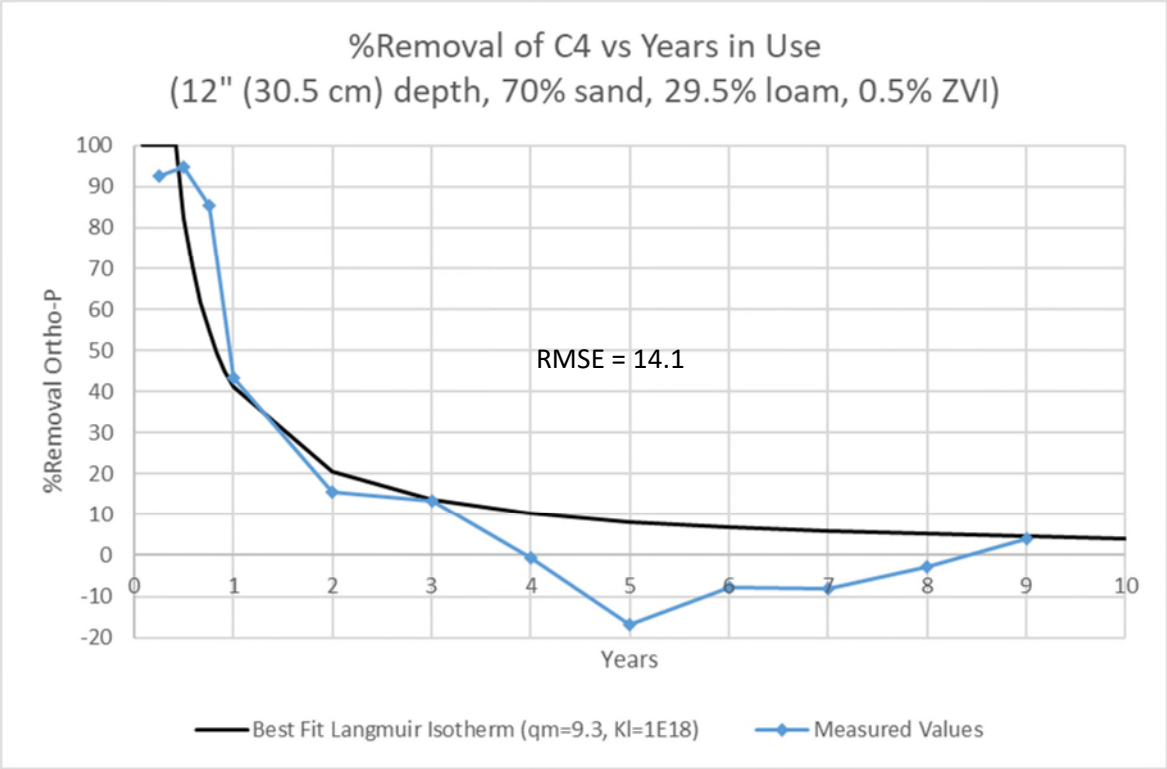

Figure 54: Column 4 comparison of percent ortho-P removal for raw values and values calculated using Langmuir rate constants determined in Figure 48

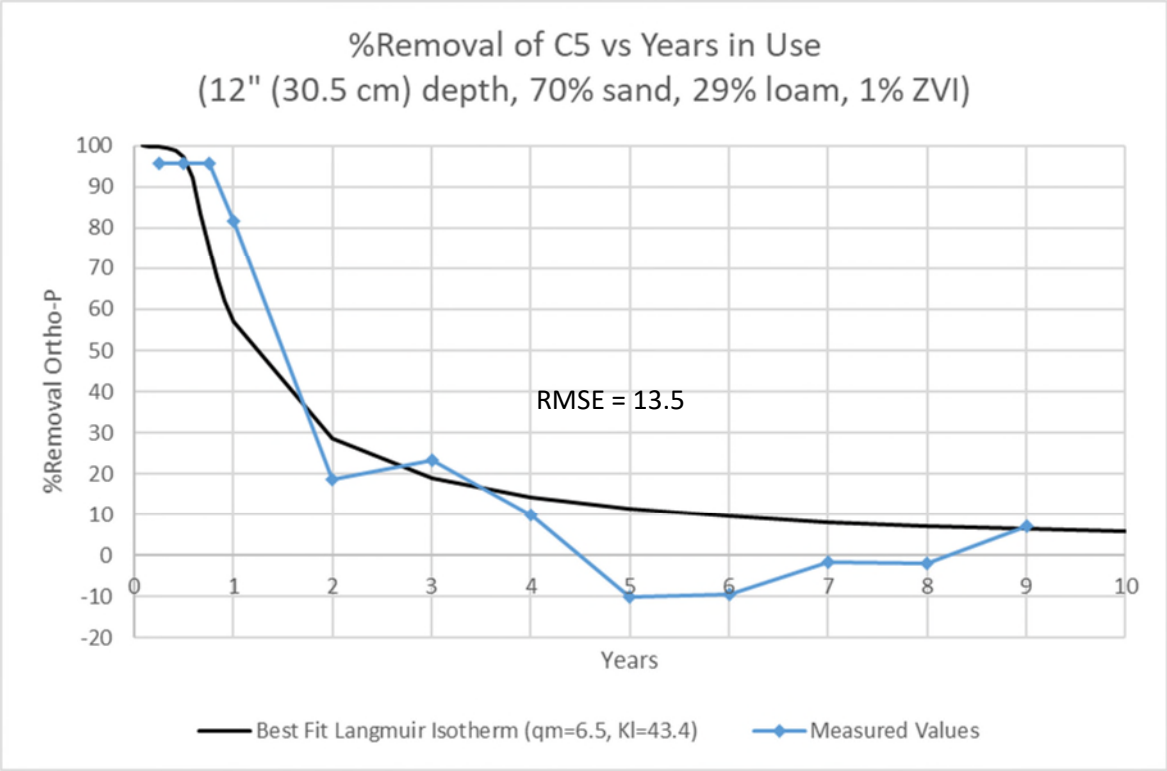

Figure 55: Column 5 comparison of percent ortho-P removal for raw values and values calculated using Langmuir rate constants determined in Figure 49

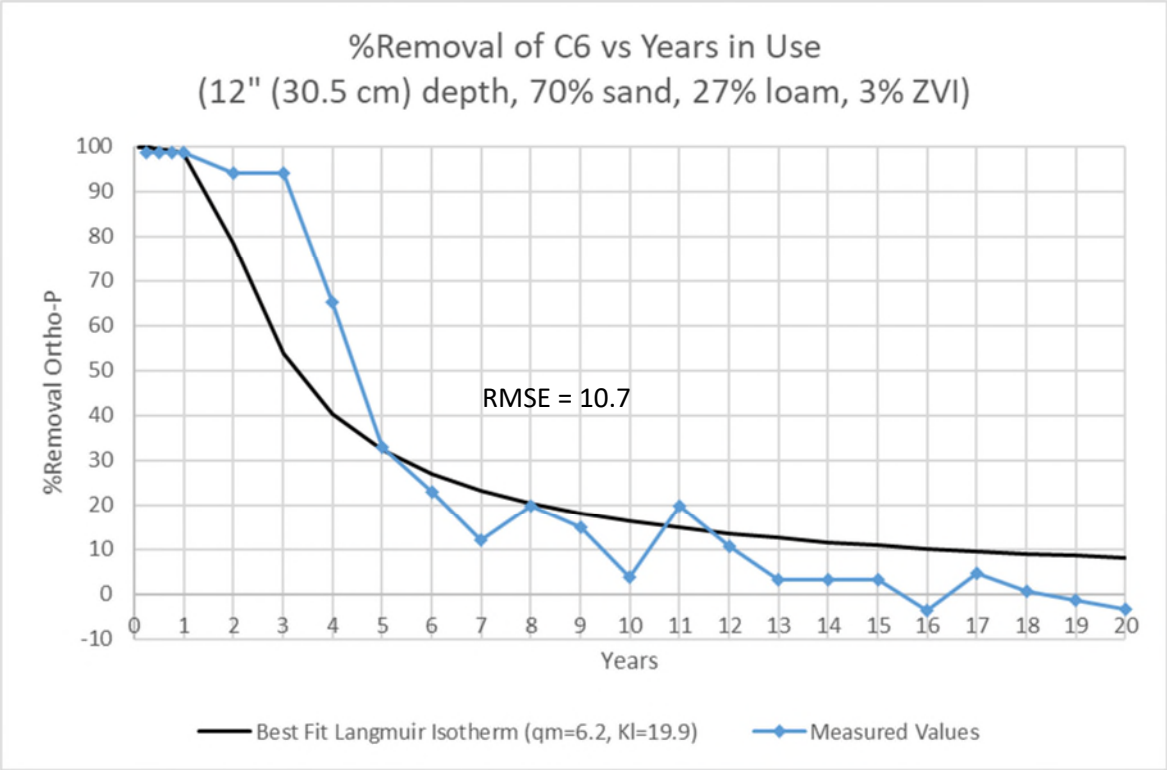

Figure 56: Column 6 comparison of percent ortho-P removal for raw values and values calculated using Langmuir rate constants determined in Figure 50

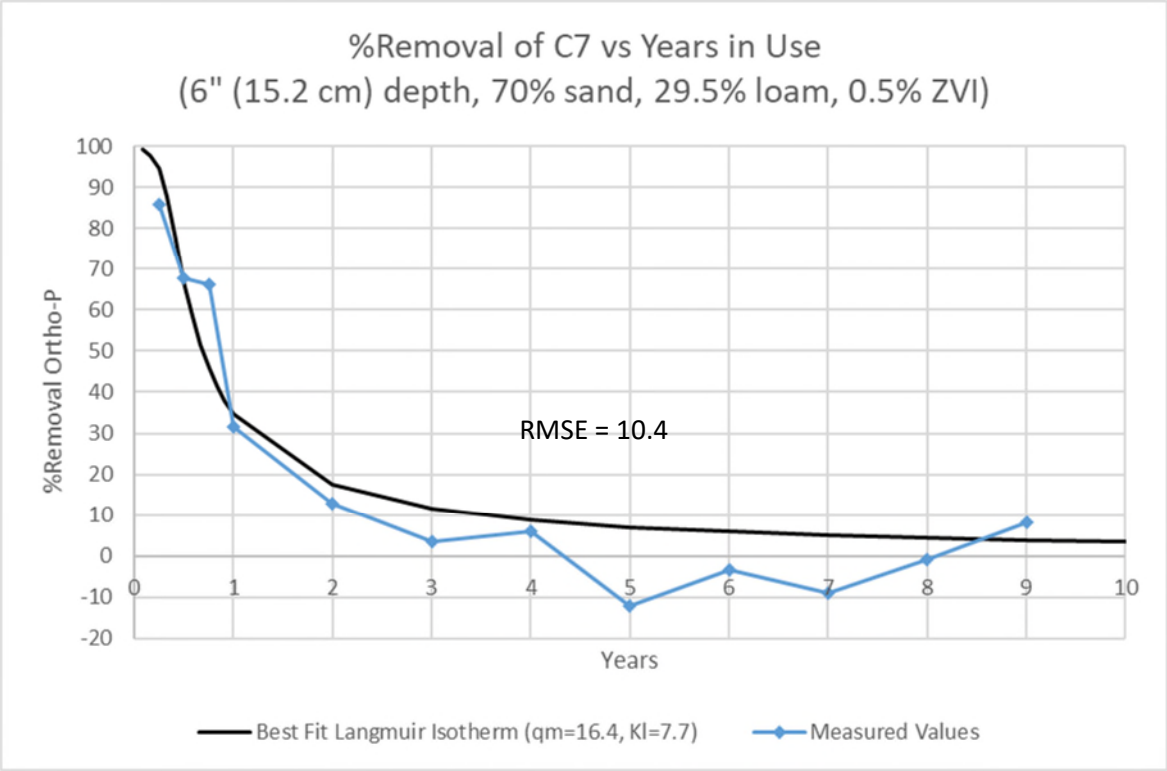

Figure 57: Column 7 comparison of percent ortho-P removal for raw values and values calculated using Langmuir rate constants determined in Figure 51

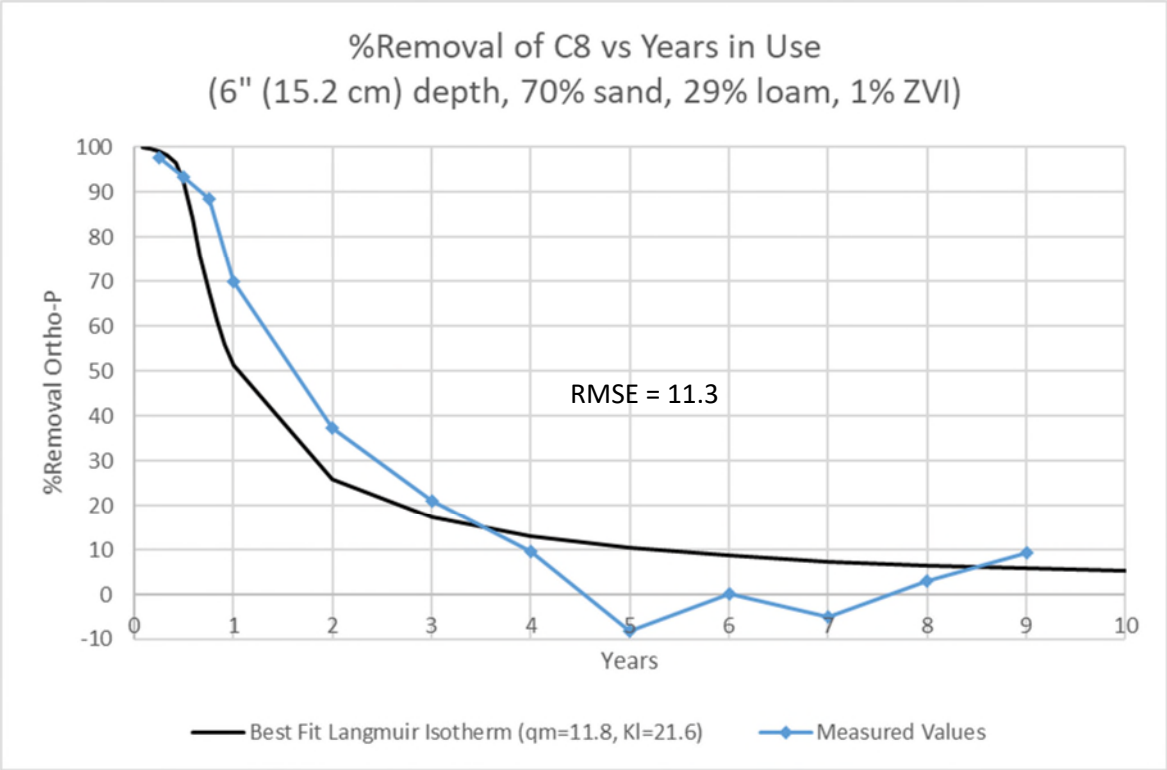

Figure 58: Column 8 comparison of percent ortho-P removal for raw values and values calculated using Langmuir rate constants determined in Figure 52

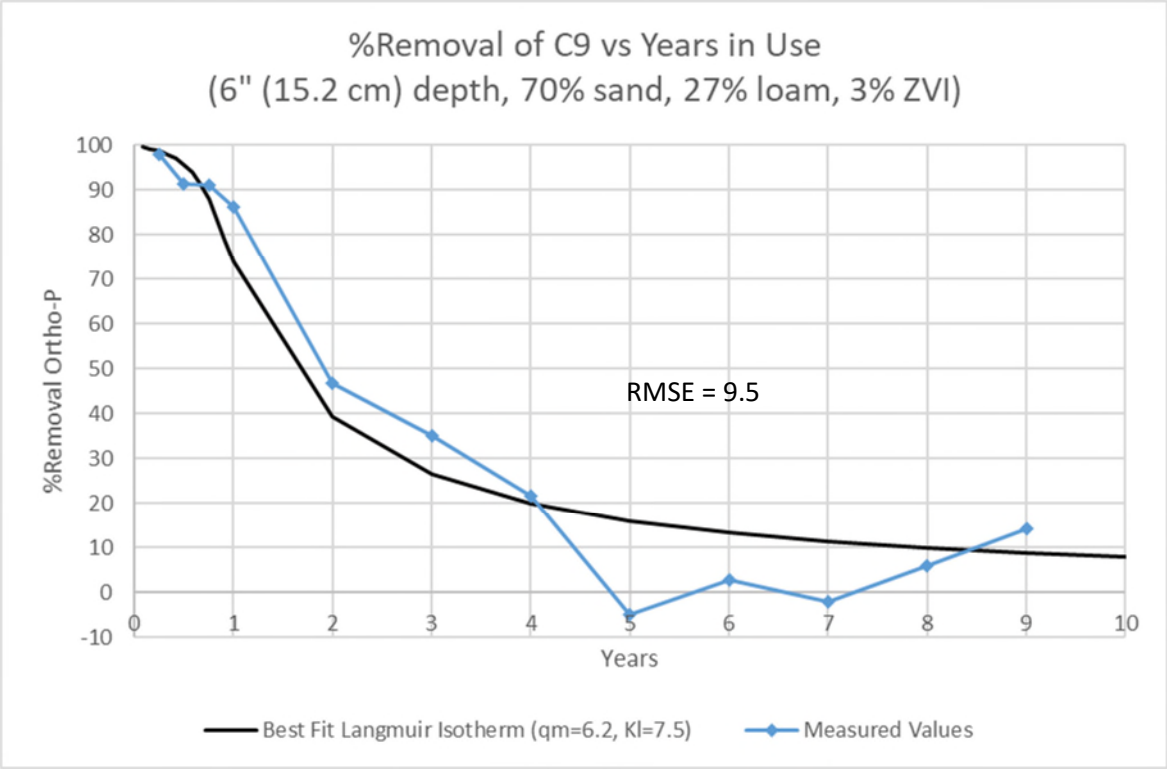

Figure 59: Column 9 comparison of percent ortho-P removal for raw values and values calculated using Langmuir rate constants determined in Figure 53

Table 9 shows a summary of Langmuir constants used in Figures 54 through 59 as well as the associated RMSE for each of these percent removal plots. The average RMSE for these columns was 11.6.

Table 9: Summary of Langmuir constants and RMSE values from percent removal plots

Column	Langmuir qm, Kl	Langmuir RMSE
4	9.3, 1E18	14.1
5	6.5, 43.4	13.5
6	6.2, 19.9	10.7
7	16.4, 7.7	10.4
8	11.8, 21.6	9.5
9	6.2, 7.5	11.6
	Average	**11.6**

Figure 60 shows a synthesis of the Langmuir q_m values determined for each column with a best fit power function. This chart is similar to multiple regression analysis for determining the Freundlich *K* in

that it is useful for predicting the lifespan of ZVI at intermediate ZVI percentages. The shape of the power function shows that higher percentages of ZVI are less efficient in retaining ortho-P. q_m describes the maximum adsorption density of the ZVI. Although these values should technically be relatively constant as the same material was used in all columns, the trend does reflect that of Figure 23 where columns with higher ZVI percentages were shown to be less efficient. It should be reiterated that Langmuir and Freundlich isotherms are only being used as convenient models for lifespan predictions and are not especially accurate when applied to these mixed-media columns. The power function method from Figure 60 was also compared against a multiple regression function shown in Table 10, but it was determined by comparing RMSEs for the columns that the power function was a better fit for the data. Further information on the comparison of these methods is available in Section 4.4.6. Equation 9 shows how the coefficients from the multiple regression analysis can be arranged within an equation to determine q_m.

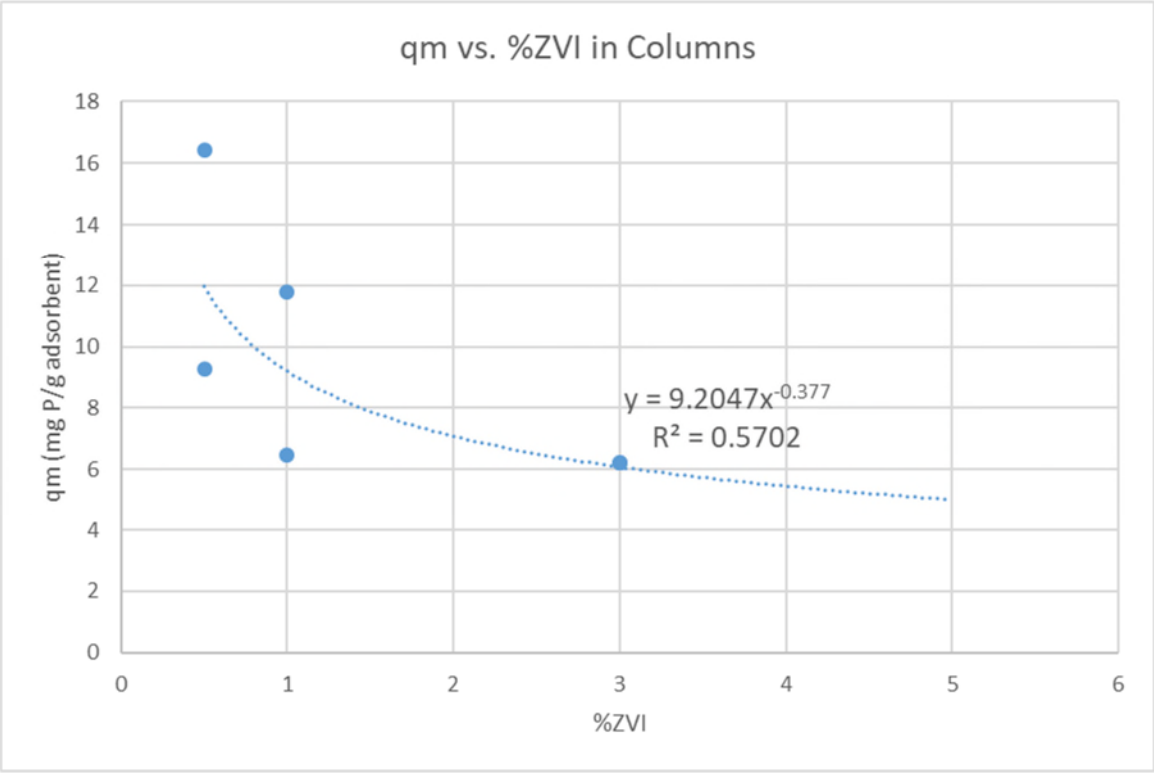

Figure 60: Synthesis of Langmuir "qm" values from each column

Table 10: Multiple regression analysis for q_m based on %ZVI and media depth

Regression Statistics	
Multiple R	0.869775834
R Square	0.756510001
Adjusted R Square	0.594183335
Standard Error	2.608843922
Observations	6

ANOVA

	df	*SS*	*MS*	*F*	*Significance F*
Regression	2	63.43822099	31.7191105	4.660417288	0.120149424
Residual	3	20.41819983	6.806066611		
Total	5	83.85642082			

	Coefficients	*Standard Error*	*t Stat*	*P-value*	*Lower 95%*	*Upper 95%*	*Lower 95.0%*	*Upper 95.0%*
Intercept	19.10012904	3.678465525	5.192417574	0.013874324	7.393610019	30.80664806	7.393610019	30.80664806
% ZVI	-2.316479267	0.986050318	-2.349250565	0.100374091	-5.454531459	0.821572925	-5.454531459	0.821572925
Depth (in)	-0.692227853	0.35501869	-1.949834957	0.146297376	-1.822055773	0.437600067	-1.822055773	0.437600067

$$q_m = (-2.32)(\%ZVI) + (-0.69)(\text{Depth (in)}) + 19.10 \qquad \text{Equation 9}$$

As with the Freundlich *n*, it was determined that the K_L value could be held constant at a median value of 20.7 with little effect on the RMSEs of each column's percent removal plot. The analysis performed to verify this is also shown in Section 4.4.6.

4.4.6 Langmuir Comparison of Methods for q_m and K_L Estimation

Following the same reasoning outlined in Section 4.4.3 for Freundlich *n* values, it was determined that RMSEs should be analyzed when the Langmuir K_L is held constant at the median value for all columns. Figures 113 through 118 in Appendix B.2.1 show the percent removal plots used to compare the RMSEs for a constant K_L versus the original best fit K_L values shown in Table 9. Table 11 shows that the RMSEs for each column are only minimally different when using a constant K_L value, so it was determined that a constant K_L would be used for all further analyses.

Table 11: Comparison of best fit q_m and K_L RMSEs to RMSEs using the best fit q_m with a constant K_L value

	RMSE			
Column	**q_m and K_L from Table 9**	**q_m Using Table 9 with Constant K_L (K_L =20.7)**	**|Difference in RMSE|**	**% Difference**
4	14.091	14.563	0.472	3.350
5	13.487	13.743	0.256	1.901
6	10.708	10.689	0.019	0.173
7	10.362	10.524	0.162	1.565
8	11.256	11.275	0.019	0.171
9	9.536	9.241	0.295	3.090
Average	**11.573**	**11.673**	**0.204**	**1.708**

After it was determined that it was reasonable for K_L to be held constant, different methods for estimating q_m at various ZVI percentages were explored, similar to the Freundlich analysis with *K*. Figure 60 showed a trendline created using q_m values from Table 9 and their corresponding ZVI percentages. Figures 119 through 124 in Appendix B.2.2 show the percent removal plots created to determine the new RMSEs based on q_m values from the Figure 60 trendline. Table 12 shows the comparison of RMSEs between the original best fit q_m and K_L values versus when q_m was determined from the Figure 60 trendline with a constant K_L value.

Table 12: Comparison of best fit q_m and K_L RMSEs to RMSEs using the q_m from the Figure 60 trendline with a constant K_L value

	RMSE			
Column	**q_m and K_L from Table 9**	**q_m Using Figure 60 with Constant K_L (K_L =20.7)**	**|Difference in RMSE|**	**% Difference**
4	14.091	13.142	0.949	6.738
5	13.487	13.379	0.108	0.802
6	10.708	10.980	0.272	2.544
7	10.362	12.607	2.245	21.670
8	11.256	16.190	4.935	43.840
9	9.536	9.301	0.234	2.457
Average	**11.573**	**12.600**	**1.457**	**13.009**

Similar to the Freundlich analysis with *K*, a multiple regression analysis was completed to estimate q_m based on both ZVI percentage and depth of media. Table 10 shows this multiple regression analysis with the coefficients for %ZVI and depth as well as the intercept. Figures 125 through 130 in

Appendix B.2.3 show the percent removal plots created to determine the new RMSEs based on q_m values from the multiple regression trend from Table 10. Table 13 shows the comparison of RMSEs between the original best fit q_m and K_L values versus when q_m was determined from the multiple regression trend from Table 10 with a constant K_L value.

Table 13: Comparison of best fit q_m and n RMSEs to RMSEs using q_m from the Table 10 multiple regression trend with a constant K_L value

	RMSE			
Column	**q_m and K_L from Table 9**	**q_m Using Table 10 with Constant K_L (K_L =20.7)**	**|Difference in RMSE|**	**% Difference**
4	14.091	14.106	0.015	0.103
5	13.487	12.650	0.836	6.201
6	10.708	18.087	7.379	68.910
7	10.362	11.285	0.923	8.912
8	11.256	10.242	1.014	9.012
9	9.536	10.919	1.384	14.509
Average	**11.573**	**12.881**	**1.925**	**17.941**

4.4.7 Freundlich and Langmuir Isotherm Model Comparisons

Table 14 shows a comparison of RMSEs based on the Freundlich and Langmuir isotherms for each column. These RMSEs come from Figures 35 through 40 for the Freundlich isotherms and Figures 54 through 59 for the Langmuir isotherms. The average RMSE across all columns for the Freundlich isotherms was 12.5 compared to an average of 10.1 for the Langmuir isotherms. Almost every RMSE value for the Langmuir isotherm was lower than its corresponding Freundlich isotherm. The Langmuir isotherm was a better fit to the experimental data based on these results. These facts suggest that the Langmuir model should be used when trying to predict the life expectancy of different percentages of ZVI under varying ortho-P and hydraulic loading conditions.

Table 14: RMSE values based on isotherm models using constants found to minimize RMSE for each column

Column	Freundlich K, n	Langmuir qm, Kl	Freundlich RMSE	Langmuir RMSE
4	9.3, 1E18	9.3, 1E18	13.7	14.1
5	5.8, 35.8	6.5, 43.4	14.8	13.5
6	4.1, 1E18	6.2, 19.9	16.9	10.7
7	15.0, 37.5	16.4, 7.7	10.9	10.4
8	11.0, 68.8	11.8, 21.6	12.0	9.5
9	4.3, 8.0	6.2, 7.5	12.6	11.6
		Average	**13.5**	**11.6**

Although the Langmuir isotherm was a better fit for the data using its best fit constants, it was important to compare the RMSEs from the percent removal plots of both Freundlich and Langmuir isotherms using the trendlines and assumptions for constants that would exist in the longevity prediction spreadsheet. Table 15 shows a summary of RMSEs from the various methods discussed in Sections 4.4.3 and 4.4.6 that were used to estimate the Freundlich *K* and the Langmuir q_m. After comparing the average RMSE among all methods, it was determined that the Langmuir isotherm would be the best option for use in the ZVI longevity prediction tool. The better method of the two tested for estimating q_m was shown to be the power function from Figure 60. This conclusion was again based on the average RMSE across all columns.

Table 15: Synthesis of RMSE values from Tables 8, 11, 12, and 13

	Freundlich RMSE		**Langmuir RMSE**	
Column	**K from Figure 41 with Constant n (n=53.2)**	**K Using Table 5 with Constant n (n=53.2)**	**q_m Using Figure 60 with Constant K_L (K_L =20.7)**	**q_m Using Table 10 with Constant K_L (K_L =20.7)**
4	13.340	14.118	13.142	14.106
5	12.465	12.383	13.379	12.650
6	16.202	26.233	10.980	18.087
7	12.822	11.869	12.607	11.285
8	18.610	11.188	16.190	10.242
9	13.960	9.752	9.301	10.919
Average	**14.567**	**14.257**	**12.600**	**12.881**

4.4.8 ZVI Longevity Prediction Spreadsheet

Eight out of the nine columns in this study had less than ten total effluent data points to use when creating a prediction model. The small sample sizes and lack of replicated testing for each column would make the statistical verification of any new prediction model almost impossible. Therefore, a ZVI lifespan prediction tool was created using a widely accepted method for fitting adsorption data. Because it was shown in Tables 14 and Table 15 that the Langmuir isotherm was more favorable than the Freundlich isotherm, a ZVI longevity prediction spreadsheet was created using the Langmuir isotherm as the foundation. As previously discussed, the basis for using the isotherms was to find best fit curves for the data that still retained physical meaning.

Figure 61 shows sample input and output values for the ZVI lifespan prediction tool. This lifespan prediction tool can be accessed through the UNH Stormwater Center website (www.unh.edu/unhsc/). The **%ZVI** and **Depth of ZVI Amended Media** parameters are directly related to the total mass of ZVI being used to treat the predicted runoff. These parameters may be chosen to best fit the site being modeled. The watershed to filter area ratio and average annual rainfall are used to determine the volume of water treated during each simulated year. The **Expected Median Influent Ortho-P Concentration** is the concentration chosen that would best represent the site in question over a long period of time. The prediction calculations assume that there is roughly 70% sand and 30% loam in the treatment system that is being simulated.

Input Parameters

%ZVI (0.5-5)	3				
Watershed Area:Filter Area Ratio	100				
Average Annual Rainfall	40	inches	**or**		cm
Depth of ZVI-Amended Media		inches	**or**	30.5	cm
Average Influent PO_4^{3-}-P Concentration (mg/L)	0.8				
Acceptable Percent Removal (%)	20				

DETERMINE LIFESPAN

Figure 61: Input parameters for determining the expected lifespan of ZVI

Figure 62 displays a curve predicting the removal efficiency of ZVI at the end of each year based on the input parameters shown in Figure 61. The "Expected Lifespan" shown in Figure 61 is represented in Figure 62 by the vertical orange line. This expected lifespan is completely dependent upon what the user deems an acceptable ortho-P percentage. In this case, the chosen **Acceptable Removal Efficiency** was 20%, which would correspond to 5.8 years of useful ZVI life. Each user would need to determine their target effluent concentration, possibly based on regulations, and then calculate the percent removal that their system must maintain to continue meeting this requirement. If the user's land was under strict effluent concentration regulations, the **Expected Median Influent Ortho-P Concentration** would be best chosen based on testing performed at the site. If the user was simply trying to employ a ZVI-amended treatment system as a best management practice and was not subject to regulations, a reasonable ortho-P concentration could be estimated using information from Section 2.1.3 of this thesis.

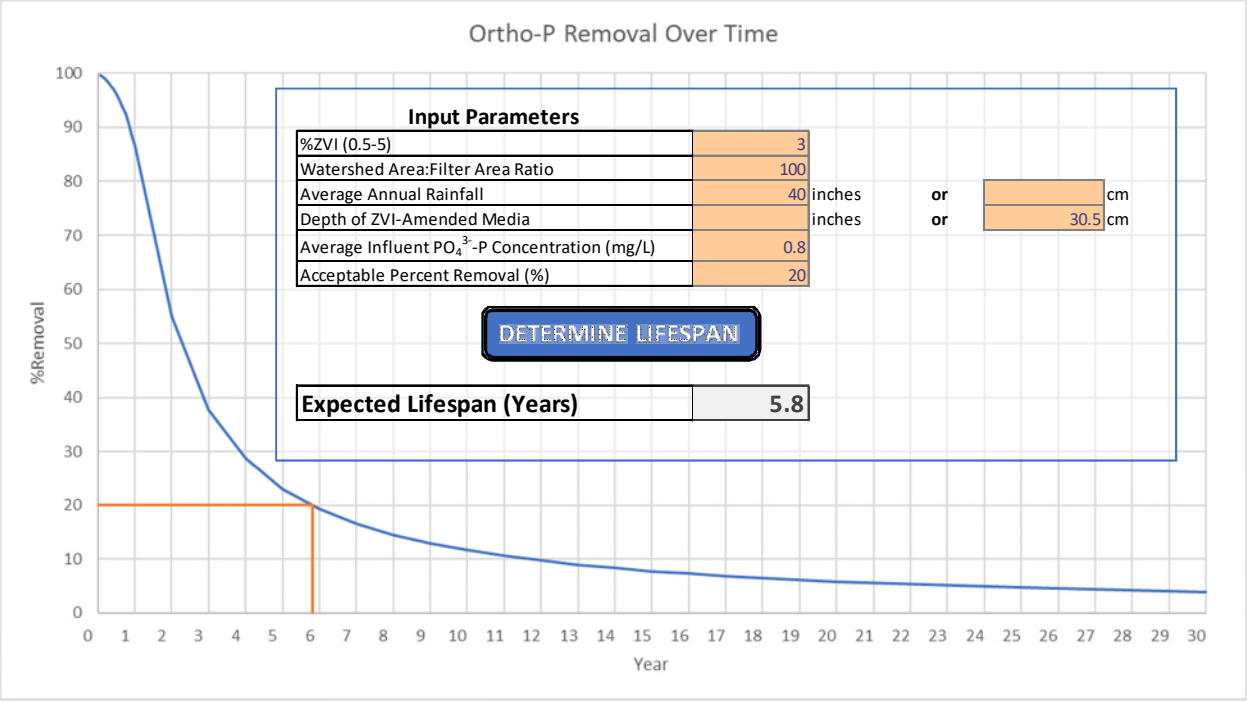

Figure 62: Predicted percent ortho-P removal over time using Langmuir isotherm

Although the accuracy of this prediction tool has not been verified through field testing, it is extremely useful for those with limited knowledge of adsorption kinetics to see how various factors may affect ZVI removal efficiency in a prospective treatment system. Due to the form of the Langmuir isotherm equation, solving for the effluent concentration for each year requires an iterative process. Even for those familiar with the Langmuir isotherm, the results shown in the prediction tool would require painstaking calculations if done by hand or other methods. The tool allows for predictions to be made quickly and clearly while allowing the input parameters to be changed at the user's discretion.

The column study used to create this prediction tool was exclusively focused on ortho-P removal from runoff. With only tap water mixed with KH_2PO_4 being used, there was little opportunity for chemicals to compete for ZVI adsorption sites. In agricultural runoff, and any other types runoff for that matter, there will be chemicals (e.g. DOC) that could adsorb to the ZVI and lower its removal efficiency with respect to ortho-P. The lack of laboratory and field data on this adsorption competition makes it difficult to incorporate into the lifespan prediction tool. Some other factors that could potentially affect ortho-P adsorption are pH, wetting and drying cycle of the media, hydraulic conductivity and contact time, particle size distribution of ZVI, differences in loam makeup, and temperature of runoff. Many of these factors would vary by site, and the scope of this column study did not allow for a full analysis of how differences in these variables could specifically affect ZVI lifespan.

Contact time could have had a significant effect on the removals from this study, but the dispenser setup did not allow for accurate monitoring of flows. Furthermore, contact time could have been estimated based on measured hydraulic conductivities, but these hydraulic conductivities clearly changed throughout testing. This change in hydraulic conductivity was what made the remixing of media necessary. Hydraulic conductivity tests were not performed before ortho-P testing was complete for fear of skewing results.

Similar to contact time, resting time could not be accurately be monitored due to columns finishing their yearly tests at different times. Often these columns would finish their tests while the laboratory was not being monitored, so a true estimation of time between tests could not be determined. It is also likely that the lack of resting time within each year of simulated runoff negatively affected the removals. The ZVI performs best when it rusts and is under aerobic conditions, but the continuous testing within each year of simulated runoff did not provide as much opportunity for interaction with the air. Under normal conditions, the ZVI would be exposed to many wetting and drying cycles throughout the span of one year.

4.4.9 ZVI Longevity Prediction Underlying Calculations

Table 16 shows the calculations being performed in the background of the spreadsheet when the "Determine Lifespan" button is selected. C_0 and M_{ad} are chosen by the user in the spreadsheet where C_0 is the **Average Influent PO_4^{3-}-P Concentration** and M_{ad} is determined from the **%ZVI** and **Depth of ZVI Amended Media**. The user can use field data collected for certain land to estimate the influent concentration or use the range of values shown in Figure 1 to choose a reasonable influent concentration. The model runs based on the assumption that the influent concentration will remain constant over the lifespan of the system. The volume treated is also chosen by the user when they input values for the **Average Annual Rainfall** and **Watershed Area:Filter Area Ratio**. This yearly volume is calculated by multiplying **Average Annual Rainfall** and **Watershed Area:Filter Area Ratio** by the cross sectional area of a column. The objective of these calculations is to find C_e, which can then easily be used to find a percent removal using Equation 7. q_m is determined by the power function dependent on ZVI percentage as shown in Figure 60 while K_L is held constant at 20.7 as previously discussed in Section 4.4.7. Because C_e is on both sides of the equation for the Langmuir isotherm as shown in Equation 4, the equation must be solved for C_e using iterations. The spreadsheet will run these iterations using the Solver add-in within a macro activated by the "Determine Lifespan" button. These iterations will be

performed until the values in Column J of Table 16 are all minimized. Once these values are minimized, it essentially means that both sides of the Langmuir equation are equal and the correct value for C_e was determined. The spreadsheet calculates C_e at volumes that correspond to the treatment time (i.e. Year 1, Year 2, Year 3, etc.). Once C_e has been calculated at each of these points, the percent removal can be calculated as previously discussed. Because it is assumed in these calculations that the proposed treatment system would include roughly 30% loam, the loam effect is added back in and slightly boosts the percent removal. This addition is not displayed in Table 16, but it is reflected in the tool's prediction plot and "Expected Lifespan" prediction. The total loam effect for each column can be determined by dividing the cumulative mass of ortho-P retained by that column by the mass retained by its corresponding control column (see Figure 24). The total loam effect on removal percentage is determined using the multiple regression analysis coefficients shown in Table 17. Equation 10 shows how the coefficients from the multiple regression analysis can be arranged within an equation to determine the total loam effect percentage. Once the total loam effect percentage is determined, this percentage is divided equally among the data points encompassing the projected system lifespan and is added to each value in column K of Table 16. The lifespan of ZVI can then easily be determined based on these removal percentages. Although the acceptable removal threshold set by many agencies is 85%, the tool allows the user to choose any percent removal they believe will best correspond to the useful life of the media.

Table 16: Langmuir isotherm background calculations for longevity prediction tool

A	B	C	D	E	F	G	H	I	J	K
Year	V (L)	C_0 (mg/L)	C_e (mg/L)	M_{ad} (g)	q_e (mg/g)	1/(qmKL)	C_e/q_m	C_e/q_e	$\lvert[1/(q_mK_L)+C_e/q_m]-C_e/q_e\rvert$	%Removal
1/12	1.3803	4.3	0.002613	18.96	0.3128634	0.0079238	0.00043	0.00835345	5.54031E-12	99.93922117
2/12	2.7607	4.3	0.005522	18.96	0.6253032	0.0079238	0.000908	0.00883165	1.28736E-13	99.87157075
3/12	4.141	4.3	0.008779	18.96	0.9372435	0.0079238	0.001443	0.00936701	3.64351E-13	99.79583338
4/12	5.5214	4.3	0.012449	18.96	1.2485894	0.0079238	0.002046	0.00997023	1.19166E-12	99.71049482
5/12	6.9017	4.3	0.016613	18.96	1.5592208	0.0079238	0.002731	0.01065481	6.80444E-13	99.61364639
6/12	8.2821	4.3	0.021377	18.96	1.8689838	0.0079238	0.003514	0.01143798	4.17545E-12	99.50285117
7/12	9.6624	4.3	0.026877	18.96	2.1776784	0.0079238	0.004418	0.01234204	8.53827E-13	99.37495387
8/12	11.043	4.3	0.03329	18.96	2.48504	0.0079238	0.005472	0.0133963	7.55698E-14	99.22580581
9/12	12.423	4.3	0.040856	18.96	2.7907128	0.0079238	0.006716	0.01463999	3.01051E-13	99.04986003
10/12	13.803	4.3	0.049899	18.96	3.0942086	0.0079238	0.008203	0.01612649	4.19838E-14	98.83956468
11/12	15.184	4.3	0.060869	18.96	3.394844	0.0079238	0.010006	0.01792987	4.8295E-13	98.58443956
1	16.564	4.3	0.074405	18.96	3.6916408	0.0079238	0.012231	0.02015496	4.17069E-13	98.26965427
2	33.128	4.3	0.981434	18.96	5.7984519	0.0079238	0.161334	0.16925788	1.68993E-12	77.17596118
3	49.693	4.3	2.032727	18.96	5.9423277	0.0079238	0.334152	0.34207591	1.13213E-11	52.72727541
4	66.257	4.3	2.591016	18.96	5.9721356	0.0079238	0.425927	0.43385076	9.5296E-13	39.7438243
5	82.821	4.3	2.929918	18.96	5.984779	0.0079238	0.481638	0.48956161	6.90725E-13	31.86237141
6	99.385	4.3	3.156935	18.96	5.9917528	0.0079238	0.518956	0.52687998	3.59912E-12	26.58291633
7	115.95	4.3	3.319507	18.96	5.9961693	0.0079238	0.545681	0.5536047	9.88432E-13	22.80215162
8	132.51	4.3	3.441633	18.96	5.9992163	0.0079238	0.565757	0.57368045	8.23541E-12	19.96202137
9	149.08	4.3	3.536724	18.96	6.001445	0.0079238	0.581388	0.58931203	3.37319E-12	17.75061096
10	165.64	4.3	3.612857	18.96	6.0031459	0.0079238	0.593903	0.60182722	5.08593E-13	15.9800777
11	182.21	4.3	3.675185	18.96	6.0044867	0.0079238	0.604149	0.61207309	2.91318E-11	14.53058789
12	198.77	4.3	3.727149	18.96	6.0055706	0.0079238	0.612692	0.62061534	5.70566E-12	13.32211013
13	215.33	4.3	3.771136	18.96	6.0064651	0.0079238	0.619922	0.62784614	4.3535E-11	12.29916405
14	231.9	4.3	3.808851	18.96	6.0072159	0.0079238	0.626122	0.6340459	6.16012E-11	11.42207973
15	248.46	4.3	3.841545	18.96	6.0078549	0.0079238	0.631497	0.63942042	1.26865E-12	10.66174174
16	265.03	4.3	3.870159	18.96	6.0084054	0.0079238	0.6362	0.64412418	1.55431E-14	9.996298762
17	281.59	4.3	3.895412	18.96	6.0088846	0.0079238	0.640352	0.64827533	9.33897E-12	9.409031534
18	298.16	4.3	3.917862	18.96	6.0093054	0.0079238	0.644042	0.65196586	2.95097E-13	8.886930006
19	314.72	4.3	3.937952	18.96	6.0096781	0.0079238	0.647345	0.65526839	4.00058E-12	8.419718906
20	331.28	4.3	3.956035	18.96	6.0100103	0.0079238	0.650317	0.65824105	3.50775E-12	7.999175122
25	414.1	4.3	4.024772	18.96	6.0112461	0.0079238	0.661617	0.66954034	9.86822E-12	6.400655989
30	496.93	4.3	4.07061	18.96	6.0121152	0.0079238	0.669152	0.67706786	7.64578E-06	5.334651163

Table 17: Total loam effect multiple regression analysis

SUMMARY OUTPUT

Regression Statistics	
Multiple R	0.929526951
R Square	0.864020353
Adjusted R Square	0.773367255
Standard Error	7.49680458
Observations	6

ANOVA

	df	*SS*	*MS*	*F*	*Significance F*
Regression	2	1071.331068	535.6655338	9.531062625	0.050143063
Residual	3	168.6062367	56.20207891		
Total	5	1239.937304			

	Coefficients	*Standard Error*	*t Stat*	*P-value*	*Lower 95%*	*Upper 95%*	*Lower 90.0%*	*Upper 90.0%*
Intercept	26.78553348	10.5704818	2.533993624	0.085125796	-6.854457266	60.42552422	1.909348126	51.66171883
%ZVI	-9.078471263	2.833525792	-3.203948694	0.049183098	-18.09601495	-0.060927574	-15.74678725	-2.410155272
Depth (in)	3.025816646	1.020185885	2.965946394	0.059260443	-0.220870153	6.272503445	0.624948488	5.426684803

Total Loam Effect % = (-9.08)(%ZVI) + (3.02)(Depth (in)) + 26.79 Equation 10

4.5 Longevity Prediction Comparison to Similar Studies

Erickson et al. (February 23, 2010) estimated that sand filtration systems with 5% iron filings could remove at least 80% ortho-P for more than thirty years. Similarly, it was estimated that a 2% ZVI system could remove at least 80% ortho-P for roughly fifteen years and a 0.3% system could remove at least 30% ortho-P for five years. These results were compared against predictions using the longevity prediction tool developed in this study. Figures 63 through 65 show the output curves from the longevity prediction tool when matching the testing parameters from Erickson et al. (February 23, 2010). The input parameters shown in the plots correspond to the various ZVI percentages, a hydraulic loading rate of 5.6 m/year (220.47 in/year), media depth of 40 cm (18.11 in), and a flow volume weighted mean influent concentration of 0.340 mg PO_4-P/L. As previously discussed in Section 2.2.1, Erickson et al. (February 23, 2010) estimated that systems with 5% iron filings could capture 80% of DP for more than thirty years, 2% iron filings could lead to roughly fifteen years of 80% DP capture, and 0.3% iron filings could remove more than 30% of DP for five years. Figure 63 and Figure 64 show that this study's

longevity tool also predicts high removals over a long period of time. The plots demonstrate that after thirty years a 5% ZVI system could maintain removals as high as 95% while a 2% ZVI system could maintain 90% removals at that point. It is important to note that the added removal effect of loam was removed from predictions in Figures 63 through 65 for comparison to the sand-ZVI filtration system from Erickson et al. (February 23, 2010). Figure 63 shows that after thirty years a 5% ZVI system could maintain removals as high as 95% while Figure 64 shows 90% removals for 2% ZVI system after thirty years. These removals are higher than what Erickson et al. (February 23, 2010) predicted, and Figure 65 shows removals that are significantly higher than what was predicted in that study for 0.3% ZVI. It predicts that a 0.3% ZVI system could still maintain 50% removal after 30 years. There were several major differences between the two studies that could have contributed to these discrepancies. Erickson et al. (February 23, 2010) did not test the iron filings to exhaustion, likely because of the relatively low ortho-P concentrations would cause an extremely long testing period. Testing to exhaustion could have allowed for the comparison of cumulative retained ortho-P masses, but the comparisons must be limited to model predictions based on the available data. Coarser iron filings were also used for that testing which could have contributed to less adsorptive capacity based on the smaller potential surface area. Figure 66 shows a comparison between the particle size distribution that Erickson et al. (February 23, 2010) used versus the one used for this column study.

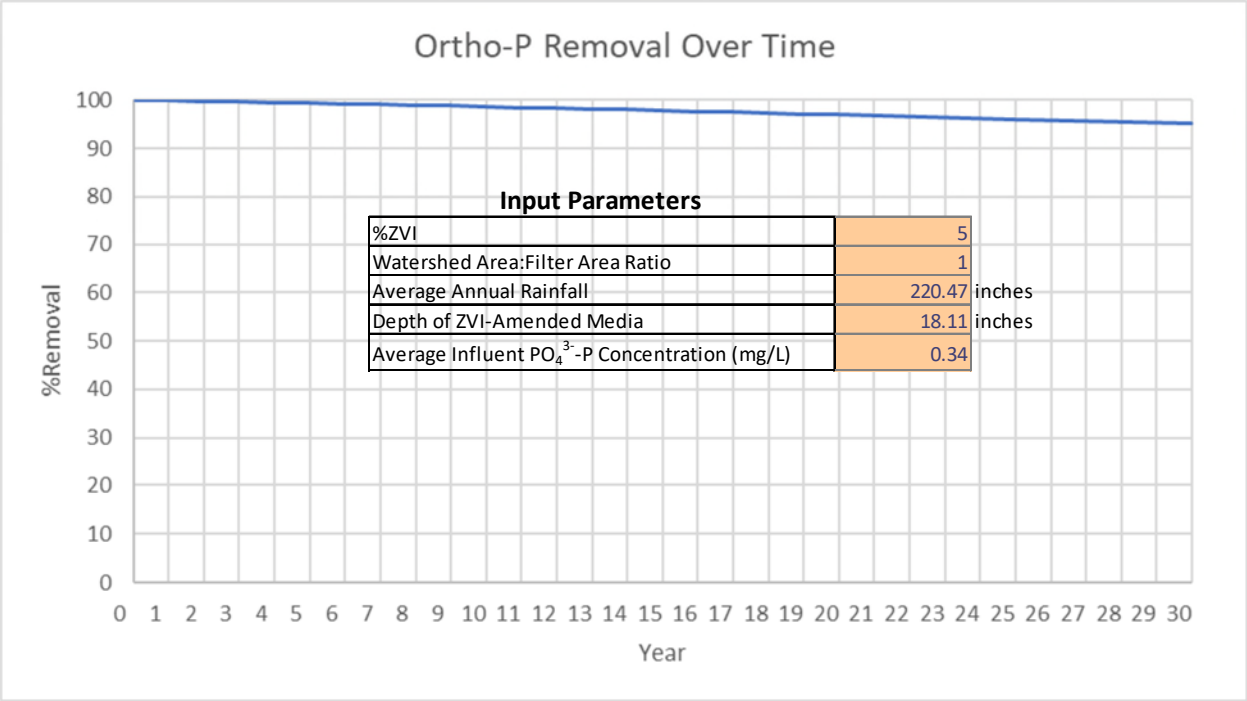

Figure 63: Predicted percent removal curve for 5% ZVI based on input parameters from Erickson et al. (February 23, 2010)

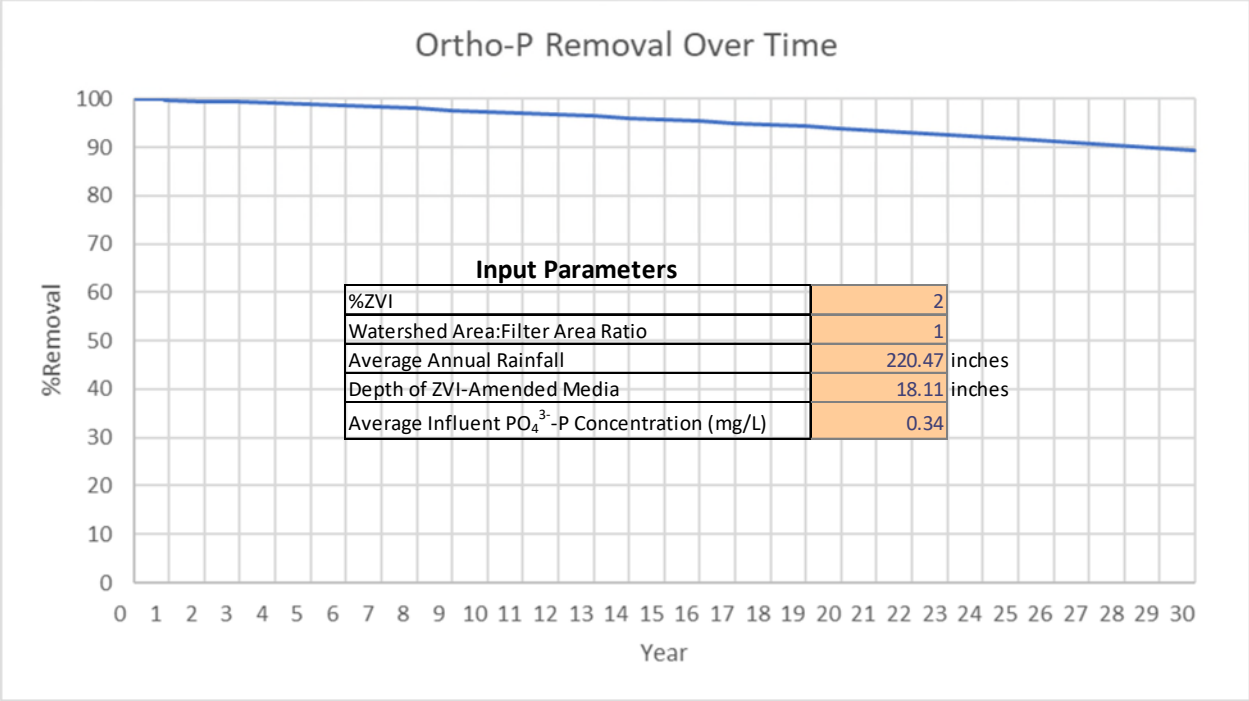

Figure 64: Predicted percent removal curve for 2% ZVI based on input parameters from Erickson et al. (February 23, 2010)

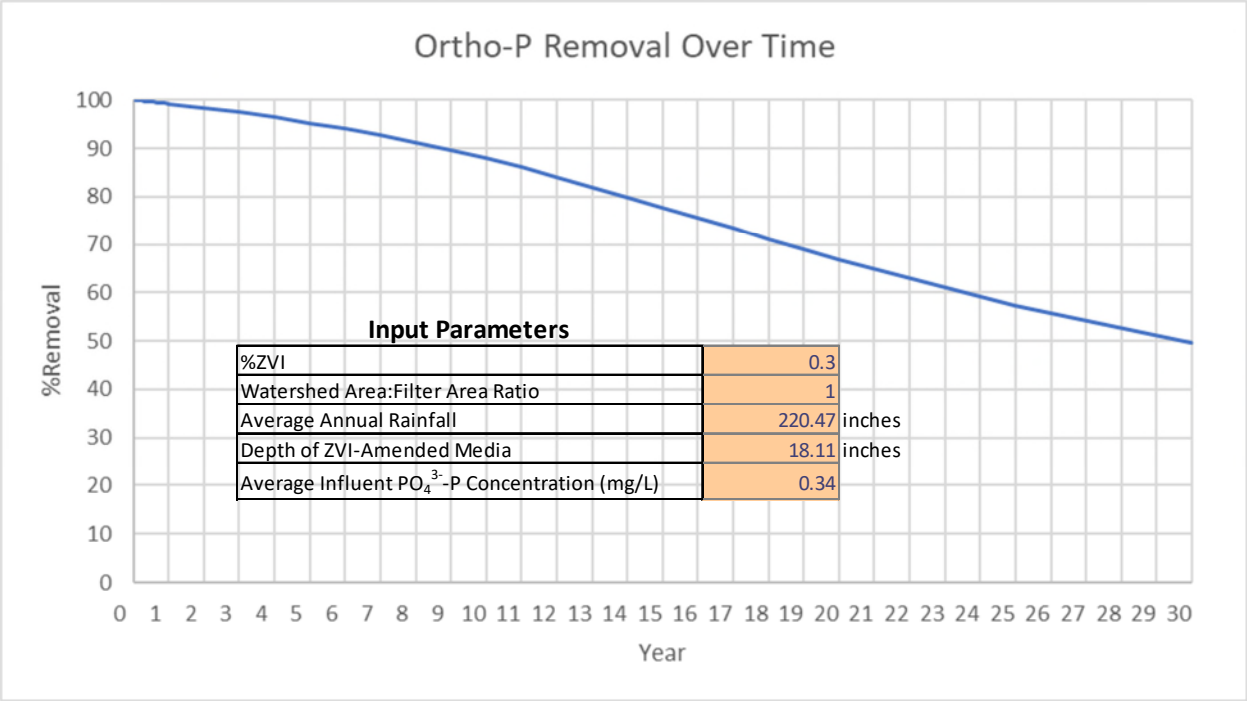

Figure 65: Predicted percent removal curve for 0.3% ZVI based on input parameters from Erickson et al. (February 23, 2010)

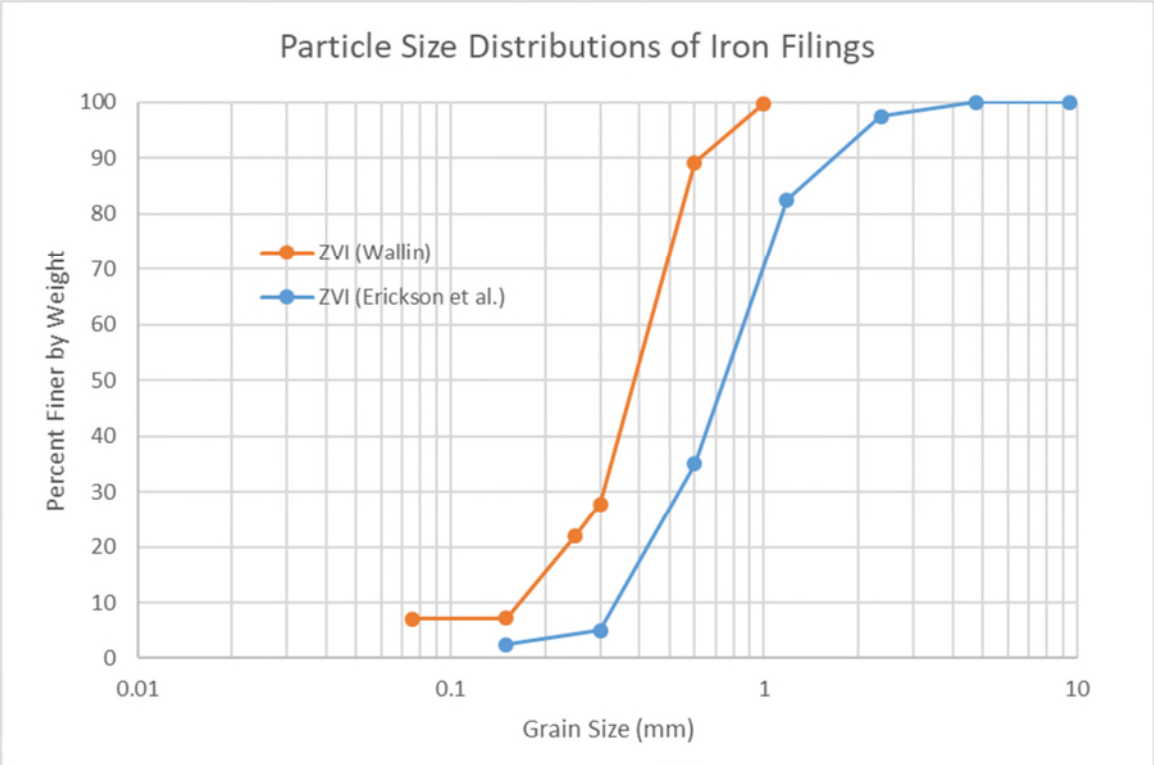

Figure 66: Comparison of particle size distributions for iron filings

Barbu et al. (2014) conducted several column experiments with ZVI amended bioretention media as previously discussed in Section 2.2.1. Results from those experiments can be compared to results from the longevity prediction tool shown in Figures 67 through 70. Each of these plots offers a percent removal comparison to a specific column from Barbu et al. (2014). The input parameters for the longevity prediction tool were based on those outlined in Barbu et al. (2014) where ZVI percentage, watershed area to filter area ratio, and depth of media varied between columns. The influent concentration in the column study was roughly 0.29 mg PO_4-P/L, and ten storms with a cumulative depth of 8.7 inches were tested. For simplicity, this 8.7 inches was assumed to be one year's worth of rainfall so that the corresponding removal efficiency could easily be shown on the longevity prediction plot. The removal efficiency for this 8.7-inch depth of runoff is shown in Figures 67 through 70 where the orange lines intersect. All these longevity prediction plots reported a removal efficiency of 100% after treating the 8.7 inches of runoff. When comparing the removal percentages to those determined by Barbu et al. (2014), the difference is less than 2% for three of the comparisons and is only 6.5% different at the most. These high removal percentages were to be expected with such a low volume of runoff treated and relatively low P concentrations when compared to agricultural runoff. Results, though limited by the relatively small amount of volume treated, were in line with the longevity tool predictions.

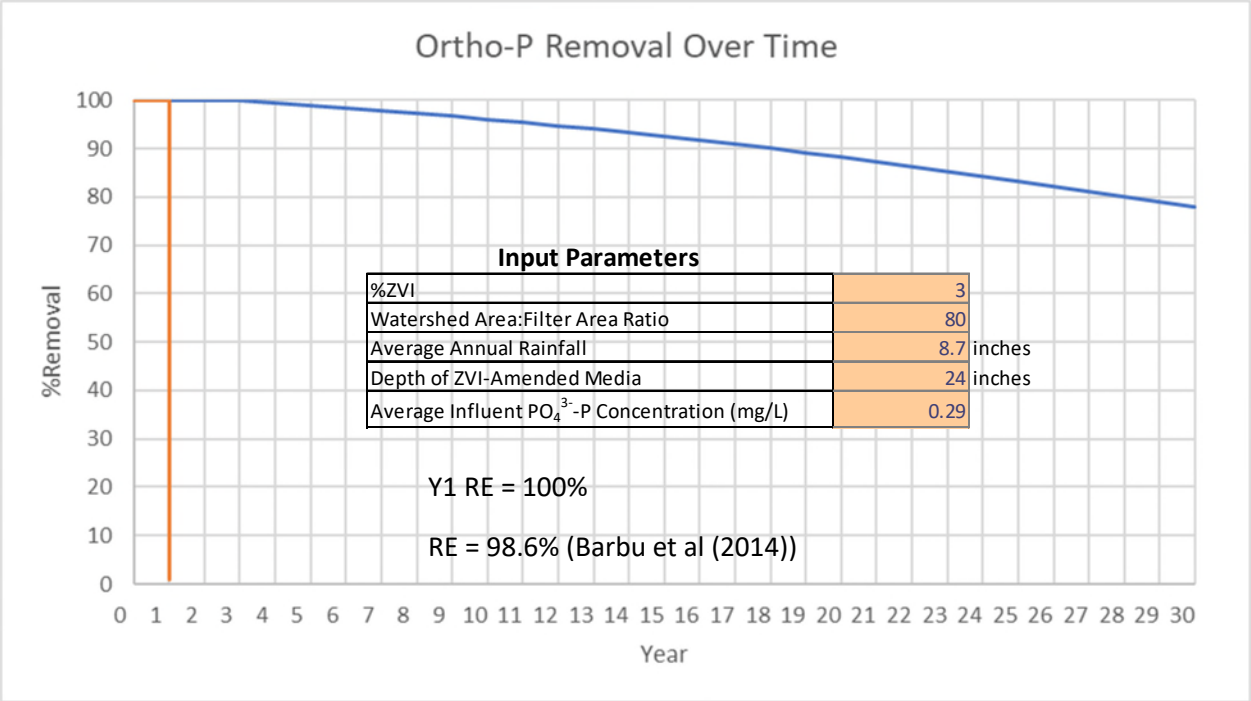

Figure 67: Predicted percent removal curve for 3% ZVI with a 24-inch media depth based on input parameters from (Barbu, Ballestero, & Ballestero, 2014)

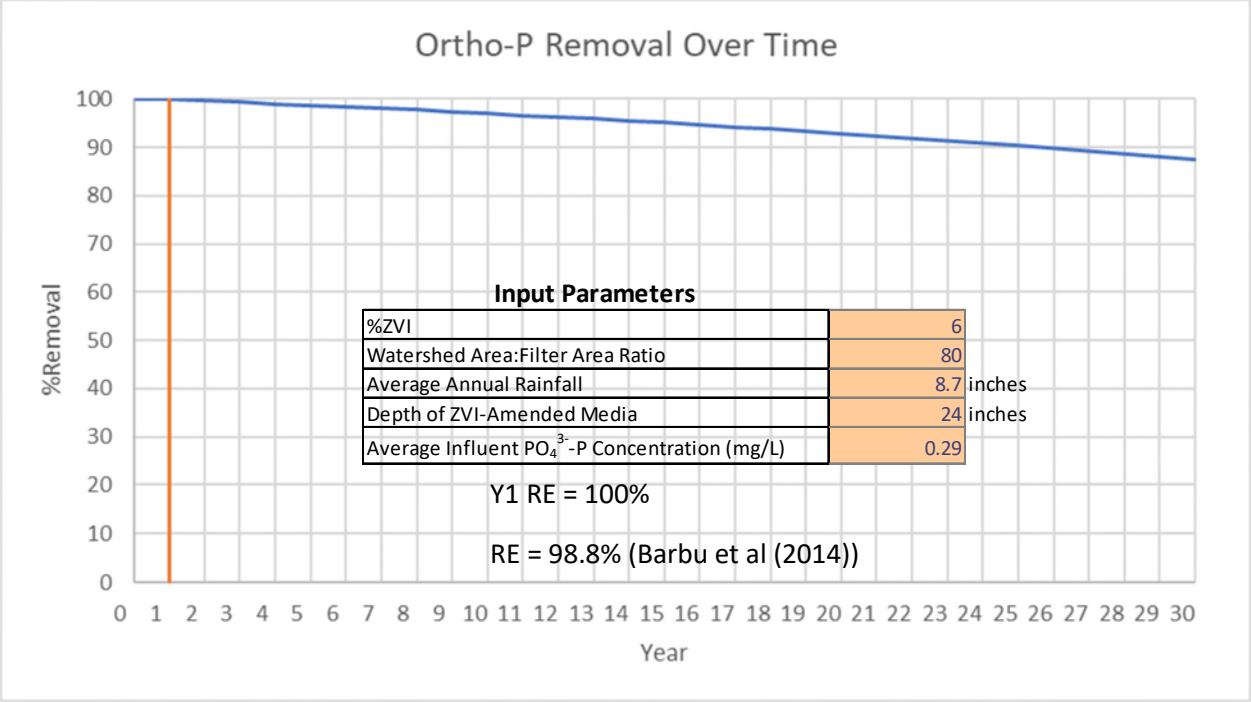

Figure 68: Predicted percent removal curve for 6% ZVI with a 24-inch media depth based on input parameters from (Barbu, Ballestero, & Ballestero, 2014)

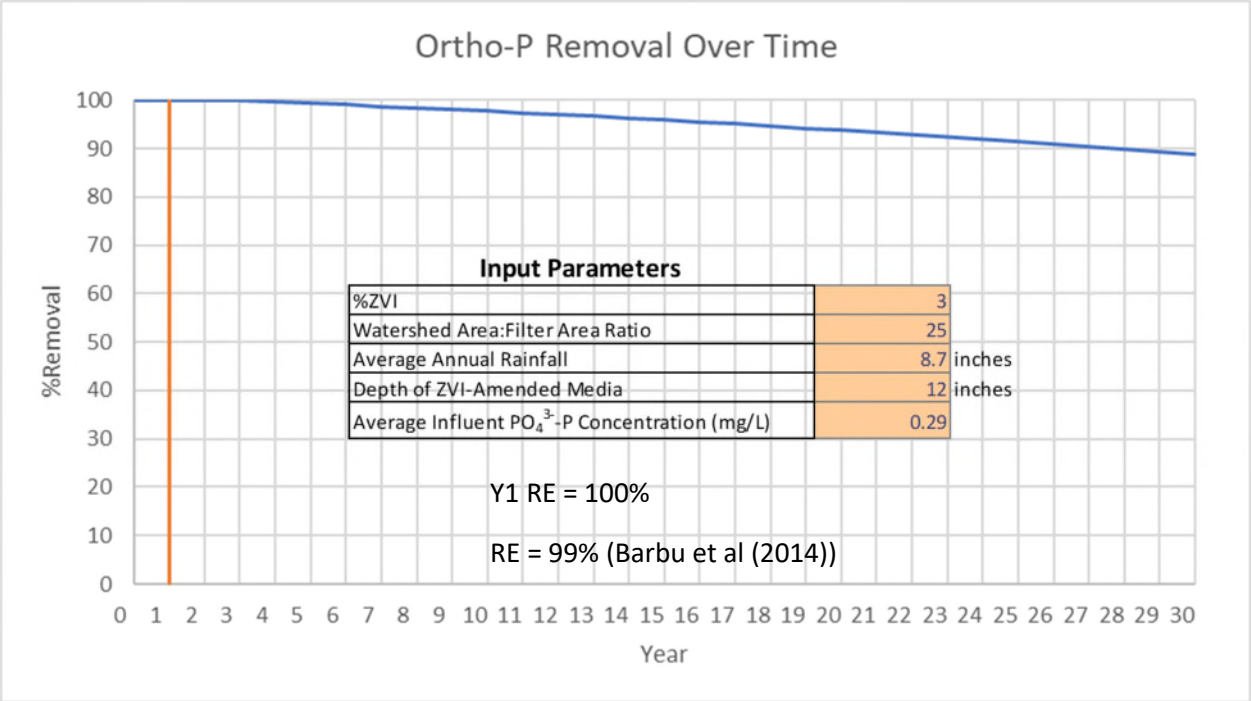

Figure 69: Predicted percent removal curve for 3% ZVI with a 12-inch media depth based on input parameters from (Barbu, Ballestero, & Ballestero, 2014)

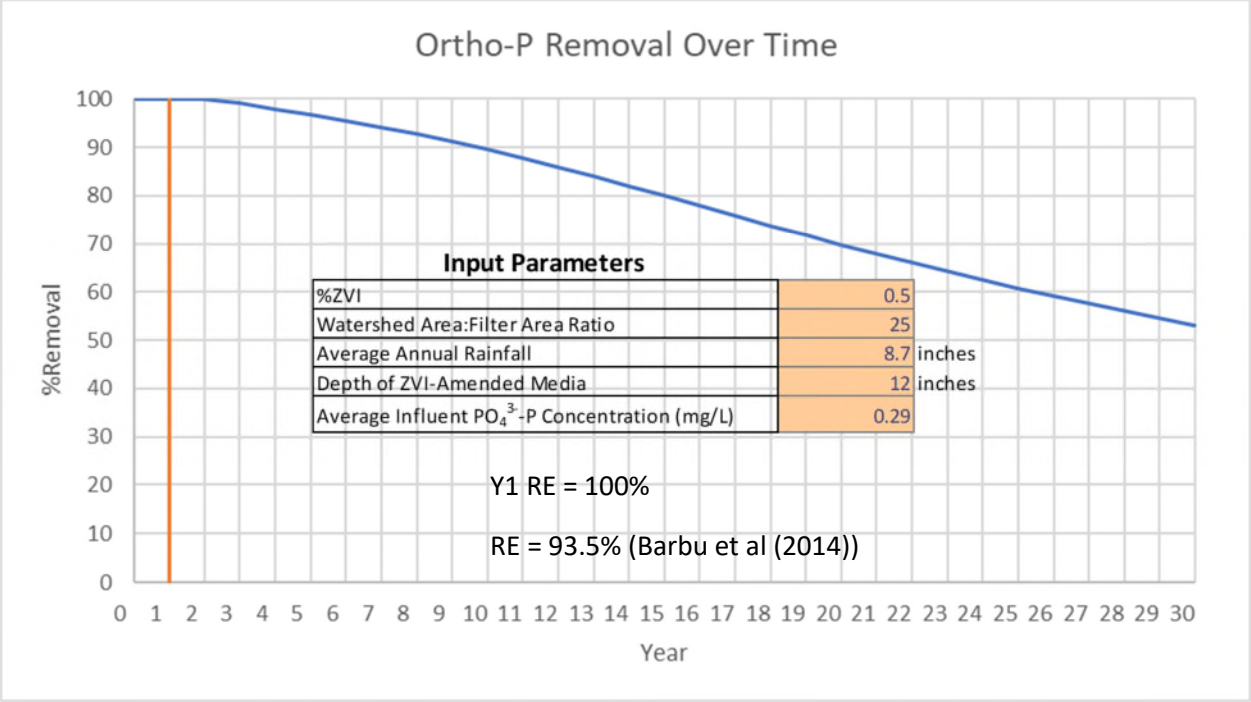

Figure 70: Predicted percent removal curve for 0.5% ZVI with a 12-inch media depth based on input parameters from (Barbu, Ballestero, & Ballestero, 2014)

4.6 Longevity Prediction Summary Plots

Figures 71 through 82 show the predictive percent removal curves for ortho-P for various soil depths, ZVI percentages, and ortho-P concentrations. These curves were created using the previously described longevity prediction tool. Ortho-P concentrations were chosen based on the range of reasonable ortho-P concentrations expected from agricultural runoff discussed in Section 2.1.3. These concentrations included 0.12 mg-P/L as a baseline comparison to the national median stormwater DP concentration for municipalities from Pitt et al. (2005). These plots assume a watershed area to filter area ratio of 16:1 as this is maximum acceptable ratio for many agencies (I. Barbu, personal communication, April 9, 2018). The predictive curves in these plots show, as expected, that lower influent concentrations lead to higher removal percentages over longer periods. They also demonstrate that as the depth of media and ZVI percentages increase, higher removal percentages are predicted. Because these curves are derived from the somewhat complex Langmuir isotherm model, simplified correlations between the percent removal curves under varying conditions are difficult to obtain. For example, one might expect that the 0.5 mg/L curve from Figure 71 to drop to 50% removal two times faster than the same curve in Figure 72 due to it having half the ZVI content. However, this is not the case and it is due to both the nonlinear shape of these curves as well as the underlying function in the longevity prediction tool to determine q_m based on ZVI percentage (shown in Figure 60). Furthermore Figures 16 through 21 demonstrate the need for a longevity prediction tool as the removal percentage comparisons between columns do not translate to simple ratio correlations.

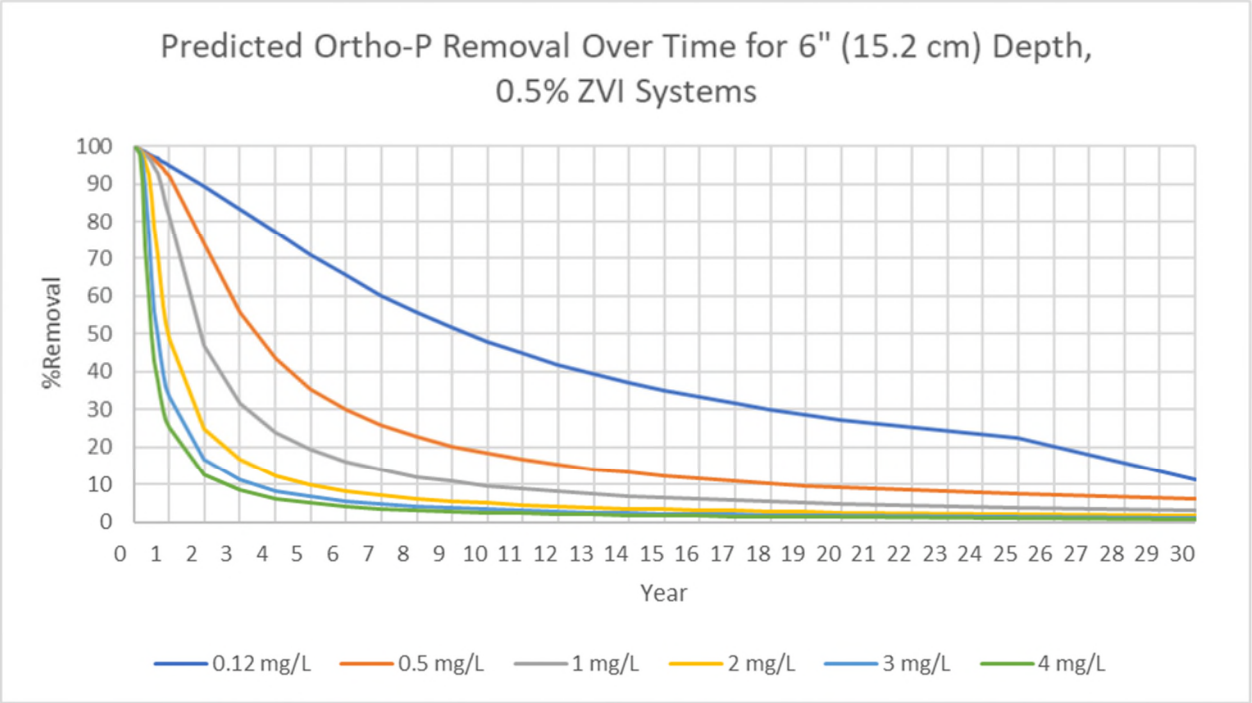

Figure 71: Predictive percent removal curves for systems with 6” media depth and 0.5% ZVI under varying ortho-P loadings, a watershed area to filter area ratio of 16:1, and 40 inches of annual rainfall

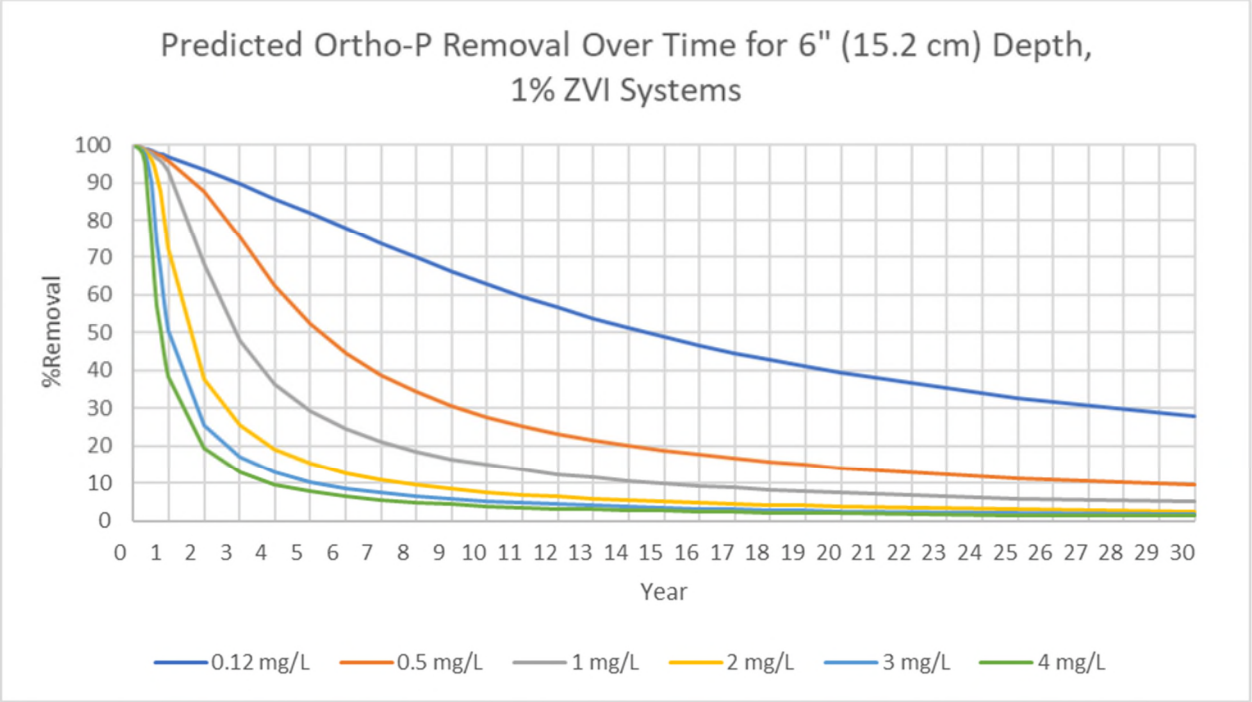

Figure 72: Predictive percent removal curves for systems with 6” media depth and 1% ZVI under varying ortho-P loadings, a watershed area to filter area ratio of 16:1, and 40 inches of annual rainfall

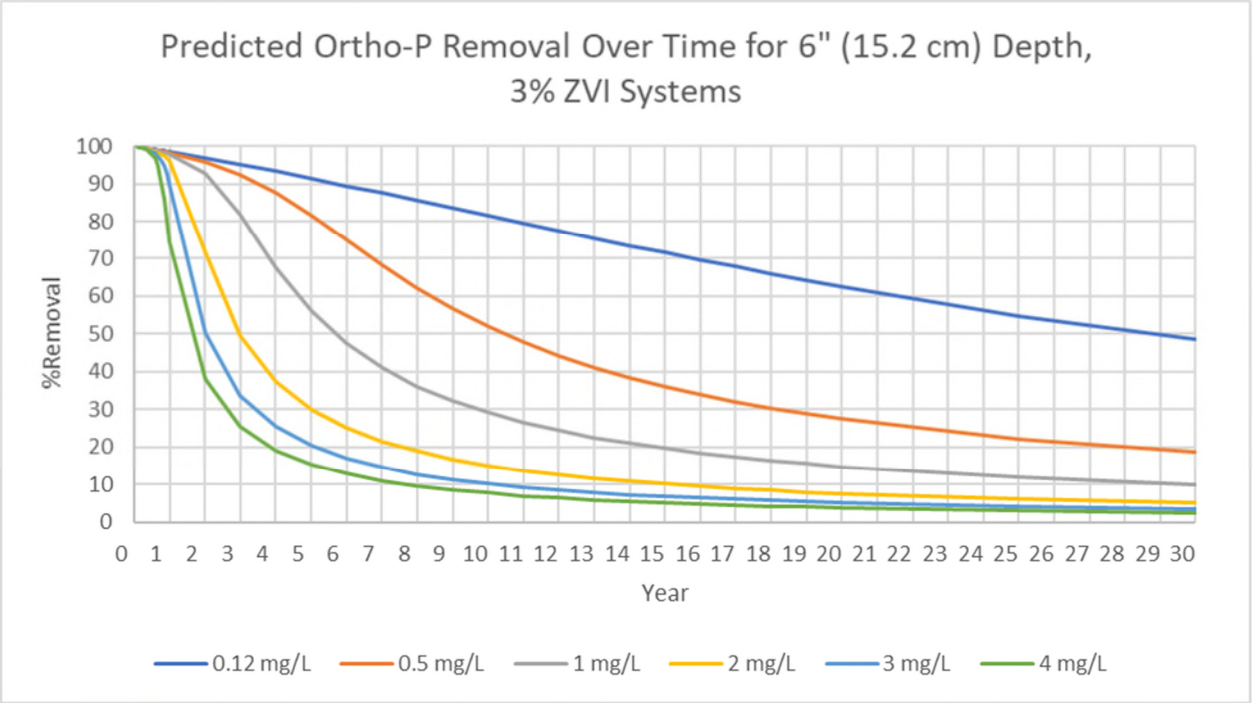

Figure 73: Predictive percent removal curves for systems with 6” media depth and 3% ZVI under varying ortho-P loadings, a watershed area to filter area ratio of 16:1, and 40 inches of annual rainfall

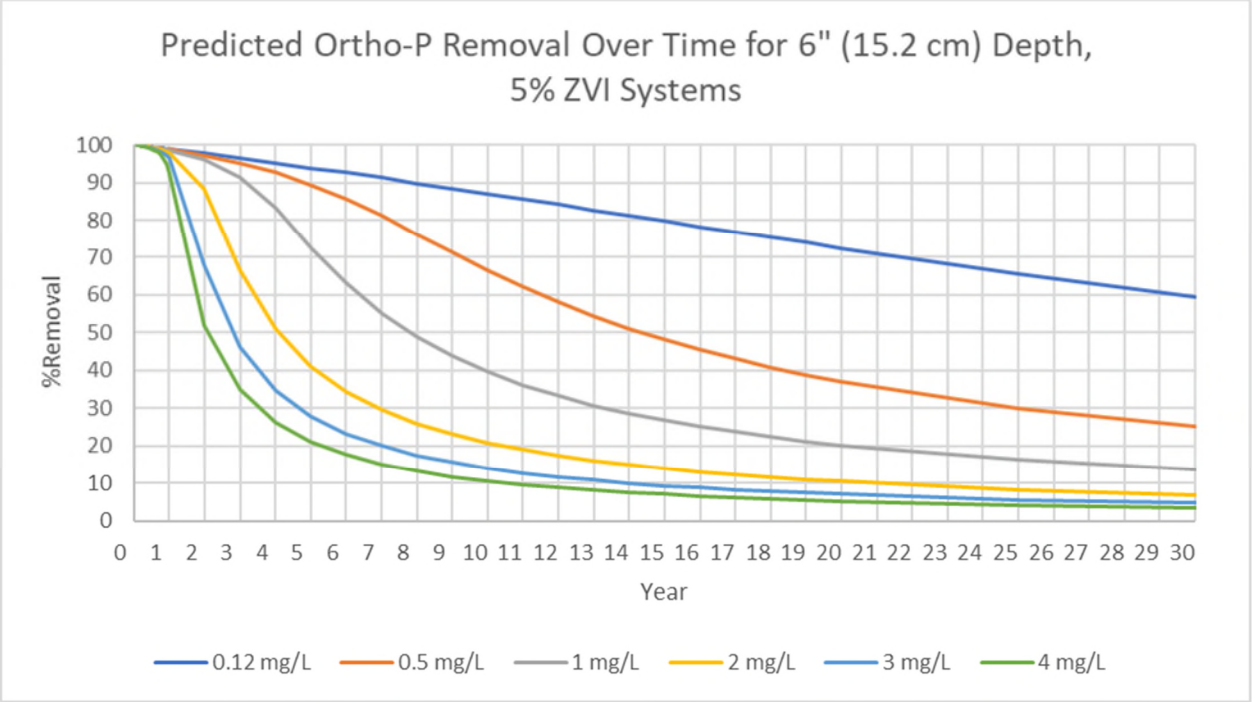

Figure 74: Predictive percent removal curves for systems with 6” media depth and 5% ZVI under varying ortho-P loadings, a watershed area to filter area ratio of 16:1, and 40 inches of annual rainfall

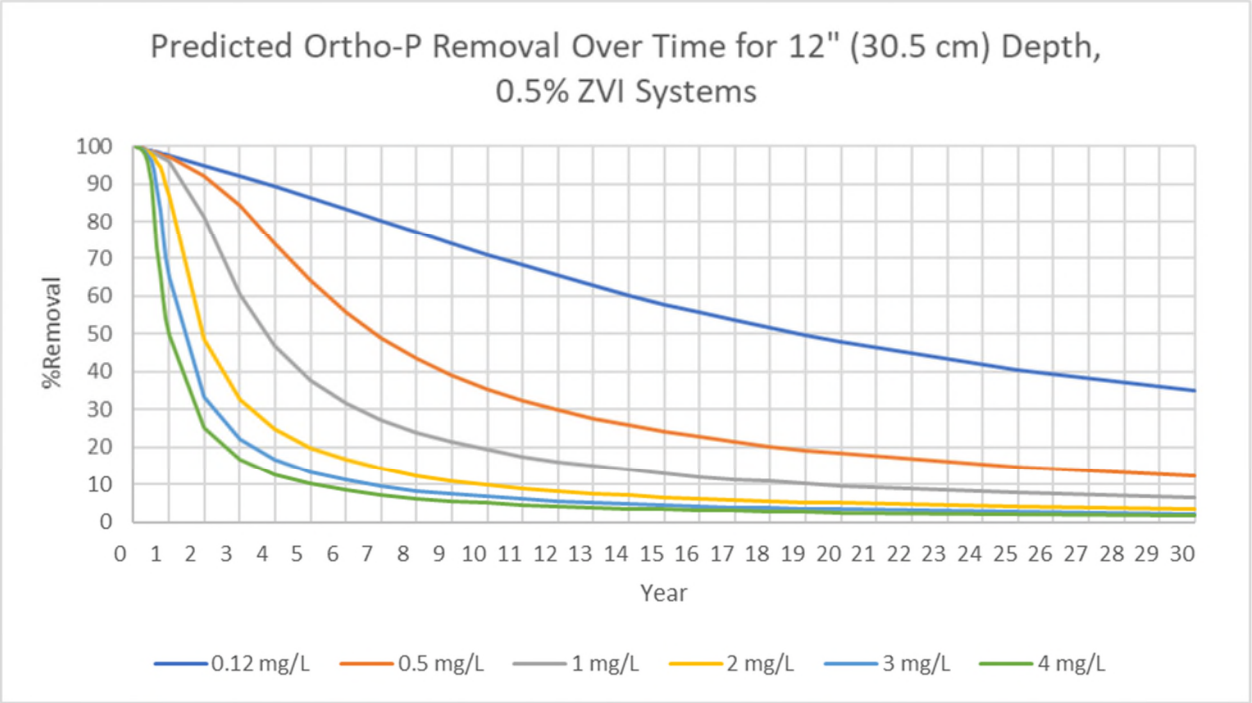

Figure 75: Predictive percent removal curves for systems with 12” media depth and 0.5% ZVI under varying ortho-P loadings, a watershed area to filter area ratio of 16:1, and 40 inches of annual rainfall

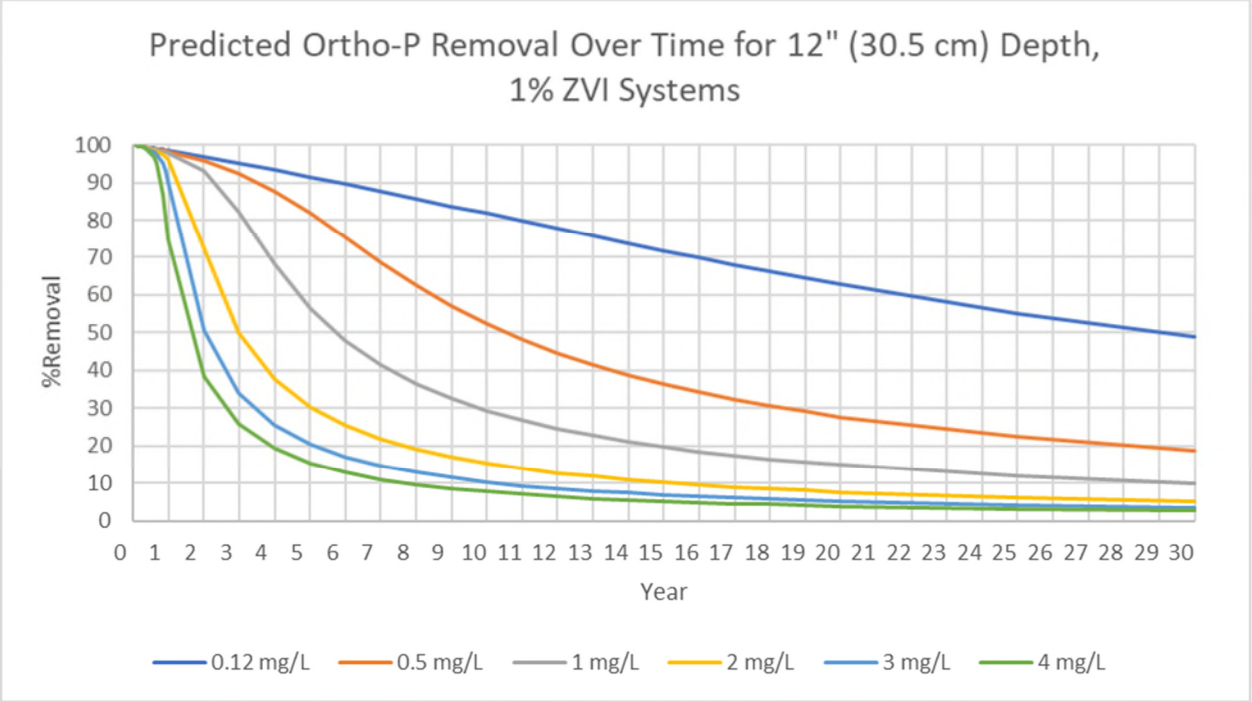

Figure 76: Predictive percent removal curves for systems with 12” media depth and 1% ZVI under varying ortho-P loadings, a watershed area to filter area ratio of 16:1, and 40 inches of annual rainfall

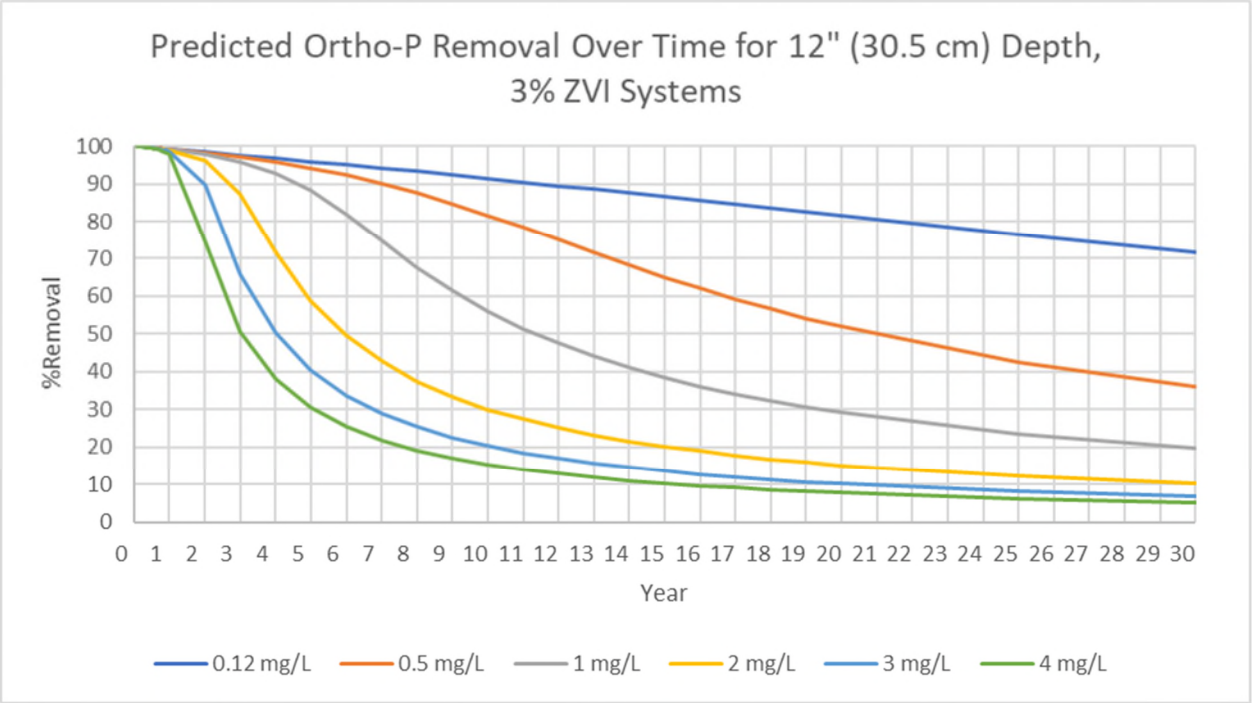

Figure 77: Predictive percent removal curves for systems with 12” media depth and 3% ZVI under varying ortho-P loadings, a watershed area to filter area ratio of 16:1, and 40 inches of annual rainfall

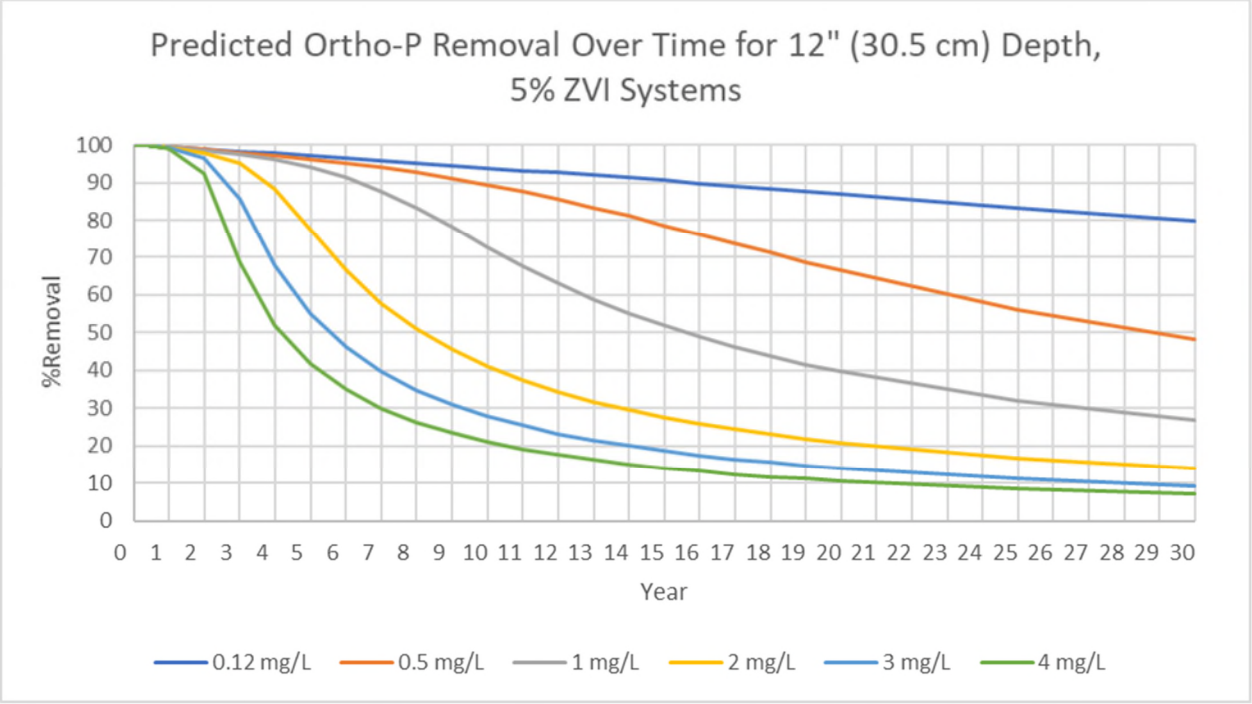

Figure 78: Predictive percent removal curves for systems with 12” media depth and 5% ZVI under varying ortho-P loadings, a watershed area to filter area ratio of 16:1, and 40 inches of annual rainfall

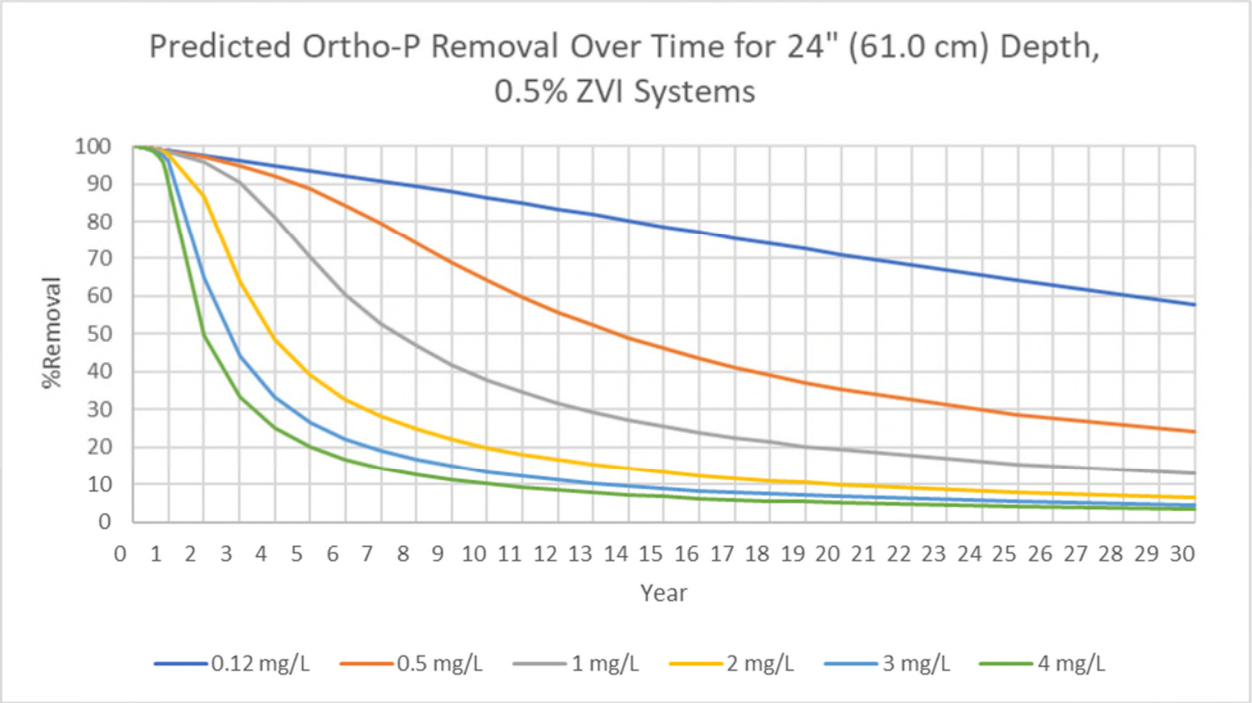

Figure 79: Predictive percent removal curves for systems with 24” media depth and 0.5% ZVI under varying ortho-P loadings, a watershed area to filter area ratio of 16:1, and 40 inches of annual rainfall

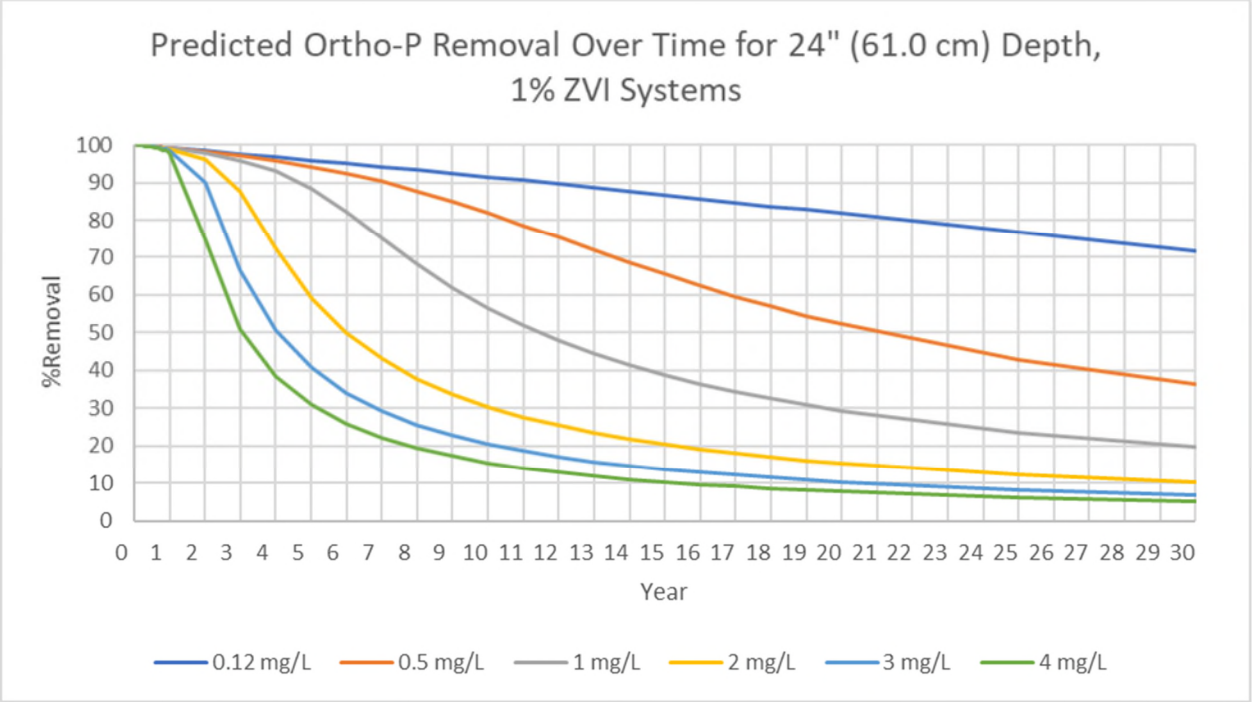

Figure 80: Predictive percent removal curves for systems with 24” media depth and 1% ZVI under varying ortho-P loadings, a watershed area to filter area ratio of 16:1, and 40 inches of annual rainfall

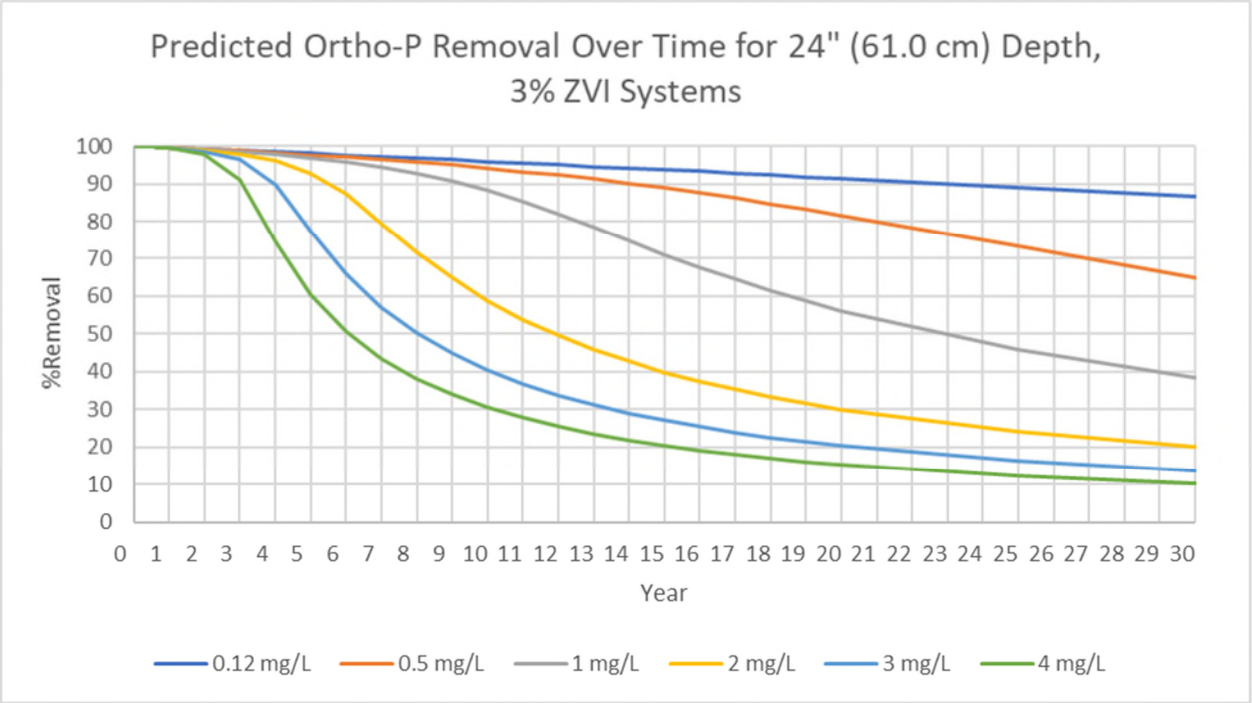

Figure 81: Predictive percent removal curves for systems with 24” media depth and 3% ZVI under varying ortho-P loadings, a watershed area to filter area ratio of 16:1, and 40 inches of annual rainfall

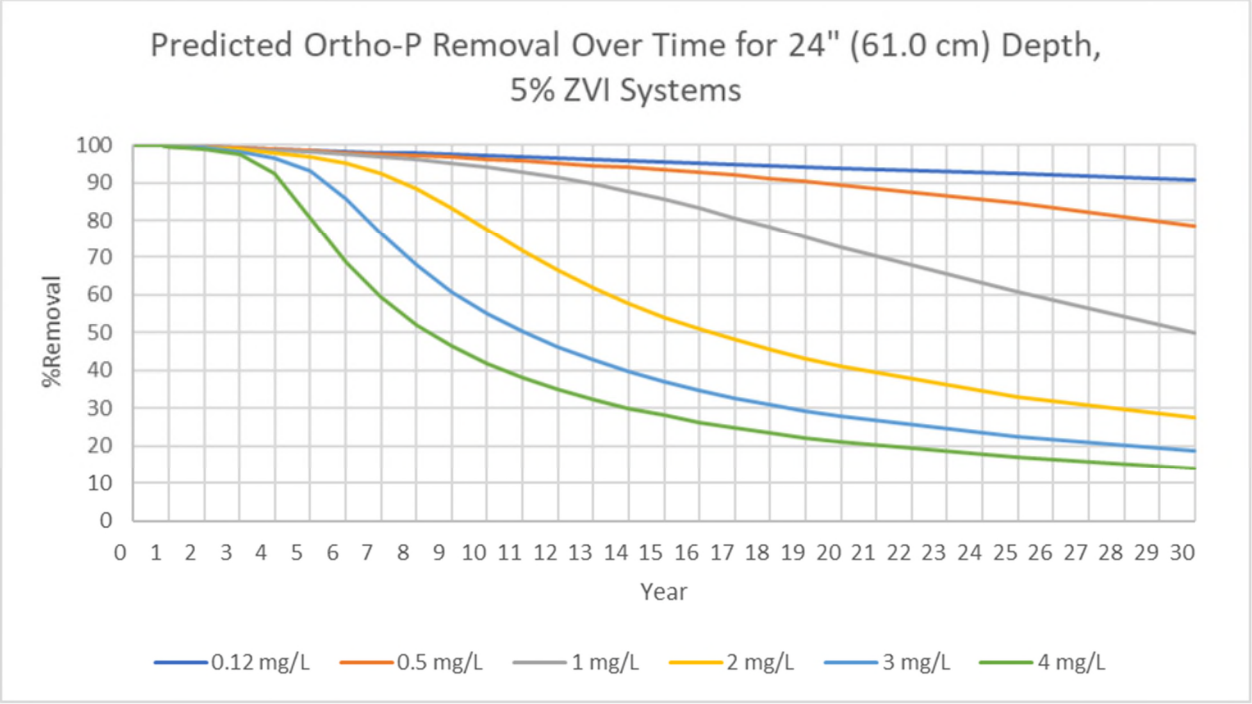

Figure 82: Predictive percent removal curves for systems with 24” media depth and 5% ZVI under varying ortho-P loadings, a watershed area to filter area ratio of 16:1, and 40 inches of annual rainfall

4.7 Ortho-P Mass Retained Prediction Summary Plots

Figures 83 through 94 were created using output from the longevity prediction tool that was reconfigured to show cumulative mass of ortho-P retained per acre treated instead of percent removal. These figures use the same assumptions as those from Section 4.6 where the average annual rainfall was assumed to be 40 inches and the watershed to filter area ratio was chosen as 16:1. As Figures 83 through 94 are a simple reconfiguration of the data shown in Figures 71 through 82, the same general conclusions apply. However, plots showing cumulative mass retained are useful for demonstrating what the removal percentages mean in terms of physical processes occurring in the media. The curves shown in Figures 83 through 94 also allow for easier interpolation between influent concentrations as their shapes are much more uniform than those in Figures 71 through 82.

These figures are also useful for comparing the overall treatment potentials for the various system options. For example, if a person wanted to find a system that could treat water to the same level as the 24-inch, 0.5% ZVI system, they could see that the 6”, 5% system would have similar performance as shown in Figure 91 and Figure 86.

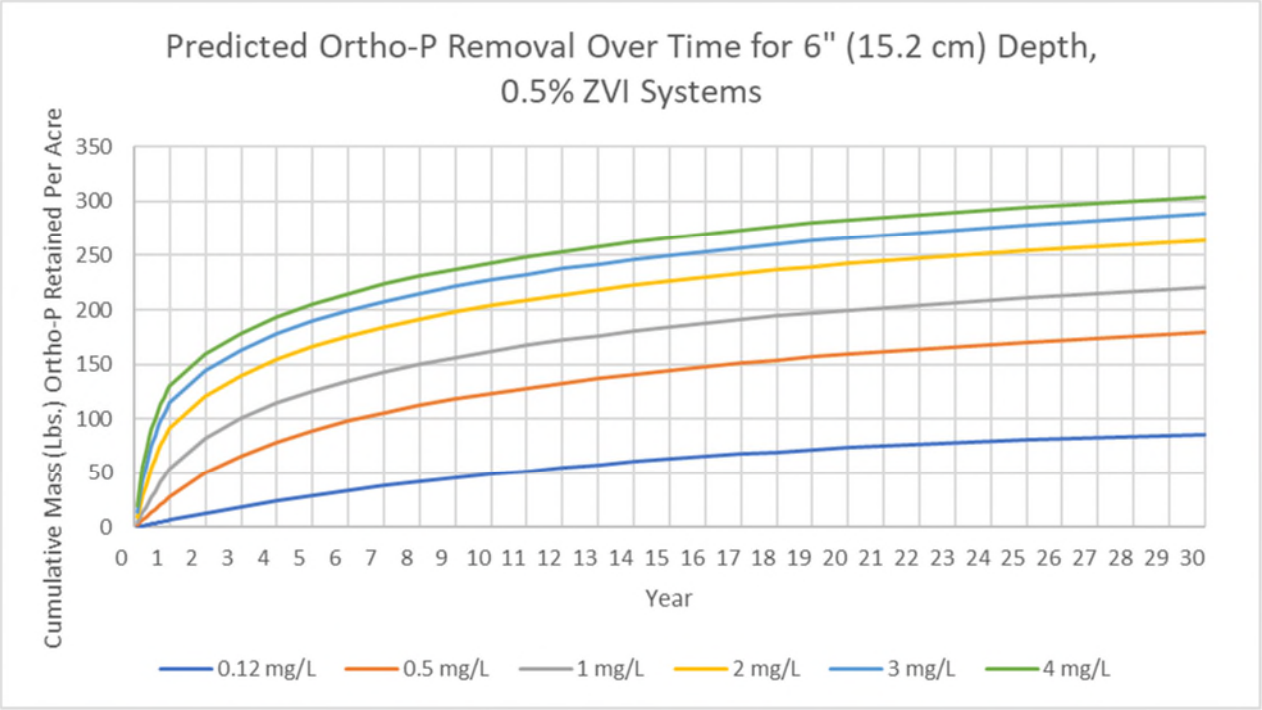

Figure 83: Predictive mass removal curves for systems with 6” media depth and 0.5% ZVI under varying ortho-P loadings, a watershed area to filter area ratio of 16:1, and 40 inches of annual rainfall

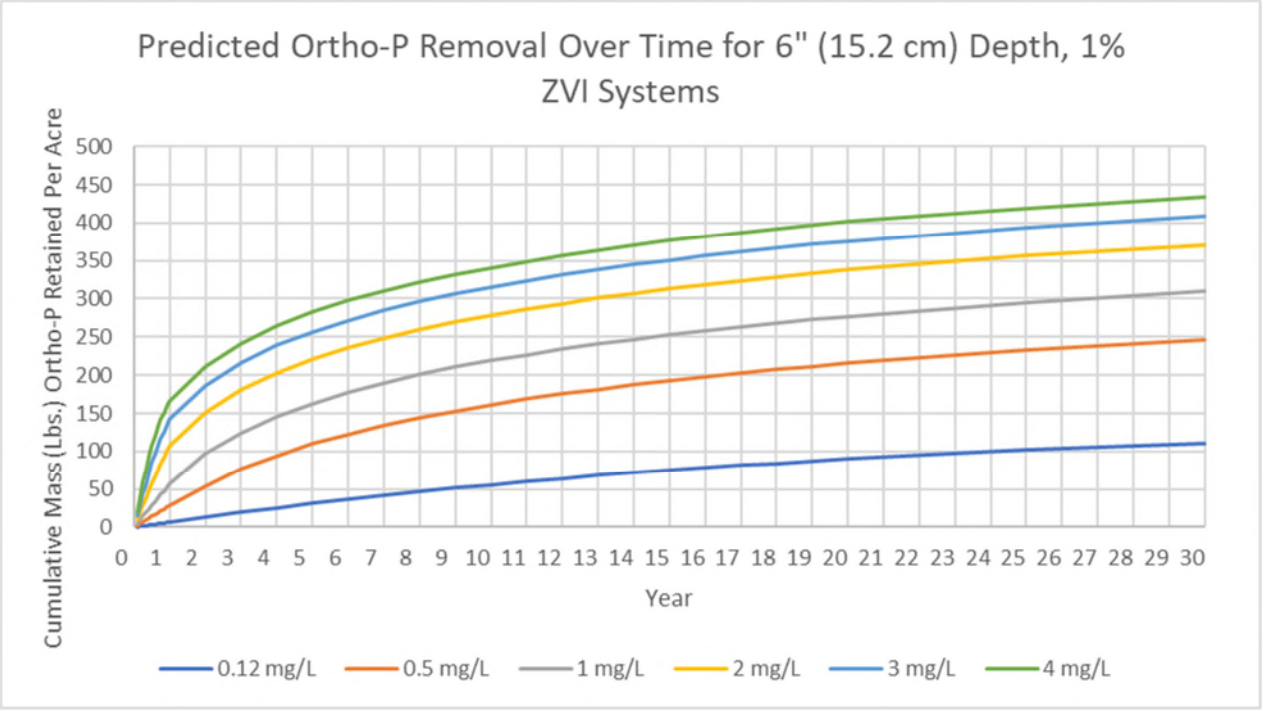

Figure 84: Predictive mass removal curves for systems with 6” media depth and 1% ZVI under varying ortho-P loadings, a watershed area to filter area ratio of 16:1, and 40 inches of annual rainfall

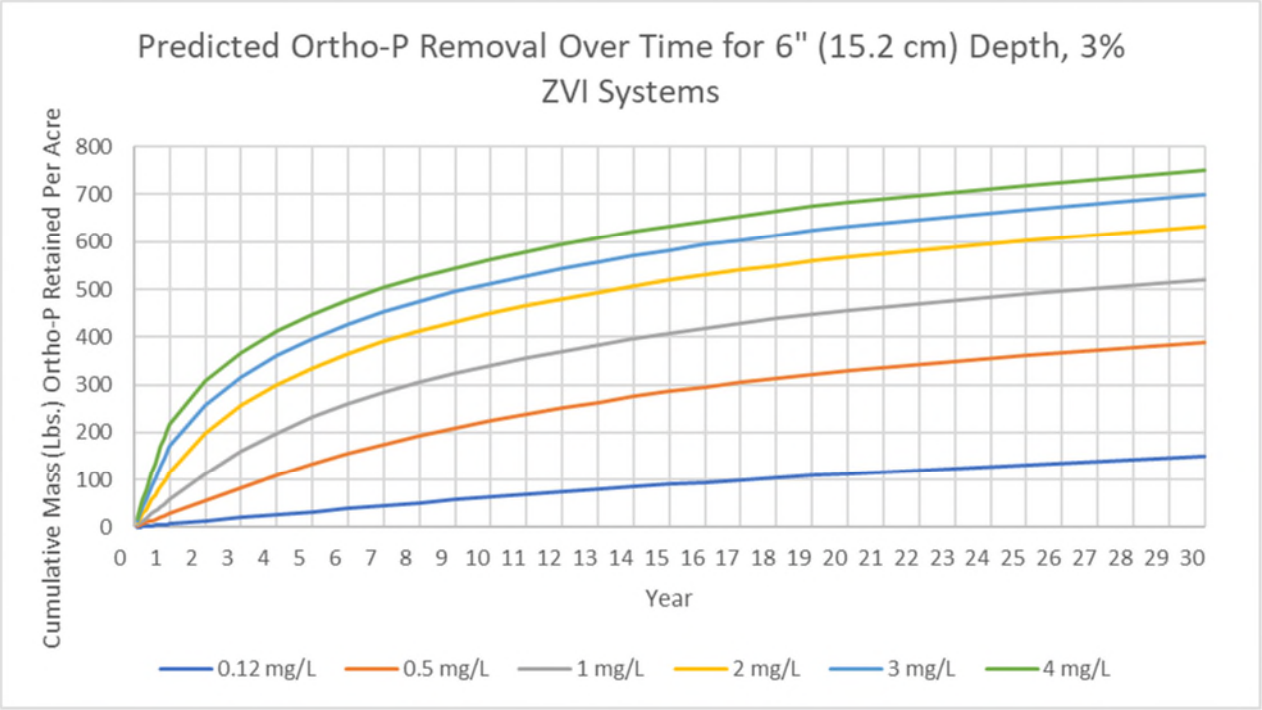

Figure 85: Predictive mass removal curves for systems with 6” media depth and 3% ZVI under varying ortho-P loadings, a watershed area to filter area ratio of 16:1, and 40 inches of annual rainfall

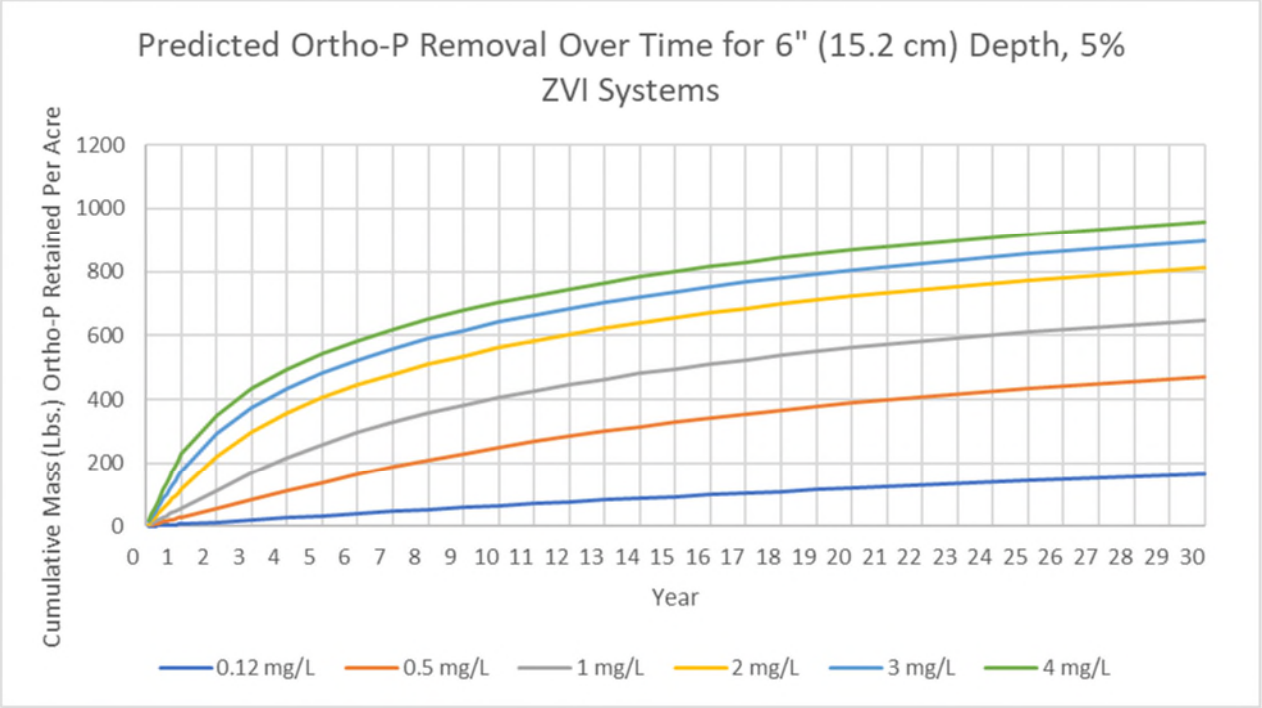

Figure 86: Predictive mass removal curves for systems with 6” media depth and 5% ZVI under varying ortho-P loadings, a watershed area to filter area ratio of 16:1, and 40 inches of annual rainfall

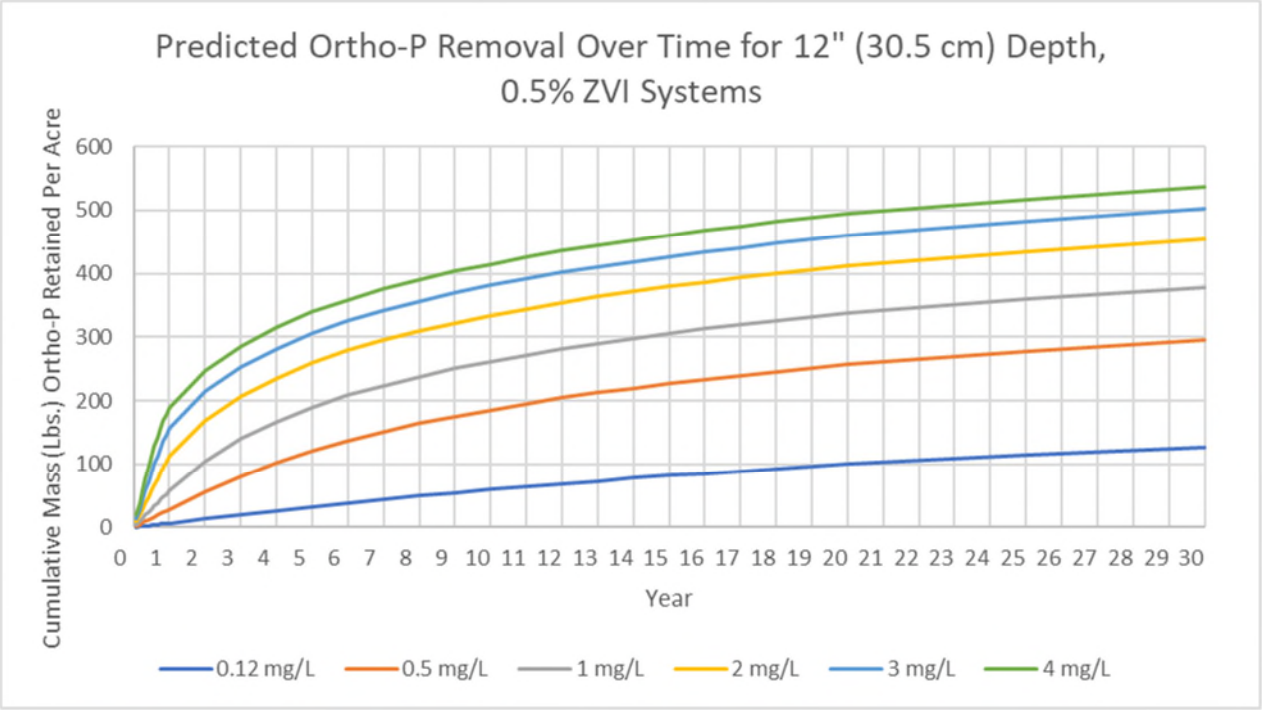

Figure 87: Predictive mass removal curves for systems with 12” media depth and 0.5% ZVI under varying ortho-P loadings, a watershed area to filter area ratio of 16:1, and 40 inches of annual rainfall

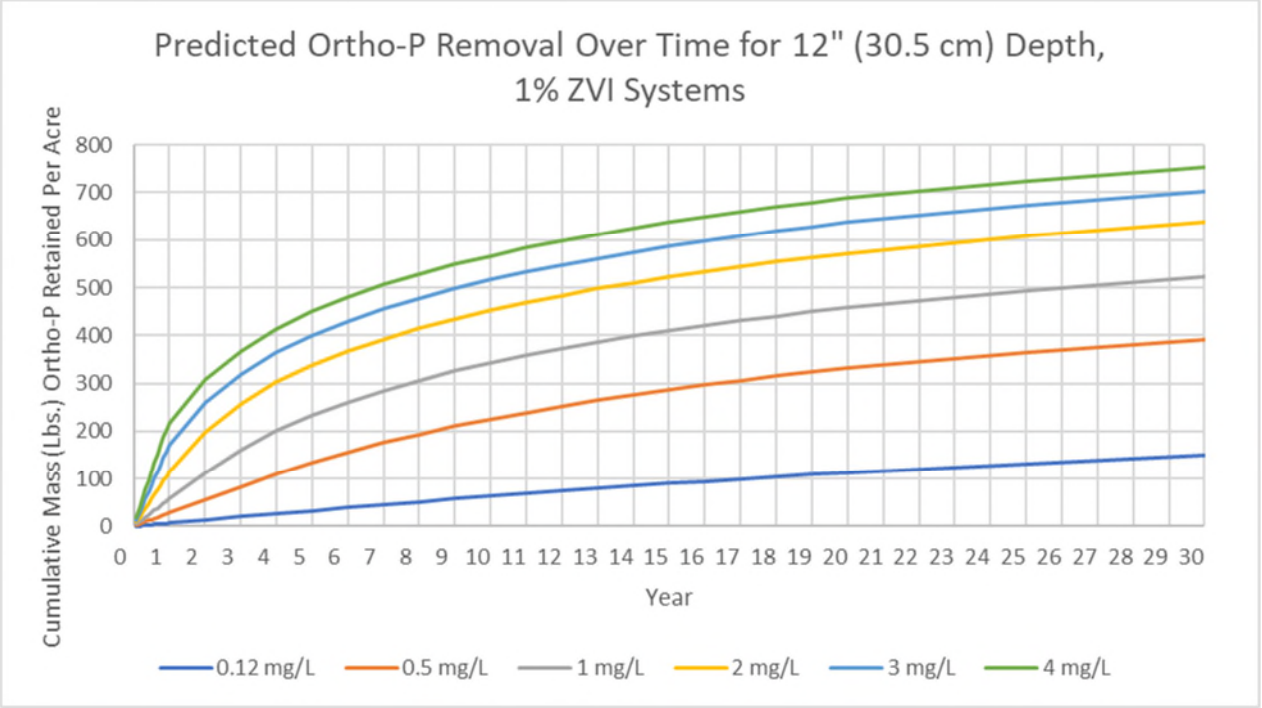

Figure 88: Predictive mass removal curves for systems with 12” media depth and 1% ZVI under varying ortho-P loadings, a watershed area to filter area ratio of 16:1, and 40 inches of annual rainfall

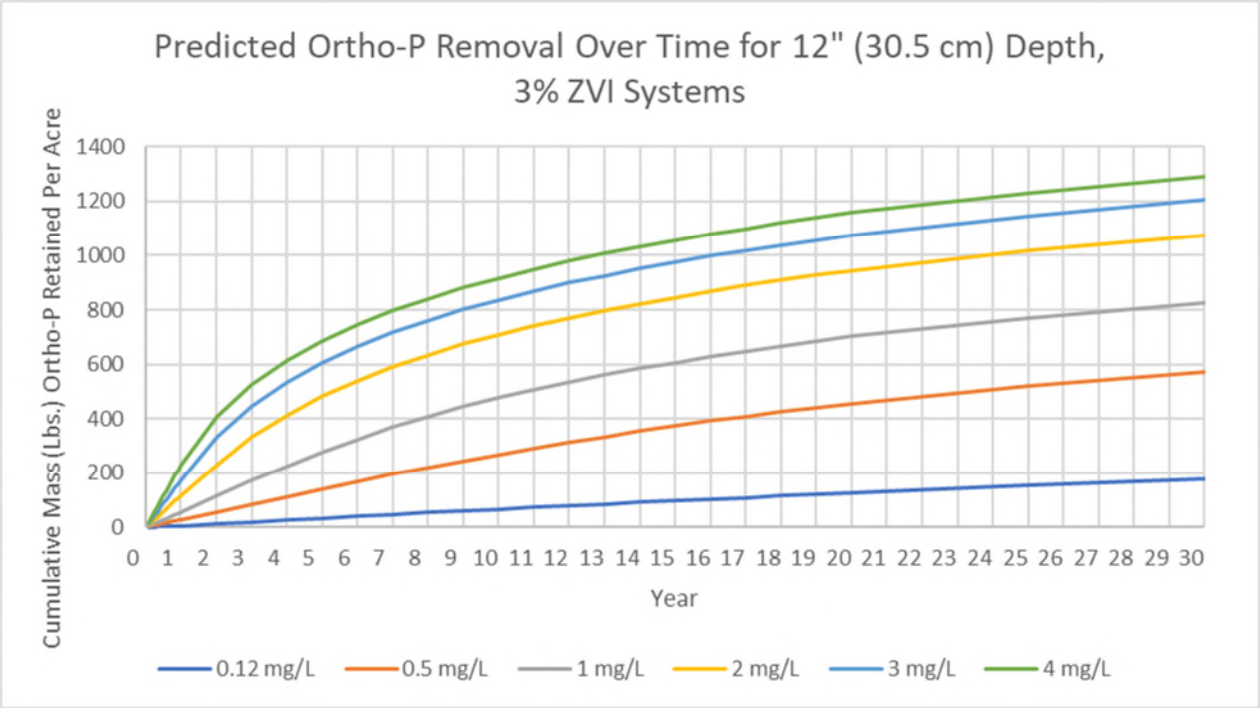

Figure 89: Predictive mass removal curves for systems with 12” media depth and 3% ZVI under varying ortho-P loadings, a watershed area to filter area ratio of 16:1, and 40 inches of annual rainfall

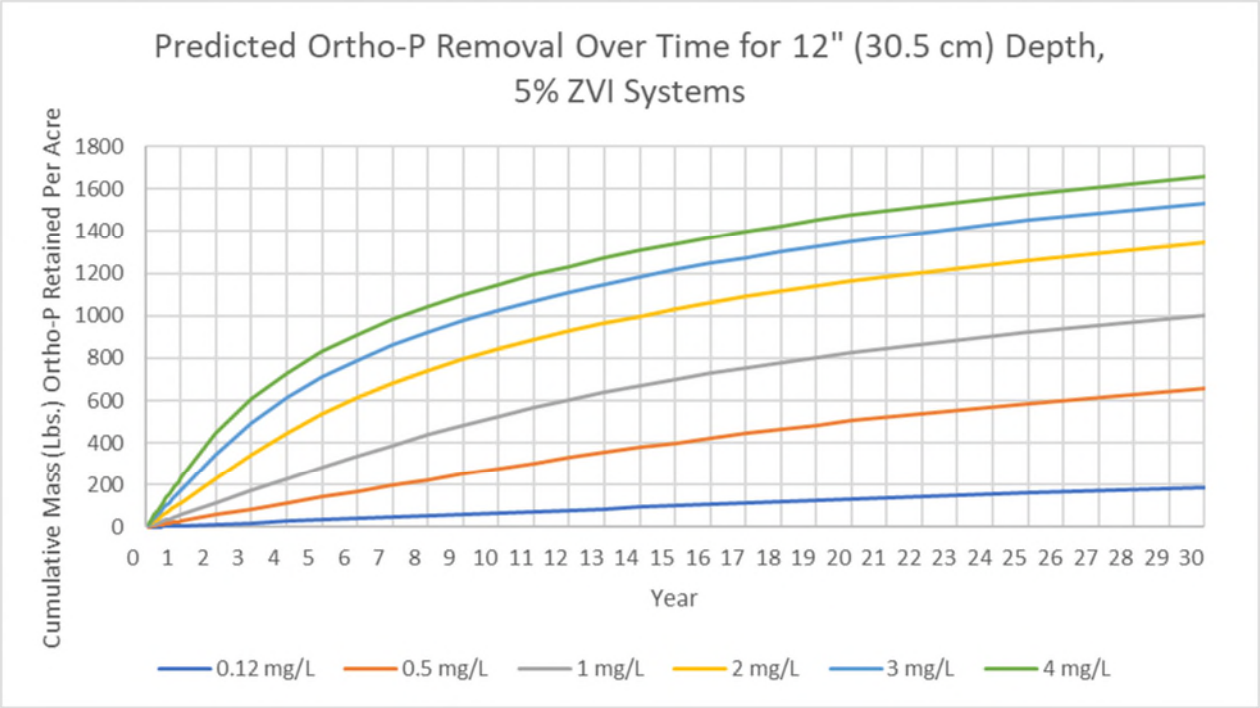

Figure 90: Predictive mass removal curves for systems with 12” media depth and 5% ZVI under varying ortho-P loadings, a watershed area to filter area ratio of 16:1, and 40 inches of annual rainfall

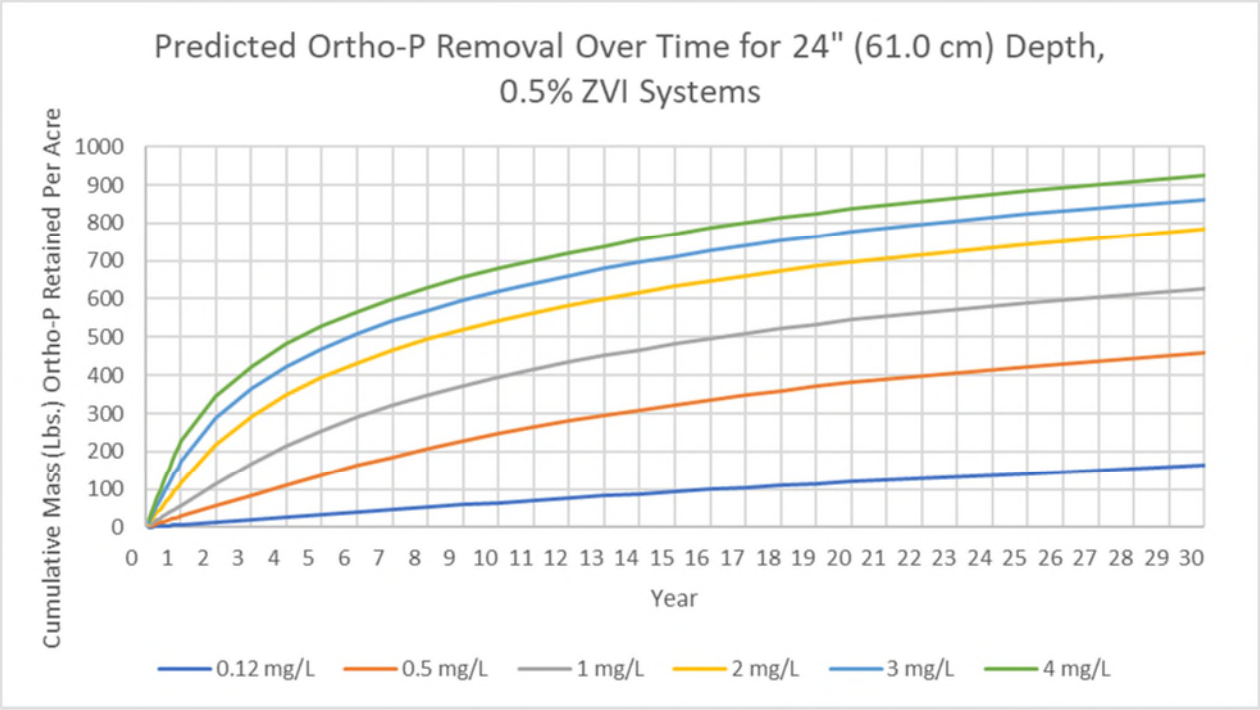

Figure 91: Predictive mass removal curves for systems with 24” media depth and 0.5% ZVI under varying ortho-P loadings, a watershed area to filter area ratio of 16:1, and 40 inches of annual rainfall

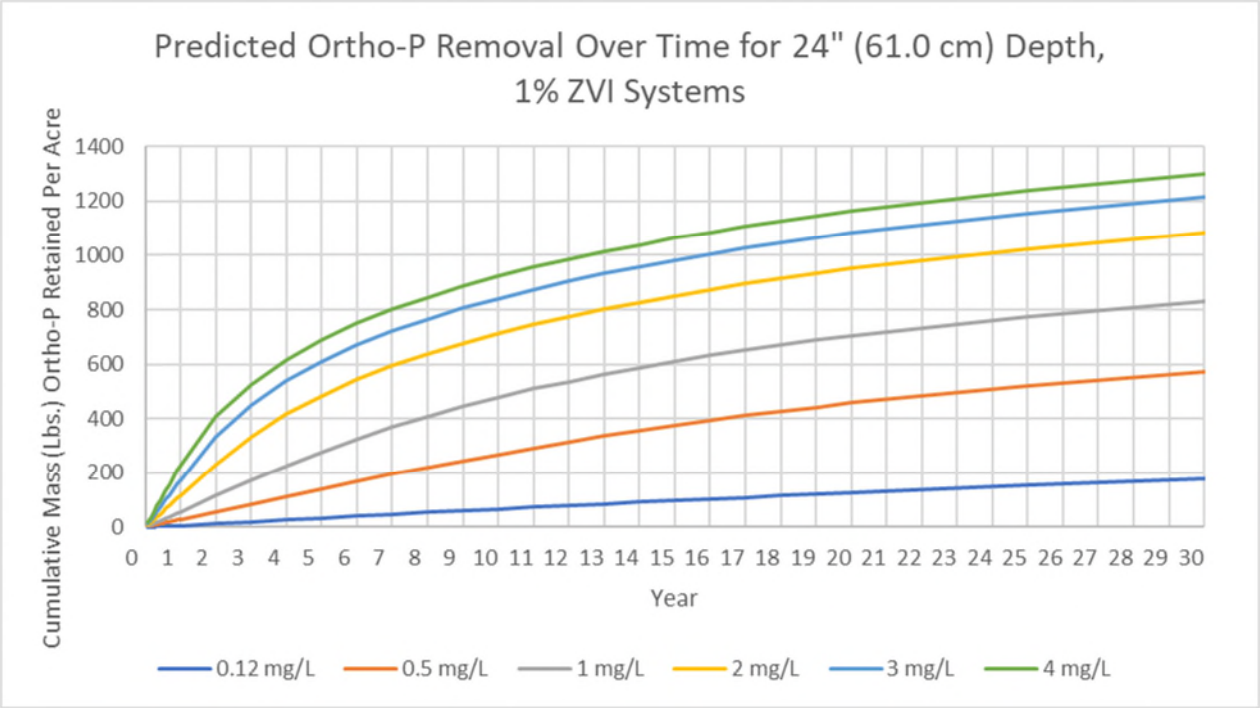

Figure 92: Predictive mass removal curves for systems with 24” media depth and 1% ZVI under varying ortho-P loadings, a watershed area to filter area ratio of 16:1, and 40 inches of annual rainfall

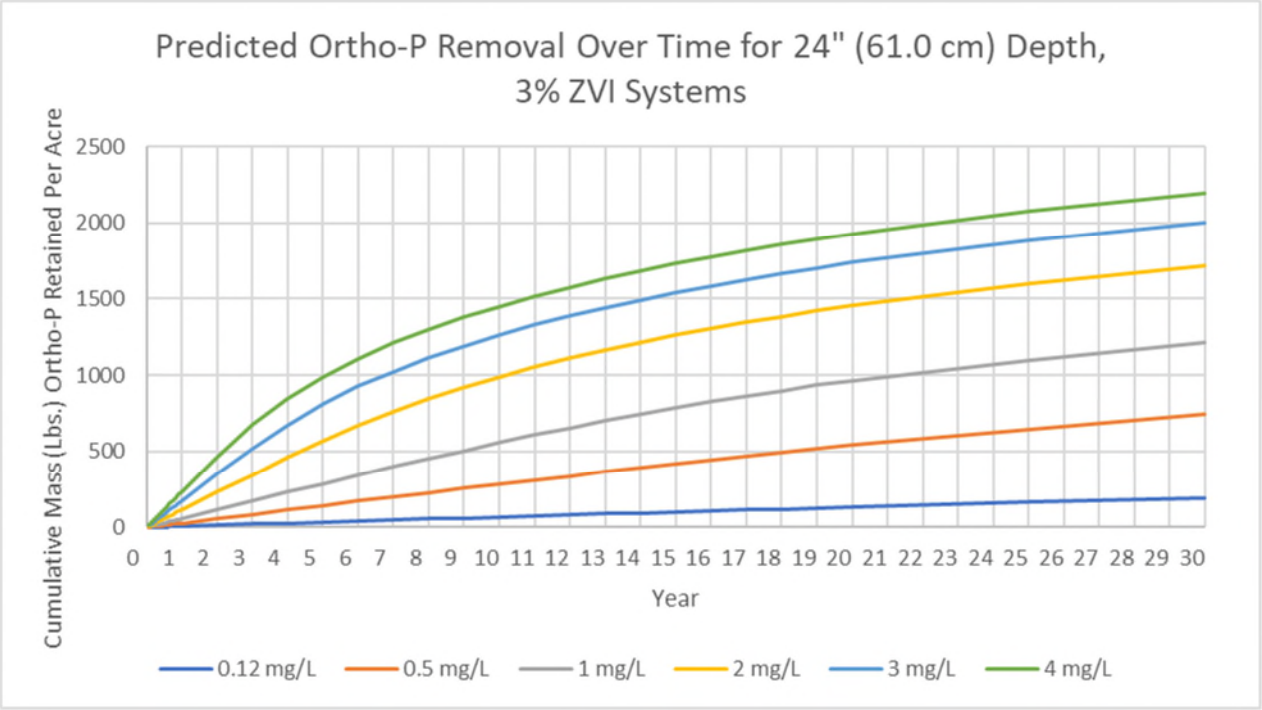

Figure 93: Predictive mass removal curves for systems with 24” media depth and 3% ZVI under varying ortho-P loadings, a watershed area to filter area ratio of 16:1, and 40 inches of annual rainfall

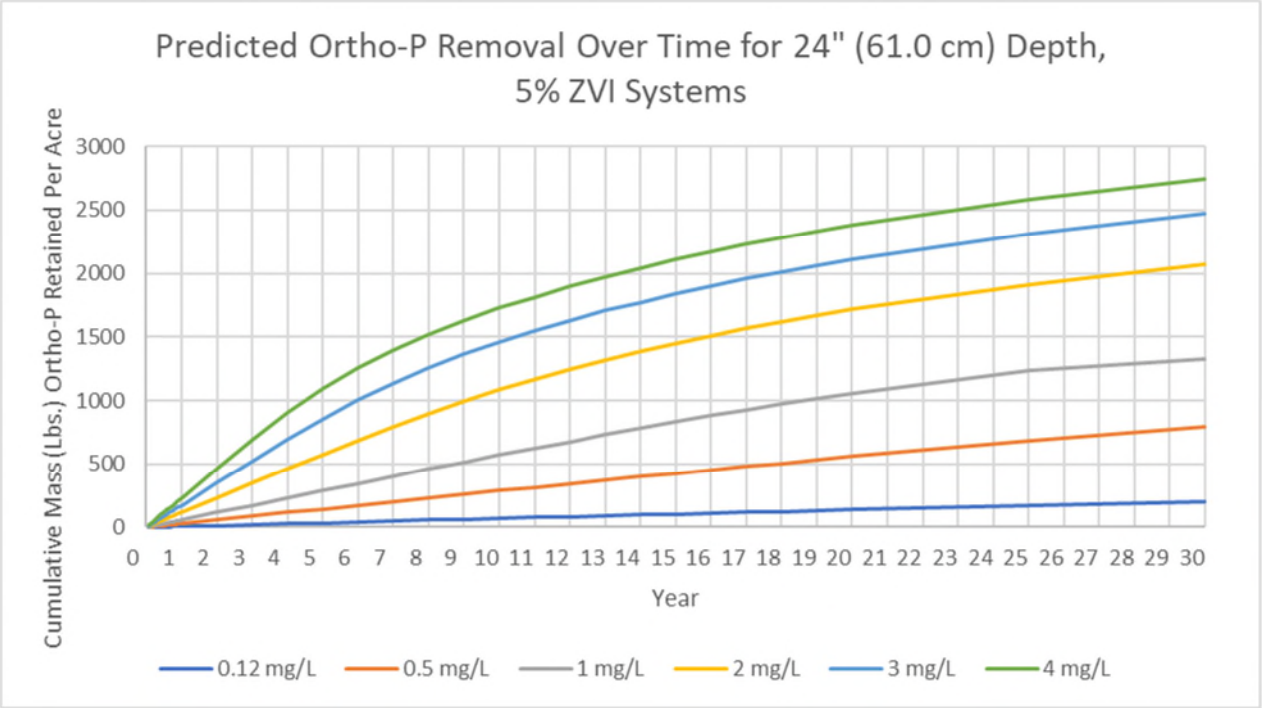

Figure 94: Predictive mass removal curves for systems with 24” media depth and 5% ZVI under varying ortho-P loadings, a watershed area to filter area ratio of 16:1, and 40 inches of annual rainfall

Chapter 5: Conclusions and Future Research

5.1 Summary of Conclusions

The addition of ZVI to stormwater management systems treating simulated agricultural runoff was clearly shown to bolster the media's retention of ortho-P. Regardless of ZVI percentage or media depth, all columns containing ZVI showed higher median ortho-P removal efficiencies than any of the control columns and sustained higher removal efficiencies during most simulated years. In general, it can be concluded that ZVI is an effective media amendment for dissolved ortho-P treatment in runoff, but its degree of effectiveness is largely dependent on the overall mass of ZVI present in the engineered media. The use of ZVI in stormwater treatment systems could dramatically decrease both the depth and area of the systems as it was shown that ZVI addition was significantly more effective at removing ortho-P than systems that only include loam.

5.1.1 Effect of Media Depth on Ortho-P Removal

Greater media depth was shown to increase ortho-P adsorption in the columns. When comparing columns with equal ZVI percentages, the columns with 12-inch (30.5 cm) media depths outperformed those with only 6 inches (15.2 cm). This trend was shown in the median removal percentages for years one through nine, and the yearly data shows higher removals by the 12-inch (30.5 cm) columns for almost all years before the ZVI adsorption capacity was lost. However, increased media depth was not shown to proportionally increase removals with all other variables held constant. This lack of proportional effect necessitates the longevity prediction tool and plots like those shown in Section 4.7 as it would be very difficult to predict what changing the media depth could accomplish otherwise. Although the media depth itself may have had an indirect effect on the overall removal efficiency of a column, it is more likely that the overall ZVI mass was the key factor when comparing columns of differing media depths but the same ZVI percentage. Columns with 12-inch (30.5 cm) depths

had twice as much ZVI mass as their 6-inch (15.2 cm) counterparts of the same ZVI percentage. This additional ZVI mass would allow for more contact, and contact time, with ortho-P and present extra opportunity for adsorption. When put in terms of the Langmuir equation, the percent removal of ortho-P is directly proportional to the mass of ZVI adsorbent (M_{ad}):

$$\%Removal = 100\left(\frac{q_m K_L C_e M_{ad}}{(1 + K_L C_e)VC_0}\right) \quad \text{Equation 11}$$

Therefore, anytime there is more ZVI being used to treat the simulated runoff, there should be a higher ortho-P removal percentage at common snapshots in time.

5.1.2 Effect of ZVI Percentage on Ortho-P Removal

When comparing columns of similar media depth, higher ZVI percentages increased the removal efficiency due to the additional adsorbent mass in the media. Increases in adsorbent mass should directly correspond to higher removal percentages as previously discussed. Columns with higher ZVI percentages consistently outperformed columns of similar media depth and lower ZVI percentages until adsorption capacities were exhausted. Systems with depth constraints could use higher percentages of ZVI to achieve similar removals to those with greater media depths. Column 9, for example, had half the media depth of Column 4 but was still able to retain roughly double the cumulative ortho-P mass. This performance is directly attributable to having a higher percentage, and mass, of ZVI in the column.

5.1.3 Effect of Loam on Ortho-P Removal

The loam used in this column study showed significant ortho-P removal capacity in the first simulated year of testing, but its efficiency quickly dwindled after this point. When considering the high concentrations of ortho-P that the columns were subjected to, it is possible that loam could have a much longer impact on the ortho-P removal from sites with less dramatic loadings. But because the specific makeup of loam can vary greatly by location, these results may not be duplicated with loam from other sources. Furthermore, many people do not have the training or experience to determine

what soils are truly loam, so it is quite possible that mischaracterized soils could be used in stormwater treatment infrastructure and underperform. Loam contains roughly 40% sand, 20% clay, and 40% silt based its soil textural classification (Angima, Terry, Dobkowski, & Zabowski, 2011). With the sand control column showing essentially no ortho-P removal capacity, it is clear that the silt and clay in the media allow for adsorption to occur. It is also possible that the removal capacity of loam was significantly underrepresented in this study. Due to time and other experimental constraints, the hydraulic conductivity needed to be increased in all the columns and a significant portion of the fines was removed before testing began. These fines were likely to provide abundant adsorption sites that could have significantly impacted the removal efficiencies of each column. Throughout testing, small amounts of media were also found in the effluent collected from the columns. In a field application such as a bioretention system, it is unlikely that so much of these fines would be flushed out during treatment, especially with smaller watershed to filter area ratios. These facts are promising for the true effectiveness of loam in field applications when used in conjunction with ZVI as a media amendment.

5.1.4 Effect of Ortho-P Concentration

The effect of ortho-P concentration on ZVI lifespan could be easily seen when adjusting the parameter in the longevity prediction spreadsheet. Although this column study did not specifically use varying ortho-P concentrations in the columns to test these effects, the Langmuir isotherm is a widely accepted model that clearly shows how adsorption capacity decreases as the volume treated increases. The volume treated, in this case, directly corresponds to a certain amount of time-based on the watershed size and expected annual rainfall feeding the treatment infrastructure. It is likely that many agricultural sites would not have steady ortho-P concentrations as high as the target influent for this study. This means that the lifespan of ZVI in their treatment infrastructure could last much longer than the ZVI in this column study. This increased longevity would be assuming that competing chemicals or other factors in the field would not have a significant impact on the ZVI.

5.1.5 Adsorption Efficiency of Media

When comparing the cumulative ortho-P mass retained by the ZVI for each column, it was clear that columns with lower percentages of ZVI showed much less retention capacity. However, these columns proved to be more efficient when comparing their ortho-P retention per gram of ZVI used in the columns. The highest efficiency column had the lowest overall mass of ZVI while the lowest efficiency column had the highest ZVI mass.

Applying these results to treatment infrastructure in the field would need to be completely based on the goals for that system. The following example shows how the decision-making process could play out. A farmer is under a mandate to reduce ortho-P levels in the field runoff below 2.3 mg/L from a median influent of 4.6 mg/L before it discharges to a regulated waterway. 4.6 mg/L was also the target influent concentration in this column study, so 2.3 mg/L here represents 50% removal. If the farmer used the low efficiency (in terms of ortho-P retained per gram of ZVI), 3% ZVI, twelve-inch depth like Column 6, the 2.3 mg/L regulations could be met for roughly four and a half years without replacing the ZVI. If the high efficiency (in terms of ortho-P retained per gram of ZVI), 0.5% ZVI were used, six-inch depth like Column 7, he would only be able to meet regulations for roughly one year. The farmer would need to weigh the costs of replacing less ZVI more frequently versus replacing more ZVI less frequently, along with factors such as labor costs.

5.1.6 The ZVI Longevity Prediction Tool

The ZVI longevity prediction model could be a very valuable tool for those searching for the ideal percentage of ZVI and depth of media for their ortho-P treatment system. In the previous example of a farmer looking for the most cost-effective ZVI system for his land, they would not likely have a fundamental knowledge of adsorption kinetics to help him predict the longevity of his system. Even if they did have this knowledge, the calculations could be very time consuming if done by other means. This tool would allow them to easily look at options for ZVI percentage and media depth and compare

their projected ortho-P removals over time. At the same time, they could be using their knowledge of ZVI cost, soil costs and availability, labor costs, and ZVI disposal costs to choose the least expensive option that will help them meet their treatment requirements or goals. This tool significantly simplifies an otherwise daunting task of comparing many removal efficiency curves using the Langmuir isotherm.

5.2 Future Research

Those interested in using ZVI as a treatment method for ortho-P from runoff, whether it be agricultural or not, would benefit greatly from expanded research in this area. This study and others like it have displayed the clear viability of ZVI as an ortho-P treatment method, but much is still unknown about how specific variables can affect the ZVI's removal efficiency.

A limitation of this study was a lack of replicated data points for each column's testing. Ideally, testing would have included many columns with the same ZVI percentages so that trends and data points could be more rigorously scrutinized by statistical methods. With such few data points for each column and simulated year in this study, it was impossible to determine if any points were outliers. Ideally, for each mix, there would be a cluster of data points at every simulated year. These additional points would allow for more confidence when fitting isotherms to the data and when projecting removals for other mixes. Future projects could use the same column setup and methods as this study to verify or refute conclusions and to create more accurate ZVI longevity predictions. Even if the influent ortho-P concentrations in a future study were different, the results would be very useful when comparing to the predictive curves given by the longevity prediction tool.

Another natural next step in researching agricultural runoff treatment using ZVI would be to test full-scale field systems. Many conditions exist in nature that cannot be replicated in a laboratory setting. Although variables cannot be controlled as easily outside the laboratory, it would be very informative to see how a ZVI-enhanced bioretention system would respond to actual agricultural ortho-P loading over time.

Before a system is tested in the field, it would be helpful to determine via column study if the system could get similar removals whether the ZVI is mixed into the media or in its own single layer. It would be ideal if the ZVI performed just as well without being mixed into the media. A single layer of ZVI would be easier to extract and dispose of when its adsorption capacity was exhausted. It could greatly reduce labor time and costs while making it easier to reuse the other media in the treatment infrastructure.

Another significant knowledge gap in this study involves how contact time affected ortho-P adsorption. Due to many limitations, contact time could not be easily controlled across all columns. A future study could test how hydraulic conductivity, infiltration rate, and contact time affect removals in the columns. If the mix was held constant across several columns and contact time varied significantly, results may show a relationship between ortho-P removal efficiency and contact time between the media and simulated runoff. Elrashidi et al. (2005) reported that in a batch study that up to 95% of ortho-P could be adsorbed within ten minutes, indicating that the contact time necessary for ortho-P adsorption may actually be very short.

Other studies could include column studies using different loam in the mix, different percentages of loam and ZVI, or different ZVI particle size distributions. It is possible that ZVI with smaller particles could eventually leach through the system and no longer provide the intended treatment. This leaching could also have potential environmental impacts. Tests exploring possible unintended consequences such as iron leaching could be helpful in determining the overall feasibility of ZVI-enriched treatment systems moving forward.

References

Allred, B. J., & Racharaks, R. (2014). Laboratory comparison of four iron-based filter materials for drainage water phosphate treatment. *Water Environment Research, 86*(9), 852-862.

Almeelbi, T., & Bezbaruah, A. (2012, March). Aqueous phosphate removal using nanoscale zero-valent iron. *Journal of Nanoparticle Research, 14*(900).

Aly, O. M., & Faust, S. D. (1964). Studies on the fate of 2,4-D and ester derivatives in natural surface waters. *Journal of Agricultural and Food Chemistry, 12*(6), 541-546.

Angima, S., Terry, T. A., Dobkowski, A., & Zabowski, D. (2011). Best management practices for maintaining soil productivity in the Douglas-fir region. *EM, 9023*.

Baker, J. L., Campbell, K. L., Johnson, H. P., & Hanway, J. J. (1974, August). Nitrate, phosphorus, and sulfate in subsurface drainage water. *Journal of Environmental Quality, 4*(3), 406-412.

Barbu, I., Ballestero, T., & Ballestero, H. (2014). *Investigation of bioretention soil media and amendments for treatment of nutrients from stormwater runoff.* Durham, NH: University of New Hampshire Stormwater Center.

Bartsch, A. F. (1972). *Role of phosphorus in eutrophication.* National Environmental Research Center. Corvallis, Oregan: EPA.

Benjamin, M. M. (2002). *Water Chemistry.* New York, NY: McGraw-Hill.

Berg, R. D., & Carter, D. L. (1980). Furrow erosion and sediment losses on irrigated cropland. *Journal of Soil and Water Conservation, 35*(6), 267-270.

Borchardt, J. A. (1970). Secondary effects of nitrogen in water. *Nitrate and water supply: source and control* (pp. 66-76). University of Illinois, Urbana, Ill: Twelfth Sanitary Engineering Conference.

Burt, T. P., & Slattery, M. C. (2006). 118 land use and land cover effects on runoff processes: Agricultural effects. In *Encyclopedia of Hydrological Sciences* (Vol. 10, p. 118).

Carpenter, S. R. (2005, July). Eutrophication of aquatic ecosystems: Bistability and soil phosphorus. *PNAS, 102*(29), 10002-10005.

Chiu, P., Imhoff, P., & Culver, T. (2016). *Simultaneous removal of nitrogen and phosphorus from stormwater by zero-valent iron and biochar in bioretention cells.* University of Delaware, Department of Civil and Environmental Engineering. Newark, DE: Virginia Center for Transportation Innovation and Research.

DePinto, J. V., Young, T. C., & Salisbury, D. K. (1986). Impact of phosphorus availability on modelling phytoplankton dynamics. *Hydrobiological Bulletin, 20*, 225-243.

Elrashidi, M. A., Mays, M. D., Harder, J., Shroeder, D., & Brakhage, P. (2005, July). Loss of phosphorus by runoff for agricultural watersheds. *Soil Science, 170*(7), 543-558.

Erickson, A. J., & Gulliver, J. S. (2010). *Performance assessment of an iron-enhanced sand filtration trench for capturing dissolved phosphorus.* Minneapolis, MN.

Erickson, A. J., Gulliver, J. S., & Weiss, P. T. (2007, May). Enhanced sand filtration for storm water phosphorus removal. *Journal of Environmental Engineering*, 485-497.

Erickson, A. J., Gulliver, J. S., & Weiss, P. T. (2017, September). PhosphaterRemoval from agricultural tile drainage with iron enhanced sand. *Water, 9*(672).

Erickson, A. J., Gulliver, J. S., Weiss, P. T., & Huser, B. J. (February 23, 2010). Iron-enhanced sand filtration for stormwater phosphorus removal. *17th Congress of the Asia and Pacific Division of the International Association of Hydraulic Engineering and Research incorporating the 7th International Urban Watershed Management Conference (IAHR-APD-IUWMC 2010).* Auckland, NZ.

Fry, F. E. (1969). Some possible physiological stresses induced by eutrophication. In *Eutrophication: causes, consequences, correctives* (pp. 531-536). Washington D. C.: National Academy of Sciences.

Gillingham, A. G., Thorrold, B. S., Wheeler, D. M., Power, I. L., Gray, M. H., & Blennerhassett, J. D. (1997). Factors influencing phosphate losses in surface runoff water. *H. Furness (ed.) Proceedings of the 24th NZFMRA Technical Conference* (pp. 144-153). Invercargill: New Zealand Fertiliser Manufacturer's Research Association.

Hart, M. R., Quin, B. F., & Nguyen, M. L. (2004, November). Phosphorus runoff from agricultural land and direct fertilizer effects. *Journal of Environmental Quality, 33*, 1954-1972.

Haygarth, P. M., & Jarvis, S. C. (1997). Soil derived phosphorus in surface runoff from grazed grassland lysimeters. *Water Research, 31*, 140-148.

He, Z. L., Zhang, M. K., Stoffella, P. J., Yang, X. E., & Banks, D. J. (2006, June). Phosphorus concentrations and loads in runoff water under crop production. *Soil Science Society of America Journal, 70*(5), 1807-1816.

Jenkins, D., Ferguson, J. F., & Menar, A. B. (1971). Chemical processes for phosphate removal. *Water Research, 5*, 369.

Johnson, H. P., & Baker, J. L. (1984). *Field-to-stream transport of agricultural chemicals and sediment in an Iowa watershed: part II. Data base for model testing (1979-1980).* Environmental Research Laboratory. Athens, GA: EPA.

Kinniburgh, D. G. (1986). General purpose adsorption isotherms. *Environmental Science and Technology, 20*, 895-904.

LeVan, M. D., & Vermeulen, T. (1981). Binary Langmuir and Freundlich isotherms for ideal adsorbed solutions. *Journal of Physical Chemistry*, 3247-3250.

Li, J., Wang, Z., Cao, X., Wang, Z., & Zheng, Z. (2015). Effect of orthophosphate and bioavailability of dissolved organic phosphorous compounds to typically harmful cyanobacterium Microcystis aeruginosa. *Marine Pollution Bulletin*, 52-88.

Nichols, D. J., Edwards, D., & Edwards, D. R. (1994). Nutrient runoff from pasture after incorporation of poultry litter or inorganic fertilizer. *Soil Science Society of America Journal, 58*(4), 1224-1228.

Nutrient pollution policy and data. (2018). Retrieved from epa.gov: https://www.epa.gov/nutrient-policy-data

Pitt, R., Maestre, A., Morquecho, R., Brown, T., Swann, C., Cappiella, K., & Schueler, T. (2005). *Evaluation of NPDES Phase 1 municipal stormwater monitoring data.* University of Alabama and the Center for Watershed Protection.

Reddy, K. R., Xie, T., & Dastgheibi, S. (2014, January). Nutrients removal from urban stormwater by different filter materials. *Water Air and Soil Pollution, 225*(1778).

Rinker, K. R., & Powell, R. T. (2006, November). Dissolved organic phosphorus in the Mississippi River plume during spring and fall 2002. *Marine Chemistry, 102*(1-2), 170-179.

Sellner, B. (2016). Evaluating steel byproducts and natural minerals for phosphate adsorption from agricultural subsurface drainage. *Theses and Dissertations, Paper 1025*.

Sharpley, A. N. (1993). Assessing phosphorus bioavailability in agricultural soils and runoff. *Fertilizer Research, 36*, 259-272.

Sharpley, A. N., & Syers, J. K. (1976). Phosphorus transport in surface run-off as influenced by fertiliser and grazing cattle. *New Zealand Journal of Science, 19*, 277-282.

Sharpley, A. N., Daniel, T., Sims, T., Lemunyon, J., Stevens, R., & Parry, R. (2003, September). Agricultural phosphorus and eutrophication. *ARS-149, 2*.

Sharpley, A. N., Daniels, T. C., Sims, J. T., & Pote, J. T. (1996). Determining environmentally sound soil phosphorus levels. *Journal of Soil and Water Conservation, 51*(1), 160-166.

Sharpley, A. N., Robinson, J. S., & Smith, S. J. (1995, June). Bioavailable phosphorus dynamics in agricultural soils and effects on water quality. *Geoderma, 67*(1-2), 1-15.

Sharpley, A. N., Smith, S. J., & Menzel, R. G. (1989). Phosphorus dynamics in agricultural runoff and reservoirs in Oklahoma. *Lake and Reservoir Management, 5*(2), 75-81.

Sharpley, A. N., Smith, S. J., Jones, O. R., Berg, W. A., & Coleman, G. A. (1992, January). The transport of bioavailable phosphorus in agricultural runoff. *Journal of Environmental Quality, 21*(1), 30-35.

Stewart, B. A., Woolhiser, D. A., Wischmeier, W. H., Caro, J. H., & Frere, M. H. (1975). *Control of water pollution from cropland: Volume I.* Washington D.C.: EPA, USDA.

Stewart, B. A., Woolhiser, D. A., Wischmeier, W. H., Caro, J. H., & Frere, M. H. (1976). *Control of water pollution from cropland: Volume II* (Vol. 2). Washington D.C.: EPA, USDA.

Stone, R. M. (2013). Evaluation and optimization of bioretention design for nitrogen and phosphorus removal. *Thesis*.

Stone, R. M. (2013). *Evaluation and optimization of bioretention design for nitrogen and phosphorus removal.* Civil Engineering. University of New Hampshire.

Stumm, W., & Morgan, J. J. (1981). *Aquatic chemistry: An introduction emphasizing chemical equilibria in natural waters.* New York: Wiley.

UNHSC. (2017, February). *UNHSC Bioretention Soil Specification.* Retrieved from https://www.unh.edu/unhsc/sites/default/files/media/unhsc_bsm_spec_2-28-17_0.pdf

University of New Hampshire Stormwater Center 2012 Biennial Report. (2012). Retrieved from https://www.unh.edu/unhsc/

Withers, P. J., Clay, S. D., & Breeze, V. G. (2001). Phosphorus transfer in runoff following application of fertilizer, manure and sewage sludge. *Journal of Environmental Quality, 30*, 180-188.

Yan, W., Huang, M., Zhang, S., & Tang, Y. (2001, October). Phosphorus export by runoff from agricultural field plots with different crop cover in Lake Taihu watershed. *Journal of Environmental Sciences, 13*(4), 502-507.

Yin, C., Lan, Z., Zhao, M., & Bernhardt, H. (1992). Determination of phosphorus concentration threshold for algal growth in eutrophic Chaohu Lake, China. *Journal of Environmental Science and Health. Part A: Environmental Science and Engineering and Toxicology, 27*(2), 443.

Zhang, H., Cao, Z., Wang, G., Zhang, H., & Wong, M. H. (2003, September). Winter runoff losses of phosphorus from paddy soils in the Taihu Lake Region of South China. *Chemosphere, 52*(9), 1461-1466.

Appendix A: Laboratory and Testing Data

Table 18: Ortho-P results from Absolute Resource Associates laboratory

Bag ID	Media Depth (in)	%ZVI	Field ID	Year	Column	Ortho-Phosphate as P Result (mg/L)	
22458			blank			0.5	
22479	0	0	M3-Y1-influent	0.25	influent	4.6	
22480	12	0	M3-Y1-C1	0.25	C1	0.7	
22481	6	0	M3-Y1-C2	0.25	C2	2.4	
22483	12	0.5	M3-Y1-C4	0.25	C4	0.1	
22484	12	1	M3-Y1-C5	0.25	C5	0	(a)
22485	12	3	M3-Y1-C6	0.25	C6	0	(a)
22486	6	0.5	M3-Y1-C7	0.25	C7	0.5	
22487	6	1	M3-Y1-C8	0.25	C8	0	(a)
22488	6	3	M3-Y1-C9	0.25	C9	0	(a)
22489	0	0	M6-Y1-influent	0.5	influent	4.5	
22490	12	0	M6-Y1-C1	0.5	C1	1.5	
22491	6	0	M6-Y1-C2	0.5	C2	2.9	
22493	12	0.5	M6-Y1-C4	0.5	C4	0	(a)
22494	12	1	M6-Y1-C5	0.5	C5	0	(a)
22495	12	3	M6-Y1-C6	0.5	C6	0	(a)
22496	6	0.5	M6-Y1-C7	0.5	C7	1.3	
22497	6	1	M6-Y1-C8	0.5	C8	0.2	
22498	6	3	M6-Y1-C9	0.5	C9	0.3	
22499	0	0	M9-Y1-influent	0.75	influent	4.3	
22500	12	0	M9-Y1-C1	0.75	C1	2	
22501	6	0	M9-Y1-C2	0.75	C2	3.4	
22503	12	0.5	M9-Y1-C4	0.75	C4	0.4	
22504	12	1	M9-Y1-C5	0.75	C5	0	(a)
22505	12	3	M9-Y1-C6	0.75	C6	0	(a)
22506	6	0.5	M9-Y1-C7	0.75	C7	1.3	
22507	6	1	M9-Y1-C8	0.75	C8	0.4	
22508	6	3	M9-Y1-C9	0.75	C9	0.3	
22509	0	0	Y1-influent	1	influent	4.3	
22510	12	0	Y1-C1	1	C1	3.3	
22511	6	0	Y1-C2	1	C2	4.1	
22512	6	0	Y1-C3	1	C3	4.4	
22513	12	0.5	Y1-C4	1	C4	2.2	(b)
22514	12	1	Y1-C5	1	C5	0.6	
22515	12	3	Y1-C6	1	C6	0	(a)
22516	6	0.5	Y1-C7	1	C7	2.8	
22517	6	1	Y1-C8	1	C8	1.2	
22518	6	3	Y1-C9	1	C9	0.5	
22519	0	0	Y2-influent	2	influent	4.3	
22520	12	0	Y2-C1	2	C1	3.8	
22521	6	0	Y2-C2	2	C2	3.8	
22522	6	0	Y2-C3	2	C3	4.3	
22523	12	0.5	Y2-C4	2	C4	3.4	
22524	12	1	Y2-C5	2	C5	3.3	
22525	12	3	Y2-C6	2	C6	0.2	

(Cont.)

Bag ID	Media Depth (in)	%ZVI	Field ID	Year	Column	Ortho-Phosphate as P Result (mg/L)	
22526	6	0.5	Y2-C7	2	C7	3.6	
22527	6	1	Y2-C8	2	C8	2.6	
22528	6	3	Y2-C9	2	C9	2.2	
22529	0	0	Y3-influent	3	influent	4.3	
22530	12	0	Y3-C1	3	C1	3.8	
22531	6	0	Y3-C2	3	C2	4	
22532	6	0	Y3-C3	3	C3	4.3	
22533	12	0.5	Y3-C4	3	C4	3.5	
22534	12	1	Y3-C5	3	C5	3.1	
22535	12	3	Y3-C6	3	C6	0.2	
22536	6	0.5	Y3-C7	3	C7	4	(c)
22537	6	1	Y3-C8	3	C8	3.3	
22538	6	3	Y3-C9	3	C9	2.7	
22539	0	0	Y4-influent	4	influent	4.2	
22540	12	0	Y4-C1	4	C1	4.1	
22541	6	0	Y4-C2	4	C2	4.1	
22542	6	0	Y4-C3	4	C3	4.2	(d)
22543	12	0.5	Y4-C4	4	C4	4	
22544	12	1	Y4-C5	4	C5	3.6	
22545	12	3	Y4-C6	4	C6	1.4	
22546	6	0.5	Y4-C7	4	C7	3.8	
22547	6	1	Y4-C8	4	C8	3.7	
22548	6	3	Y4-C9	4	C9	3.2	
22549	0	0	Y5-influent	5	influent	3.5	
22550	12	0	Y5-C1	5	C1	4.1	
22551	6	0	Y5-C2	5	C2	3.9	
22552	6	0	Y5-C3	5	C3	3.9	
22553	12	0.5	Y5-C4	5	C4	3.9	
22554	12	1	Y5-C5	5	C5	3.7	(e)
22555	12	3	Y5-C6	5	C6	2.3	
22556	6	0.5	Y5-C7	5	C7	3.8	
22557	6	1	Y5-C8	5	C8	3.7	
22558	6	3	Y5-C9	5	C9	3.6	
22559	0	0	Y6-influent	6	influent	4.1	
22560	12	0	Y6-C1	6	C1	4.1	
22561	6	0	Y6-C2	6	C2	4	
22562	6	0	Y6-C3	6	C3	4.2	(f)
22563	12	0.5	Y6-C4	6	C4	4.2	
22564	12	1	Y6-C5	6	C5	4.3	
22565	12	3	Y6-C6	6	C6	3.1	
22566	6	0.5	Y6-C7	6	C7	4.1	
22567	6	1	Y6-C8	6	C8	4	
22568	6	3	Y6-C9	6	C9	3.9	
22569	0	0	Y7-influent	7	influent	3.7	
22570	12	0	Y7-C1	7	C1	3.9	
22571	6	0	Y7-C2	7	C2	4	
22572	6	0	Y7-C3	7	C3	4	(g)

(Cont.)

Bag ID	Media Depth (in)	%ZVI	Field ID	Year	Column	Ortho-Phosphate as P Result (mg/L)	
22573	12	0.5	Y7-C4	7	C4	3.8	
22574	12	1	Y7-C5	7	C5	3.6	
22575	12	3	Y7-C6	7	C6	3.2	
22576	6	0.5	Y7-C7	7	C7	3.9	
22577	6	1	Y7-C8	7	C8	3.8	
22578	6	3	Y7-C9	7	C9	3.7	
22579	0	0	Y8-influent	8	influent	3.8	
22580	12	0	Y8-C1	8	C1	3.9	
22581	6	0	Y8-C2	8	C2	3.9	
22582	6	0	Y8-C3	8	C3	3.9	
22583	12	0.5	Y8-C4	8	C4	3.7	
22584	12	1	Y8-C5	8	C5	3.7	
22585	12	3	Y8-C6	8	C6	3	(h)
22586	6	0.5	Y8-C7	8	C7	3.7	
22587	6	1	Y8-C8	8	C8	3.6	
22588	6	3	Y8-C9	8	C9	3.5	
22589	0	0	Y9-influent	9	influent	4.3	
22590	12	0	Y9-C1	9	C1	3.9	
22591	6	0	Y9-C2	9	C2	3.9	(i)
22592	6	0	Y9-C3	9	C3	4	
22593	12	0.5	Y9-C4	9	C4	3.9	
22594	12	1	Y9-C5	9	C5	3.8	
22595	12	3	Y9-C6	9	C6	3.6	
22596	6	0.5	Y9-C7	9	C7	3.8	
22597	6	1	Y9-C8	9	C8	3.8	
22598	6	3	Y9-C9	9	C9	3.6	
22599	0	0	Y10-influent	10	influent	4	(j)
22600	12	3	Y10-C6	10	C6	3.8	
22601	0	0	Y11-influent	11	influent	3.8	
22602	12	3	Y11-C6	11	C6	3	
22603	0	0	Y12-influent	12	influent	4.2	
22604	12	3	Y12-C6	12	C6	3.7	
22605	0	0	Y13-influent	13	influent	4.3	
22606	12	3	Y13-C6	13	C6	4.1	
22607	0	0	Y14-influent	14	influent	4.5	
22608	12	3	Y14-C6	14	C6	4.3	
22609	0	0	Y15-influent	15	influent	4.4	(k)
22610	12	3	Y15-C6	15	C6	4.2	
22611	0	0	Y16-influent	16	influent	4.5	
22612	12	3	Y16-C6	16	C6	4.6	
22613	0	0	Y17-influent	17	influent	5.1	
22614	12	3	Y17-C6	17	C6	4.8	
22615	0	0	Y18-influent	18	influent	5	
22616	12	3	Y18-C6	18	C6	4.9	
22617	0	0	Y19-influent	19	influent	4.8	
22618	12	3	Y19-C6	19	C6	4.8	
22619	0	0	Y20-influent	20	influent	4.9	

(Cont.)

Bag ID	Media Depth (in)	%ZVI	Field ID	Year	Column	Ortho-Phosphate as P Result (mg/L)
22620	12	3	Y20-C6	20	C6	5

(a) Below reporting limit of 0.1 mg/L

(b) The recovery for the matrix spike was 65%. The acceptance criteria is 90-110%. All other associated QC samples were acceptable.

(c) The recovery for the matrix spike was 46%. The acceptance criteria is 90-110%. All other associated QC samples were acceptable.

(d) The recovery for the matrix spike was 45%. The acceptance criteria is 90-110%. All other associated QC samples were acceptable.

(e) The recovery for the matrix spike was 70%. The acceptance criteria is 90-110%. All other associated QC samples were acceptable.

(f) The recovery for the matrix spike was 57%. The acceptance criteria is 90-110%. All other associated QC samples were acceptable.

(g) The recovery for the matrix spike was 57%. The acceptance criteria is 90-110%. All other associated QC samples were acceptable.

(h) The recovery for the matrix spike was 78%. The acceptance criteria is 90-110%. All other associated QC samples were acceptable.

(i) The recovery for the matrix spike was 52%. The acceptance criteria is 90-110%. All other associated QC samples were acceptable. The RPD for the sample duplicate, run as internal QC, was outside the 10% acceptance range. The duplicate analysis showed a concentration of 5.6 mg/L.

(j) The recovery for the matrix spike was 75%. The acceptance criteria is 90-110%. All other associated QC samples were acceptable.

(k) The recovery for the matrix spike was 36%. The acceptance criteria is 90-110%. All other associated QC samples were acceptable.

Table 19: Influent and effluent pH and temperature measurements for simulated years 6 through 9

pH, T (°C) by Simulated Year and Column

		Influent	C-1	C-2	C-3	C-4	C-5	C-6	C-7	C-8	C-9
Y6	pH, T	7.54, 18.7	7.71, 18.7	7.81, 18.7	7.9, 18.7	7.73, 18.6	7.73, 18.7	7.81, 18.7	7.8, 18.8	7.75, 18.8	7.78, 18.7
Y7	pH, T	7.8, 18.3	7.87, 18.2	7.98, 18.1	7.99, 18.1	7.93, 17.9	7.9, 17.9	7.93, 17.9	7.94, 18.2	7.93, 18.2	7.94, 18.3
Y8	pH, T	7.19, 19.0	7.43, 18.6	7.35, 18.5	7.33, 18.4	7.47, 18.3	7.48, 18.3	7.61, 18.3	7.35, 18.5	7.42, 18.4	7.42, 18.5
Y9	pH, T	7.86, 18.6	7.56, 18.2	7.62, 18.1	7.79, 18.0	7.6, 17.9	7.58, 18.0	7.72, 17.9	7.62, 18.0	7.64, 17.9	7.64, 17.8
Y10	pH, T	7.18, 20.4	-	-	-	-	-	7.57, 18.8	-	-	-
Y11	pH, T	7.58, 18.8	-	-	-	-	-	7.80, 17.0	-	-	-
Y12	pH, T	7.85, 19.1	-	-	-	-	-	7.98, 17.7	-	-	-
Y13	pH, T	7.51, 20.1	-	-	-	-	-	7.69, 18.7	-	-	-
Y14	pH, T	7.85, 19.5	-	-	-	-	-	7.91, 18.4	-	-	-
Y15	pH, T	7.28, 19.9	-	-	-	-	-	7.54, 18.5	-	-	-
Y16	pH, T	7.59, 22.0	-	-	-	-	-	7.73, 19.9	-	-	-
Y17	pH, T	7.42, 19.4	-	-	-	-	-	7.59, 17.8	-	-	-
Y18	pH, T	7.10, 21.6	-	-	-	-	-	7.59, 19.8	-	-	-
Y19	pH, T	7.59, 20.4	-	-	-	-	-	7.65, 18.4	-	-	-
Y20	pH, T	7.41, 20.1	-	-	-	-	-	7.70, 18.8	-	-	-

*Data not available for Years 1-5

Appendix B: Freundlich and Langmuir Methods Comparison

This appendix is intended to display the process for choosing the underlying model for the longevity prediction tool and the best methods for determining its constant parameters (i.e. K, n, q_m, and K_L). All percent removal plots in this appendix include corrections for the effects of loam on each column's ortho-P removal.

B.1 Freundlich Analysis

B.1.1 Constant *n*

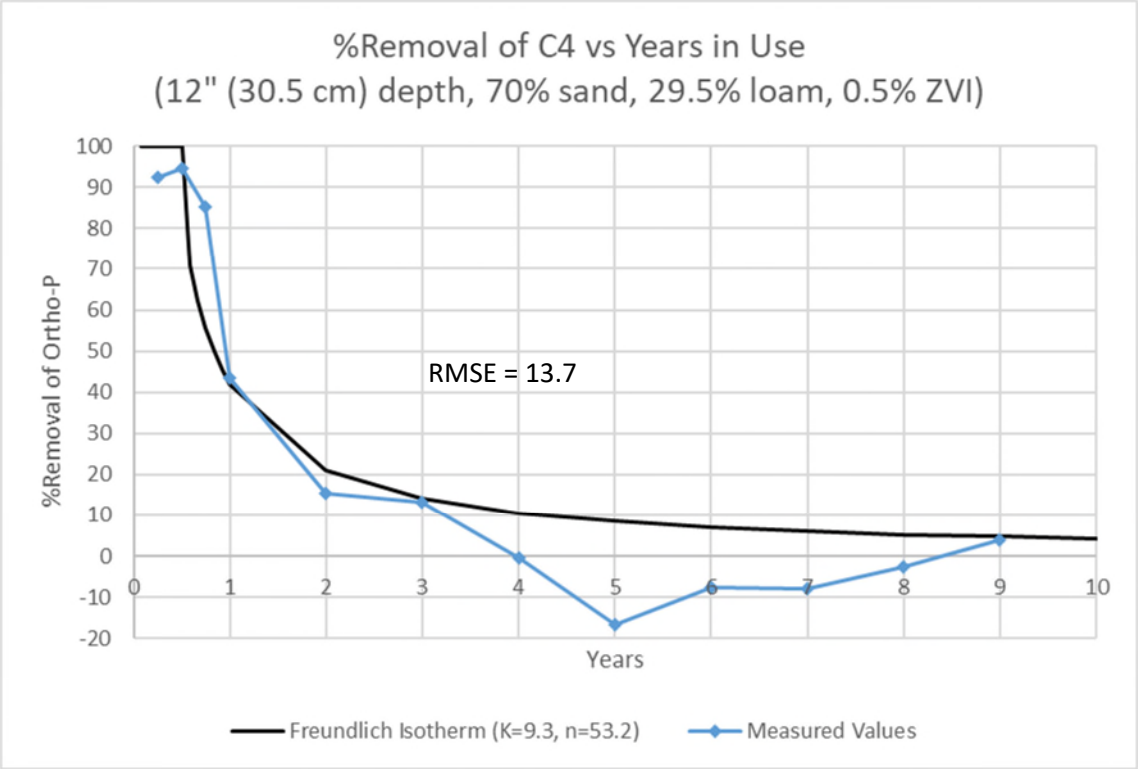

Figure 95: Column 4 comparison of percent ortho-P removal for raw values and values calculated using K from Table 14 and the median n value across all columns

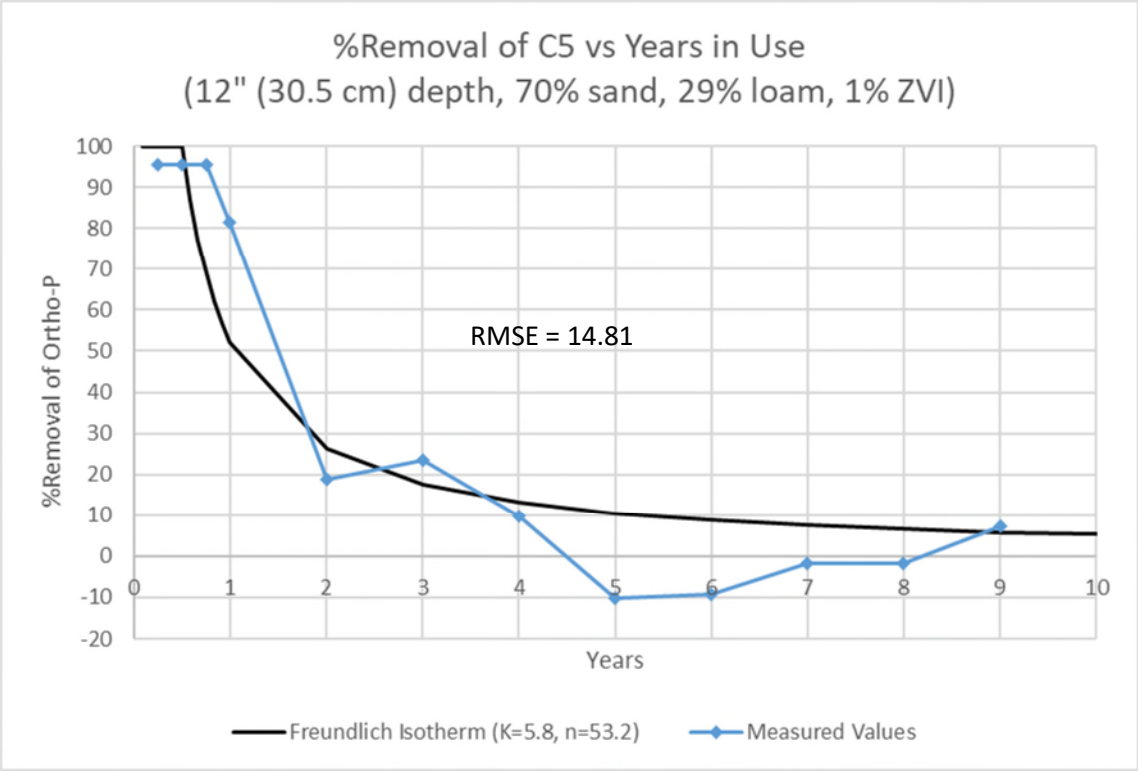

Figure 96: Column 5 comparison of percent ortho-P removal for raw values and values calculated using *K* from Table 14 and the median *n* value across all columns

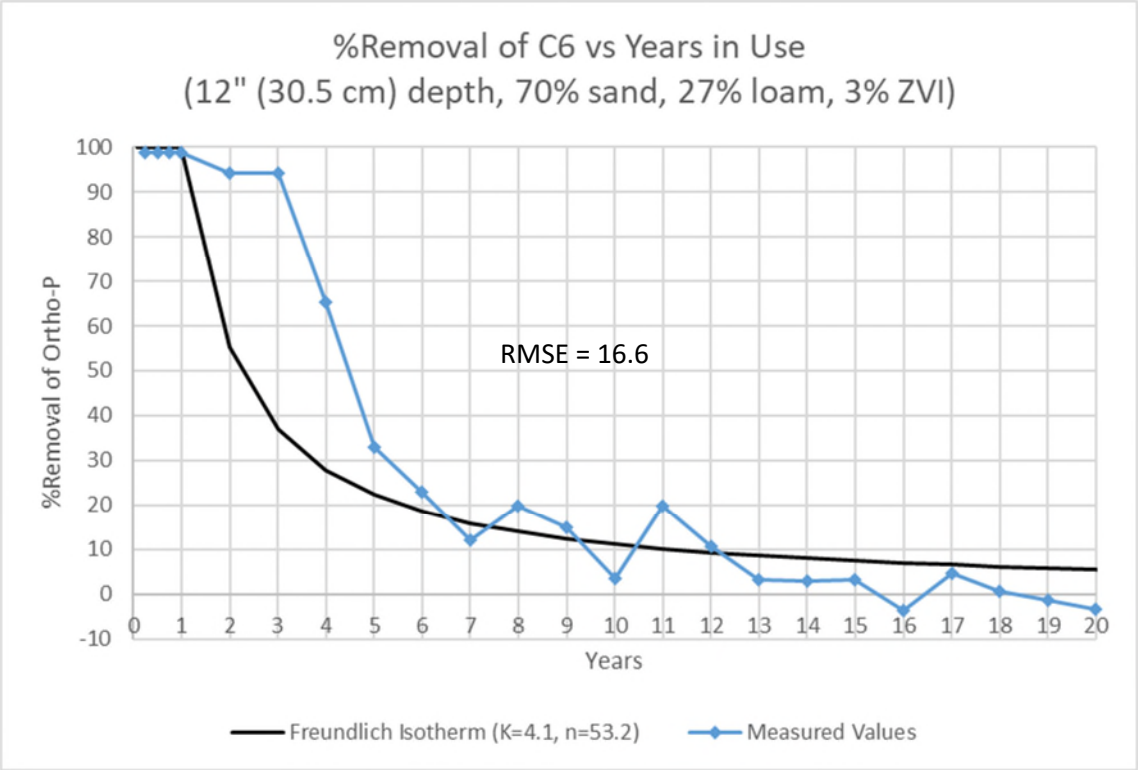

Figure 97: Column 6 comparison of percent ortho-P removal for raw values and values calculated using *K* from Table 14 and the median *n* value across all columns

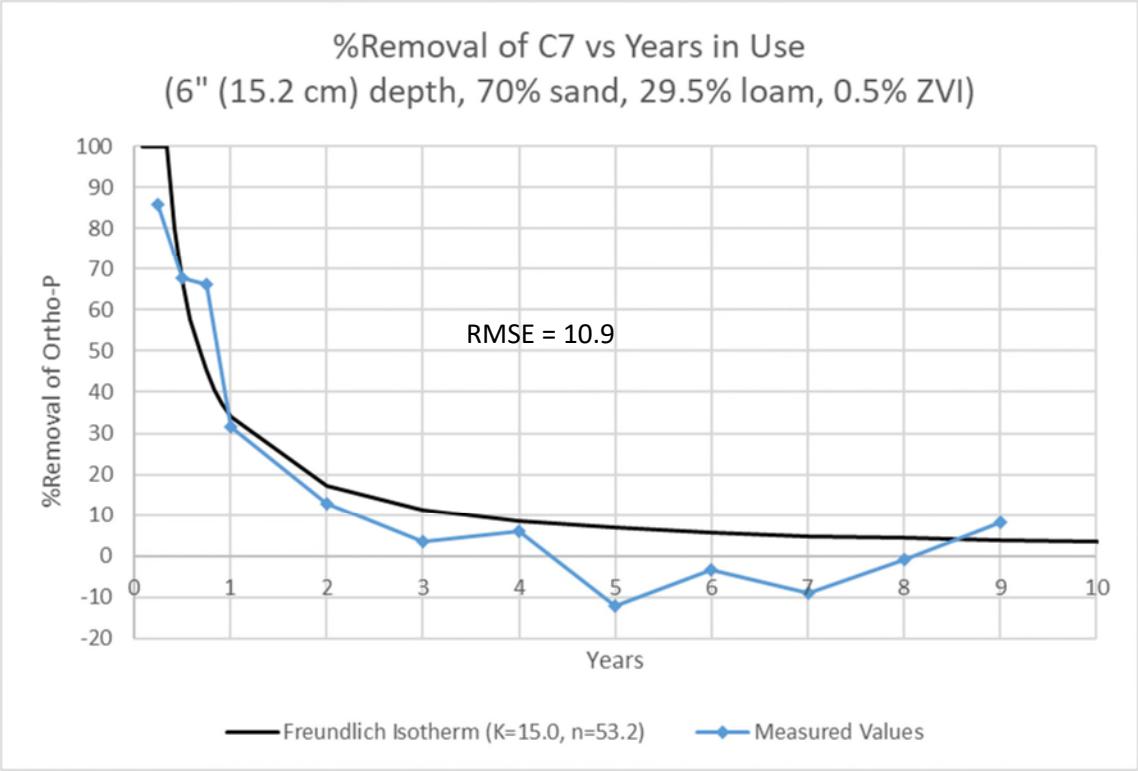

Figure 98: Column 7 comparison of percent ortho-P removal for raw values and values calculated using *K* from Table 14 and the median *n* value across all columns

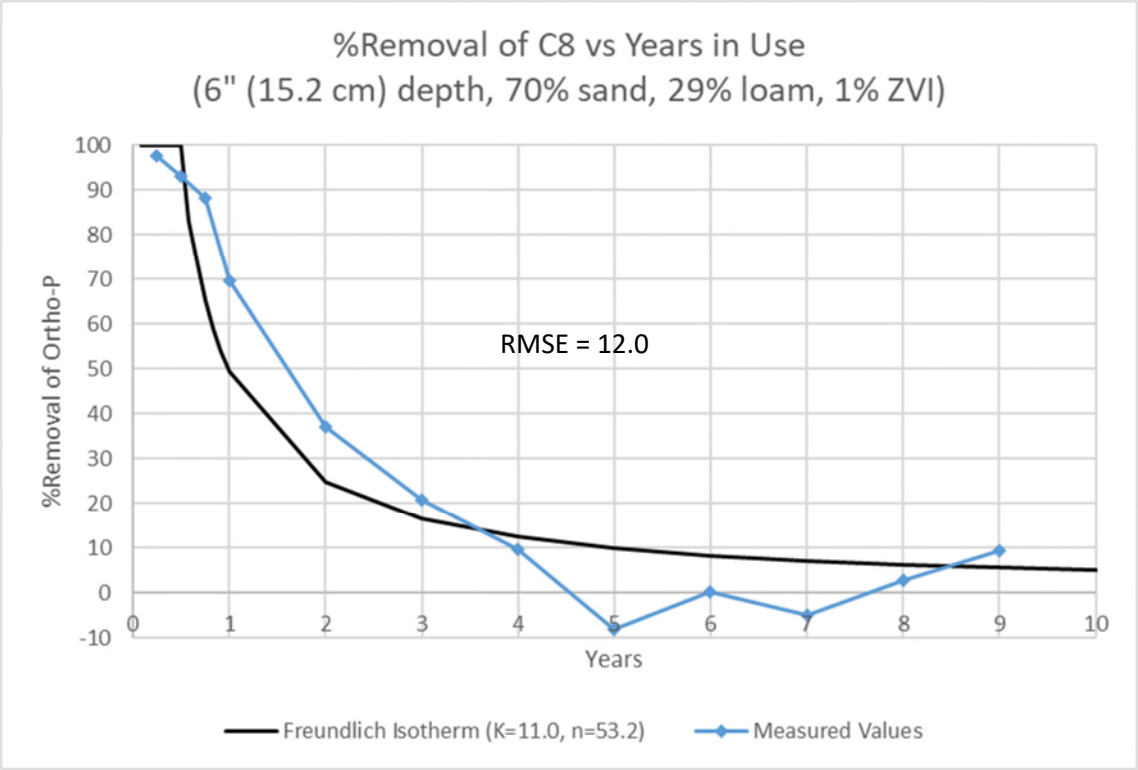

Figure 99: Column 8 comparison of percent ortho-P removal for raw values and values calculated using *K* from Table 14 and the median *n* value across all columns

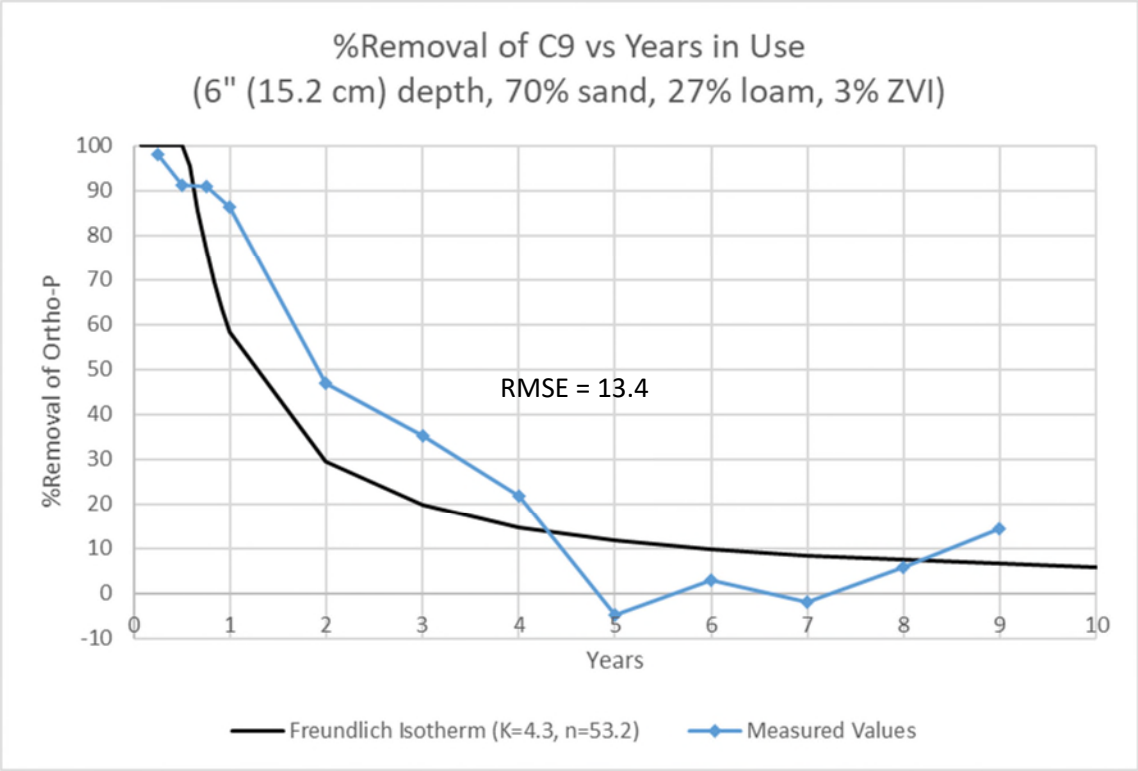

Figure 100: Column 9 comparison of percent ortho-P removal for raw values and values calculated using *K* from Table 14 and the median *n* value across all columns

B.1.2 *K* from Trendline with Constant *n*

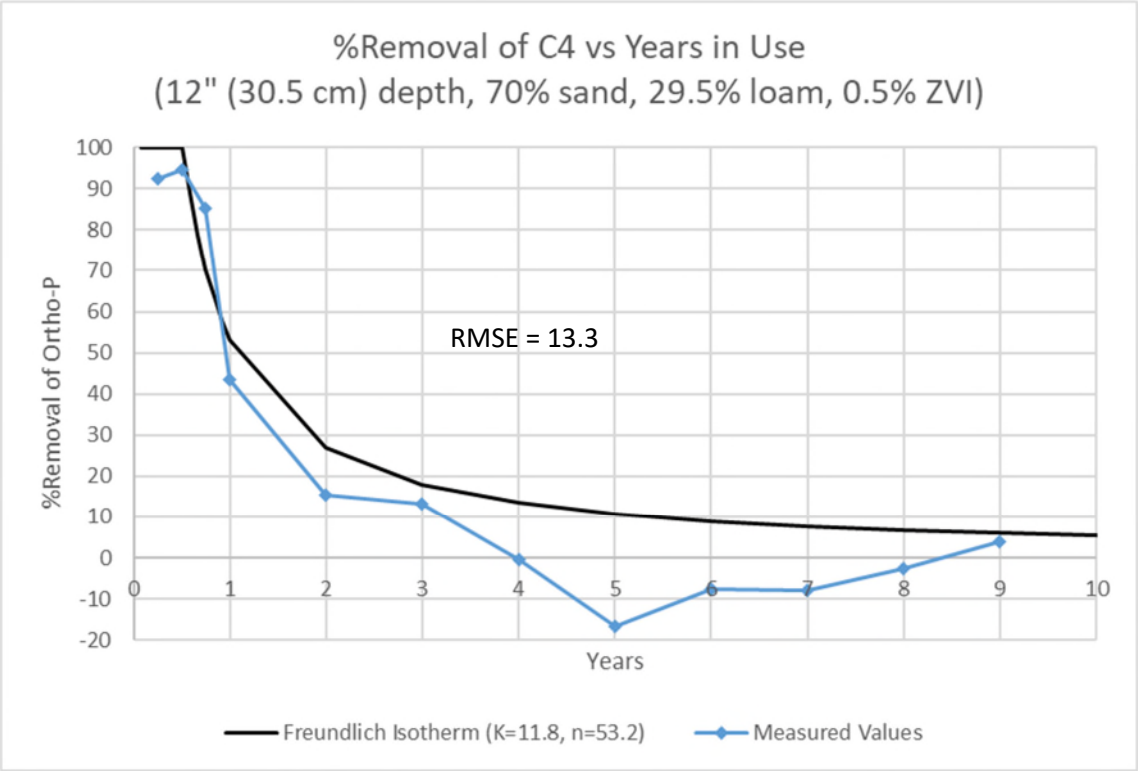

Figure 101: Column 4 comparison of percent ortho-P removal for raw values and values calculated using *K* from the trendline of Figure 41 and a constant *n* value

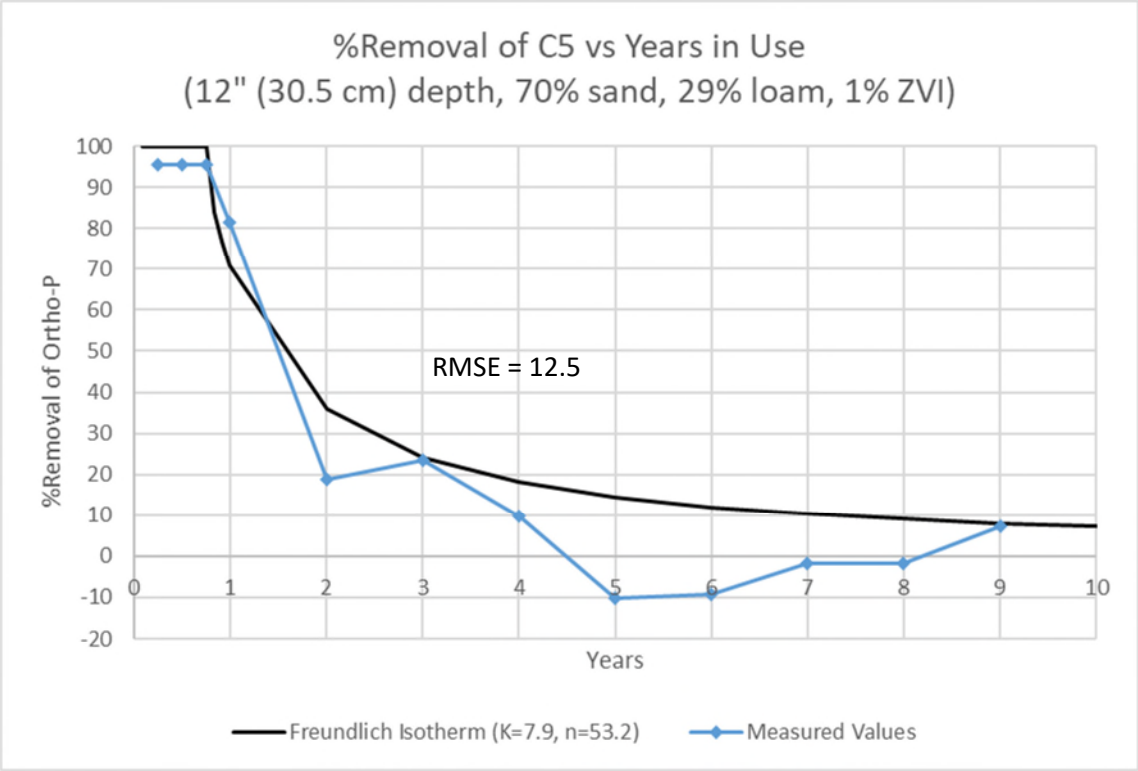

Figure 102: Column 5 comparison of percent ortho-P removal for raw values and values calculated using *K* from the trendline of Figure 41 and a constant *n* value

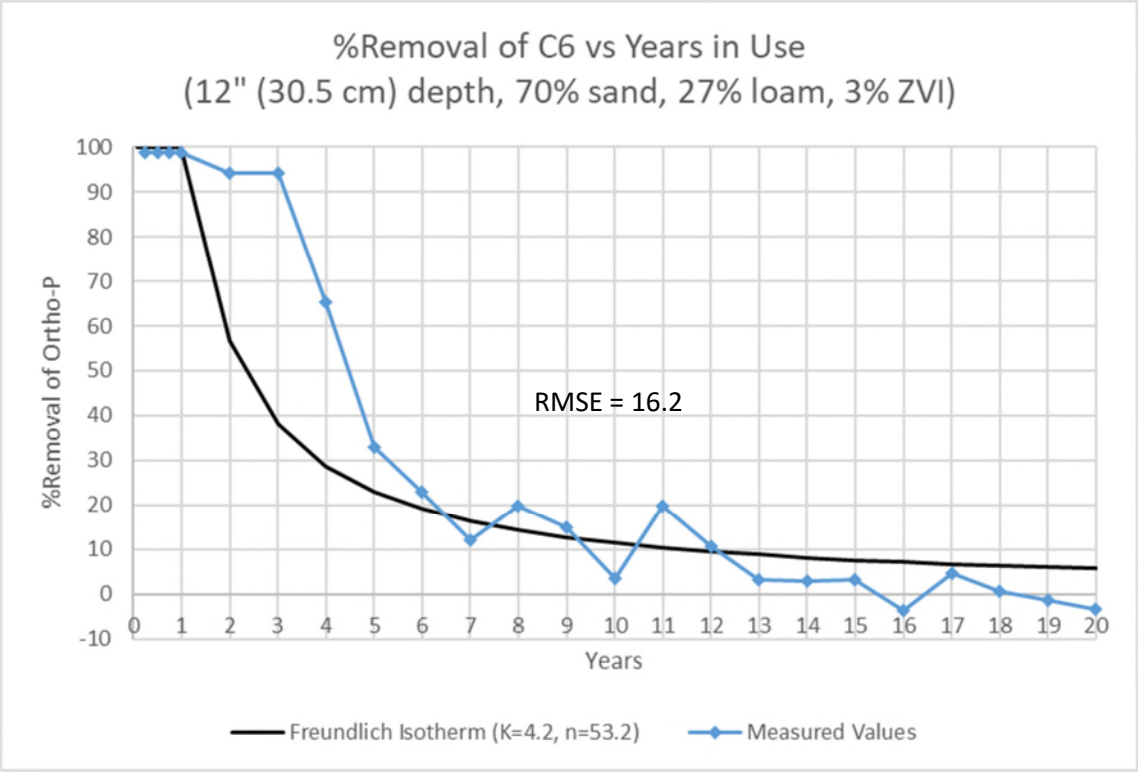

Figure 103: Column 6 comparison of percent ortho-P removal for raw values and values calculated using *K* from the trendline of Figure 41 and a constant *n* value

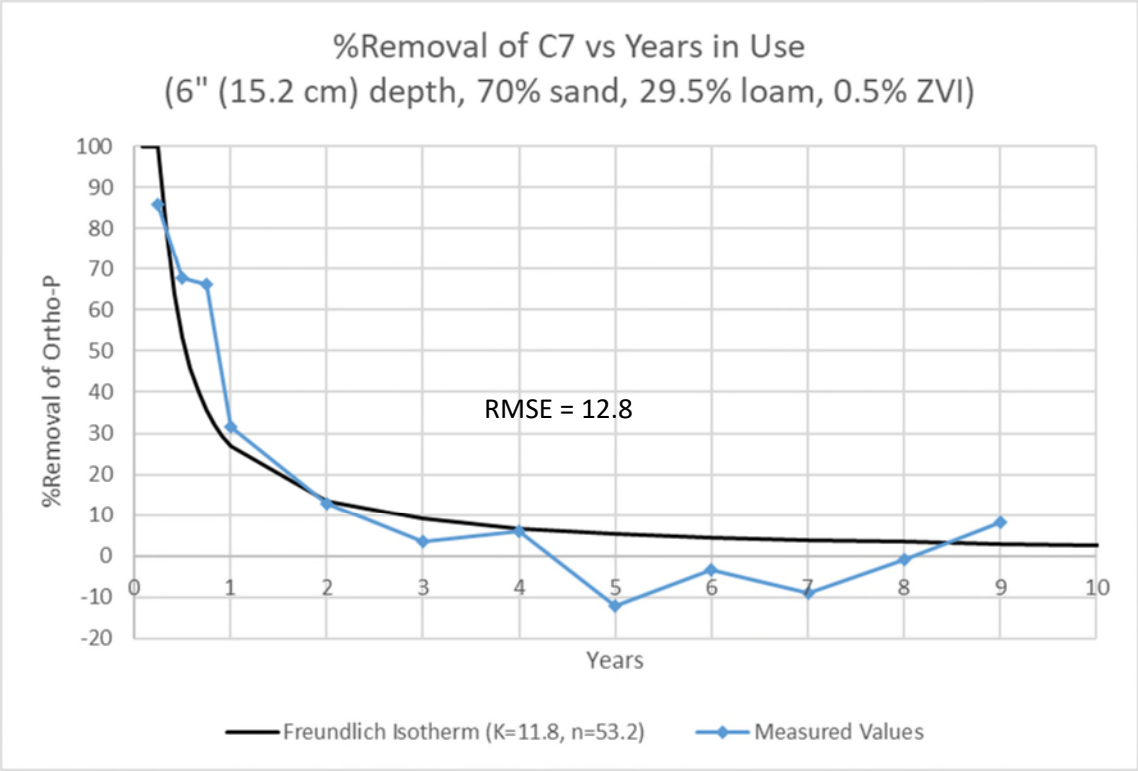

Figure 104: Column 7 comparison of percent ortho-P removal for raw values and values calculated using *K* from the trendline of Figure 41 and a constant *n* value

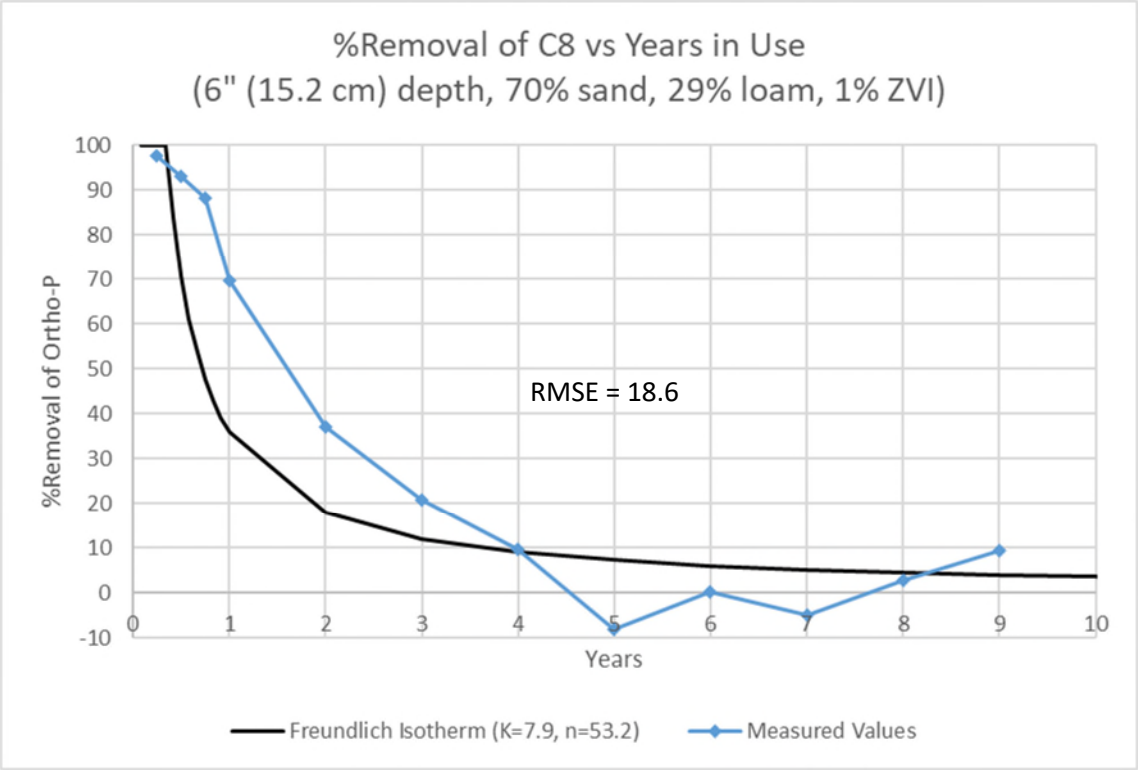

Figure 105: Column 8 comparison of percent ortho-P removal for raw values and values calculated using *K* from the trendline of Figure 41 and a constant *n* value

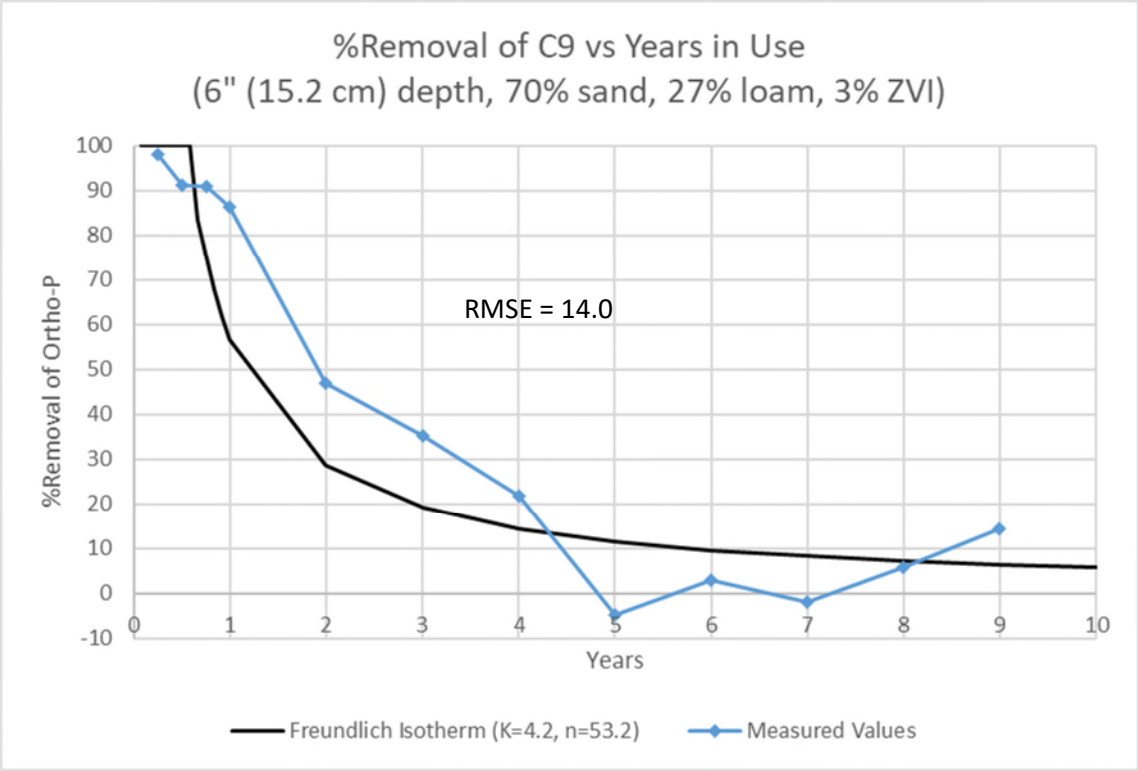

Figure 106: Column 9 comparison of percent ortho-P removal for raw values and values calculated using *K* from the trendline of Figure 41 and a constant *n* value

B.1.3 *K* from Multiple Regression Analysis with Constant *n*

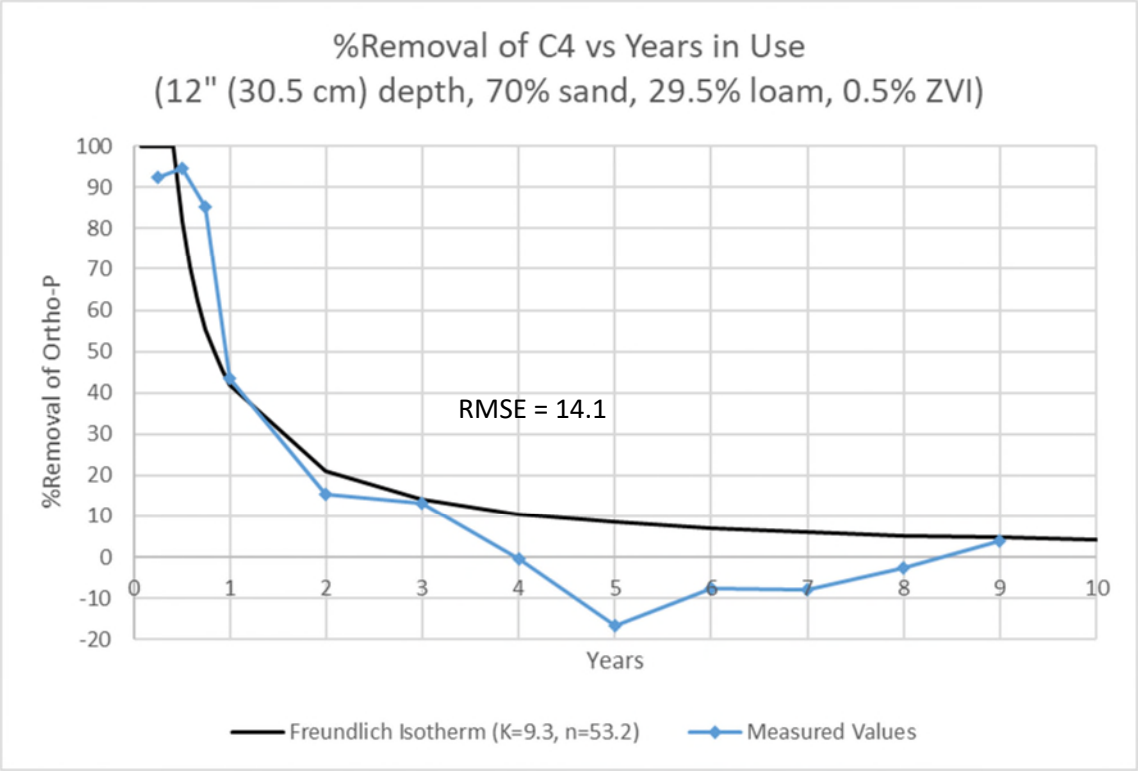

Figure 107: Column 4 comparison of percent ortho-P removal for raw values and values calculated using *K* from the multiple regression trend of Table 5 and a constant *n* value

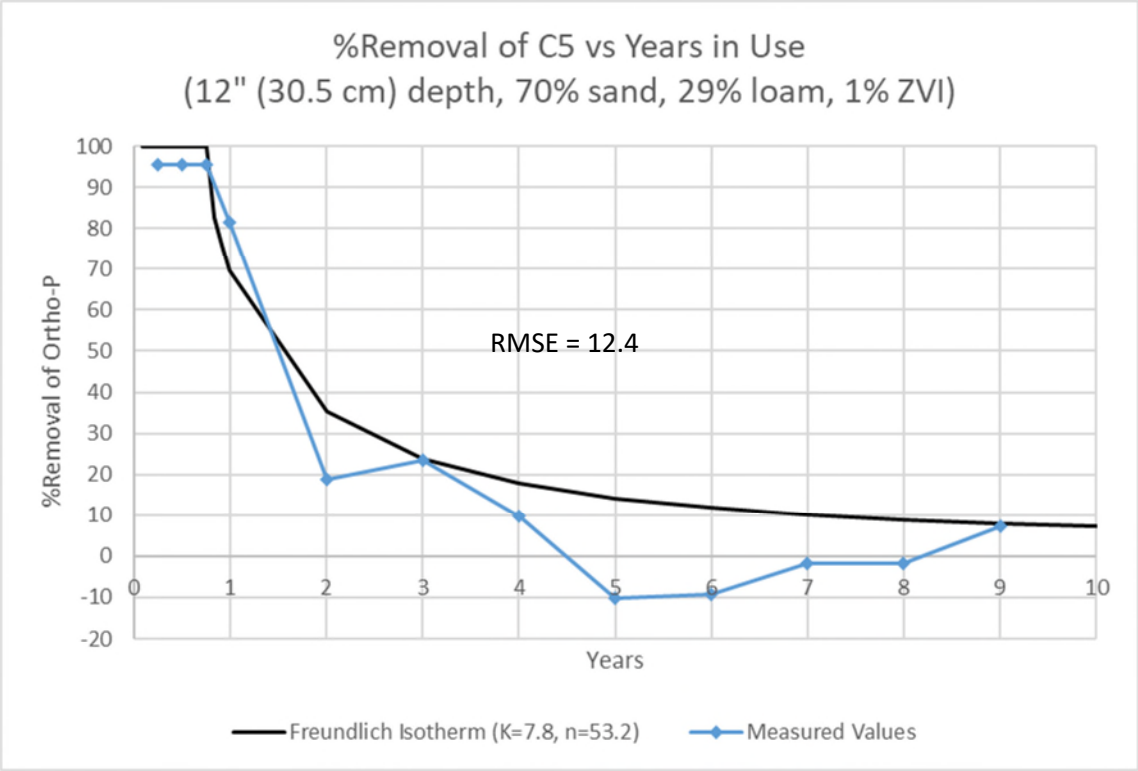

Figure 108: Column 5 comparison of percent ortho-P removal for raw values and values calculated using *K* from the multiple regression trend of Table 5 and a constant *n* value

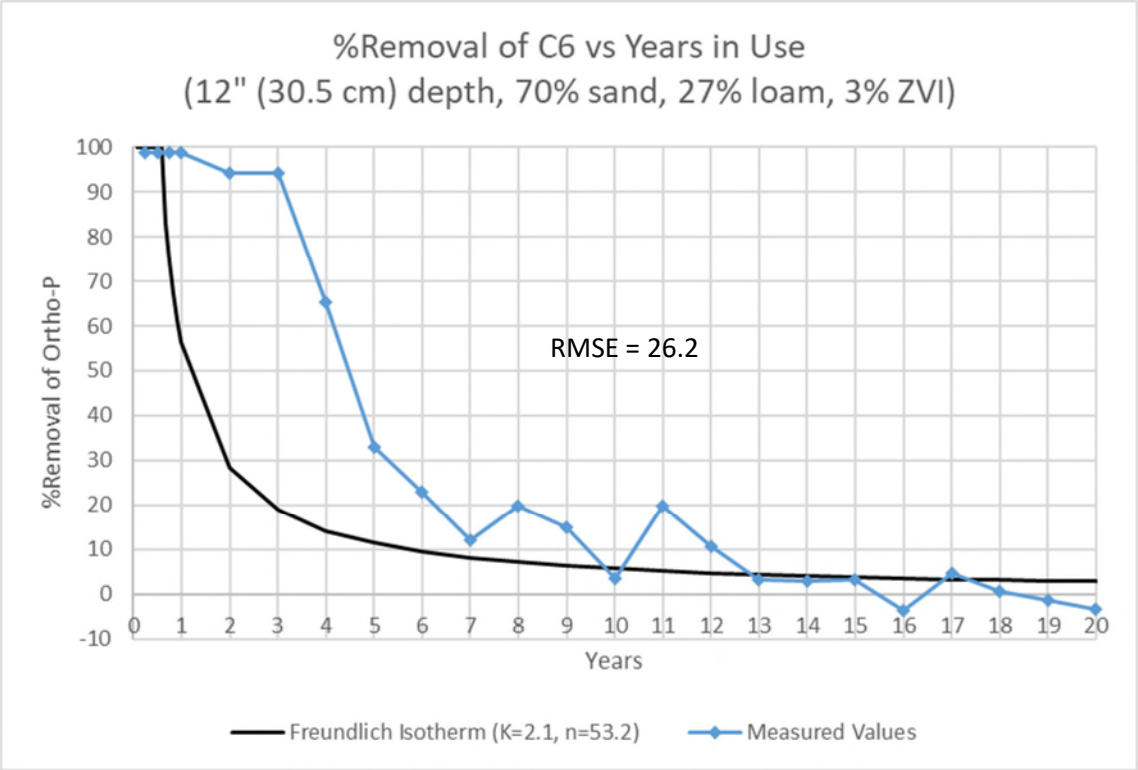

Figure 109: Column 6 comparison of percent ortho-P removal for raw values and values calculated using *K* from the multiple regression trend of Table 5 and a constant *n* value

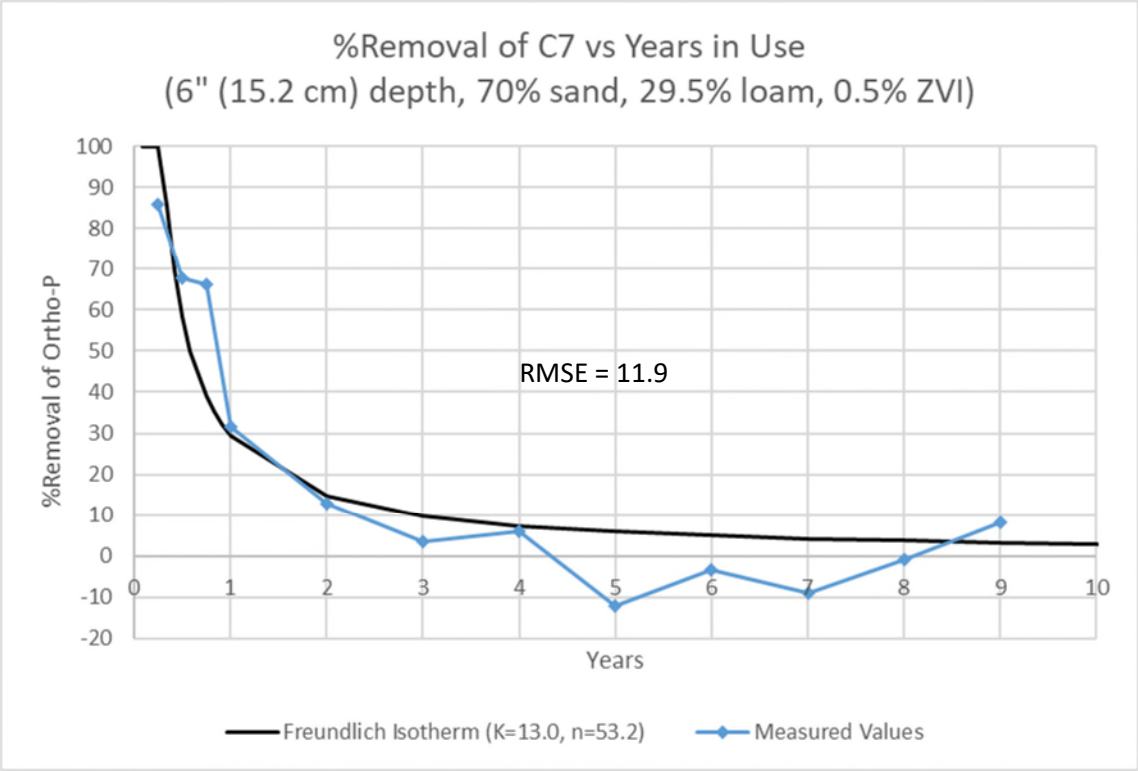

Figure 110: Column 7 comparison of percent ortho-P removal for raw values and values calculated using *K* from the multiple regression trend of Table 5 and a constant *n* value

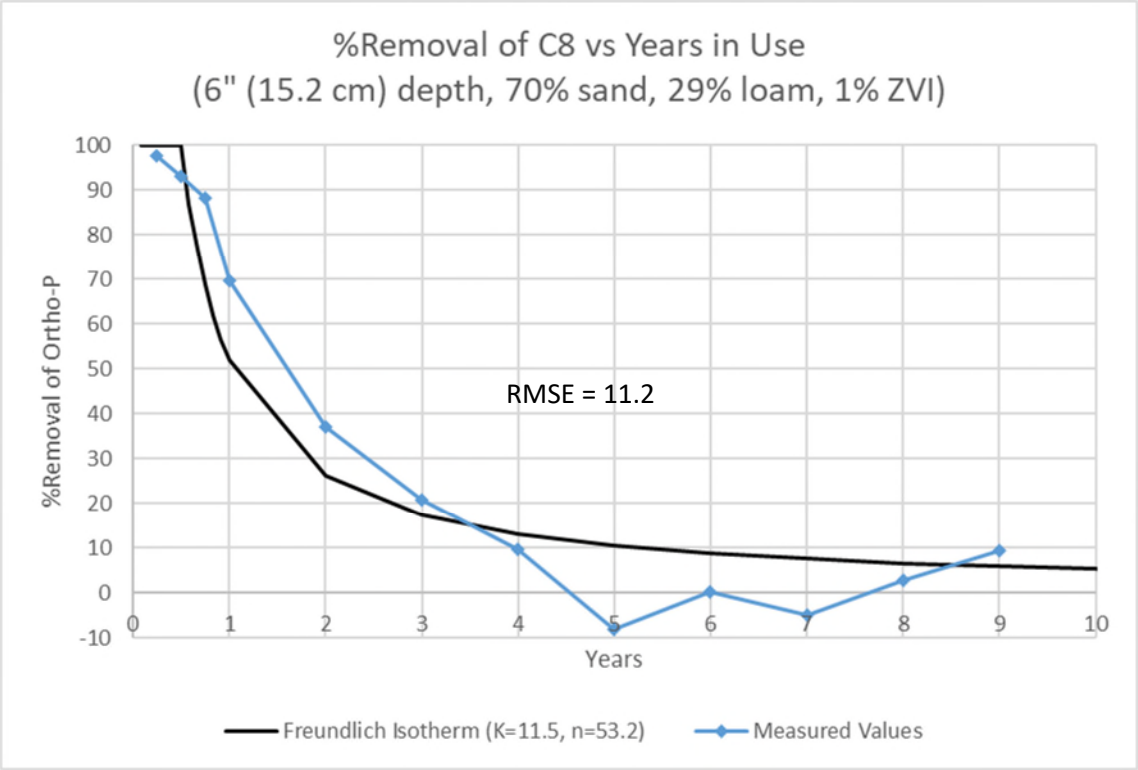

Figure 111: Column 8 comparison of percent ortho-P removal for raw values and values calculated using *K* from the multiple regression trend of Table 5 and a constant *n* value

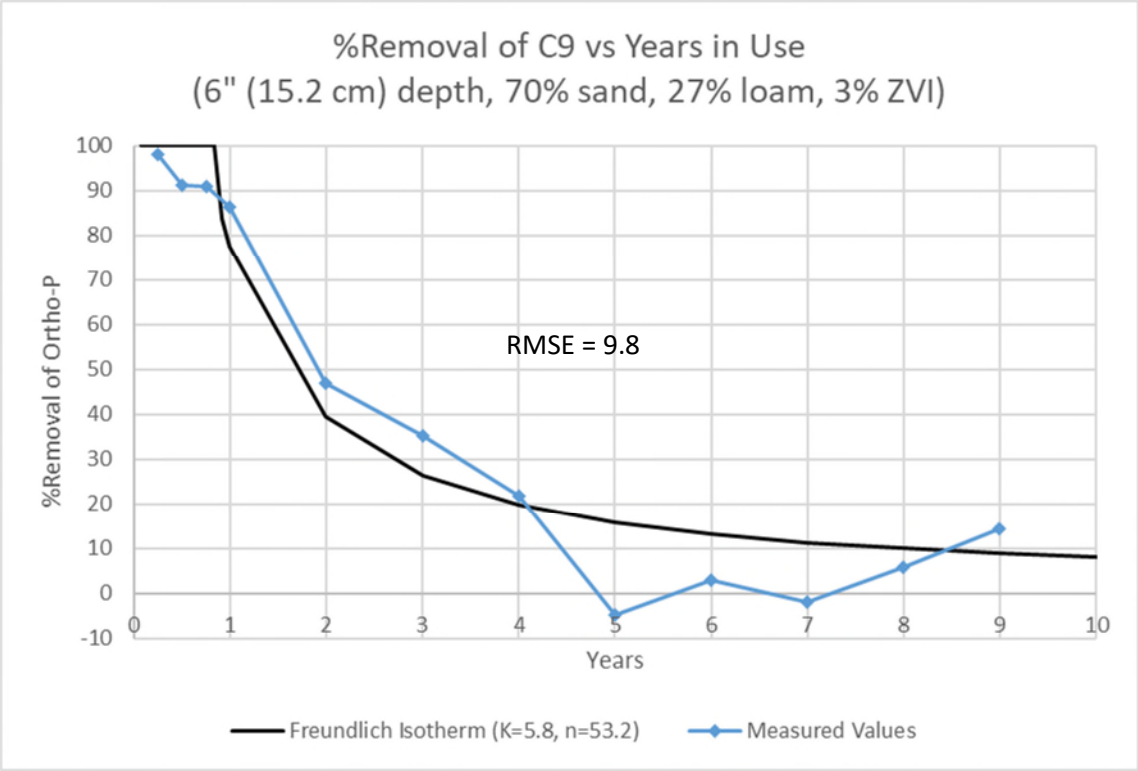

Figure 112: Column 9 comparison of percent ortho-P removal for raw values and values calculated using *K* from the multiple regression trend of Table 5 and a constant *n* value

B.2 Langmuir Analysis

B.2.1 Constant K_L

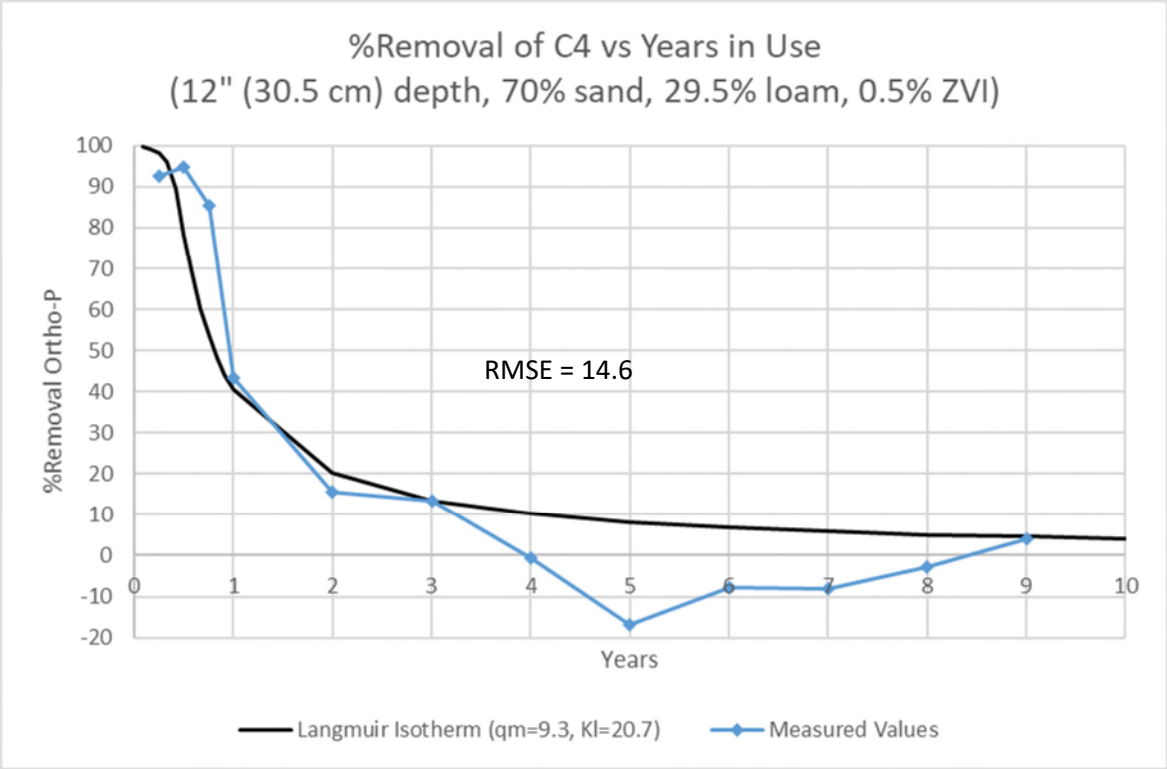

Figure 113: Column 4 comparison of percent ortho-P removal for raw values and values calculated using q_m from Table 14 and the median K_L value across all columns

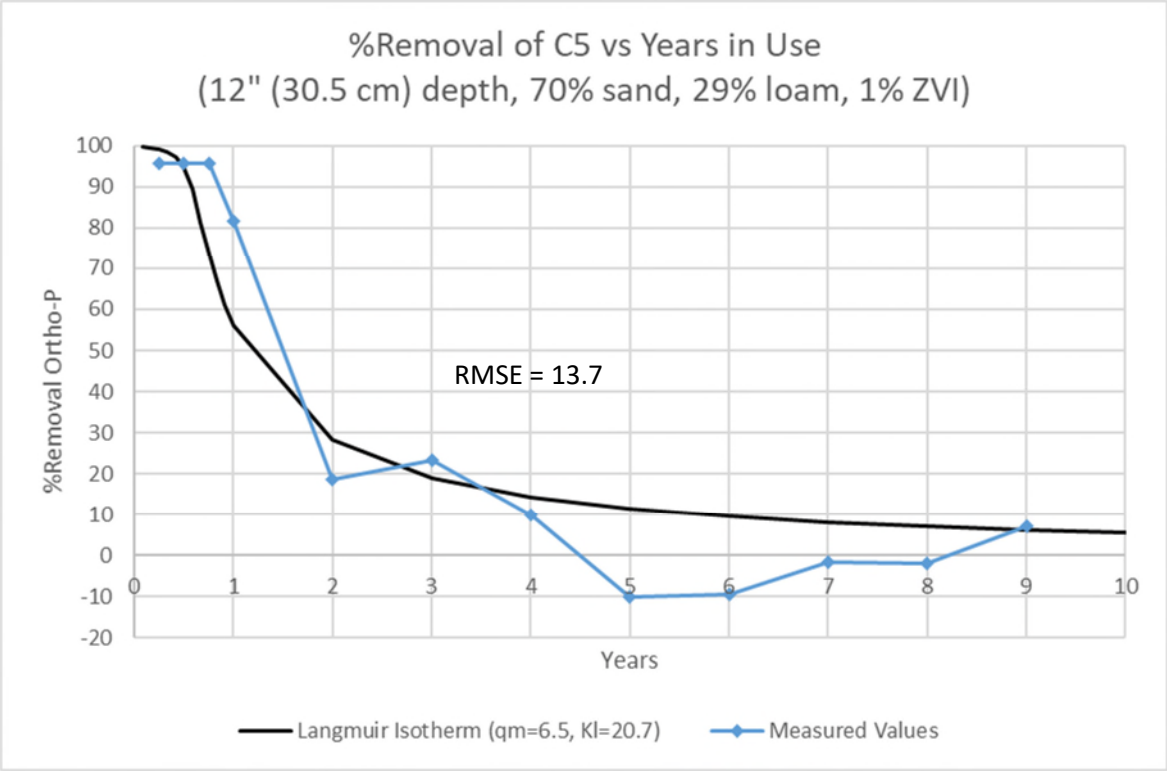

Figure 114: Column 5 comparison of percent ortho-P removal for raw values and values calculated using q_m from Table 14 and the median K_L value across all columns

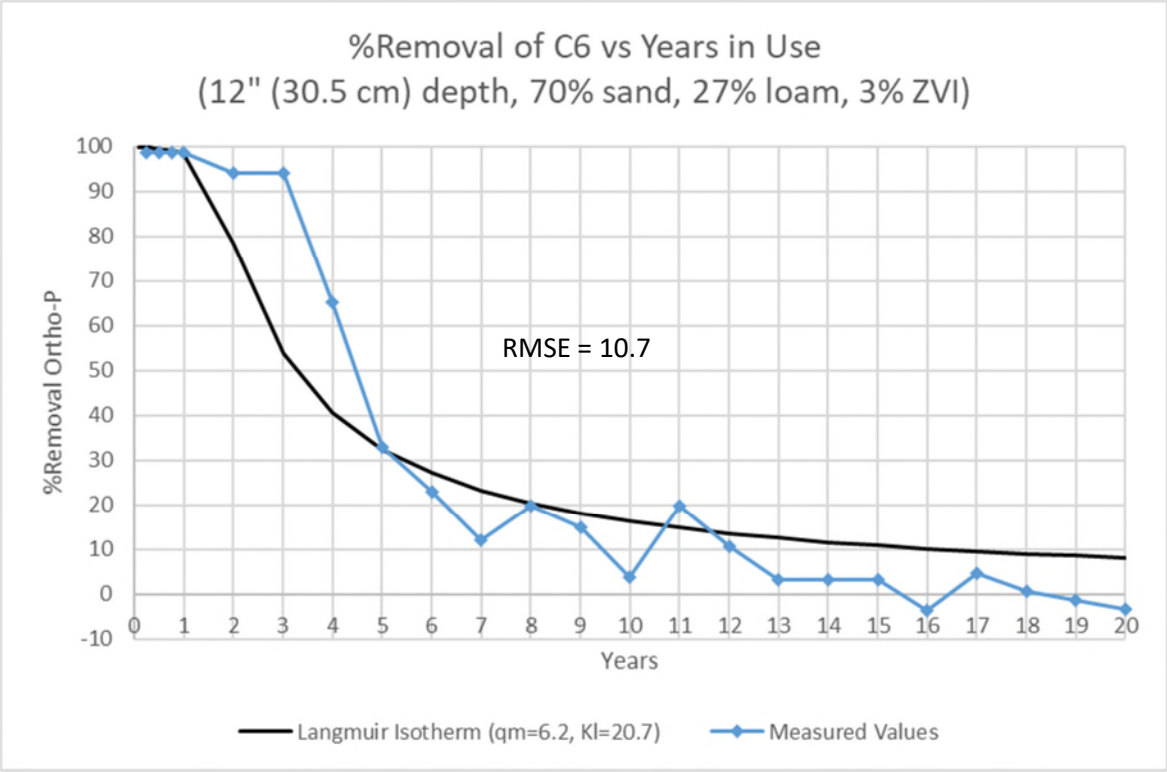

Figure 115: Column 6 comparison of percent ortho-P removal for raw values and values calculated using q_m from Table 14 and the median K_L value across all columns

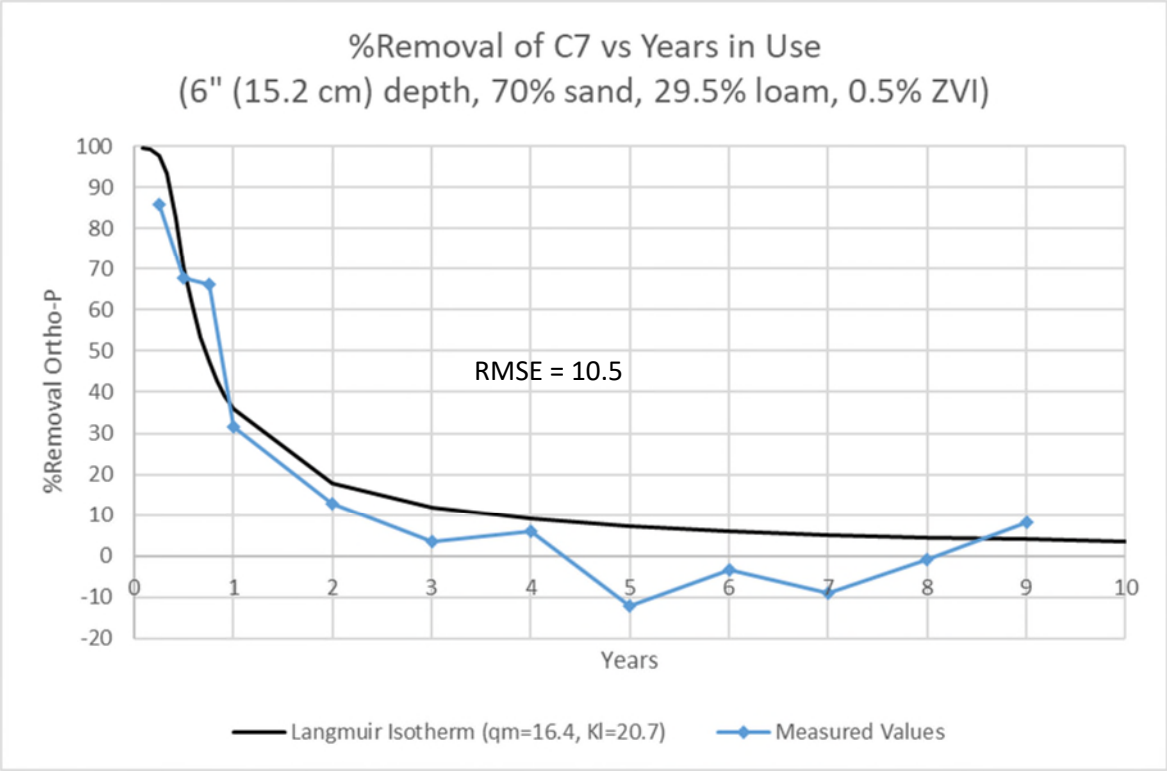

Figure 116: Column 7 comparison of percent ortho-P removal for raw values and values calculated using q_m from Table 14 and the median K_L value across all columns

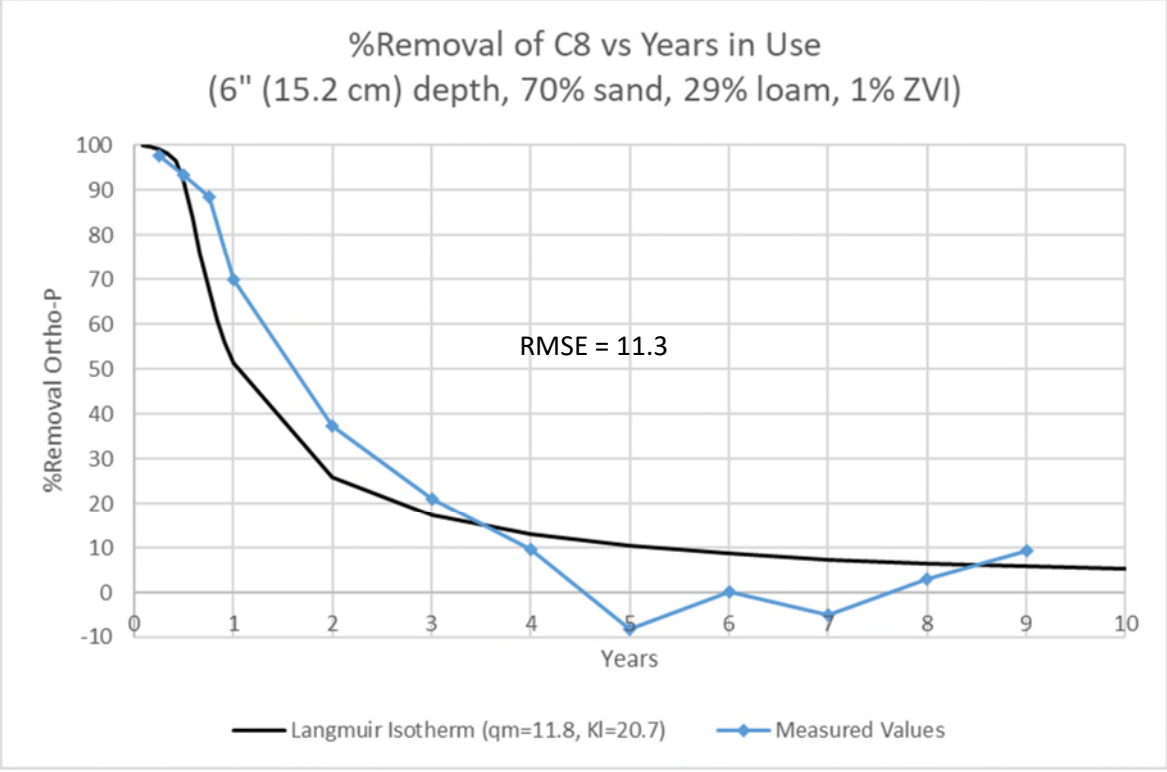

Figure 117: Column 8 comparison of percent ortho-P removal for raw values and values calculated using q_m from Table 14 and the median K_L value across all columns

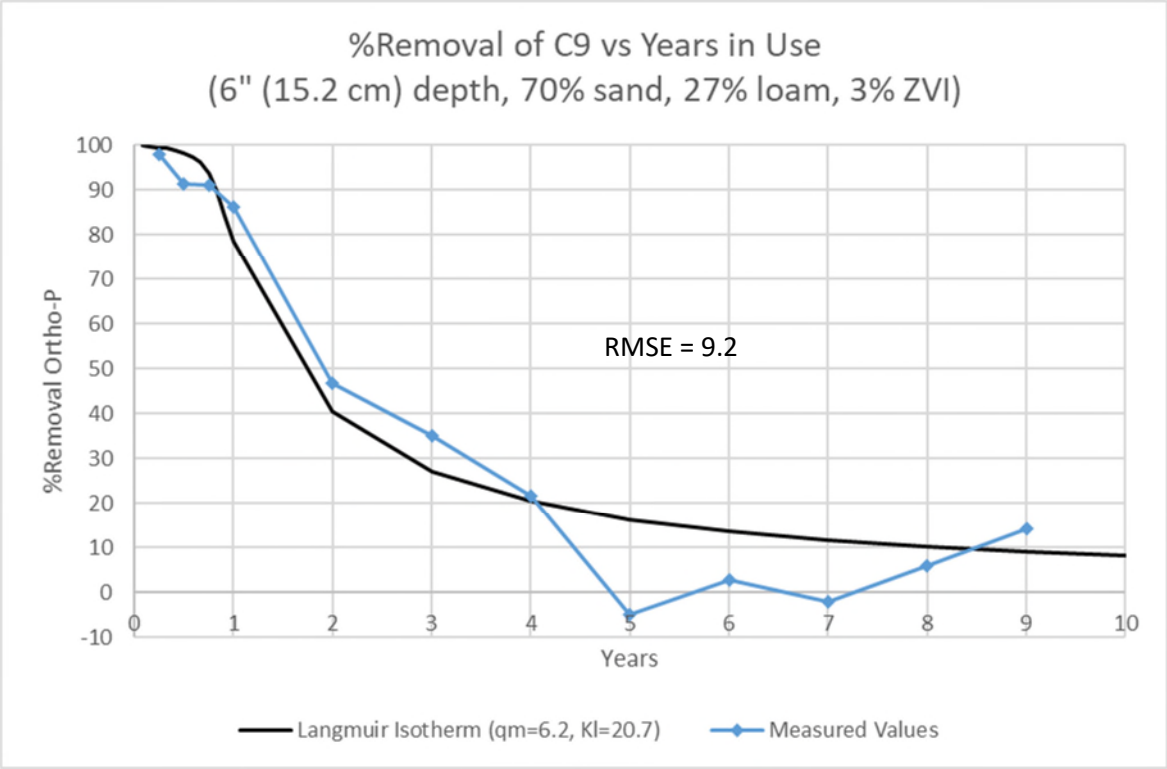

Figure 118: Column 9 comparison of percent ortho-P removal for raw values and values calculated using q_m from Table 14 and the median K_L value across all columns

B.2.2 q_m from Trendline with Constant K_L

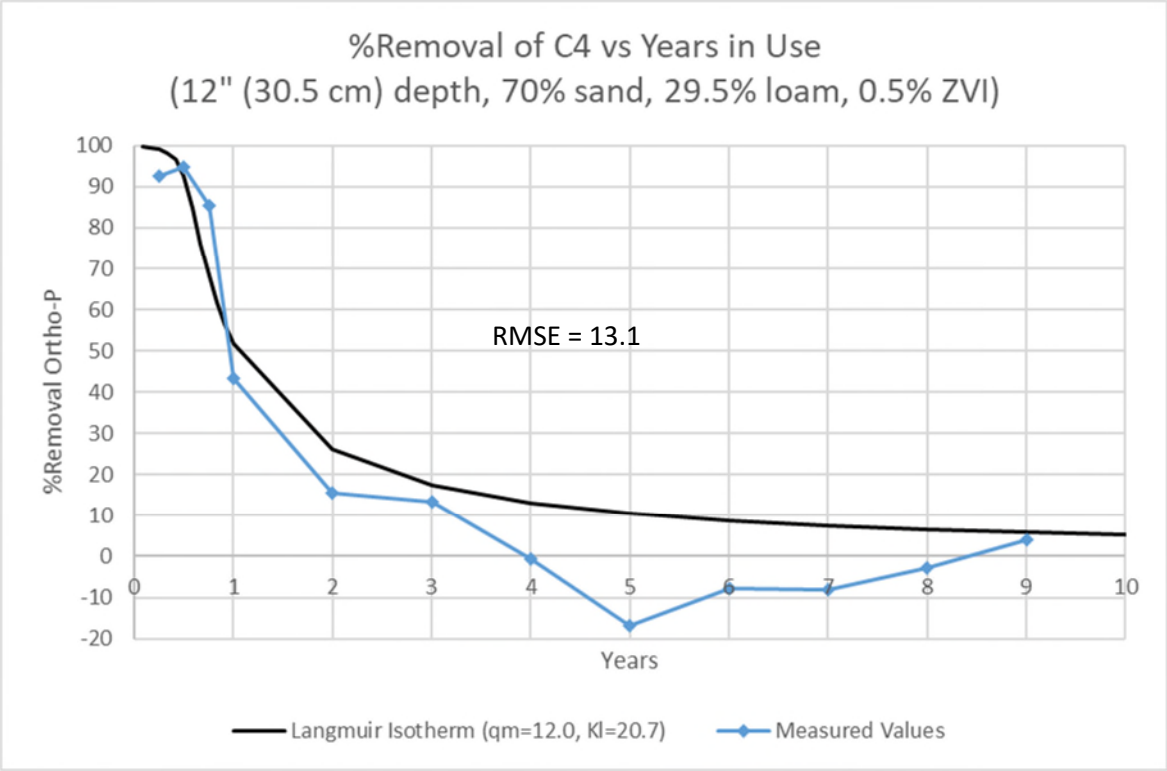

Figure 119: Column 4 comparison of percent ortho-P removal for raw values and values calculated using *K* from the trendline of Figure 60 and a constant K_L value

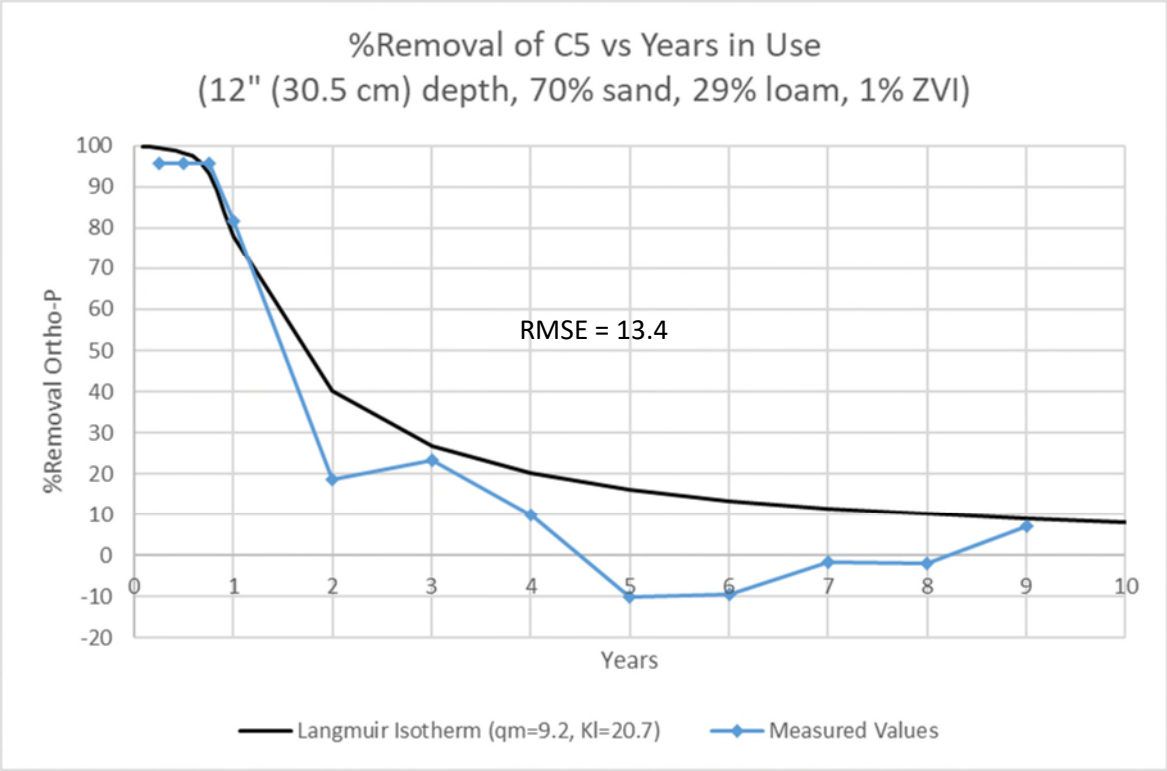

Figure 120: Column 5 comparison of percent ortho-P removal for raw values and values calculated using *K* from the trendline of Figure 60 and a constant K_L value

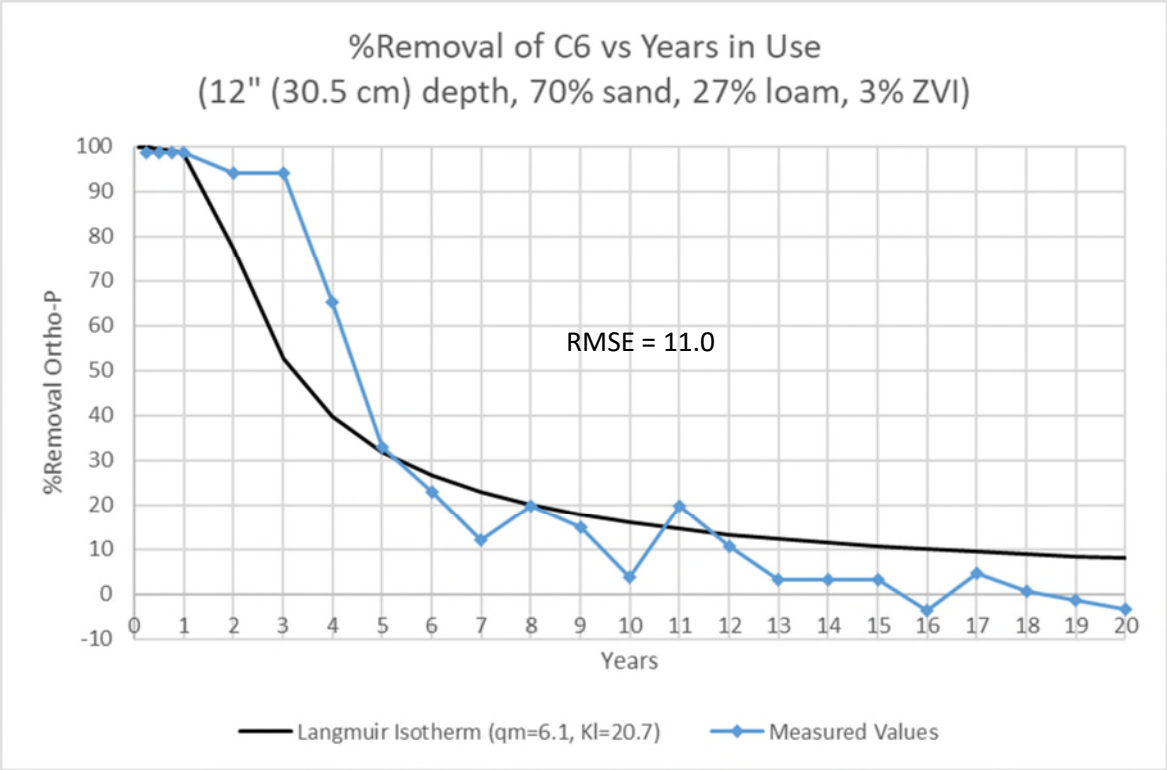

Figure 121: Column 6 comparison of percent ortho-P removal for raw values and values calculated using *K* from the trendline of Figure 60 and a constant K_L value

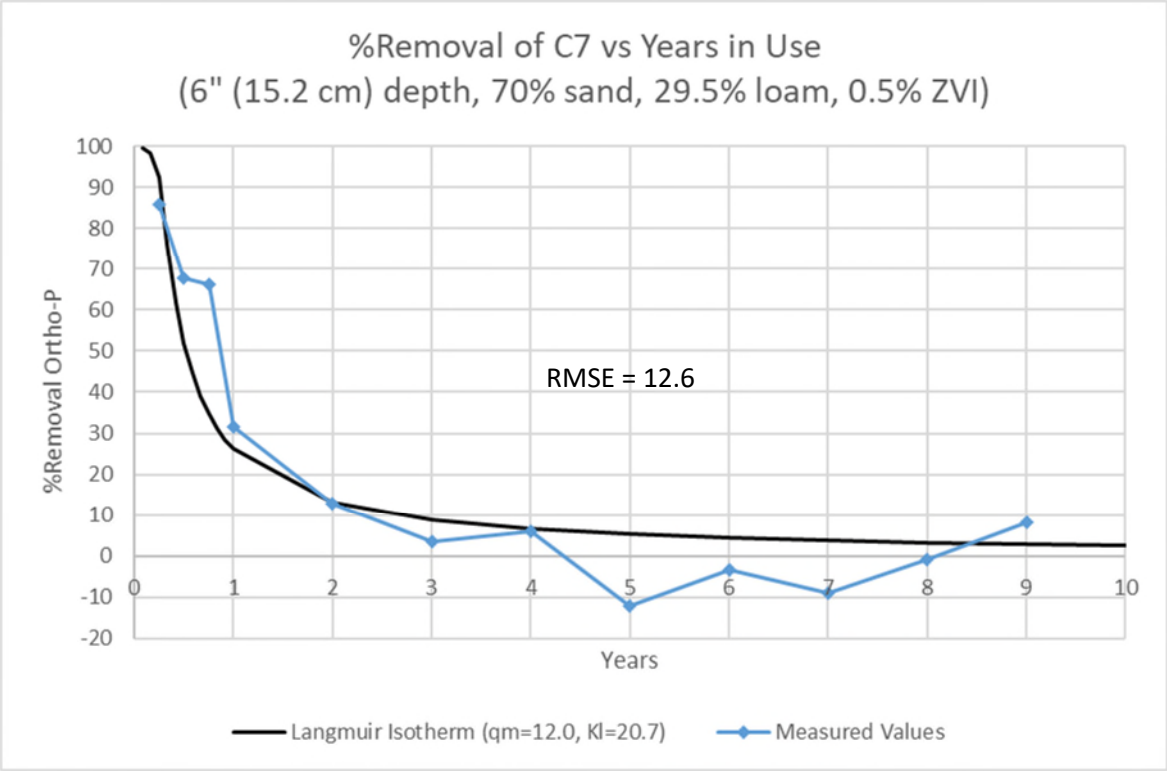

Figure 122: Column 7 comparison of percent ortho-P removal for raw values and values calculated using *K* from the trendline of Figure 60 and a constant K_L value

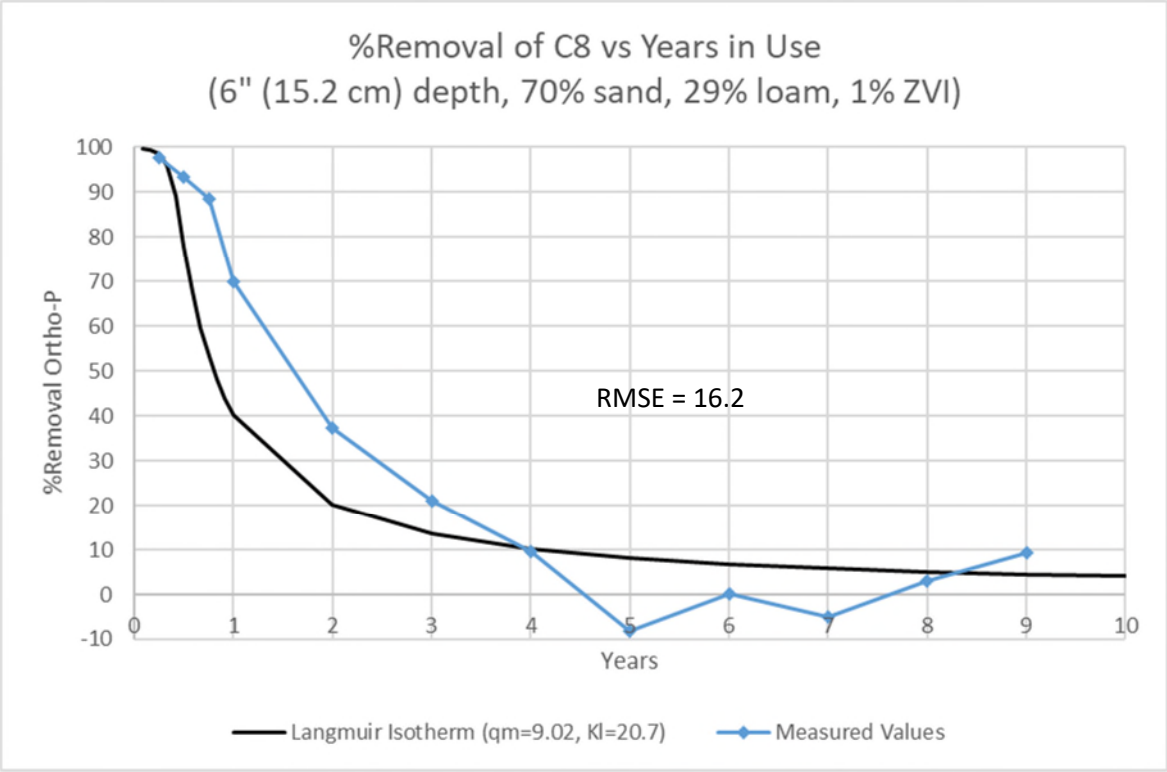

Figure 123: Column 8 comparison of percent ortho-P removal for raw values and values calculated using *K* from the trendline of Figure 60 and a constant K_L value

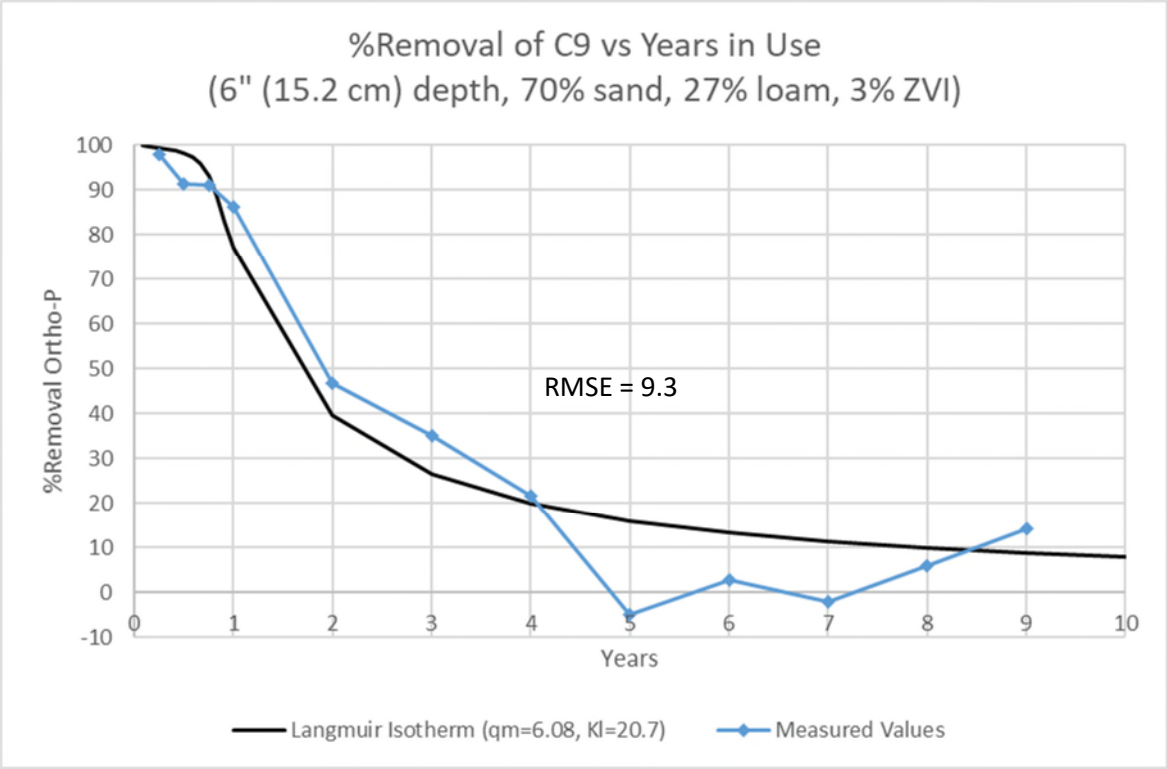

Figure 124: Column 9 comparison of percent ortho-P removal for raw values and values calculated using *K* from the trendline of Figure 60 and a constant K_L value

B.2.3 q_m from Multiple Regression Analysis with Constant K_L

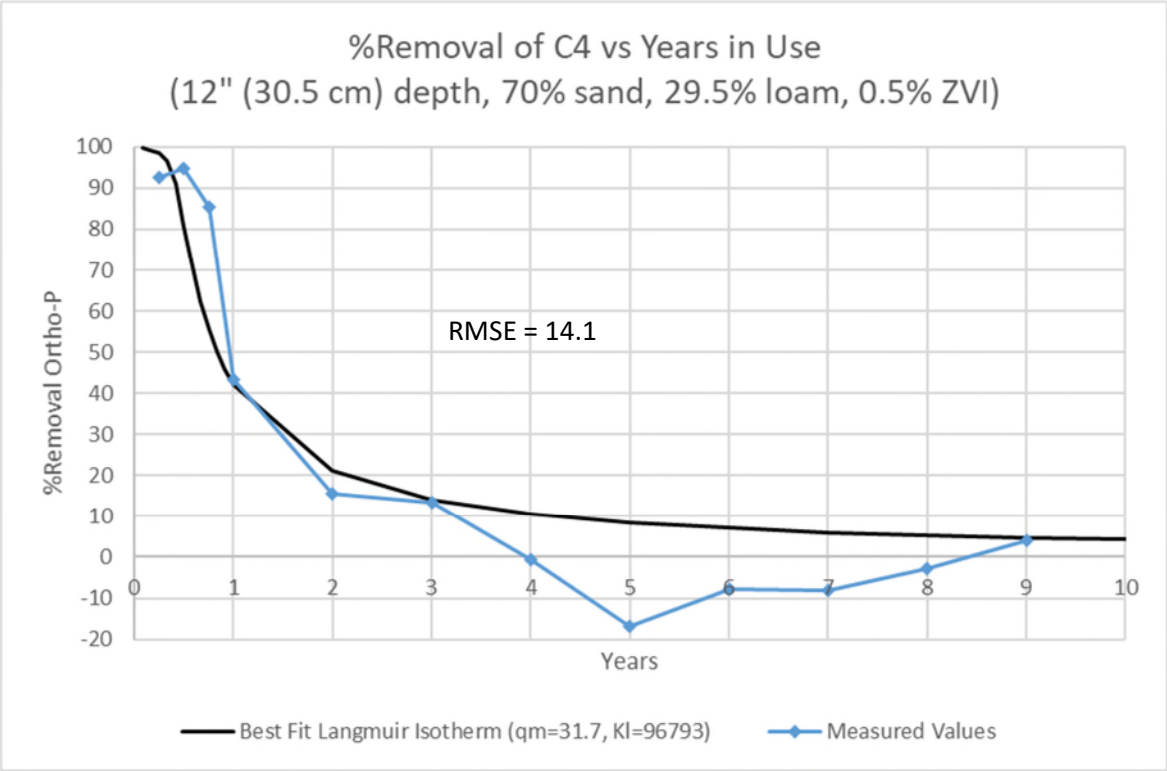

Figure 125: Column 4 comparison of percent ortho-P removal for raw values and values calculated using q_m from the multiple regression trend of Table 10 and a constant K_L value

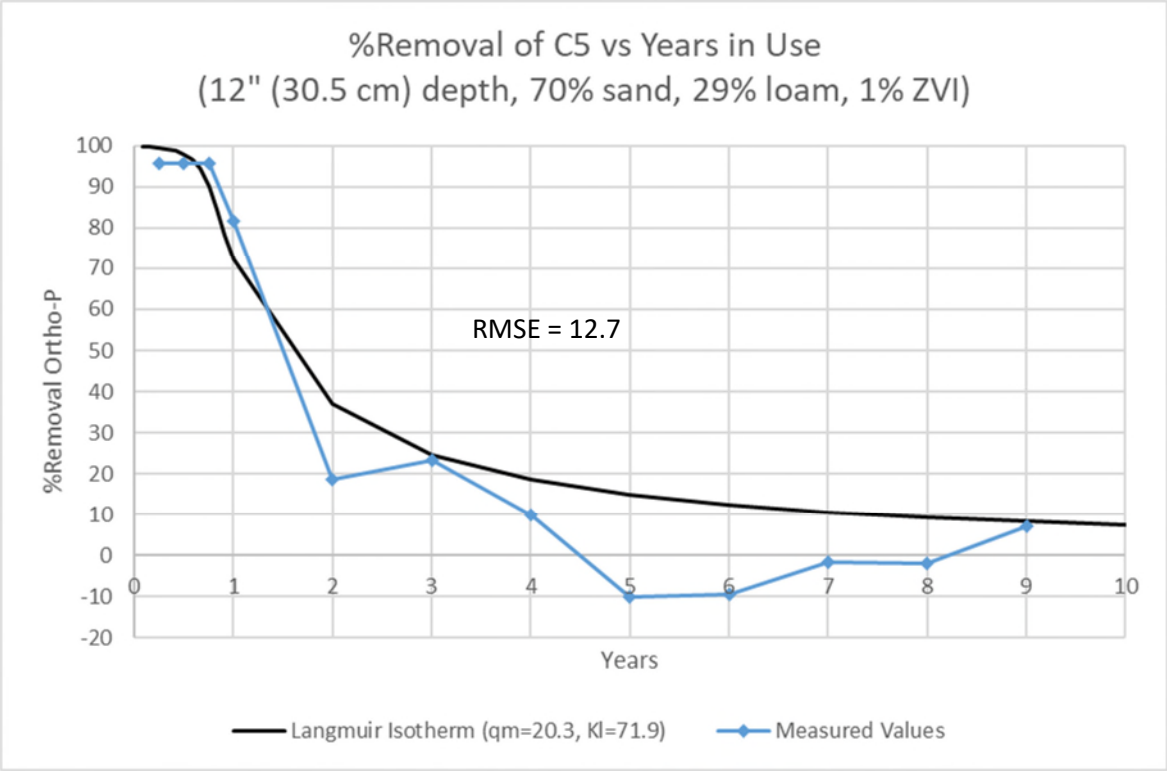

Figure 126: Column 5 comparison of percent ortho-P removal for raw values and values calculated using q_m from the multiple regression trend of Table 10 and a constant K_L value

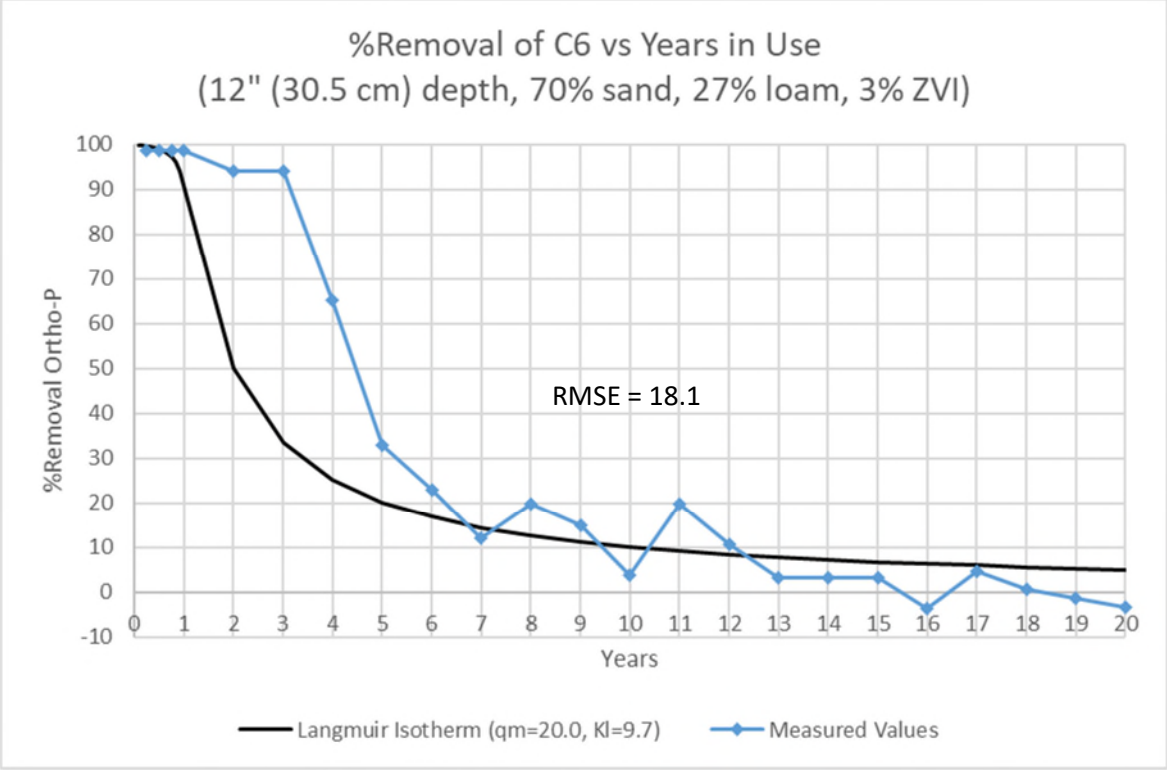

Figure 127: Column 6 comparison of percent ortho-P removal for raw values and values calculated using q_m from the multiple regression trend of Table 10 and a constant K_L value

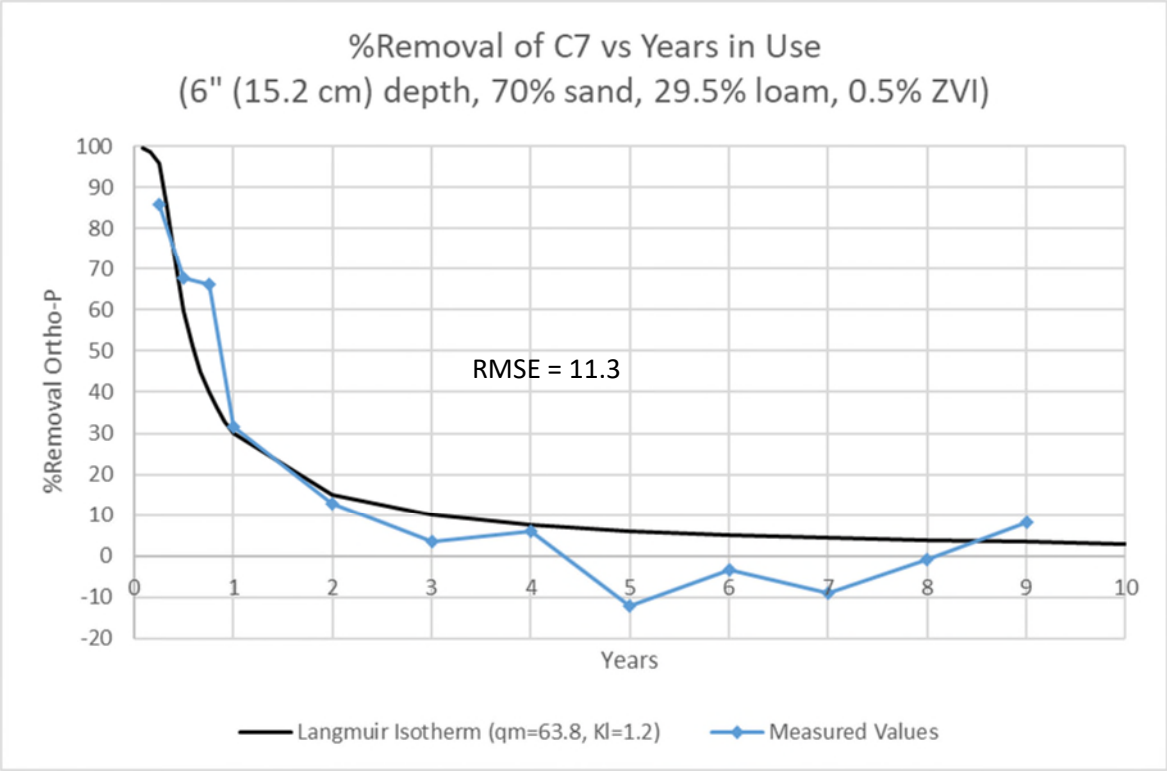

Figure 128: Column 7 comparison of percent ortho-P removal for raw values and values calculated using q_m from the multiple regression trend of Table 10 and a constant K_L value

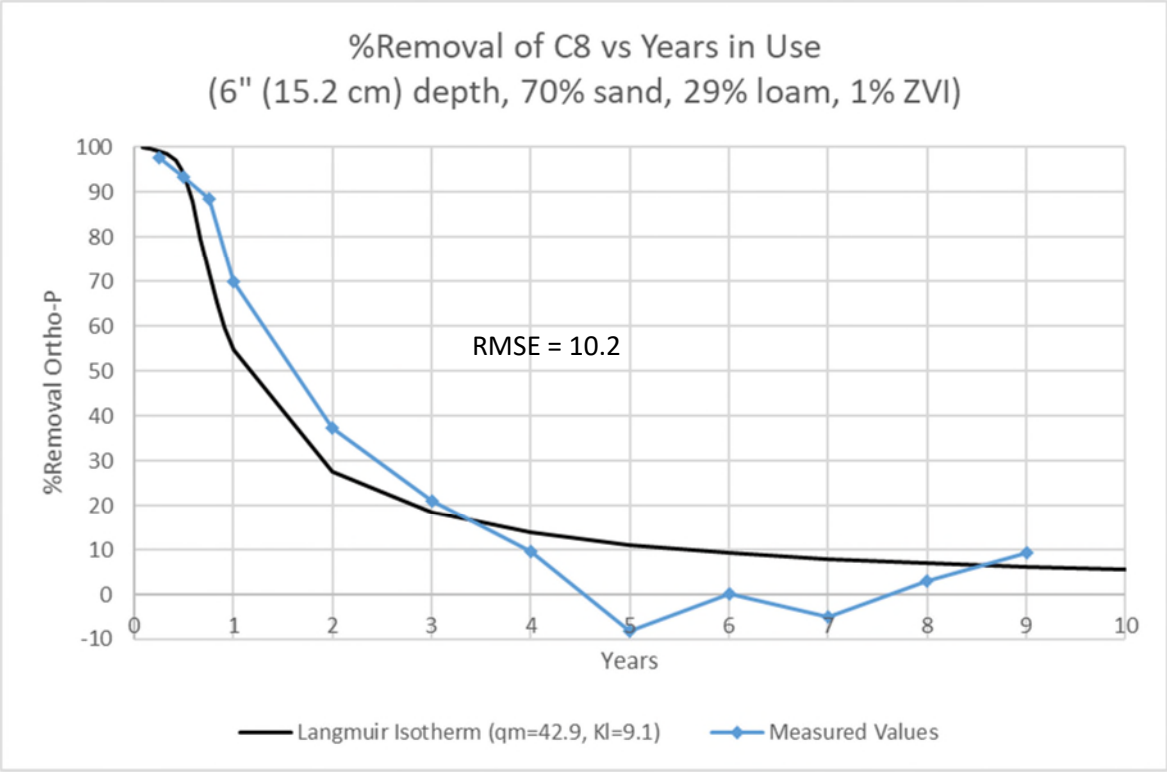

Figure 129: Column 8 comparison of percent ortho-P removal for raw values and values calculated using q_m from the multiple regression trend of Table 10 and a constant K_L value

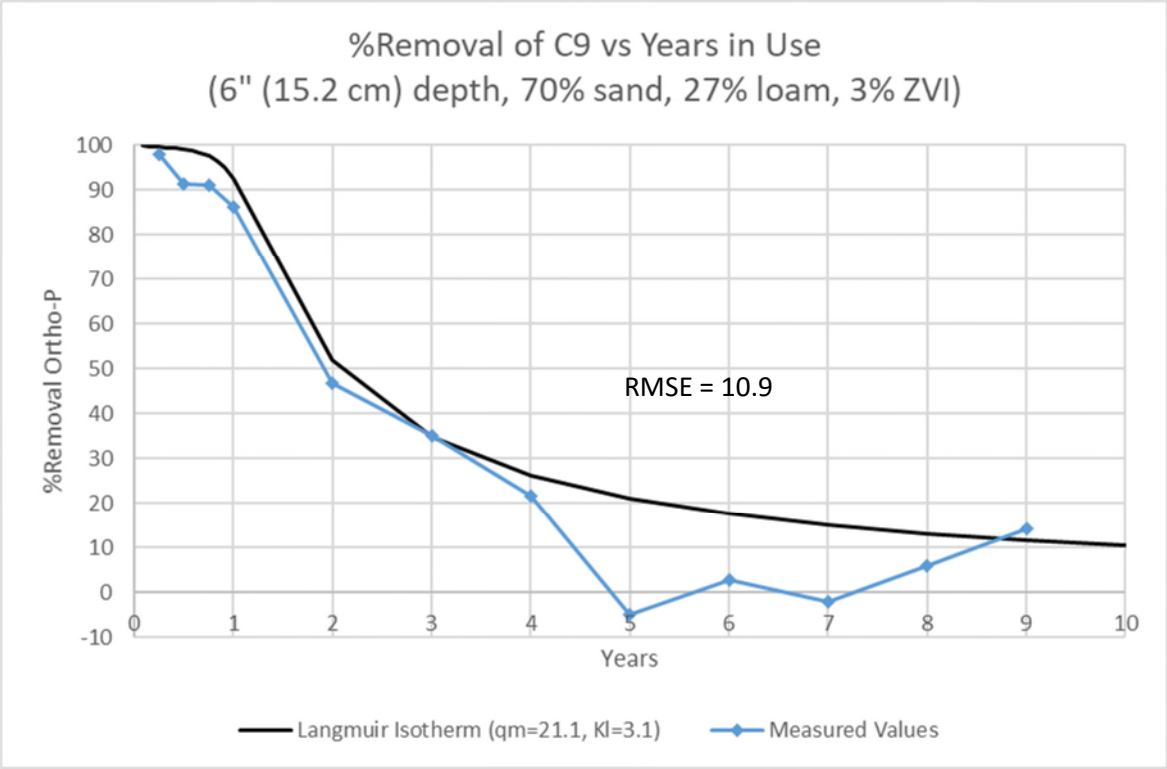

Figure 130: Column 9 comparison of percent ortho-P removal for raw values and values calculated using q_m from the multiple regression trend of Table 10 and a constant K_L value

Appendix C: Soil Data

Table 20: Hydraulic conductivity raw data and results for control columns prior to ortho-P testing

Column	Outlet Height (ft)[a]	Water Height (ft)[a]	L (in)[a]	ΔH (in)	ΔV (mL)[a]	ΔV (in^3)	Δt (min)[a]	Δt (h)	Q (in^3/h)	q (in/h)	K (in/h)	ΔH/L	k (in^2)	Re
C1	3.14	3.73	12	7.08	62	3.8	20	0.33	11.4	6.4	**11**	0.59	1.09E-08	0.0001
	3.14	3.97	12	9.96	96	5.9	20	0.33	17.6	9.9	**12**	0.83	1.20E-08	0.0002
	3.14	4.2	12	12.72	97	5.9	15	0.25	23.7	13.4	**13**	1.06	1.26E-08	0.0002
C2	2.8	3.22	6	5.04	105	6.4	20	0.33	19.2	10.9	**13**	0.84	1.29E-08	0.0002
	2.8	3.72	6	11.04	120	7.3	10	0.17	43.9	24.9	**14**	1.84	1.35E-08	0.0004
	2.8	4.22	6	17.04	207	12.6	10	0.17	75.8	42.9	**15**	2.84	1.51E-08	0.0008
C3	2.79	3.22	6	5.16	165	10.1	10	0.17	60.4	34.2	**40**	0.86	3.97E-08	0.0011
	2.79	3.72	6	11.16	173	10.6	5	0.08	126.7	71.7	**39**	1.86	3.85E-08	0.0022
	2.79	4.22	6	17.16	266	16.2	5	0.08	194.8	110.2	**39**	2.86	3.85E-08	0.0034

[a] Measured input value

Note: Water temperature = 73°F

Table 21: Hydraulic conductivity raw data and results for all columns after ortho-P testing completion

Column	Outlet Height (ft)[a]	Water Height (ft)[a]	L (in)[a]	ΔH (in)	ΔV (mL)[a]	ΔV (in^3)	Δt (min)[a]	Δt (h)	Q (in^3/h)	q (in/h)	K (in/h)	ΔH/L	k (in^2)	Re
	3.16	3.47	12	3.72	372	22.7	10	0.17	136.2	77.1	**249**	0.31	3.32E-07	0.0051
C1	3.16	3.8	12	7.68	426	26.0	10	0.17	156.0	88.3	**138**	0.64	1.84E-07	0.0044
	3.16	4.13	12	11.64	469	28.6	10	0.17	171.7	97.2	**100**	0.97	1.34E-07	0.0041
	3.16	4.13	6	11.64	468	28.6	3	0.05	571.2	323.2	**167**	1.94	2.22E-07	0.0177
C2	3.16	3.77	6	7.32	479	29.2	3	0.05	584.6	330.8	**271**	1.22	3.62E-07	0.0231
	2.8	3.12	6	3.84	414	25.3	10	0.17	151.6	85.8	**134**	0.64	1.79E-07	0.0042
	3.05	4.1	6	12.6	380	23.2	12	0.20	115.9	65.6	**31**	2.10	4.17E-08	0.0016
C3	3.05	3.78	6	8.76	271	16.5	15	0.25	66.1	37.4	**26**	1.46	3.42E-08	0.0008
	3.05	3.44	6	4.68	169	10.3	20	0.33	30.9	17.5	**22**	0.78	2.99E-08	0.0004
	3.3	4.1	12	9.6	498	30.4	5	0.08	364.7	206.4	258	0.80	3.44E-07	0.0140
C4	3.3	3.77	12	5.64	247	15.1	5	0.08	180.9	102.4	218	0.47	2.91E-07	0.0064
	3.3	3.43	12	1.56	176	10.7	15	0.25	43.0	24.3	187	0.13	2.49E-07	0.0014
	3.22	4.1	12	10.56	483	29.5	2	0.03	884.2	500.4	**569**	0.88	7.59E-07	0.0505
C5	3.22	3.77	12	6.6	432	26.4	3	0.05	527.2	298.4	**542**	0.55	7.24E-07	0.0294
	3.22	3.43	12	2.52	267	16.3	5	0.08	195.5	110.6	**527**	0.21	7.03E-07	0.0108
	3.27	4.1	12	9.96	371	22.6	3	0.05	452.8	256.2	**309**	0.83	4.12E-07	0.0191
C6	3.27	3.77	12	6	356	21.7	3	0.05	434.5	245.9	**492**	0.50	6.56E-07	0.0231
	3.27	3.44	12	2.04	204	12.4	10	0.17	74.7	42.3	**249**	0.17	3.32E-07	0.0028
	2.59	3.43	6	10.08	539	32.9	1.5	0.03	1315.7	744.5	**443**	1.68	5.91E-07	0.0664
C7	2.59	3.1	6	6.12	352	21.5	2	0.03	644.4	364.7	**358**	1.02	4.77E-07	0.0292
	2.59	2.78	6	2.28	346	21.1	5	0.08	253.4	143.4	**377**	0.38	5.03E-07	0.0118
	2.62	3.42	6	9.6	441	26.9	2	0.03	807.3	456.9	**286**	1.60	3.81E-07	0.0327
C8	2.62	3.1	6	5.76	360	22.0	3	0.05	439.4	248.6	**259**	0.96	3.46E-07	0.0169
	2.62	2.76	6	1.68	185	11.3	5	0.08	135.5	76.7	**274**	0.28	3.65E-07	0.0054
	2.59	3.43	6	10.08	434	26.5	3	0.05	529.7	299.7	**178**	1.68	2.38E-07	0.0170
C9	2.59	3.1	6	6.12	324	19.8	4	0.07	296.6	167.8	**165**	1.02	2.20E-07	0.0091
	2.59	2.76	6	2.04	234	14.3	10	0.17	85.7	48.5	**143**	0.34	1.90E-07	0.0025

[a] Measured input value

Note: Water temperature = 66°

Hydraulic Conductivity Testing Definitions and Equations:

L = thickness of media in column

ΔH = height of water above media (constant during each trial)

ΔV = volume of water collected from outlet

Δt = run time for each test

Q = discharge from column = ΔV/Δt Equation 12

q = velocity = Q/cross sectional area of media Equation 13

K = hydraulic conductivity = qL/ΔH Equation 14

ΔH/L = hydraulic gradient

k = intrinsic permeability = Kv/g Equation 15

where: v = kinematic viscosity of water

g = acceleration due to gravity

Re = Reynolds number = $\frac{K\sqrt{0.6k}}{v}$ Equation 16

Table 22: Soil analysis results from UNH Soil Testing Program

Test Category	Sand	Loam	3% ZVI, 27% Loam, 70% Sand Mix
pH, SME[1]	7.2	6.0	6.50
CEC[2]	0.8	10.7	4.0
Total P[1] (P_2O_5)	0.05%	0.10%	0.06%
% Organic Carbon[1]	0.0%	2.20%	0.60%
Mehlich 3 P[2]	4 ppm	83 ppm	49 ppm

1. From the compost analysis
2. From the soil analysis (Mehlich3 extraction)

Notes: Mehlich 3 P is reported in terms of P and not P_2O_5. P_2O_5 can be found by multiplying P by 2.29.

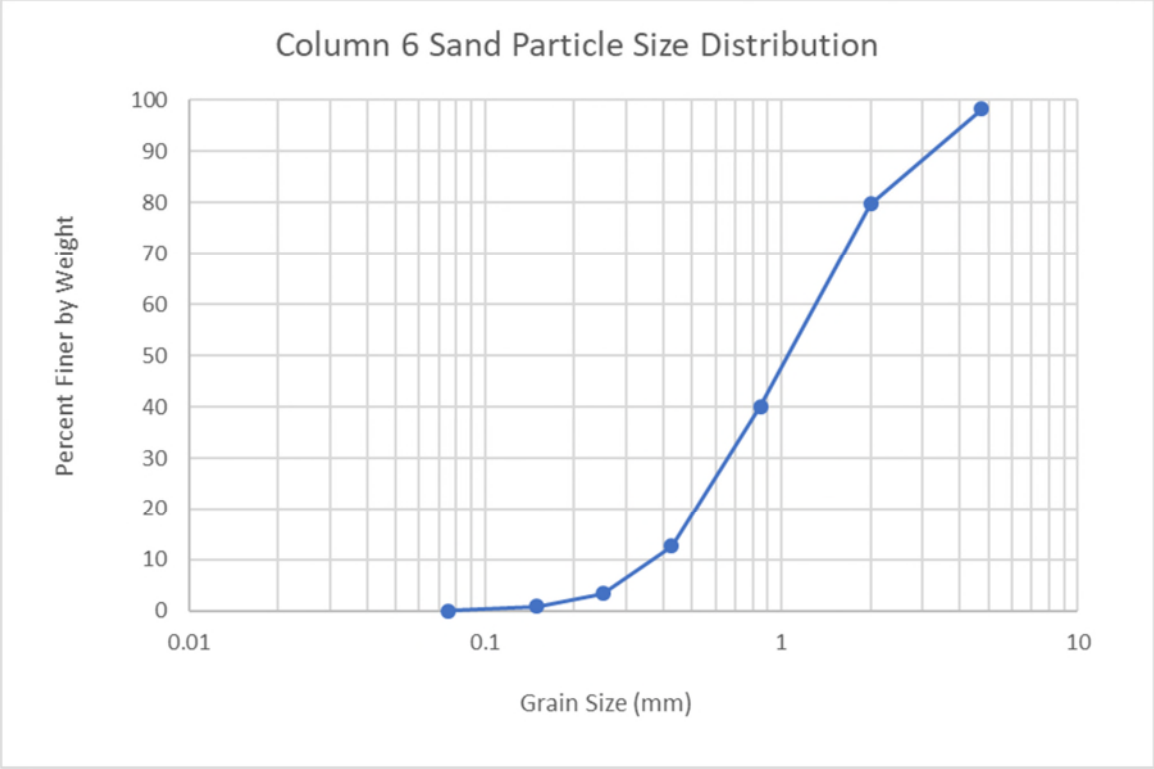

Figure 131: Particle size distribution for sand used in Column 6

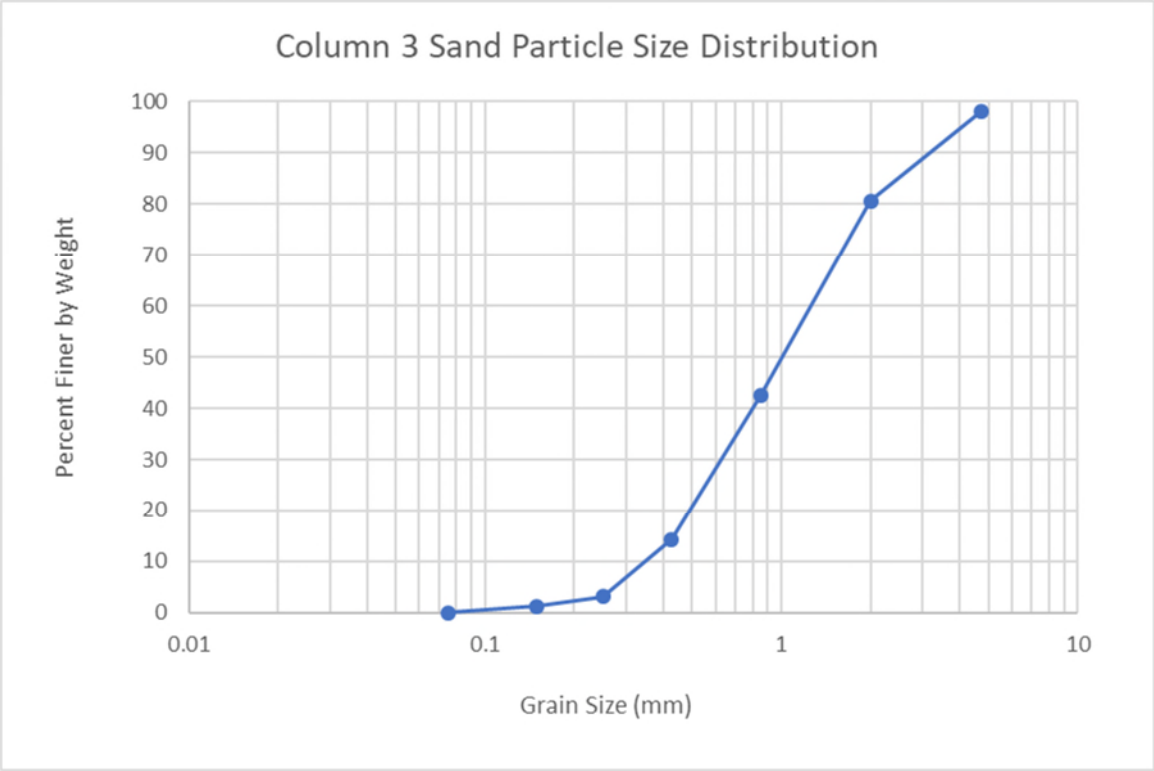

Figure 132: Particle size distribution for sand used in Column 3

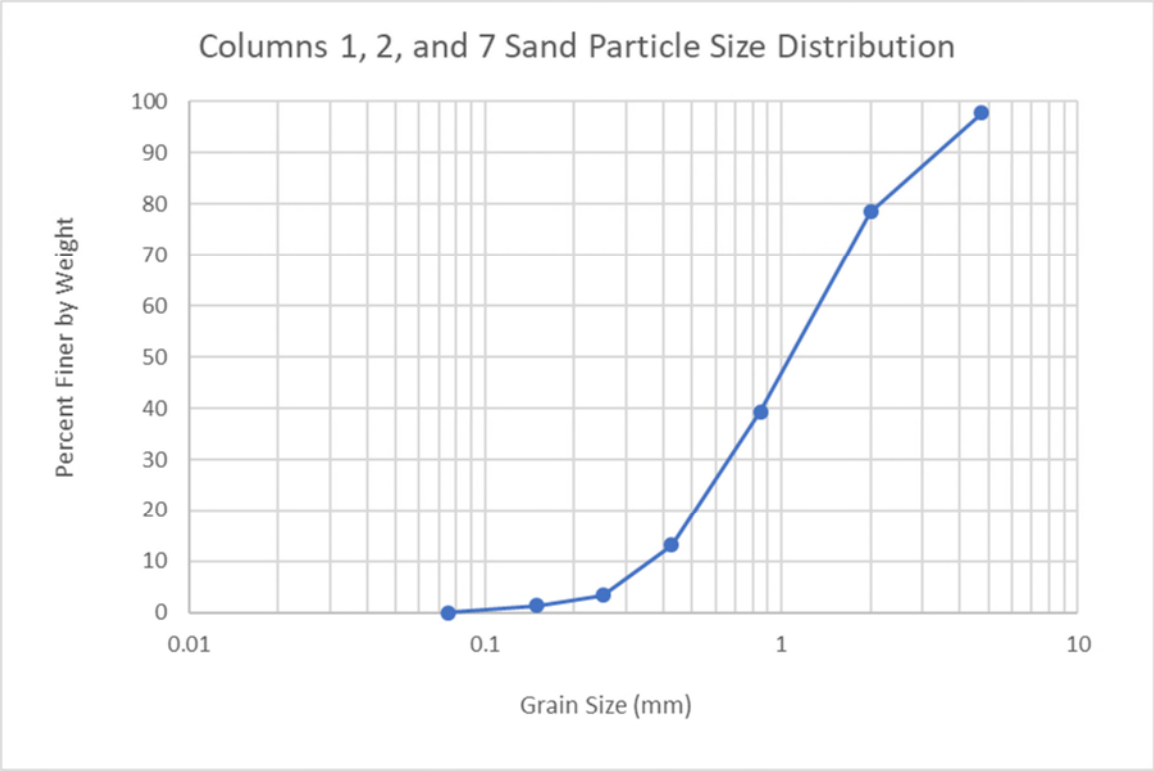

Figure 133: Particle size distribution for sand used in Columns 1, 2, and 7

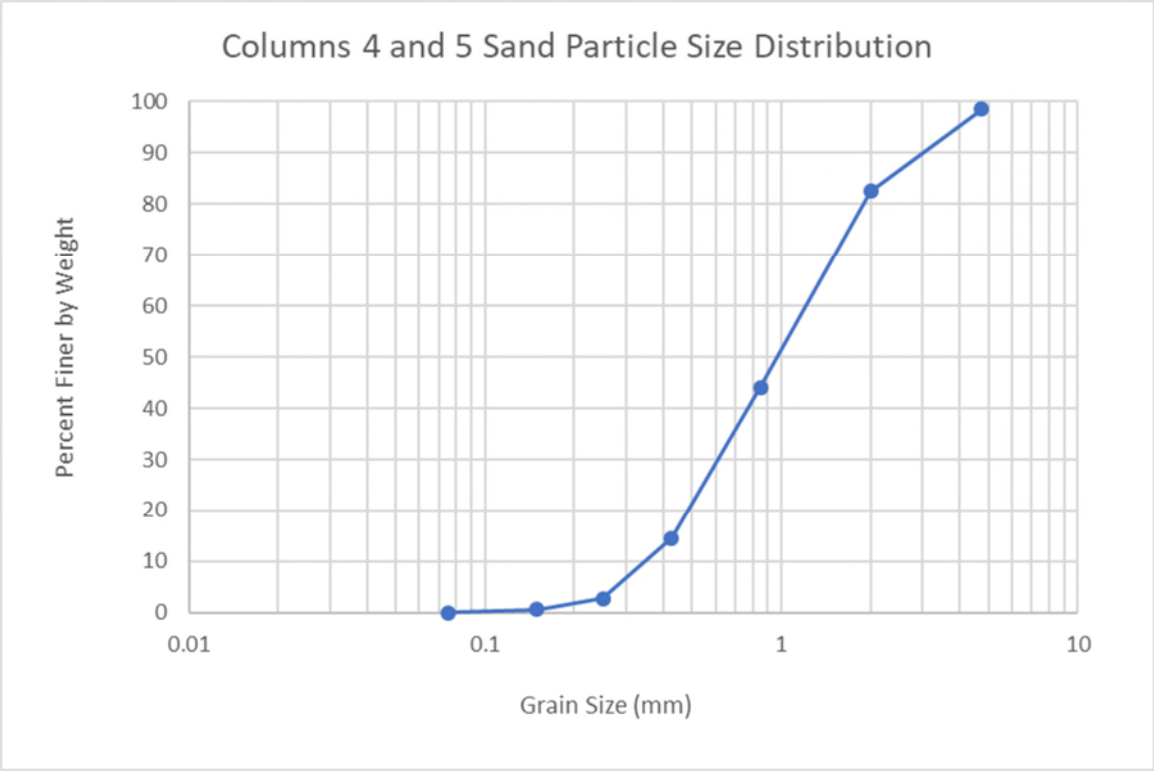

Figure 134: Particle size distribution for sand used in Columns 4 and 5

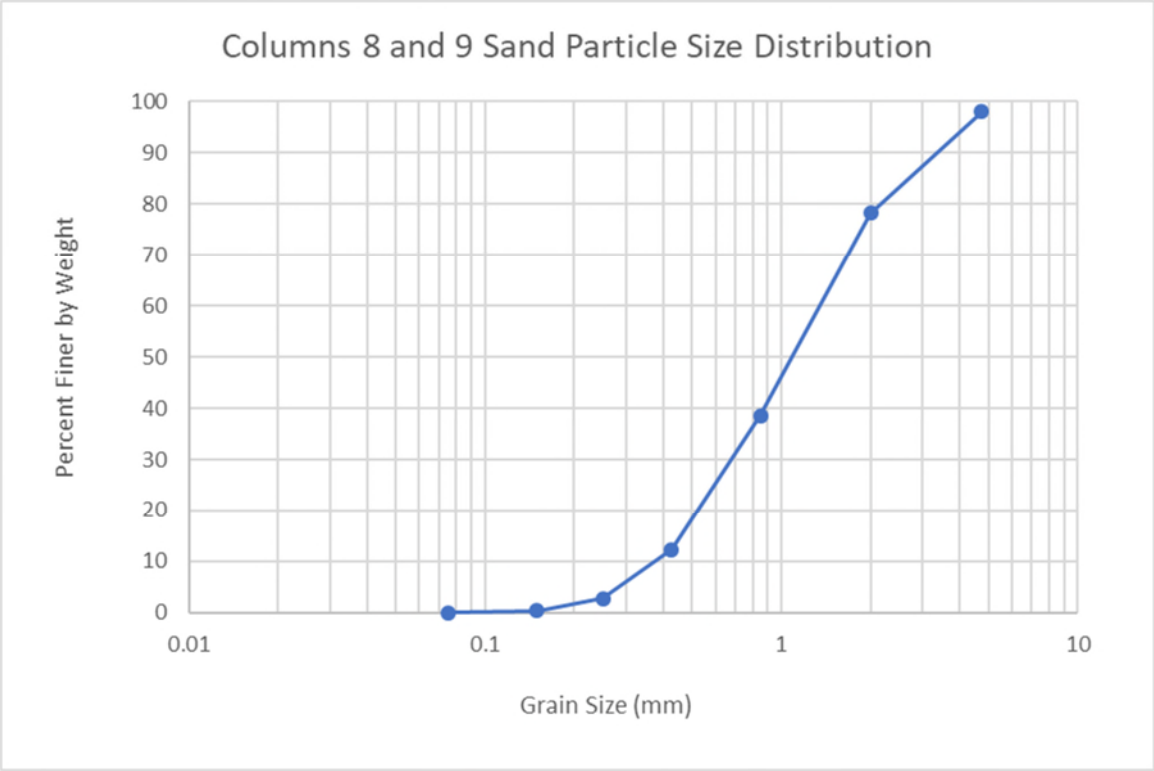

Figure 135: Particle size distribution for sand used in Columns 8 and 9

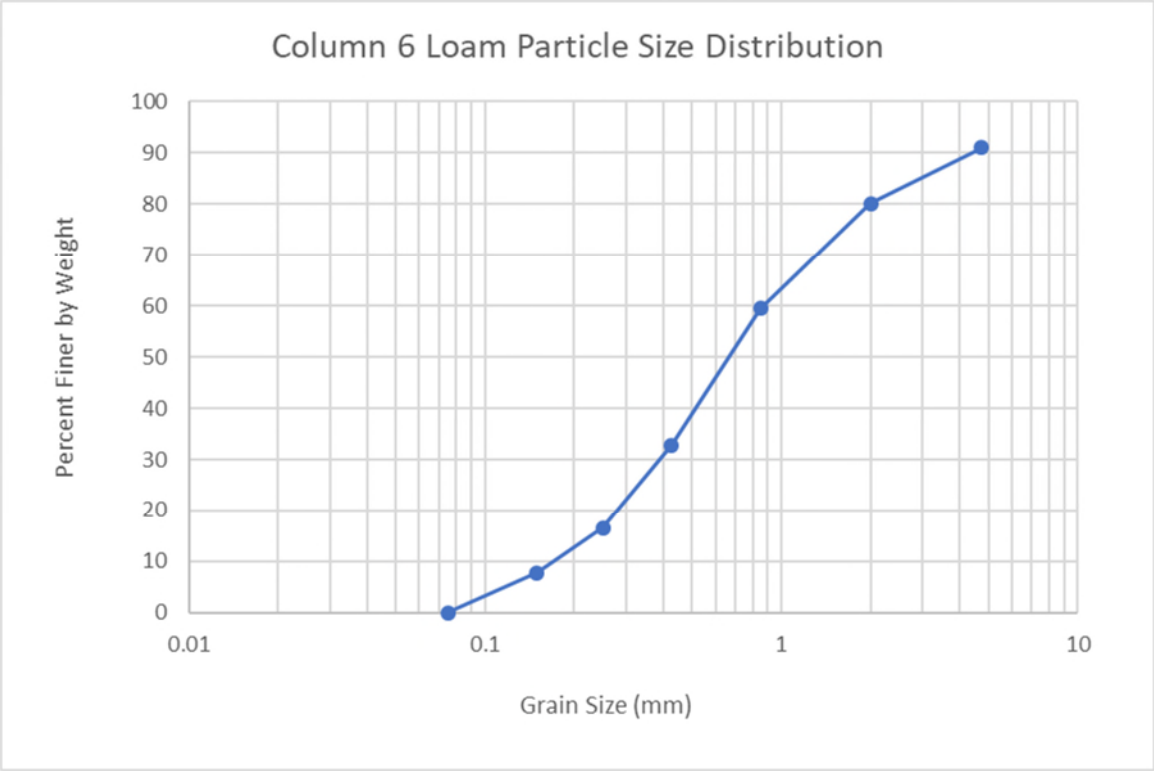

Figure 136: Particle size distribution for loam used in Column 6

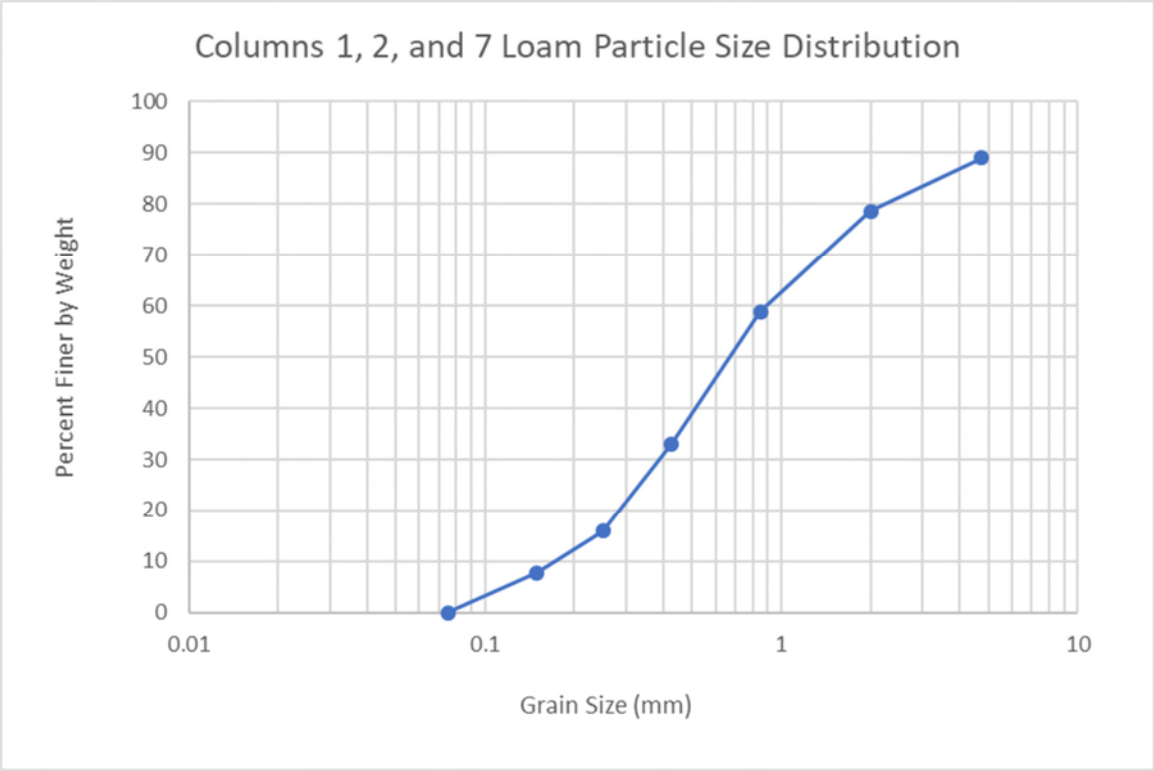

Figure 137: Particle size distribution for loam used in Columns 1, 2, and 7

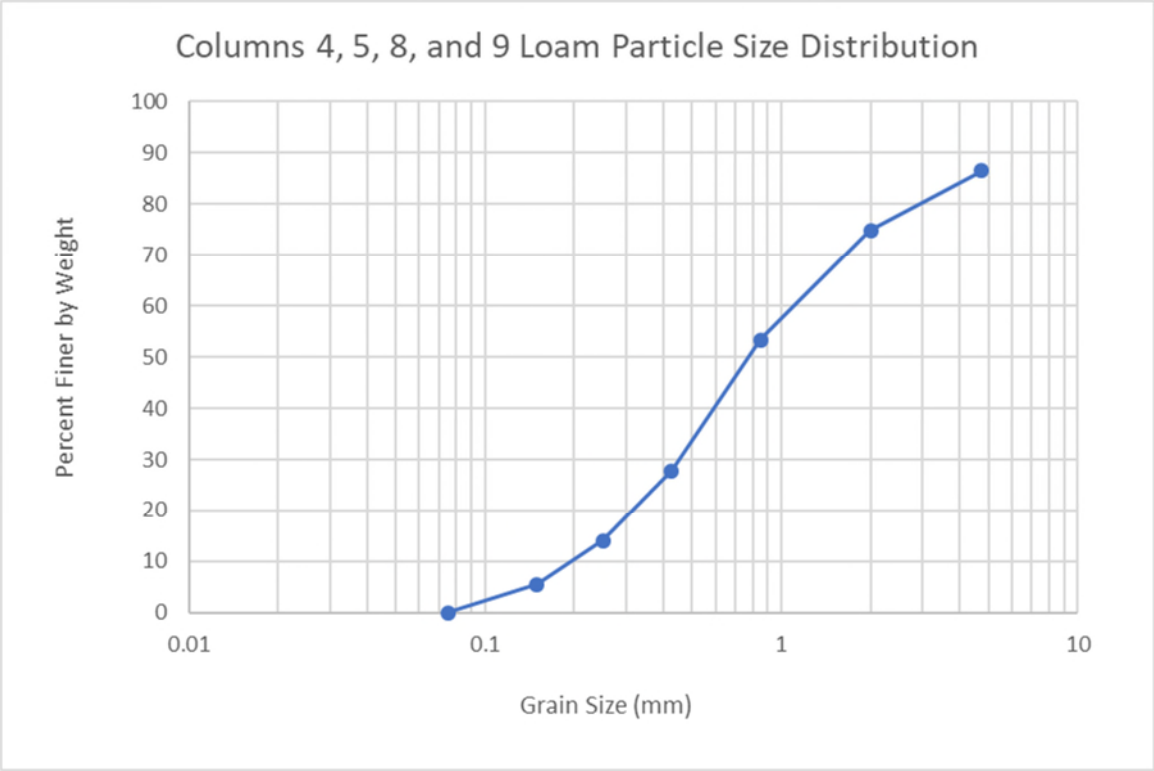

Figure 138: Particle size distribution for loam used in Columns 4, 5, 8, and 9

Table 23: Moisture, ash, and organic content analysis for overall loam batch

Moisture Content:		
pan mass =	113.5	
pan + wet sediment mass =	186.6	
wet sediment mass =	73.1	= A
pan + dry sediment mass =	178.9	
dry sediment mass =	65.4	= B
Moisture Content, % = [(A-B)x100]/A =	**10.5**	This calculation is used primarily for agriculture, forestry, energy, and horticulture purposes and the result should be referred to as the moisture content as a percentage of as-received or total mass.
Moisture Content, % = [(A-B)x100]/B =	**11.8**	This calculation is used primarily for geotechnical purposes and the result should be referred to as the moisture content as a percentage of oven-dried mass.
Organic Matter Content :		
crucible mass =	113.5	
crucible + wet sediment mass =	186.6	
wet sediment mass =	73.1	= A
crucible + dry sediment mass =	178.9	
dry sediment mass =	65.4	= B
Moisture Content, % = [(A-B)x100]/A =	10.5	This calculation is used primarily for agriculture, forestry, energy, and horticulture purposes and the result should be referred to as the moisture content as a percentage of as-received or total mass.
Moisture Content, % = [(A-B)x100]/B =	11.8	This calculation is used primarily for geotechnical purposes and the result should be referred to as the moisture content as a percentage of oven-dried mass.
crucible + ash mass =	175.5	
ash mass =	62	= C
organic matter mass =	3.4	
Ash Content, % = (C x 100)/B =	**94.8**	= D
Organic Matter, % = 100 - D =	**5.2**	

Note: Loam originated from East Coast Excavating in Groveland, MA where it was screened and blended using a combination of fill, compost, and other materials

Appendix D: Longevity Prediction Spreadsheet Instructions and Explanation of Background Calculations

Please note: For clarity and to accommodate use as a standalone document, this Appendix does not conform to the Equations, Tables, and Figures numbering schemes of the previous sections of the thesis.

D.1 Instruction Manual:

This instruction manual is to be used with the ZVI-Amended Bioretention Longevity Prediction spreadsheet.

Notice: This program may not work on Apple computers due to no macro support.

Step 1: Enable content

Excel will warn you to stay in Protected View, but disregard this message and click Enable Editing. This enables the macros that run this program.

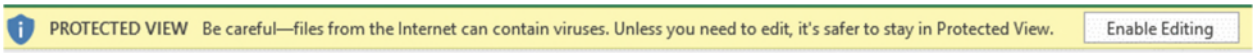

Step 2: Solver Add-in

Install/activate Solver as an Add-in.

Go to the developer tab and select Excel Add-ins.

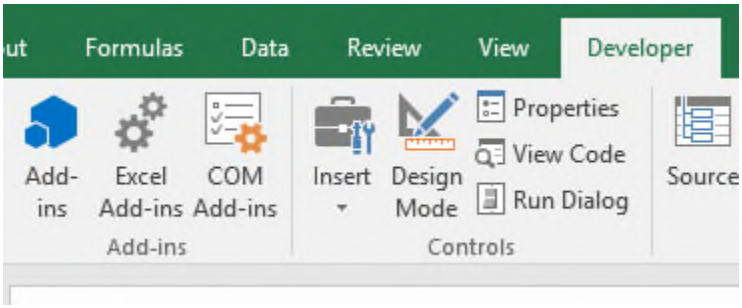

Check the box for Solver Add-in.

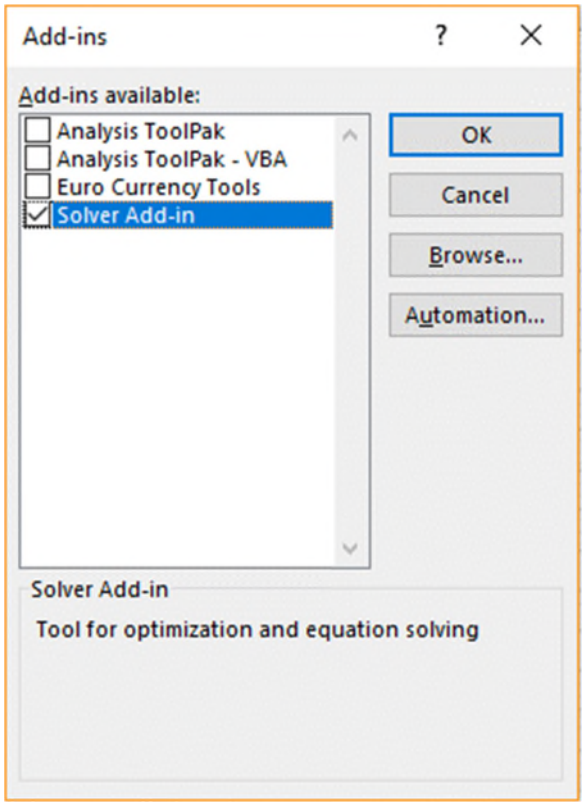

Step 3: Configure macro settings

Under the developer tab, click on the Macros button.

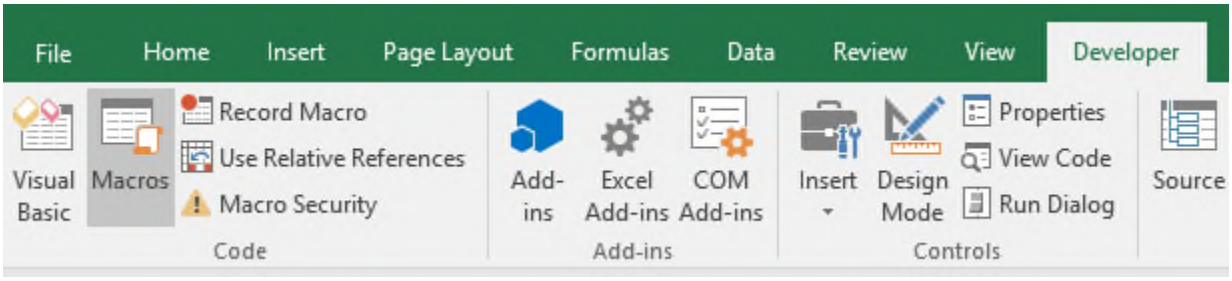

Select "isotherm" and click the edit button.

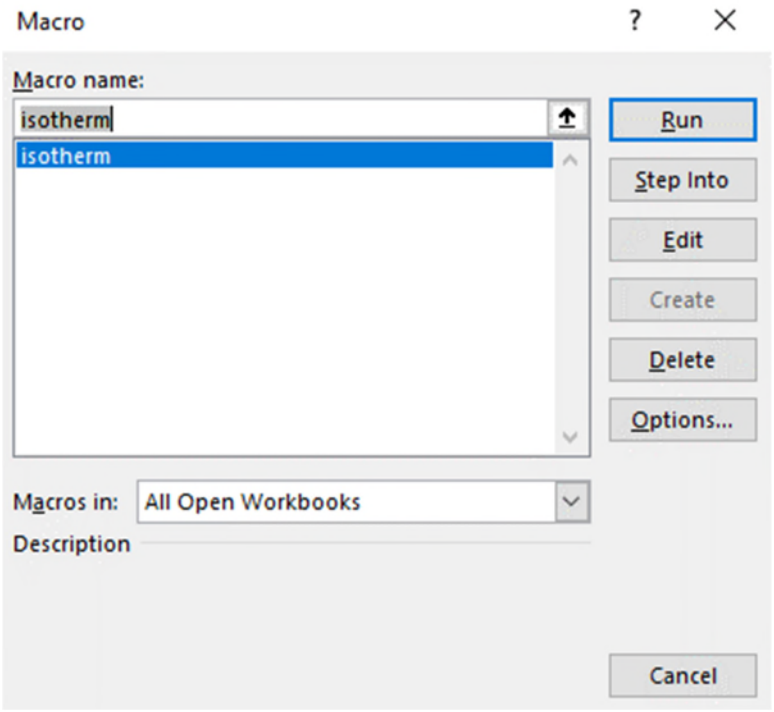

Go to the tools tab and click on References.

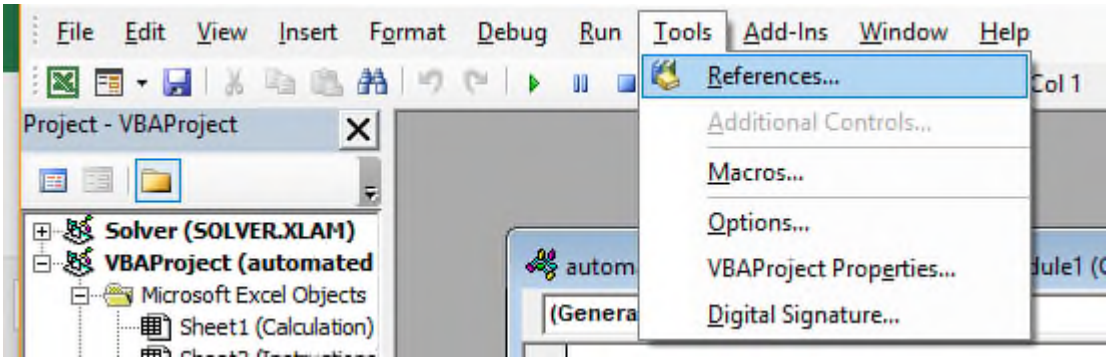

Make sure the Solver option has a check mark and click OK.

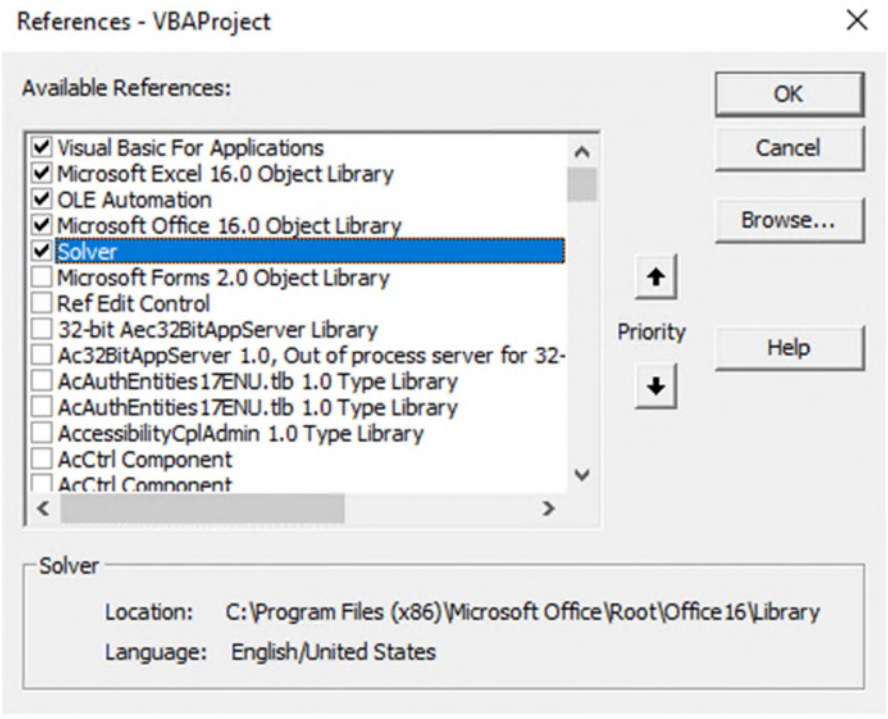

Step 4: Click on the Calculation worksheet tab.

Enter your expected design parameters, and click the "Determine Lifespan" button to get results! (The program may take a minute to run the calculation.)

Input Parameters

%ZVI (0.5-5)	3					
Watershed Area:Filter Area Ratio	14.3					
Average Annual Rainfall		inches	**or**	101.6	cm	
Depth of ZVI-Amended Media		inches	**or**	30.48	cm	
Average Influent PO_4^{3-}-P Concentration (mg/L)	4.3					
Acceptable Percent Removal (%)	20					

DETERMINE LIFESPAN

%ZVI – the percentage of ZVI intended for use in the treatment system

Watershed Area:Filter Area Ratio – the treatment system's watershed area divided by its own surface area

Average Annual Rainfall – the rainfall expected for the area feeding the treatment system in a year

Depth of ZVI-Amended Media – the depth of media from the treatment system's surface to where treated water will exit

Average Influent PO_4^{3-}P Concentration – the average expected influent concentration of ortho-P for any given runoff event

Acceptable Percent Removal – the removal percentage required for the system to keep meeting regulations, if applicable, or the percent removal that the user deems acceptable

If you change any of the parameters in the input boxes after running the program, you will need to click the "Determine Lifespan" button again for new results.

Once the program runs the calculation, you will see the Expected Lifespan prediction and the predicted %Removal curve.

Expected Lifespan (Years)	**8.0**

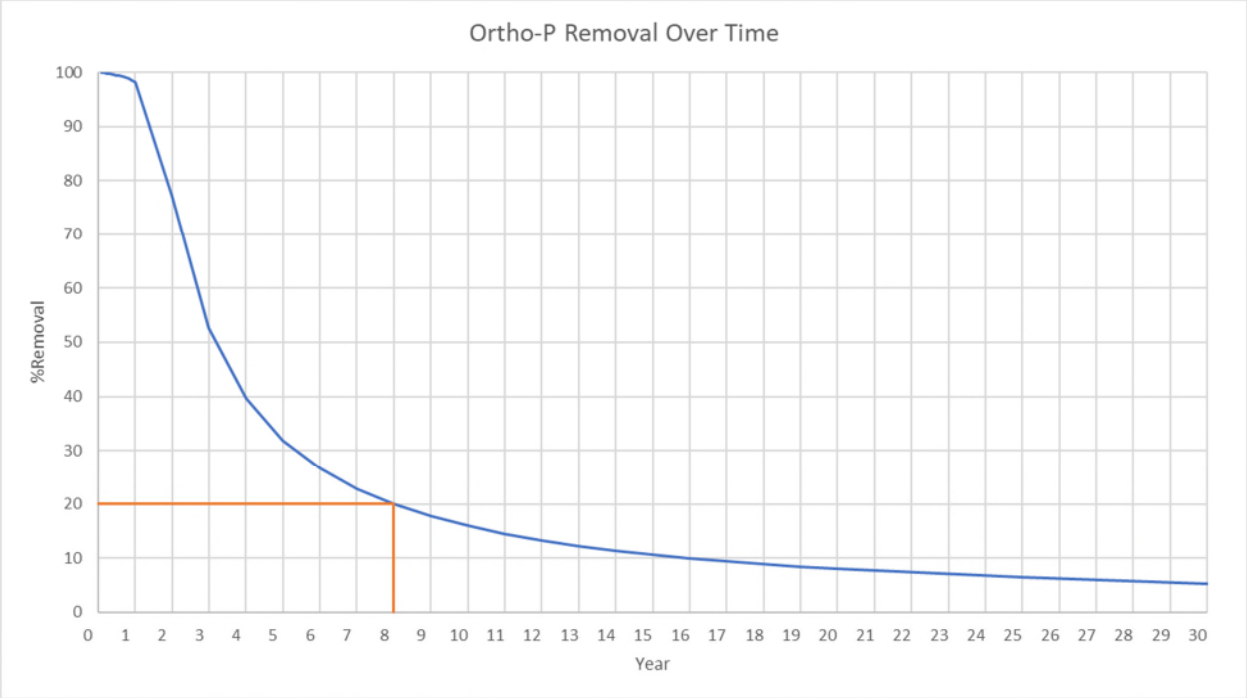

D.2 Explanation of Calculations

Please note: To accommodate use as a standalone from the main thesis body, this

The lifespan of ZVI predicted in the Calculation worksheet uses the Langmuir adsorption isotherm model. As phosphate ions in the stormwater come in contact with iron particles, the iron adsorbs these phosphate ions and effectively removes them from the water. However, the iron will lose its capacity to adsorb these ions over time because its adsorption sites become full.

The Langmuir equation is shown below:

$$q_e = \frac{(C_0 - C_e)V}{M_{ad}} = \frac{q_m K_L C_e}{1 + K_L C_e}$$

C_0 = influent phosphate concentration (mg/L)

C_e = effluent phosphate concentration (mg/L)

V = volume treated (L)

M_{ad} = mass of adsorbent (ZVI in this case)

q_m = Maximum adsorbent-phase concentration when surface sites are saturated (mg/g)

K_L = Langmuir adsorption constant (L/mg)

q_m and K_L values were determined from data collected during a column study. In this column study, six columns of varying depths of media and percentages of ZVI were used to remove phosphate from simulated stormwater. The water was run through these columns until it was determined that they had no more removal capacity. For each trial, the influent and effluent concentrations were reported for the columns. Figure 1 shows how q_m and K_L values were determined for each column by minimizing the root mean squared error (RMSE) as iterations of q_m and K_L were applied. The raw effluent concentrations were adjusted to account for the increased adsorption effect from loam in the columns. Percent removal plots as shown in Figure 2 were then created with the best fit Langmuir isotherm

curves (based on the determined q_m and K_L values for each column) plotted against the reported percent removal values (corrected for the loam effect). The RMSEs for these curves were calculated. It was determined after further analysis that although each column originally returned a unique value for K_L, there was not a large difference in RMSE when the median K_L value across all columns was applied to each plot like Figure 2. From these results, it was determined that K_L would be held constant at a value of 20.7 L/mg. The q_m values for all columns were plotted against their respective percentages of ZVI and a function was determined using a best fit curve. Figure 3 shows the best fit equation for q_m using the data from all columns. When a user enters a value into the "%ZVI" cell in the spreadsheet, the spreadsheet automatically calculates the values for q_m based on the chosen percent ZVI.

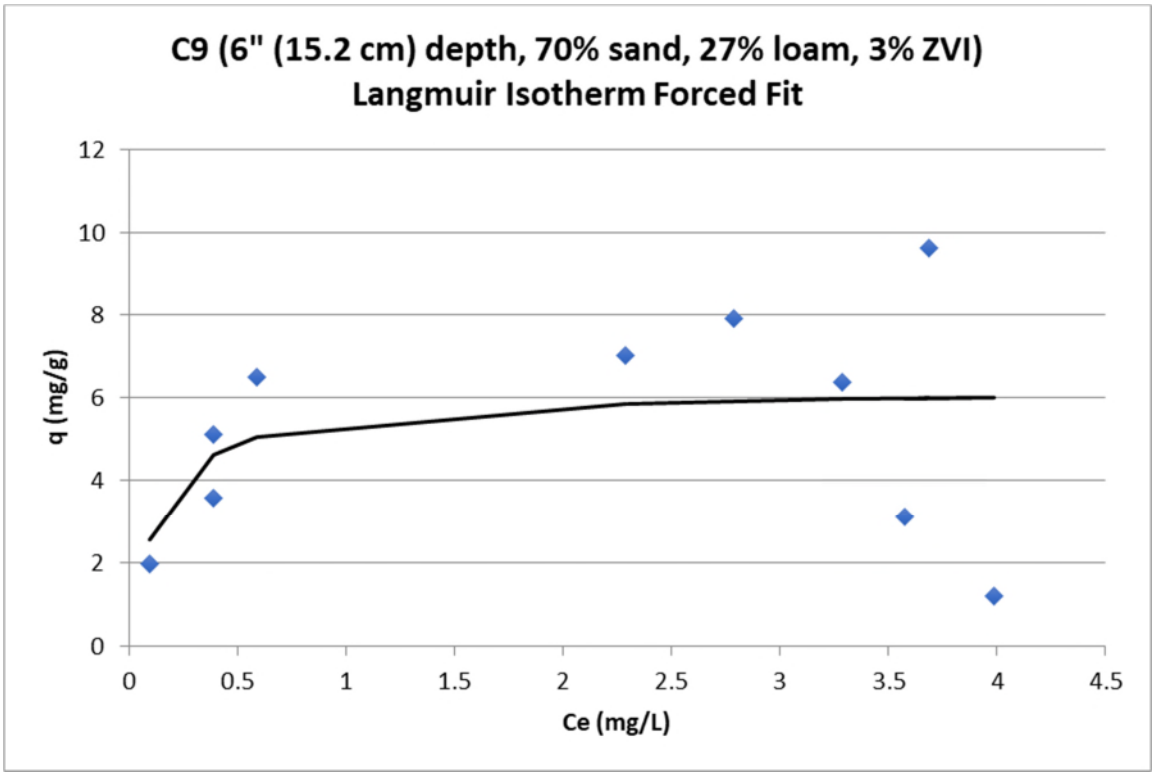

Figure 1: Langmuir isotherm fit line for Column 9 where RMSE is minimized

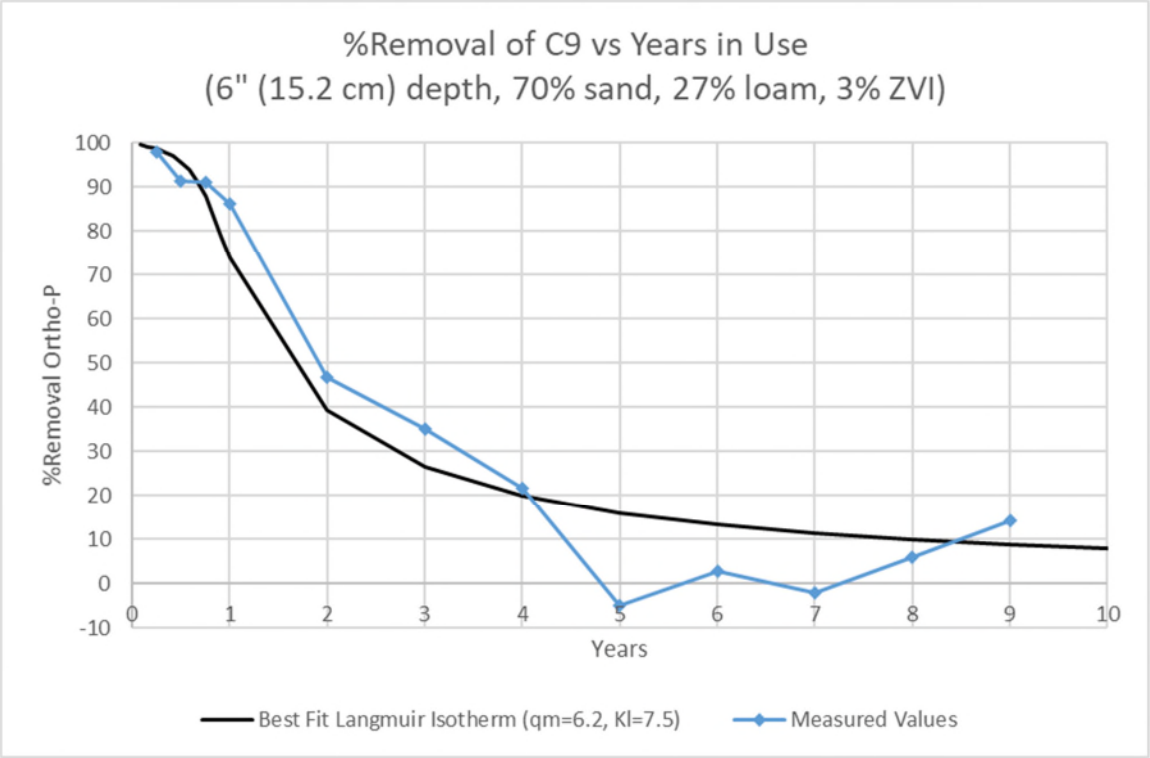

Figure 2: Best fit Langmuir isotherm curve compared to reported percent removal values

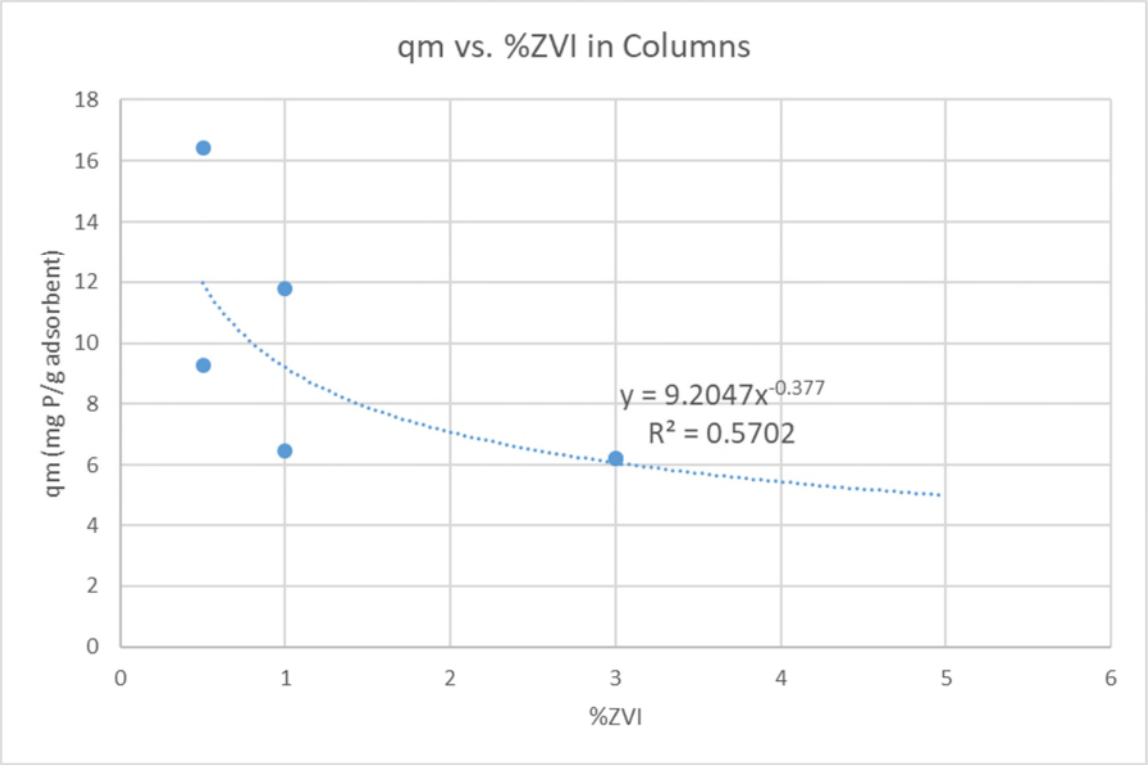

Figure 3: q_m based on percentage of ZVI

Table 1 shows the calculations being performed in the background of the spreadsheet when the "Determine Lifespan" button is pushed. C_0 and M_{ad} are chosen by the user in the spreadsheet where C_0 is the "Average Influent PO_4^{3-}-P Concentration" and M_{ad} is determined from the "%ZVI" and "Depth of ZVI Amended Media". The model runs based on the assumption that the influent concentration will remain constant over the lifespan of the system. The volume treated is also chosen by the user when they input values for the "Average Annual Rainfall" and "Watershed Area:Filter Area Ratio". This yearly volume is calculated by multiplying "Average Annual Rainfall" and "Watershed Area:Filter Area Ratio" by the cross sectional area of a column. q_m is determined by the power function dependent on ZVI percentage as shown in Figure 3 while K_L is held constant at 20.7. Because C_e is on both sides of the equation, the equation must be solved for C_e using iterations. The spreadsheet will run these iterations using the Solver add-in within a macro activated by the "Determine Lifespan" button. These iterations will be performed until the values in Column J of Table 1 are all minimized. Once these values are

minimized, it essentially means that both sides of the Langmuir equation are equal and the correct value for C_e was determined. The spreadsheet calculates C_e at volumes that correspond to the treatment time (i.e. Year 1, Year 2, Year 3, etc.). Once C_e has been calculated at each of these points, the percent removal can be calculated using C_0 and C_e. Because it is assumed in these calculations that the proposed treatment system would include roughly 30% loam, the loam effect is added back in and slightly boosts the percent removal. This addition is not displayed in Table 1, but it is reflected in the tool's prediction plot and "Expected Lifespan" prediction. The total loam effect for each column was determined by dividing the cumulative mass of ortho-P retained by that column by the mass retained by its corresponding control column (see Figure 4). The total loam effect on removal percentage is determined using the multiple regression analysis coefficients shown in Table 2. Once the total loam effect percentage is determined, this percentage is divided equally among the data points encompassing the projected system lifespan and is added to each value in column K of Table 1. The lifespan of ZVI can then easily be determined based on these removal percentages.

Table 1: Langmuir isotherm background calculations

A	B	C	D	E	F	G	H	I	J	K
Year	V (L)	C_0 (mg/L)	C_e (mg/L)	M_{ad} (g)	q_e (mg/g)	1/(qmKL)	C_e/q_m	C_e/q_e	$\lvert[1/(q_mK_L)+C_e/q_m]-C_e/q_e\rvert$	%Removal
1/12	1.3803	4.3	0.002613	18.96	0.3128634	0.0079238	0.00043	0.00835345	5.54031E-12	99.93922117
2/12	2.7607	4.3	0.005522	18.96	0.6253032	0.0079238	0.000908	0.00883165	1.28736E-13	99.87157075
3/12	4.141	4.3	0.008779	18.96	0.9372435	0.0079238	0.001443	0.00936701	3.64351E-13	99.79583338
4/12	5.5214	4.3	0.012449	18.96	1.2485894	0.0079238	0.002046	0.00997023	1.19166E-12	99.71049482
5/12	6.9017	4.3	0.016613	18.96	1.5592208	0.0079238	0.002731	0.01065481	6.80444E-13	99.61364639
6/12	8.2821	4.3	0.021377	18.96	1.8689838	0.0079238	0.003514	0.01143798	4.17545E-12	99.50285117
7/12	9.6624	4.3	0.026877	18.96	2.1776784	0.0079238	0.004418	0.01234204	8.53827E-13	99.37495387
8/12	11.043	4.3	0.03329	18.96	2.48504	0.0079238	0.005472	0.0133963	7.55698E-14	99.22580581
9/12	12.423	4.3	0.040856	18.96	2.7907128	0.0079238	0.006716	0.01463999	3.01051E-13	99.04986003
10/12	13.803	4.3	0.049899	18.96	3.0942086	0.0079238	0.008203	0.01612649	4.19838E-14	98.83956468
11/12	15.184	4.3	0.060869	18.96	3.394844	0.0079238	0.010006	0.01792987	4.8295E-13	98.58443956
1	16.564	4.3	0.074405	18.96	3.6916408	0.0079238	0.012231	0.02015496	4.17069E-13	98.26965427
2	33.128	4.3	0.981434	18.96	5.7984519	0.0079238	0.161334	0.16925788	1.68993E-12	77.17596118
3	49.693	4.3	2.032727	18.96	5.9423277	0.0079238	0.334152	0.34207591	1.13213E-11	52.72727541
4	66.257	4.3	2.591016	18.96	5.9721356	0.0079238	0.425927	0.43385076	9.5296E-13	39.7438243
5	82.821	4.3	2.929918	18.96	5.984779	0.0079238	0.481638	0.48956161	6.90725E-13	31.86237141
6	99.385	4.3	3.156935	18.96	5.9917528	0.0079238	0.518956	0.52687998	3.59912E-12	26.58291633
7	115.95	4.3	3.319507	18.96	5.9961693	0.0079238	0.545681	0.5536047	9.88432E-13	22.80215162
8	132.51	4.3	3.441633	18.96	5.9992163	0.0079238	0.565757	0.57368045	8.23541E-12	19.96202137
9	149.08	4.3	3.536724	18.96	6.001445	0.0079238	0.581388	0.58931203	3.37319E-12	17.75061096
10	165.64	4.3	3.612857	18.96	6.0031459	0.0079238	0.593903	0.60182722	5.08593E-13	15.9800777
11	182.21	4.3	3.675185	18.96	6.0044867	0.0079238	0.604149	0.61207309	2.91318E-11	14.53058789
12	198.77	4.3	3.727149	18.96	6.0055706	0.0079238	0.612692	0.62061534	5.70566E-12	13.32211013
13	215.33	4.3	3.771136	18.96	6.0064651	0.0079238	0.619922	0.62784614	4.3535E-11	12.29916405
14	231.9	4.3	3.808851	18.96	6.0072159	0.0079238	0.626122	0.6340459	6.16012E-11	11.42207973
15	248.46	4.3	3.841545	18.96	6.0078549	0.0079238	0.631497	0.63942042	1.26865E-12	10.66174174
16	265.03	4.3	3.870159	18.96	6.0084054	0.0079238	0.6362	0.64412418	1.55431E-14	9.996298762
17	281.59	4.3	3.895412	18.96	6.0088846	0.0079238	0.640352	0.64827533	9.33897E-12	9.409031534
18	298.16	4.3	3.917862	18.96	6.0093054	0.0079238	0.644042	0.65196586	2.95097E-13	8.886930006
19	314.72	4.3	3.937952	18.96	6.0096781	0.0079238	0.647345	0.65526839	4.00058E-12	8.419718906
20	331.28	4.3	3.956035	18.96	6.0100103	0.0079238	0.650317	0.65824105	3.50775E-12	7.999175122
25	414.1	4.3	4.024772	18.96	6.0112461	0.0079238	0.661617	0.66954034	9.86822E-12	6.400655989
30	496.93	4.3	4.07061	18.96	6.0121152	0.0079238	0.669152	0.67706786	7.64578E-06	5.334651163

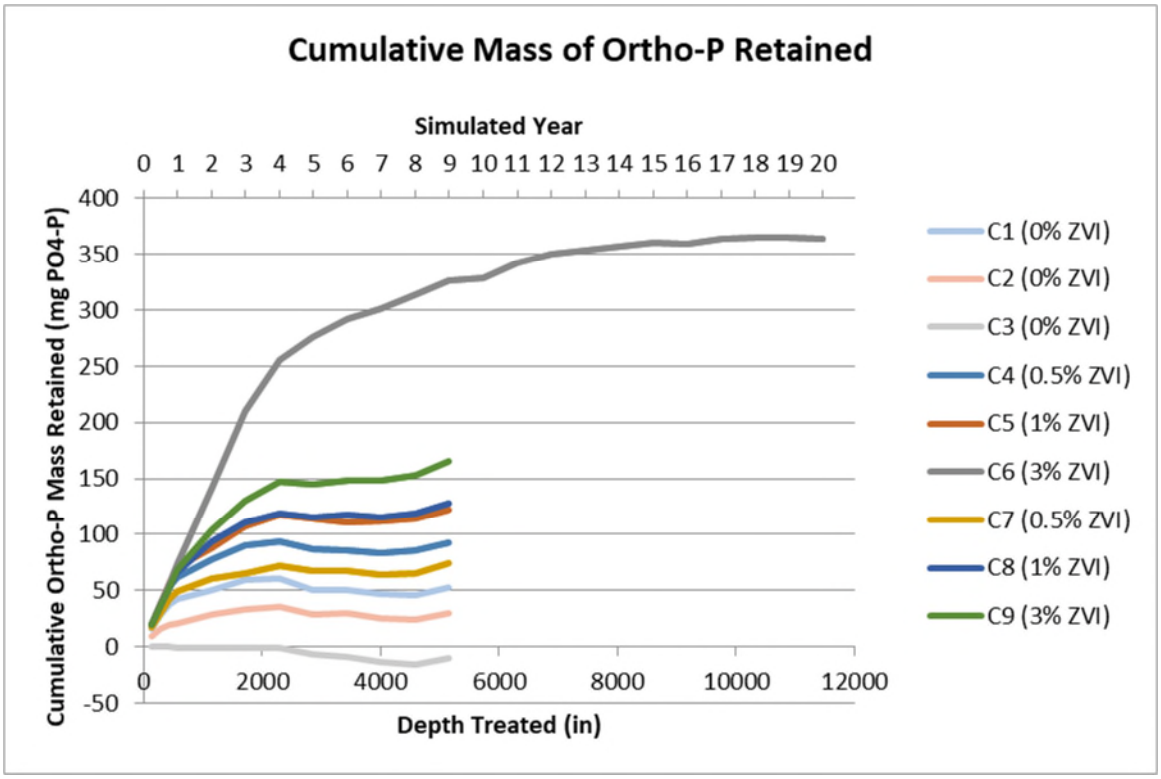

Figure 4: Cumulative mass of ortho-P retained by column

Table 2: Total loam effect multiple regression analysis

SUMMARY OUTPUT

Regression Statistics	
Multiple R	0.929526951
R Square	0.864020353
Adjusted R Square	0.773367255
Standard Error	7.49680458
Observations	6

ANOVA

	df	*SS*	*MS*	*F*	*Significance F*
Regression	2	1071.331068	535.6655338	9.531062625	0.050143063
Residual	3	168.6062367	56.20207891		
Total	5	1239.937304			

	Coefficients	*Standard Error*	*t Stat*	*P-value*	*Lower 95%*	*Upper 95%*	*Lower 90.0%*	*Upper 90.0%*
Intercept	26.78553348	10.5704818	2.533993624	0.085125796	-6.854457266	60.42552422	1.909348126	51.66171883
%ZVI	-9.078471263	2.833525792	-3.203948694	0.049183098	-18.09601495	-0.060927574	-15.74678725	-2.410155272
Depth (in)	3.025816646	1.020185885	2.965946394	0.059260443	-0.220870153	6.272503445	0.624948488	5.426684803

Total Loam Effect % = (-9.08)(%ZVI) + (3.02)(Depth (in)) + 26.79